ANALYSIS OF UPPER AND LOWER MANTLE STRUCTURE USING SHEAR WAVES

Thesis by

Thorne Lay

In Partial Fulfillment of the Requirements

for the Degree of

Doctor of Philosophy

California Institute of Technology

Pasadena, California

1983

(Submitted March 3, 1983)

To my parents

Acknowledgements

My stay in the Seismological Laboratory has been a uniquely pleasant academic experience. My enthusiasm for geophysics can be entirely attributed to the stimulating atmosphere in the lab. I thank all of the students, faculty and staff who have contributed to this environment.

My special appreciation is extended to Hiroo Kanamori, Don Helmberger and Don Anderson for their extreme patience with me and their continuing encouragement and enthusiasm for my work. They have provided a high standard of excellence toward which to strive.

I am especially grateful to Cindy Arvesen who has shared my experience at Caltech and has provided me with love and inspiration.

The research presented in this thesis, which constitutes a small fraction of the total body of work I have been involved with at Caltech, was supported in part by a National Science Foundation Graduate Fellowship, NSF grants EAR 78-14786 and 81-8616, and by the Advanced Research Projects Agency of the Department of Defense under contract numbers F49620-77-C-0022, F49620-81-C-0008.

Abstract

This thesis addresses the fundamental problem of determining the radial and lateral structure of the earth's interior using body wave observations. My approach is a cautious one, involving detailed analysis of a substantial data set in which I attempt to isolate the contributions from radial and lateral structure in both the upper and lower mantles. This is an elusive task, as I am concerned with the 2 or 3% fluctuations about standard earth models, which produce rather subtle effects on teleseismic signals. However, this is the level of precision to which the three dimensional structure of the earth must be determined if we are to map the dynamical and compositional configuration of the earth. Studies similar to those described here cannot be conducted on a detailed global basis, given the intrinsic limitations due to station and earthquake distribution, so I have repeatedly emphasized the qualitative implications of my results, as they probably provide a representative sampling of the subtle, but significant heterogeneity of the earth.

The topics addressed in the following work appear unrelated at first glance, ranging from determination of the detailed shear velocity structure at the base of the mantle to variations in attenuation and velocity structure of the upper mantle. However, the data set used throughout is largely the same, and this in itself indicates the need to consider all of the complexity discussed herein for future progress to be made in mapping the three dimensional structure of the earth with a high level of confidence.

The first chapter of the thesis presents results of a waveform

analysis of transversely polarized SH signals that propagate through the lowermost mantle. The waveforms of these phases show clear interference patterns due to interaction with a discontinuous shear velocity increase about 280 km above the core-mantle boundary. This discontinuity, which has not been detected previously, is manifested in signals sampling three widely separated portions of the lower mantle, and hence is a good candidate for a global radial earth structure. Very detailed inspection of the signals reveals evidence for lateral variations in the depth of the discontinuity, which provides a procedure by which to map the structure of the D" region in detail. Analysis of the relative amplitudes of SH and ScSH signals reveals that the velocity gradient above the core boundary is consistent with the smoothly varying gradients in most gross earth models, but evidence for local high velocity gradients at the base of the mantle is detected in ScSV signals.

Chapter II presents a travel time analysis of the same data set used in Chapter I, which was motivated by the observation of large amplitude and travel time anomalies in the S and ScS data. An emphasis is placed on isolating the portions of the S and ScS paths which are anomalous. A strong empirical case is made for the existance of localized regions with scale lengths of 1000 to 2000 km and 2% velocity anomalies within the lower mantle at depths from 1000 to 2700 km. The long period signals traversing these regions show as much as a factor of 2 amplitude enhancement or diminution. This result demonstrates that both amplitude and travel time anomalies are induced by lateral structure in the portion of the mantle assumed to

be homogeneous in most seismological studies.

The third chapter is an analysis of the influence of upper mantle variations in attenuation, velocity structure and receiver structure on the S and ScS signals analyzed in the lower mantle studies. These variations contaminate and complicate the interpretation of any data set used to study deeper earth structure. Along with evidence for very strong and abrupt variations in upper mantle properties, results are presented which indicate the inadequacy of assumptions that are frequently made about the nature of long period body-wave receiver functions.

Table of Contents

General Introduction

The principal features of the earth's radial structure were rapidly identified using seismological techniques in the first half of this century. The resulting stratified earth models have proved remarkably resilient, with only relatively minor modifications being incorporated in the last 30 years. The most significant evolution of these models has been in the upper mantle, where discontinuous changes in material properties have been identified on a global basis. There has been little modification of radial earth models for the lower mantle or core. The last few decades have been most fruitful in unveiling the regional perturbations about the radially symmetric earth models. This aspherical heterogeneity appears rather insignificant at first thought, given the ability of the gross earth models to account for body wave travel times to within 1%, yet it is only by characterizing and mapping the three dimensional structure of the earth that further significant progress in understanding the composition, dynamics and evolution of the planet can be made. This thesis addresses the adequacy of gross earth model representations of lower mantle velocity structure, as well as the nature of lateral heterogeneity in the upper and lower mantles.

With the recent development of sophisticated techniques for synthesizing displacement responses for realistic earthquake sources in realistic earth models, new procedures for determining earth structure have arisen. Simultaneous use of travel time, amplitude and waveform information allows increased resolution of structural details, but not without some pitfalls. In order to attain the

heightened resolution a detailed understanding of all propagational contributions to the signals must be mastered. This is particularly true for analysis of lower mantle or core structure, for all signals that sample these regions must also traverse the upper mantle and receiver structures as well. Waveform modeling techniques have been applied with substantial success in determining upper mantle structure, but as expected, the success has been more ambiguous for lower mantle and core studies.

The first chapter of this thesis presents a waveform modeling analysis of the shear velocity structure of the lowermost mantle; the D'' region. The exhaustive data selection and quantitative modeling employed overcome the limitations of classic travel time studies to indicate that significant velocity structure exists near the core-mantle boundary, which is itself the largest compositional discontinuity within the earth. A lower mantle shear wave triplication is observed in data sampling three distinct portions of the D'' region. Waveform modeling shows that a 2.75% velocity discontinuity exists at several places and possibly globally near 280 km above the core-mantle boundary. This feature is not present in any gross earth model, for the techniques used to derive those models are not adequately sensitive to lower mantle structure. Chapter I also presents an analysis of the lateral variations in the shear velocity structure in D'' based on modeling ScSH and ScSV waveforms and amplitudes. It is shown that lateral variations in D'' can be quantitatively modeled, with the D'' layer varying in thickness by 40 km or more. There is also strong evidence for a laterally varying

high velocity layer just above the core-mantle boundary.

The waveform information employed in Chapter I is somewhat contaminated by relatively large differential travel time (ScS-S) and amplitude (ScS/S) anomalies not accounted for by any radial earth model. To determine the cause of these variations, and their implications for the D'' velocity models, a detailed travel time study is presented in Chapter II. It is shown that upper and lower mantle heterogeneity is responsible for the differential travel time anomalies, with the direct S phases being more strongly affected than the ScS phases. Localized regions of anomalous properties are identified within the lower mantle at depths from 1000 to 2700 km. These zones have scale lengths of 1000 km with at least 2% velocity contrasts from the surrounding mantle. This result undermines the frequently made assumption that the lower mantle above the D'' region can be treated as laterally homogeneous for differential travel time and amplitude analysis. A correspondence is shown between amplitude and travel time anomalies for long period body waves traversing the lower mantle heterogeneities. This may provide an explanation for the pervasive scatter in teleseismic amplitudes that exists in earthquake modeling studies. Another important implication of such deep seated heterogeneity is that simple classification of upper mantle and receiver behavior based on surface tectonics may not reduce the amplitude scatter.

Chapter III of this study isolates the receiver and upper mantle contributions to the relative behavior of the teleseismic SH signals. Large upper mantle variations in shear velocity and attenuation

beneath North America are confirmed and quantified in this chapter. The sensitivity of broadband S wave data to variations in upper mantle properties is exploited to constrain these variations. The profound effect of receiver structure on teleseismic body waves is demonstrated, with the contributions due to variations in structure and attenuation being isolated.

All of the material presented in this thesis has been published or is in press. Chapter I is found in Lay and Helmberger (1983 a,b,c); Chapter II is presented in Lay (1983), and Chapter III is in Lay and Helmberger (1980, 1983 d,e).

References

Lay, T. (1983). Localized velocity anomalies in the lower mantle, Geophys. J. Roy. Astron. Soc., 72, 483-515.

Lay, T. and Donald V. Helmberger (1980). Body wave amplitude patterns and upper mantle attenuation variations across North America, Geophys. J. Roy. Astron. Soc., 66, 691-726.

Lay, T. and Donald V. Helmberger (1983a). A shear velocity discontinuity in the lower mantle, Geophys. Res. Letters, 10, 63-66.

Lay, T. and Donald V. Helmberger (1983b). A lower mantle S wave triplication and the shear velocity structure of D", Geophys. J. Roy. Astron. Soc., submitted.

Lay, T. and Donald V. Helmberger (1983c). The shear wave velocity gradient at the base of the mantle, J. Geophys. Res., submitted.

Lay, T. and Donald V. Helmberger (1983d). Amplitude and travel time correlations across North America, Bull. Seismol. Soc. Amer., submitted.

Lay, T. and Donald V. Helmberger (1983e). S wave amplitude and travel time variations beneath North America, Bull. Seismol. Soc. Amer., submitted.

Chapter I

Shear Velocity Structure of the D'' Region

Section I.1 A Shear Velocity Discontinuity in the Lower Mantle

Abstract

A lower mantle S wave triplication detected with short and long period WWSSN and CSN recordings indicates a substantial shear velocity discontinuity near 280 km above the core-mantle boundary. The triplication can be observed in rotated SH seismograms from intermediate and deep focus events throughout the distance range from 70^{o} to 95^{o}. Three distinct source region-receiver array combinations that have been investigated in detail demonstrate consistent travel time and relative amplitude behavior of the triplication, with slight systematic shifts in the triplication indicating up to 40 km variations in the depth of the discontinuity. Modeling of the observations with synthetic seismograms produced with the Cagniard de Hoop and Reflectivity methods constrains the shear velocity increase to be $2.75 \pm 0.25\%$, comparable to upper mantle discontinuities. Short period observations indicate that the velocity increase may be a sharp first order discontinuity, or may extend over a transition zone no more than 50 km thick. The shear velocity gradient below the discontinuity, within the D" layer, is not well-constrained by the SH data, but slightly positive or near zero velocity gradients are consistent with the long period amplitude ratios of ScSH/SH.

Introduction

The lowermost 200 km of the mantle (D" region) has long been associated with anomalously low shear velocity gradients and increased scatter in travel times and amplitudes of S waves (Bullen, 1949; Cleary et al. 1967; Hales and Roberts, 1970). Gross earth models

determined from travel times and free oscillations (e.g. Bullen, 1963; Sengupta, 1975; Gilbert and Dziewonski, 1975; Anderson and Hart, 1976; Dziewonski and Anderson, 1981) have generally indicated very smooth lower mantle velocity structures with mild positive or near zero shear velocity gradients within D". Early investigations of diffracted SH wave travel times, relying on classical ray theory interpretations, suggested very low S wave velocities at the core-mantle boundary (CMB) and attendant strong negative velocity gradients above the boundary (Cleary et al., 1967; Cleary, 1969; Bolt et al., 1970; Hales and Roberts, 1970). However, recent studies of diffracted S utilizing more complete diffraction theory and synthetic modeling capabilities have found milder positive or negative shear velocity gradients in D", generally compatible with the gross earth models (Mondt, 1977; Doornbos and Mondt, 1979; Okal and Geller, 1979; Mula and Müller, 1980). There is little agreement in the fine details of the various shear velocity models that have been determined for the base of the mantle, which may reflect the actual heterogeneity of the region, or possibly the limited resolution of the free oscillation, travel time and diffracted wave analyses which have been performed. No study of the shear velocity structure in the lower mantle has indicated any significant discontinuity near the top of D", other than smooth changes in the velocity gradient. There is clearly a large amount of lateral averaging in all of these studies, and regional variations in D" would be difficult to resolve. Any fine velocity structure such as small discontinuities, even of a global nature, could also have been completely missed because of the rather

subtle effects produced by lower mantle structure.

Analysis of the lower mantle shear velocity structure is complicated by the high attenuation of S phases in the mantle, the arrival of late P phases, and the contamination of direct S arrivals by SKS, which crosses over and arrives ahead of SV beyond 82^{o}. Yet, S waves have a major advantage over P waves for D" studies, in that the intrinsically lower shear velocities help to separate the arrivals produced by any fine structure, allowing discrete phases to be observed. Utilizing SH phases reduces the contamination of late P and SKS arrivals. In addition, the ScSH phase is completely reflected at the core and is easily observable, unlike PcP which is hard to identify over large distance ranges. Several recent attempts to utilize P waves to resolve fine structure of the lower mantle indicate that there is significant P wave velocity structure within D" (Ruff and Helmberger, 1982; Wright and Lyons, 1979, 1981); however, substantial data processing is necessary to isolate the subtle effects of this fine structure on the P waves. In this section we present a large body of S wave data which show clear evidence for major shear wave velocity structure at the top of D" and just above the CMB. In addition, since we utilize direct body wave phases which sample relatively localized regions of the lower mantle, we are able to quantify lateral variations in D" for three distinct regions. These results yield the important conclusion that the D" region is stratified, possibly on a global scale, with either a phase change or compositional change from the mantle above it. Thus, a simple model of the D" region as a thermal boundary layer with diminished velocity

gradients caused by a superadiabatic thermal gradient is inadequate.

The shear velocity models that have been proposed for the lower mantle are generally very smooth below 1000 km depth, with the only major features being low velocity zones at the base of the mantle in the few models which incorporated early estimates of diffracted S ray parameter (Randall, 1971; Robinson and Kovach, 1972). All other features in the velocity models are too small to produce a triplication or observable S wave reflections. Thus, for an intermediate or deep focus earthquake, no SH arrival is predicted between direct S and ScS at distances large enough that all surface phases arrive after ScS. This is generally substantiated by data as can be seen in Figure I.1.1. The data are rotated tangential component seismograms recorded at long period WWSSN and Canadian Seismic Network (CSN) stations in North America. The Sea of Okhotsk event shown has a focal depth of 583 km, and sS arrives later than ScS at distances greater than 44^{o}. The SH radiation to North America is near the maximum for both S and ScS so each phase is clearly observable. Note the lack of any coherent arrival between S and ScS in the range 44^{o} to 70^{o} that could be attributed to either source or deep mantle structure. There is appreciable receiver structure at some stations, notably BKS and COR, but, in general, the signals are quite simple and coherent. This coherence reflects the fact that the stations lie in a narrow azimuth range in a stable portion of the radiation pattern for this event. However, beyond 70^{o} there is a systematic arrival between S and ScS, indicated by the arrows, which interferes with the downswing of direct S, and appears to maintain a

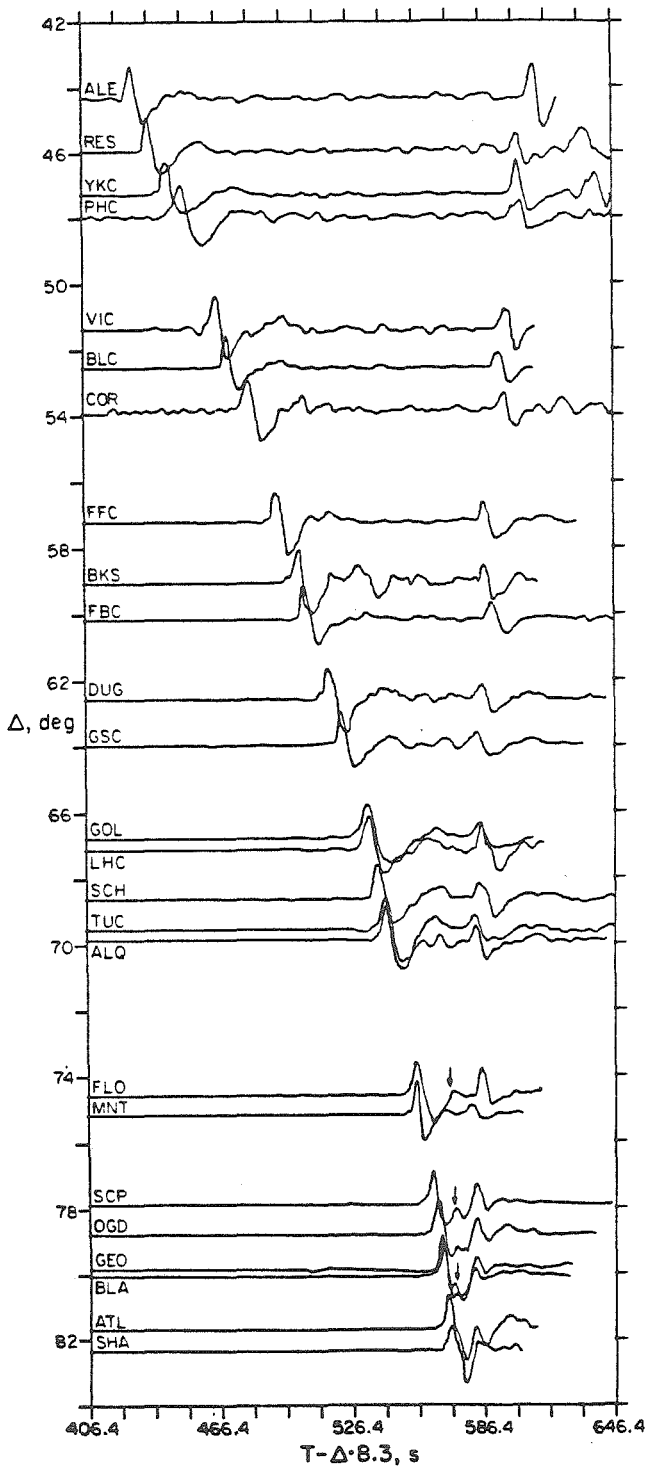

Figure I.1.1. Profile of tangential components at North American stations for the September 5, 1970 Sea of Okhotsk event (d = 583 km). Direct S is the first large arrival in each trace with ScS arriving around 580-600 sec. Station JB travel time anomalies have been removed and the amplitudes are normalized. The arrows indicate the arrival of an ScS precursor shown in greater detail in Figure I.1.6.

nearly constant separation from ScS. This feature is investigated in detail below, to determine whether it is due to source complexity, receiver structure, or lower mantle structure. Before proceeding with the data analysis, it is instructive to determine what features a lower mantle discontinuity would produce in a profile of SH data like that in Figure I.1.1.

Since the Jeffreys-Bullen (1940) S wave travel times have proved a reliable standard for lower mantle paths (e.g. Doyle and Hales, 1967; Hales and Roberts, 1970; Dziewonski and Anderson, 1981) we adopt the JB model of Press (1966) as a reference model. This model has smooth shear velocity gradients throughout the mantle except for a zero gradient within D". The only systematic departure of more recent data sets from the JB S wave model in the range 40^{o} to 100^{o} is that beyond 80^{o} the JB times are progressively early by several seconds (see Sengupta, 1975, Figs. 3-17 to 3-19 for a comparison of various models). For a surface focus event, an S wave traveling 80^{o} bottoms at a depth around 2200 km in the mantle. Therefore, below this depth it appears that the JB model is too fast. The core radius in the JB model (3473 km) also is slightly inconsistent with more recent estimates from PcP and free oscillations (Dziewonski and Haddon, 1974) and is increased to 3485 km in the models determined in this section.

Figure I.1.2 shows the lower 700 km of the mantle shear wave structure for the JB model and for a model with a 2.75% velocity discontinuity 278 km above the CMB. The latter model, SLHO, is actually that derived for the SH data from Sea of Okhotsk events recorded in North America shown below. The presence of the large,

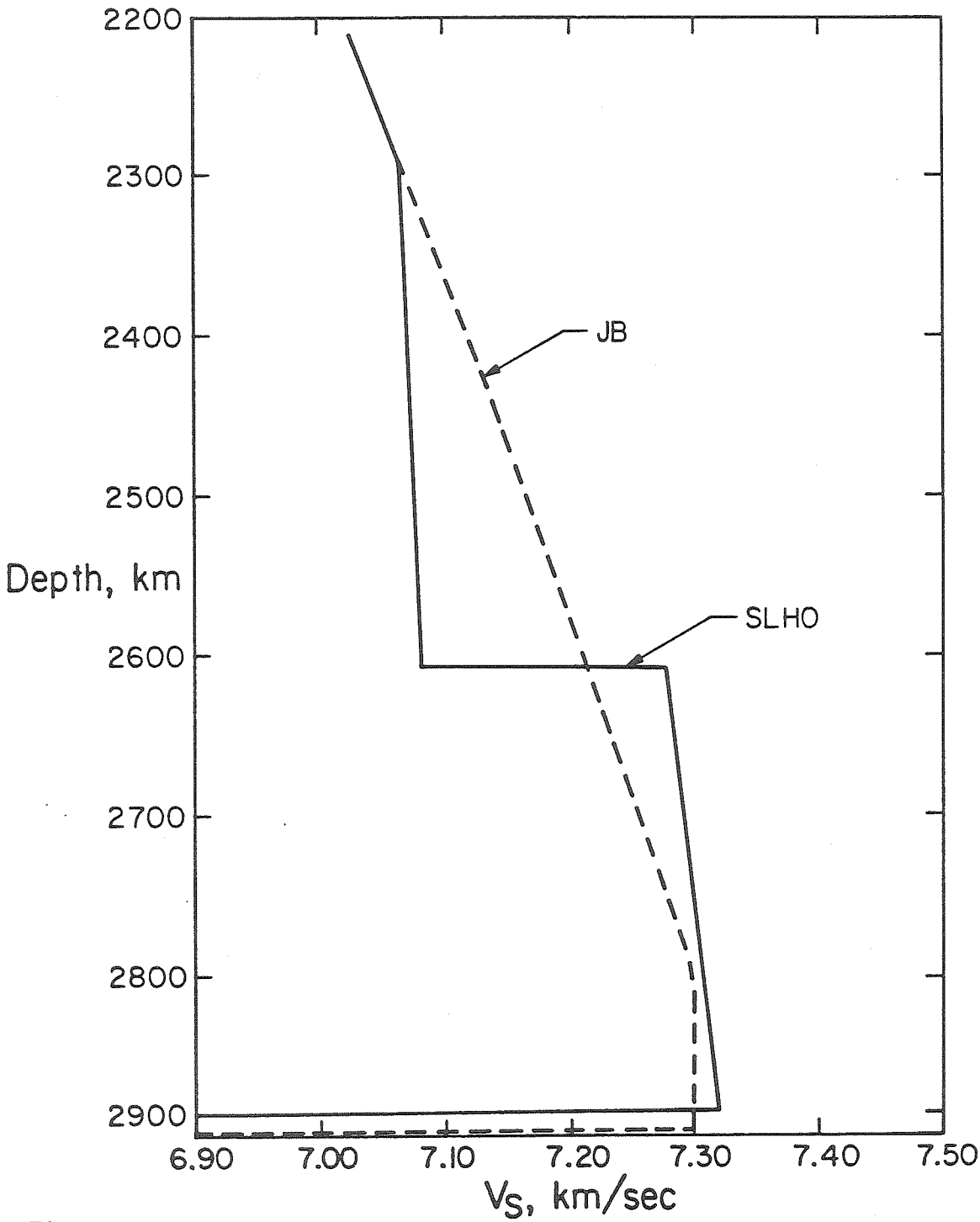

Figure I.1.2. Velocity profiles of the reference JB model and model SLHO which is derived from the Sea of Okhotsk data recorded in North America. The core radius for SLHO is 12 km greater than for the JB model. The velocity discontinuity 278 km above the core in model SLHO is a 2.75% increase. The models are identical above 2200 km.

sharp discontinuity produces a triplication not produced by the JB model. Synthetic SH seismograms for these two velocity structures are compared in Figure I.1.3. The synthetics are computed using the Cagniard de Hoop generalized ray theory method as discussed by Helmberger (1974). For the smooth JB model the only two arrivals predicted are direct S and ScS. The triplication produced by model SLHO produces the arrival between ScS and S. This arrival which corresponds to the Scd branch in standard triplication terminology, (see Figure I.1.14), is small near 70^{o} and is virtually unobservable at closer distances, particularly given the typical noise level between S and ScS shown in Figure I.1.1. By 75^{o}, Scd is quite large, and it begins to interfere with the direct S (Sab) arrival. At 80^{o} Scd is apparent in the downswing of the direct arrival and a strong interference is apparent. Note that the second arrival is actually very large, for it sharply turns the instrument downswing of the Sab arrival. At this range, Scd is as energetic as ScS, though because of the interference with Sab, the arrival is somewhat obscured. This type of interference pattern is what should be looked for in the SH data in this distance range.

Sea of Okhotsk Data Recorded in North America

The most complete S wave data set that we have gathered is for 10 intermediate and deep focus events in the Sea of Okhotsk recorded at WWSSN and CSN stations in North America. The epicenters and stations are shown in Figure I.1.4, and the hypocentral coordinates are listed in Table I.1.1. All events since 1963 with $m_b \geq 5.5$ and focal depths greater than 100 km along the Kurile trench were examined in

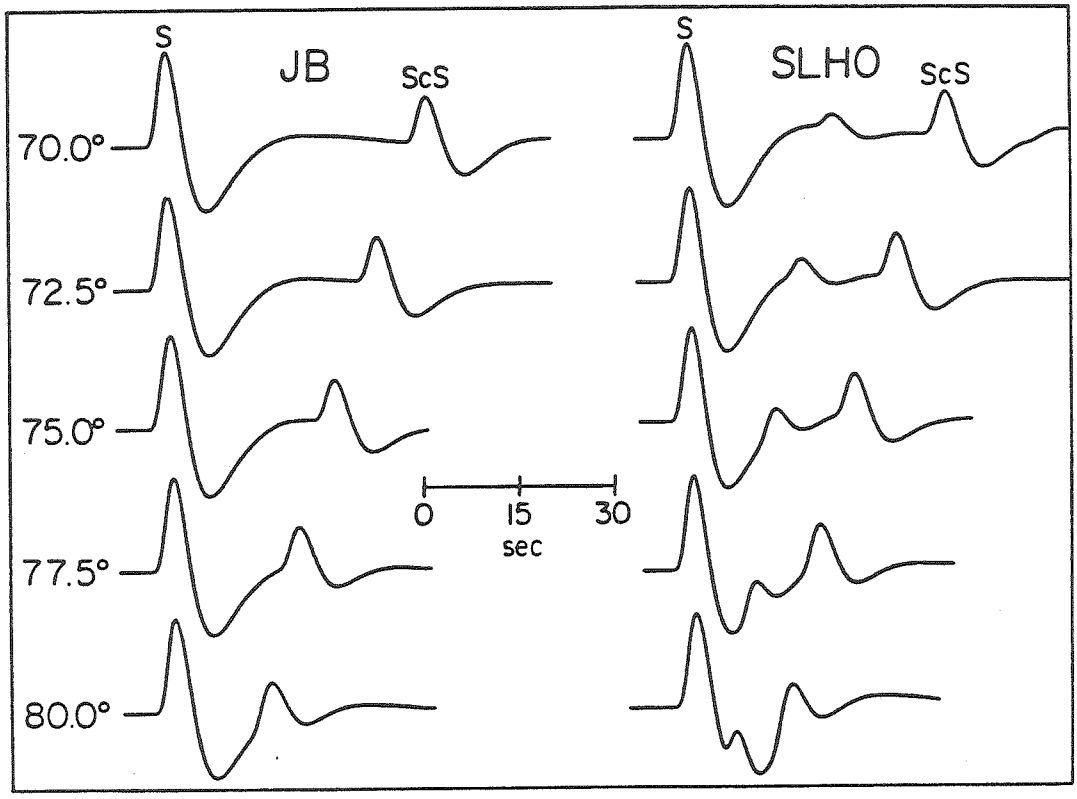

Figure I.1.3. Synthetic long period tangential component S waves for a 580 km deep source. The traces are aligned on the direct S arrival and the amplitudes are normalized. The synthetics on the left were generated using the JB model, which has smooth velocity gradients in the lower mantle and only produces the S and ScS phases. Those on the right were generated for model SLHO in Figure I.1.2, which produces the additional triplication arrival between S and ScS. Note that this phase must be very strong at 80° to produce the clear distortion of the S wave downswing.

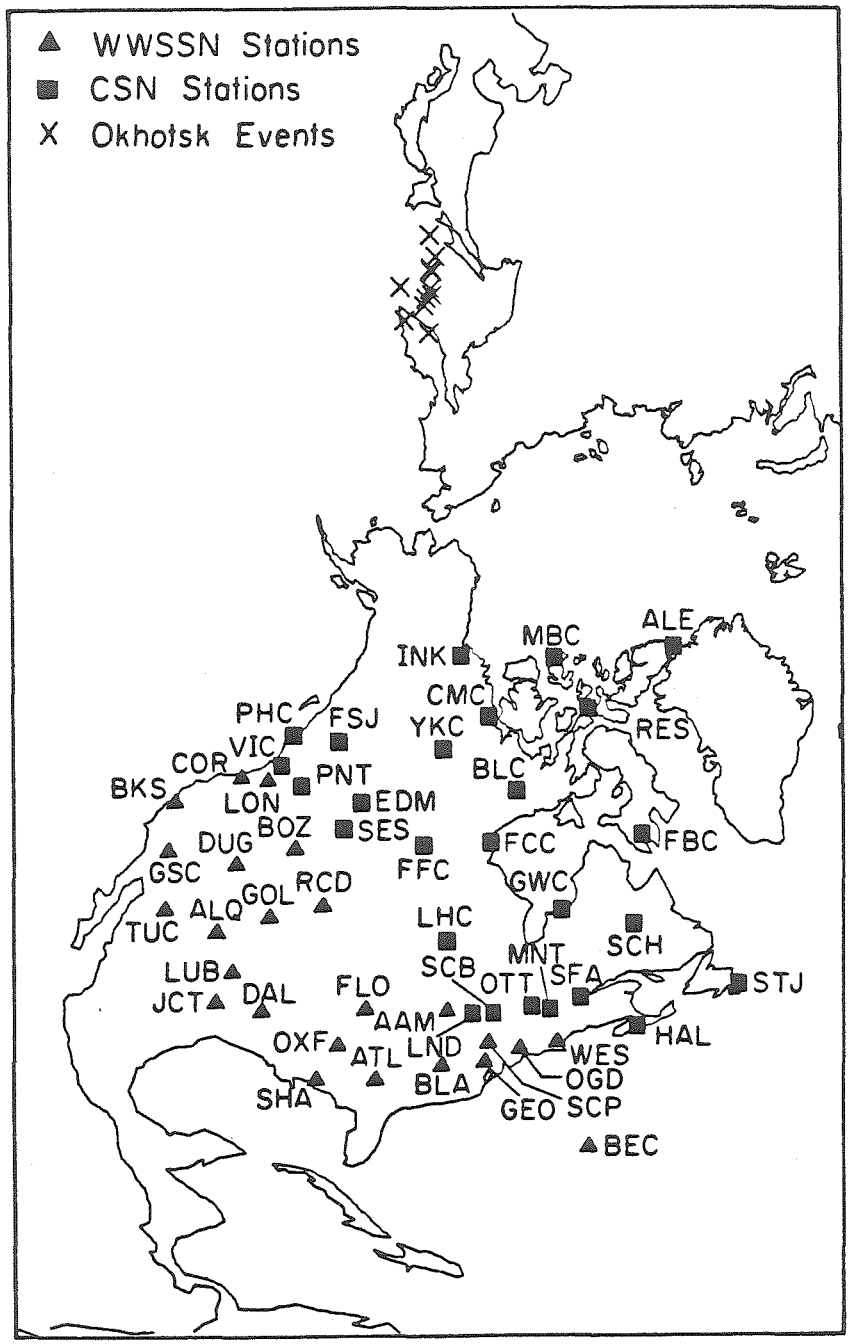

Figure I.1.4. Azimuthal equidistance projection showing the location of Sea of Okhotsk epicenters and North American stations used in this study. Station SHA ranges from 78° to 88° from the events.

Table I.1.1 Source Parameters for Events Used in This Study.

Region	Date	Origin Time	Latitude	Longitude	Depth, km	Reference	Number
Sea of Okhotsk	18 Mar. 1964	04:37:25.7 ± 0.08	52.56° ± 0.022°N	153.67° ± 0.030°E	424 ± 4.2	ISC	1
	12 Oct. 1967	12:53:45.9 ± 0.21	52.15° ± 0.018°N	152.57° ± 0.025°E	466 ± 2.7	ISC	2
	1 Dec. 1967	13:57:02.4	49.5°N	154.4°E	136	NOAA	3
	5 Sep. 1970	07:52:32.4	52.32°N	151.46°E	583	Strelitz (1975)	4
	29 Jan. 1971	21:58:06.7	51.72° ± 0.032°N	151.04° ± 0.024°E	540 ± 5.7	Veith (1974)	5
	27 May 1972	04:06:49.6 ± 0.25	54.97° ± 0.013°N	156.33° ± 0.020°E	397 ± 2.8	ISC	6
	21 Aug. 1972	06:23:48.6 ± 0.16	49.47° ± 0.012°N	147.08° ± 0.019°E	573 ± 2.2	ISC	7
	28 Jul. 1973	20:06:35.4 ± 0.15	50.45° ± 0.013°N	148.92° ± 0.022°E	585 ± 2.1	ISC	8
	21 Sep. 1974	15:54:59.1 ± 0.37	52.19° ± 0.016°N	157.44° ± 0.023°E	119 ± 3.5	ISC	9
	10 Jul. 1976	11:37:14.0 ± 0.14	47.31° ± 0.011°N	145.75° ± 0.018°E	402 ± 1.7	ISC	10
Sea of Japan	31 Mar. 1969	19:25:27.2	33.31°N	134.50°W	417	NOAA	11
	10 Sep. 1973	07:43:30.5	42.45°N	130.91°W	532	NOAA	12
Argentina	9 Dec. 1964	13:35:42.4	27.5°S	63.2°W	586	NOAA	13
	5 Mar. 1965	14:32:19.2	27.0°S	63.3°W	573	NOAA	14
	20 Dec. 1966	12:26:54.6	26.1°S	63.2°W	586	NOAA	15
	17 Jan. 1967	01:07:54.3	27.4°S	63.3°W	588	NOAA	16
	9 Sep. 1967	10:06:44.1	27.7°S	63.1°W	578	NOAA	17
	25 Jul. 1969	06:06:42.4	25.6°S	63.3°W	579	NOAA	18
	3 Jan. 1973	02:58:16.7	27.7°S	63.3°W	563	NOAA	19

collecting these data. The selection criteria imposed were: stable SH radiation patterns to North America, simple impulsive waveforms indicative of minimal source complexity, and adequate station coverage to provide dense profiles in the range of 45^{o} to 90^{o}. All short period and long period horizontal components which could be recovered were digitized over the time interval from direct S to ScS and rotated into tangential and radial components. This yielded data profiles similar to those in Figure I.1.1, for both short and long periods. While we have found that the direct evidence for a lower mantle triplication is apparent in the data only at distances greater than 68^{o}, as suggested in Figure I.1.3, inspection of the S and ScS signals at closer distances has provided a means by which to better assess the source complexity of each event.

As shown in Figure I.1.4, the North American stations span about 50^{o} in azimuth from the Okhotsk source region, along the strike of the subducting slab. Since most of the source mechanisms have a P wave nodal plane with a strike similar to that of the slab, the SH radiation is very stable to North America for both S and ScS. This is indicated in Figure I.1.5, which shows the nodal radiation orientations for P, SV, and SH signals for several of the events used. The hatchured region in the SH mechanism for the first event indicates the portion of the focal sphere covered by S and ScS rays to North American stations.

P wave first motion mechanisms for each event were taken from the literature or newly determined and the observed long period SV/SH amplitude ratios were used to redetermine each mechanism. This

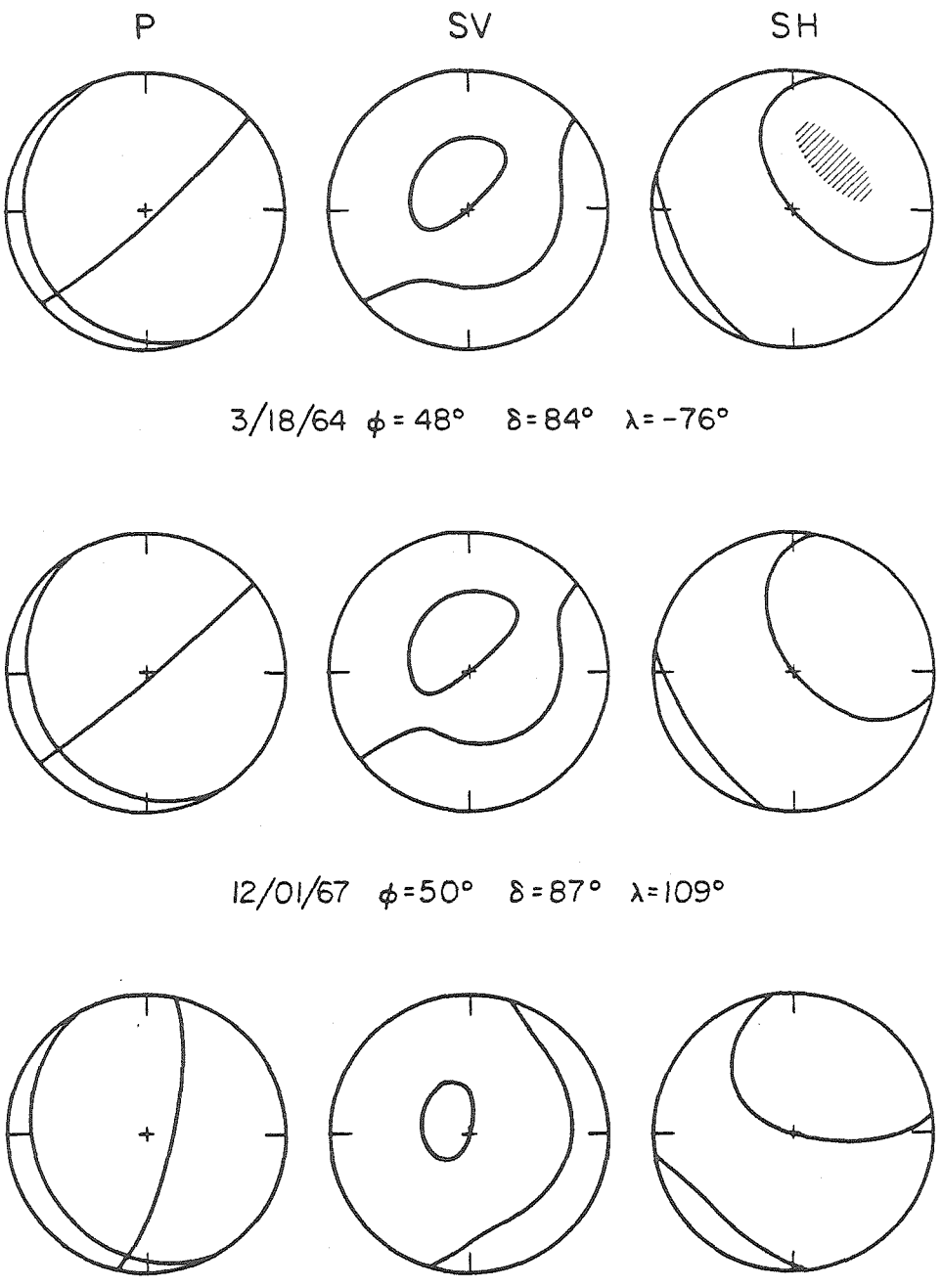

Figure I.1.5. Radiation patterns for three of the Sea of Okhotsk events. The nodal lines are plotted in the lower hemisphere of equal area projections. The hatchured area indicates the portion of the focal sphere covered by North American S and ScS observations. For the top two events both P and SV are nodal in this region, whereas for the bottom event SV and SH are comparably stable.

Table I.1.2 Fault Plane Orientations.

Date	Strike (°)	Dip (°)	Rake (°)
9 Dec. 1964	171	78	-90
5 Mar. 1965	12	26	-68
20 Dec. 1966	30	43	-42
17 Jan. 1967	28	30	-44
9 Sep. 1967	3	19	-78
3 Jan. 1973	357	28	-83
18 Mar. 1964	48	84	-76
12 Oct. 1967	30	75	-52
1 Dec. 1967	50	87	109
5 Sep. 1970	12	74	-77
29 Jan. 1971	40	77	-119
27 May 1972	25	82	-93
21 Aug. 1972	18	19	44
28 Jul. 1973	51	76	-107
21 Sep. 1974	205	79	80
10 Jul. 1976	40	81	-87

allowed us to refine the mechanisms and to select between conflicting mechanisms given in the literature for each event. The final mechanisms adopted are listed in Table I.1.2. Six of the events have mechanisms very similar to that of March 18, 1964, shown in Figure I.1.5. Both P and SV are nearly nodal in North America for these events. Two of the intermediate depth events have mechanisms similar to that of December 1, 1967, which has the same orientation as the others, but an opposite sense of motion. For two events, that of September 5, 1970 and January 1, 1971, the mechanisms are slightly rotated, which yields stable SH as well as stable SV radiation to North America. This is a fortunate occurrence, enabling us to inspect the SV data as well. The nodal character of the P and SV radiation for most of the events helps to minimize the complications due to late P arrivals and SKS. The long period SH signals generally rotate very well and appear to be free of anomalous effects due to mismatched horizontal components. The short period signals tend to be more complicated and often do not rotate as cleanly as the corresponding long periods. Thus, we emphasize the long period data in this presentation.

Figure I.1.6 shows an enlargement of the data from Figure I.1.1. The arrival between S and ScS is particularly clear from 78^{o} to 80^{o}, where the direct S downswing shows an additional arrival, Scd, not apparent in the direct S pulse at closer distances. This interference shifts systematically with distance. On the right is a profile of synthetics computed with the Cagniard de Hoop method for model SLHO (Figure I.1.2). No vertical radiation pattern is included in the

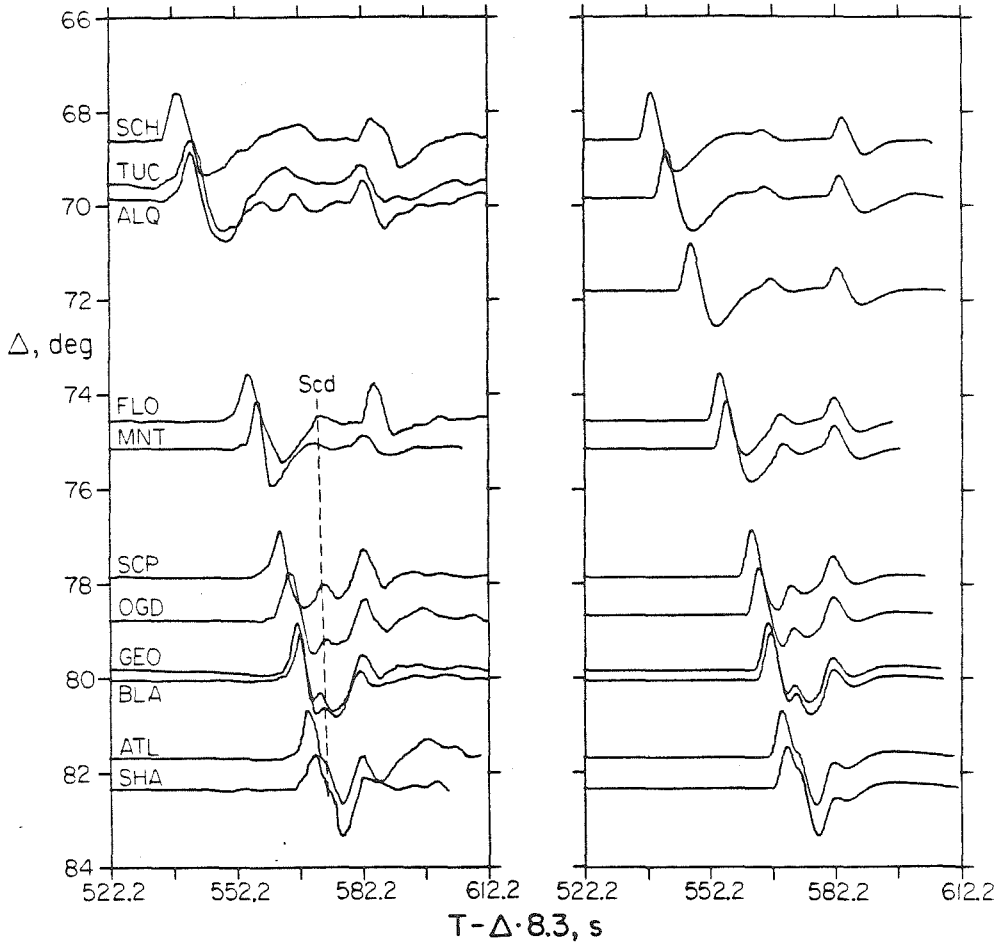

Figure I.1.6. Observed (left) and synthetic (right) profiles of long period SH seismograms for the event of September 5, 1970 (d = 583 km). The JB station residuals have been removed from the data and the amplitudes are normalized. The synthetics are for model SLHO.

synthetics, but this is of little consequence because the SH radiation is very stable between S and ScS. In constructing these synthetics we have not attempted to include individual station receiver structure, since these are not well known. Fortunately, many of the important observations are recorded at East Coast stations which have particularly simple SH receiver structures (Chapter III), so this does not appear to be a major problem. The simple, impulsive waveforms of this event and subsequent events discussed in this study are adequately reproduced by the point sources used in the modeling.

Since the direct S travel times and ScS-S differential times for all the data presented in this section are very consistent with the JB model predictions, as demonstrated in Chapter II, we used the JB model with an increased core radius of 3485 km as a starting model in the waveform modeling. We tried to find the minimum perturbations to this model that would reproduce the travel times and amplitudes of the Scd arrivals. The velocity structure above 2300 km depth was kept fixed so that direct S times, to a distance of around 82^{o}, in model SLHO are the same as for the JB model. Since the final model, SLHO, oscillates around the starting JB model, as seen in Figure I.1.2, the S and ScS-S times are very close to the original JB times and, hence, provide a good fit to the observations. This modeling procedure was greatly simplified by using the generalized ray theory technique which provides a clear interpretation of any model perturbations. The source wavelet used in the synthetics was determined by fitting a point source synthetic to the direct S observations in the range of 60^{o} to 70^{o} for each event.

In Figure I.1.6, the observed interference pattern between the direct S and Scd phases is closely matched in the synthetics. This interference pattern is sensitive to the depth and size of the discontinuity in model SLHO, and quite good resolution of the model parameters can be obtained when a range of source depths is considered.

In order to confidently interpret the Scd arrival it is clearly necessary to inspect and model many events. The possibility of systematic receiver structure effects, multiple source complexity, source region complexity, and contamination due to SKS or other phases must be considered. Since model SLHO constitutes a dramatic departure from previous lower mantle shear velocity models, we present additional data and synthetic comparisons for five other Sea of Okhotsk events at different source depths. The other four events analyzed in detail, as well as less complete data sets for several additional events are very consistent with the data shown here, but are essentially redundant because they are at similar depths to one of the events shown in this section. Profiles for these events are presented in Appendix A.1.

The SH data and synthetics for an intermediate depth event (d = 136 km) are shown in Figure I.1.7. For this source depth sS follows S by about 60 s. This phase is omitted from the synthetics. The Scd arrival is clearly apparent in the downswing of the direct S phase and model SLHO again reproduces the interference accurately. Close inspection of the traces shows that for both the observations and synthetics, ScS and Scd are shifted 5 s later relative to S than for

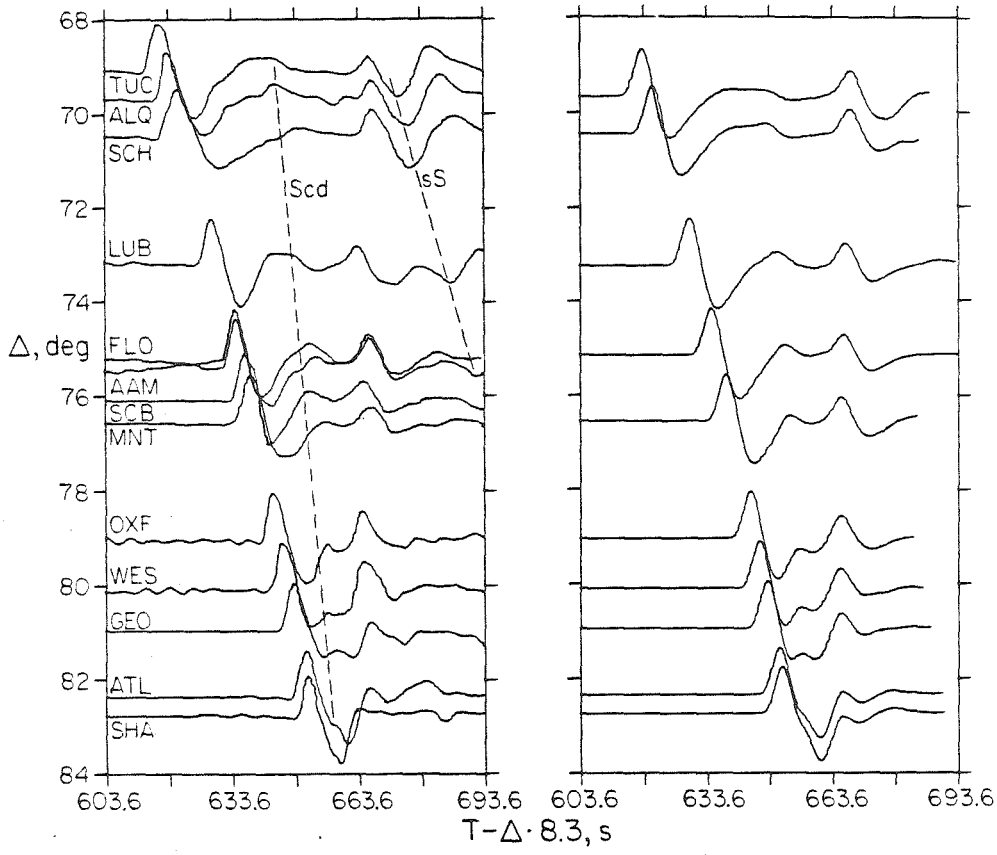

Figure I.1.7. Observed (left) and synthetic (right) profiles of long period seismograms for the event of December 1, 1967. The source depth is shallow enough (d = 136 km) that sS can be observed in the data about 60s after S. The JB station residuals have been removed from the data and the amplitudes are normalized. Note the interference in the downswing of S due to the Scd arrival. The synthetics are for model SLHO.

the deep focus event in Figure I.1.6. Many of the stations used are different, but none of the available data have been omitted except when the traces overlap and the waveforms are very similar. The fact that the ray parameter for Scd is intermediate between that of direct S and ScS, as well as the systematic shift with source depth gives strong support to the interpretation of Scd as a lower mantle phase.

Figure I.1.8 shows data for an event at 402 km depth which is recorded out to slightly greater distances. The observation at BLA is very close to the crossover distance for the triplication in model SLHO. Note the high frequency, large first pulse of this signal compared with those at SCP and DAL. This is clearly apparent in the synthetics at these distances. Scd becomes indistinguishable for distances less than about 72^{o}.

Generally the short period SH sections are too noisy to interpret; the observed signals are often very small and the profiles are sparse. One of the better quality short period sections (d = 424 km) is shown in Figure I.1.9 along with short period synthetics for model SLHO. While there is certainly a large amount of scatter in relative amplitudes and significant SH coda, it is possible to identify S, ScS and Scd in all of the traces. Strong Scd arrivals are apparent at GEO, ATL, and SHA, where model SLHO predicts that Scd is larger than ScS. The source wavelet in the synthetics was taken from the S wave at GSC which is near 65^{o}. The short period synthetics show that Scd should be observable back to at least 72^{o}, but the typical coda amplitudes in the short period traces are comparable in size to the predicted Scd amplitude, so it is difficult to confidently pick

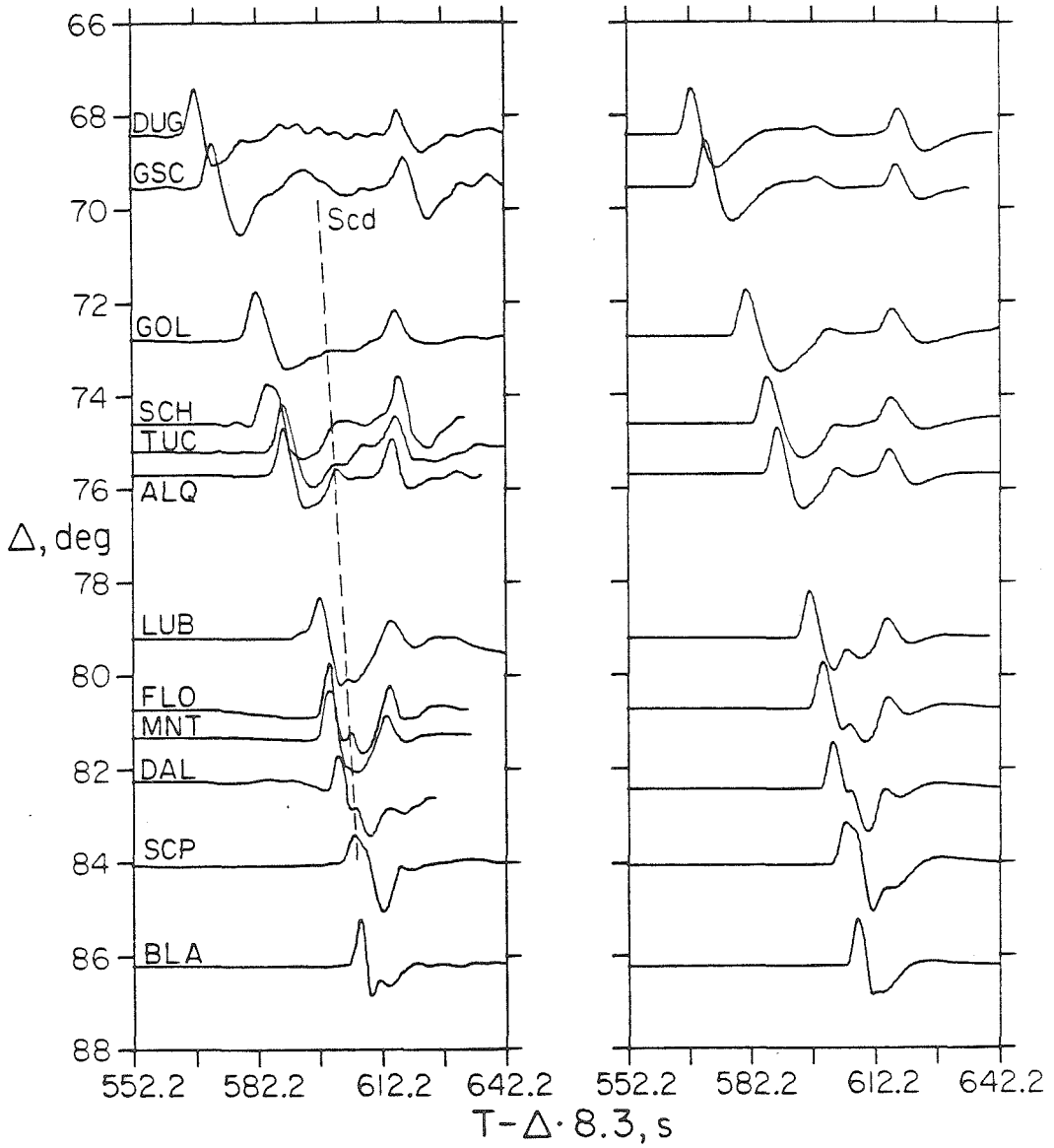

Figure I.1.8. Observed (left) and synthetic (right) profiles of long period SH seismograms for the event of July 10, 1976 (d = 402 km). The JB station residuals have been removed from the data, and the amplitudes are normalized. The synthetics are for model SLHO.

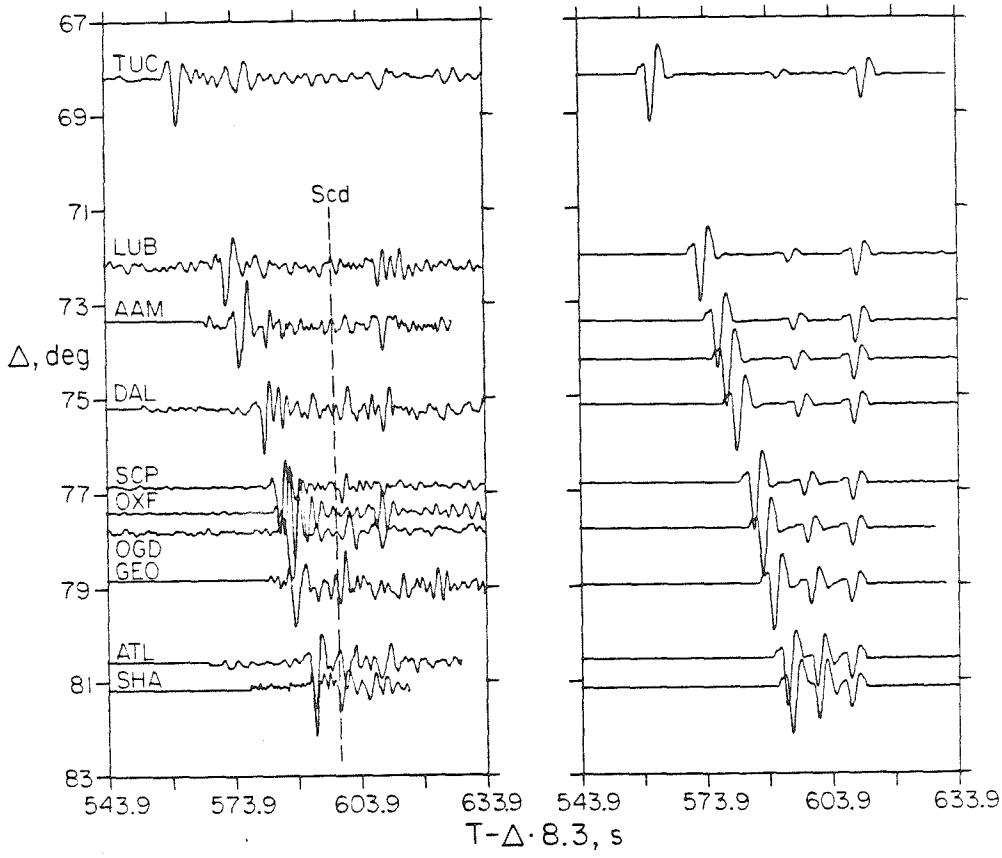

Figure I.1.9. Observed (left) and synthetic (right) profiles of short period SH seismograms for the event of March 18, 1964 (d = 424 km). The JB station residuals have been removed from the data and amplitudes are normalized. The synthetics are for model SLHO.

the arrival. The observations at AAM and LUB do show arrivals of the appropriate size, but the waveforms are rather variable, as is true of the ScS waveforms.

The long period records from the same event are shown in Figure I.1.10. These waveforms are somewhat more straightforward to interpret, particularly the strong interference at ATL, SHA, and BLA. The observation at LUB is well-modeled suggesting that the short period observations are actually Scd on the near end of the triplication. A similar event (d = 466 km) is shown in Figure I.1.11. The Scd arrival is clearly observed. A profile for a deeper event (d = 540 km) is shown in Figure I.1.12. This event has a slightly longer source process than the others, but clearly shows the Scd arrival from 74^{o} to 82^{o}.

A large data set of stable rotated SH signals is clearly needed to identify the Scd arrival. Thus, it is not surprising that such a phase has not been previously reported, since few detailed SH waveform studies have been conducted. The interference of direct S and Scd on the long period records makes it difficult to accurately time the arrival of Scd in order to invert the travel times for structure. We have attempted to avoid this difficulty by measuring the peak-to-peak differential times ScS-S and Scd-S for both data and synthetics in order to incorporate the travel time information in the modeling process. Picking the peak of the Scd arrival on long periods produces fine structure in the differential times, for at distances greater than 75^{o} this interference peak is dependent upon the source frequency content and distance. Fortunately, picking the same peak in the

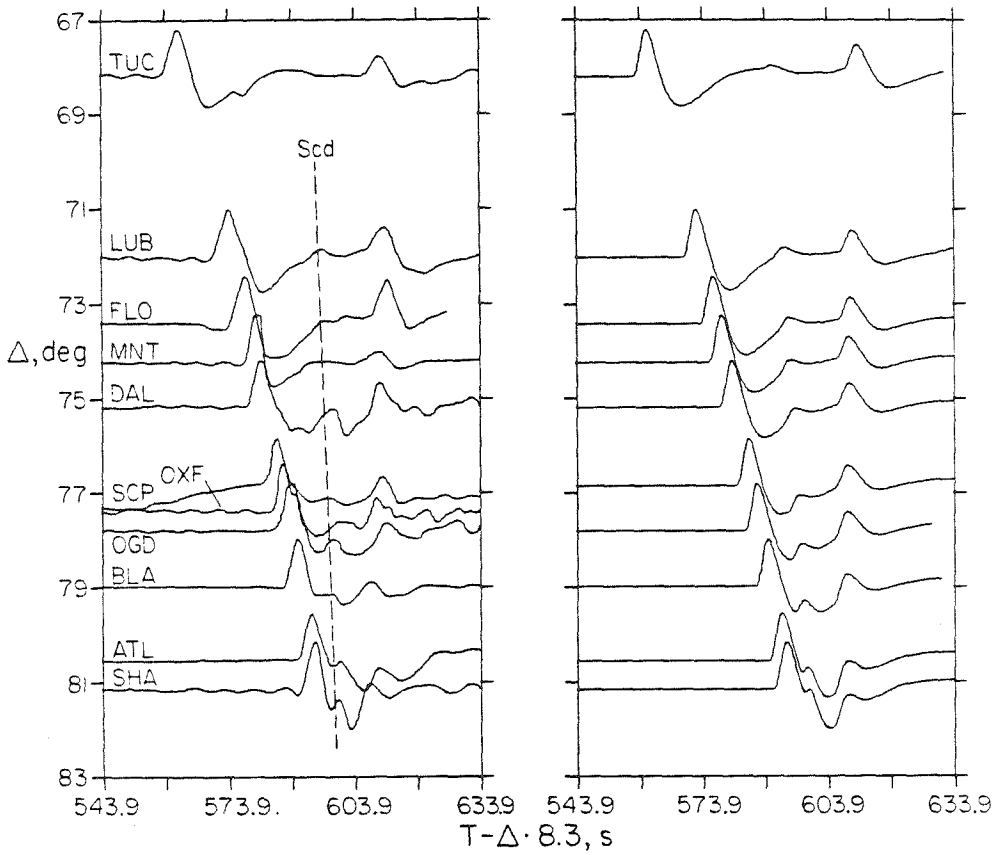

Figure I.1.10. Observed (left) and synthetic (right) profiles of long period SH seismograms for the event of March 18, 1964 (d = 424 km). The JB station residuals have been removed from the data and the amplitudes are normalized. The synthetics are for model SLHO.

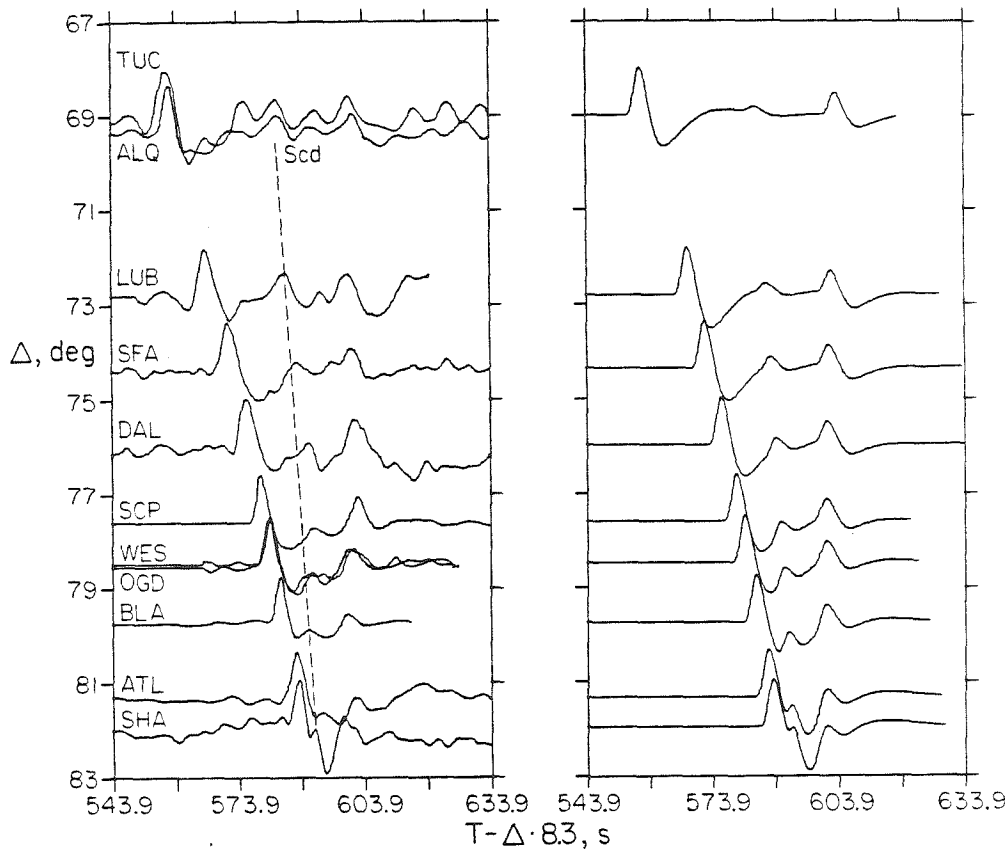

Figure I.1.11. Observed (left) and synthetic (right) profiles of long period SH seismograms for the event of October 12, 1967 (d = 466 km). The JB station residuals have been removed from the data and the amplitudes are normalized. The synthetics are for model SLHO.

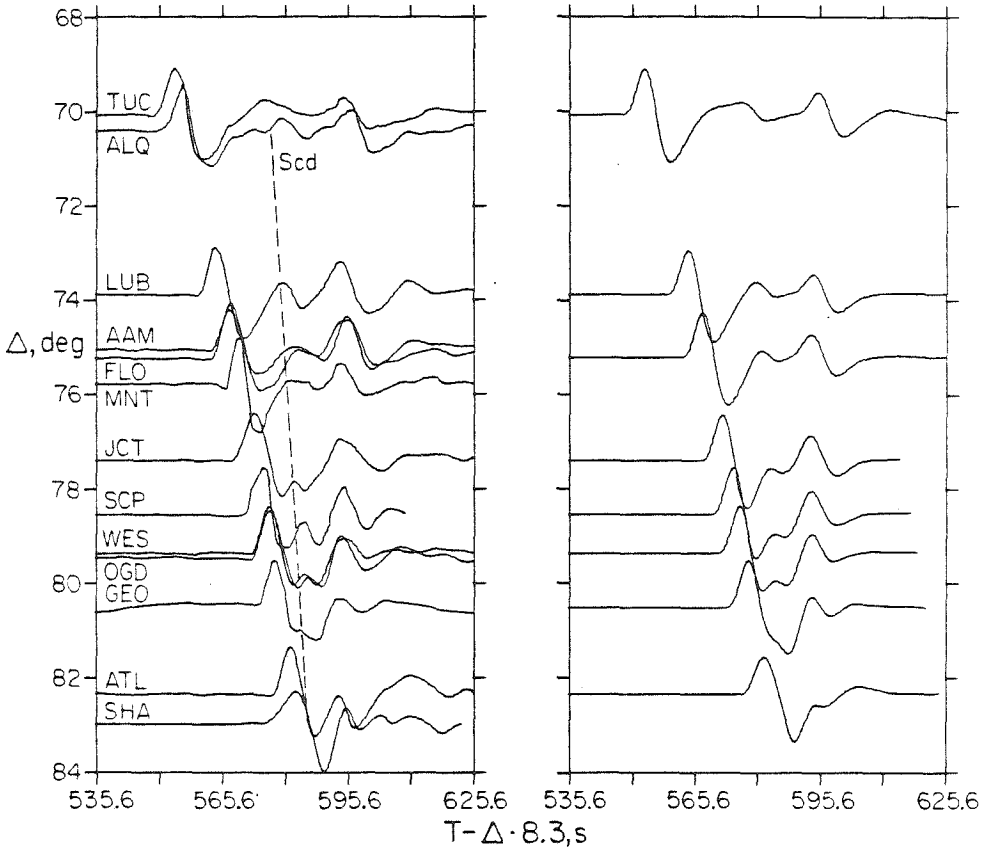

Figure I.1.12. Observed (left) and synthetic (right) profiles of long period SH seismograms for the event of January 29, 1971 (d = 540 km). The JB station residuals have been removed from the data and the amplitudes are normalized. The synthetics are for model SLHO.

synthetics accounts for the interference effects. The differential travel time data for events near six different source depths are compared with model SLHO times in Figure I.1.13. Given the nature of the travel time picks, these plots actually provide an estimate of the waveform agreement between SLHO synthetics and the data. At a given distance there may be several seconds of scatter in both ScS-S and Scd-S, part of which is due to combining several events with different frequency content, and part of which is due to azimuthal variations in the differential times. Model SLHO does an excellent job of fitting both ScS-S and Scd-S at each source depth. The shift in differential times with source depth is clearly apparent in both the data and the model. The systematic behavior of the Scd arrival for numerous sources of different frequency content, depth and distance indicates that it cannot be explained as a source complexity feature, nor as a near source multipathing phenomenon.

A surface focus geometric travel time curve for model SLHO is shown in Figure I.1.14. The crossover distance is near 89^{o} for a surface focus and shifts to near 85^{o} for a 600 km deep event. This shift in the triplication position at a given range provides a means for eliminating receiver structure as a possible explanation of the Scd observations, since any receiver complexities should be only weakly range dependent. Some comparisons of observations at a given station for several events of varying depth and distance are presented in Figure I.1.15, for four stations spanning different distance ranges from the Sea of Okhotsk events. The phases are aligned on the direct S arrival, and any systematic receiver phases should have a nearly

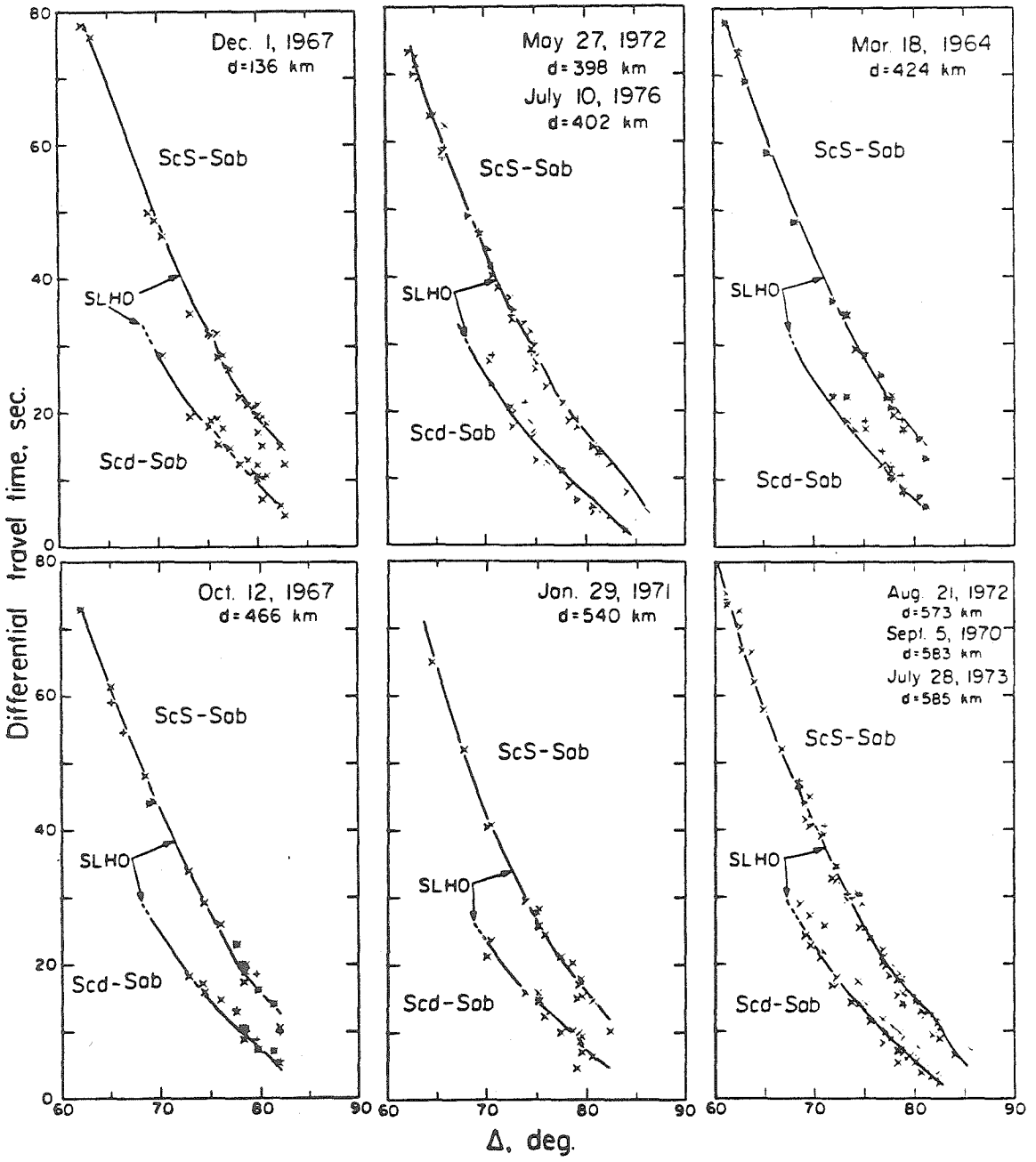

Figure I.1.13. Observed and theoretical differential travel times for Sea of Okhotsk events recorded in North America. The travel times are measured from peak-to-peak for both short period (+) and long period (x) observations. The theoretical times are similarly measured from the synthetic seismograms. The Scd branch has very low amplitude at distances less than 70°.

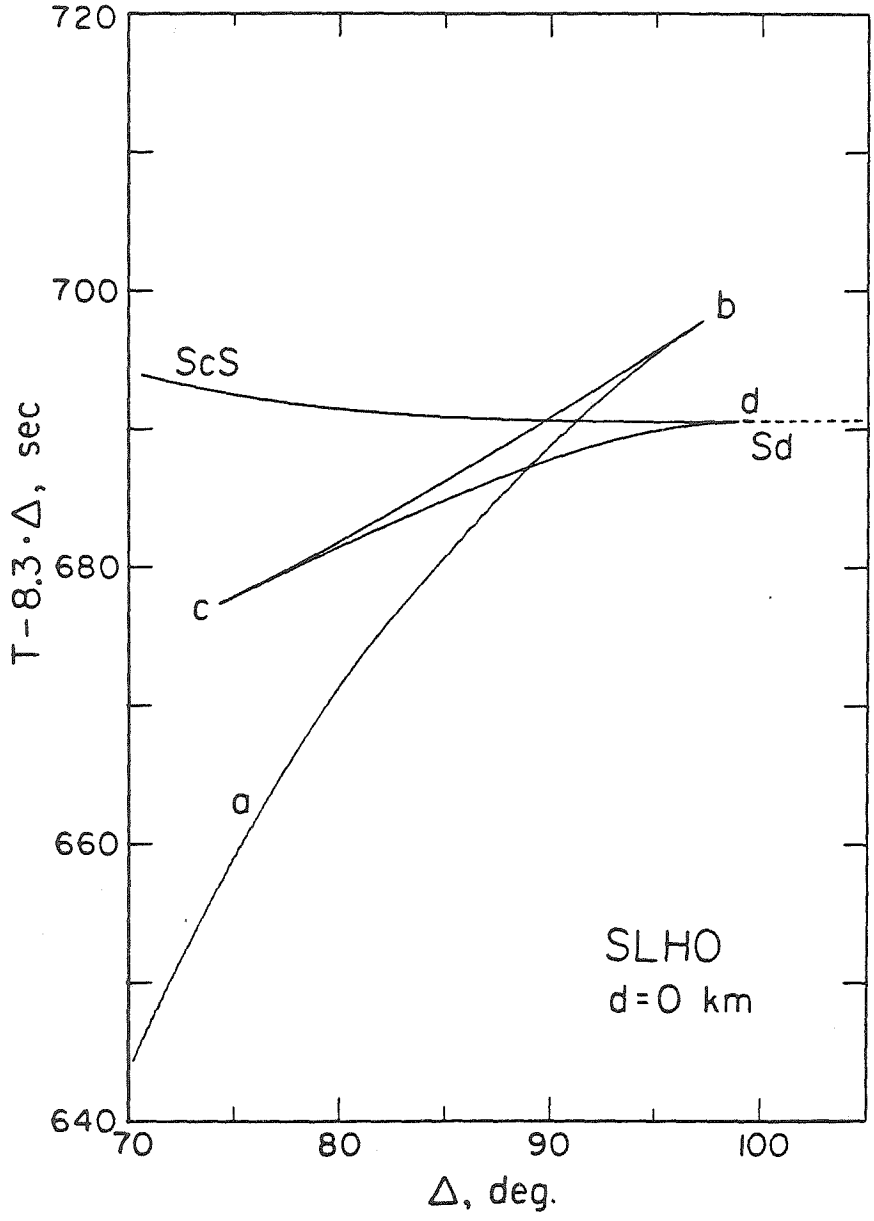

Figure I.1.14. Geometric travel time curve for model SLHO for a surface focus. The crossover distance shifts to 85° for a focal depth of 600 km.

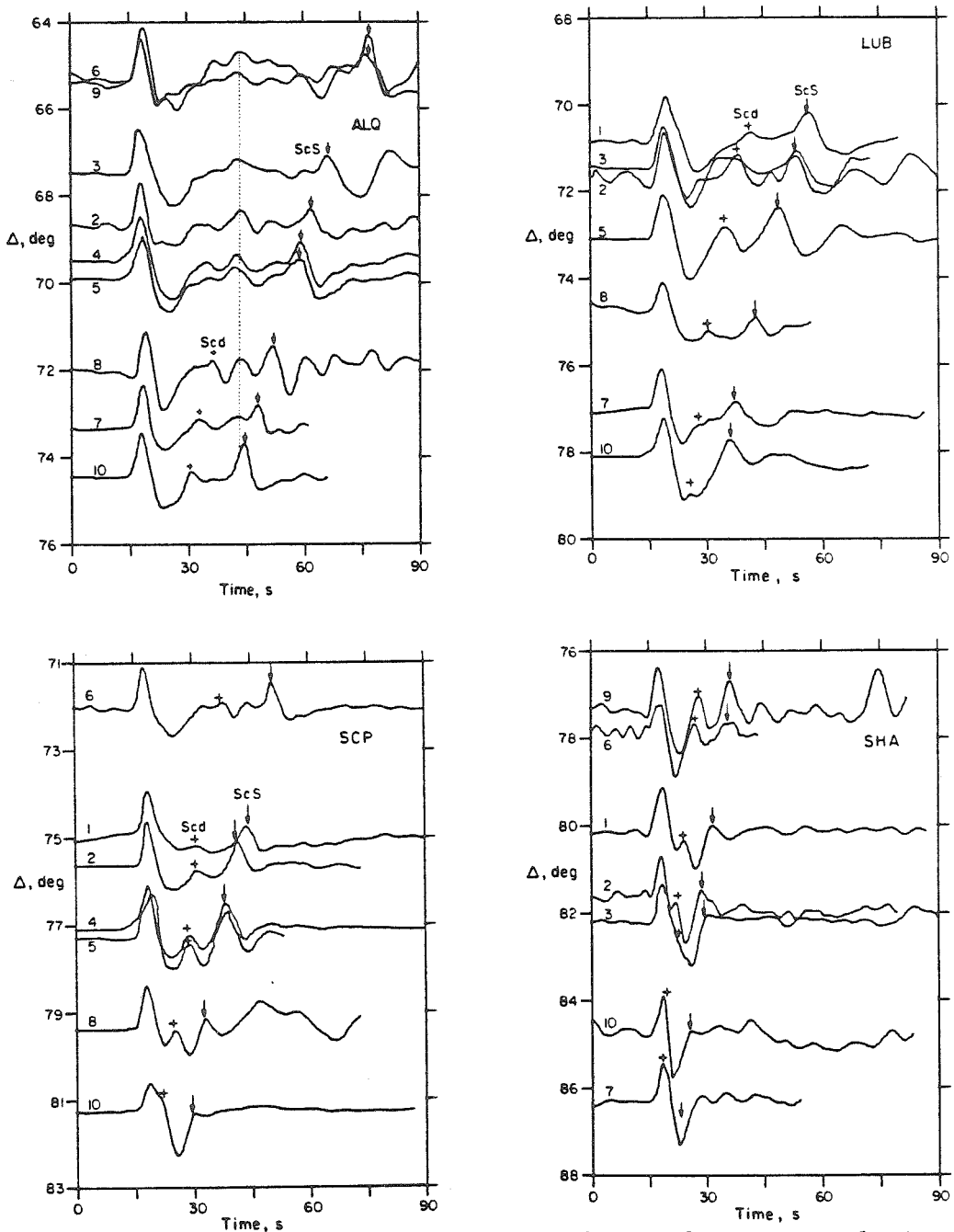

Figure I.1.15. Comparison of SH recordings from several Sea of Okhotsk events at individual stations. The possible Scd arrivals are indicated by a (+) and ScS by (⏚). The numbers indicate the event in Table I.1.1 corresponding to each trace. The traces are aligned on the S wave arrival. The distance at which each observation is plotted is such that the observed ScS-S time is the same as predicted for the JB model at that distance for a focal depth of 600 km. For station ALQ the dotted line indicates an arrival which is observed at the same time relative to S for all events, which is interpreted as a receiver phase. Note that Scd cannot be due to receiver structure and is difficult to observe closer than 71°.

constant time separation from the S arrival. At ALQ such an arrival can be seen 25 seconds behind S. This arrival interferes with ScS near 74° and could be mistakenly identified as Scd at 70°. Generally we have not found evidence for such large amplitude, late receiver phases (possibly SH reflections off of the Moho). LUB, SCP and SHA show instances where Scd and ScS clearly have similar moveout relative to S, which cannot be explained by receiver structure. Such comparisons have been made for all of the stations used in this study, along with comparisons of data from distinct source regions at a given station. The relative simplicity of the East Coast receiver structures has been confirmed by this procedure.

Only one other WWSSN station outside of North America lies along the same azimuth from the Sea of Okhotsk at slightly greater distance. This is BEC (Figure I.1.4), which ranges from 85° to 91° from the events used. For model SLHO this is in the range from crossover distance to just beyond, where Scd is predicted to become a first arrival. This crossover phenomenon is readily apparent at BEC as shown in Figure I.1.16. The synthetics are computed for the appropriate distances and source depths. The simple waveform near 86° is produced by constructive interference of Sab, Scd and ScS, all arriving essentially within the first upswing. For a shallow event such as that of September 21, 1974, the crossover is expected to shift to a somewhat larger distance, hence the observation at 88° is similar to that near 86° for the deeper source. However, a few degrees beyond crossover, near 90°, the arrivals separate by enough to broaden the first upswing. There is also a dramatic change in the ratio of

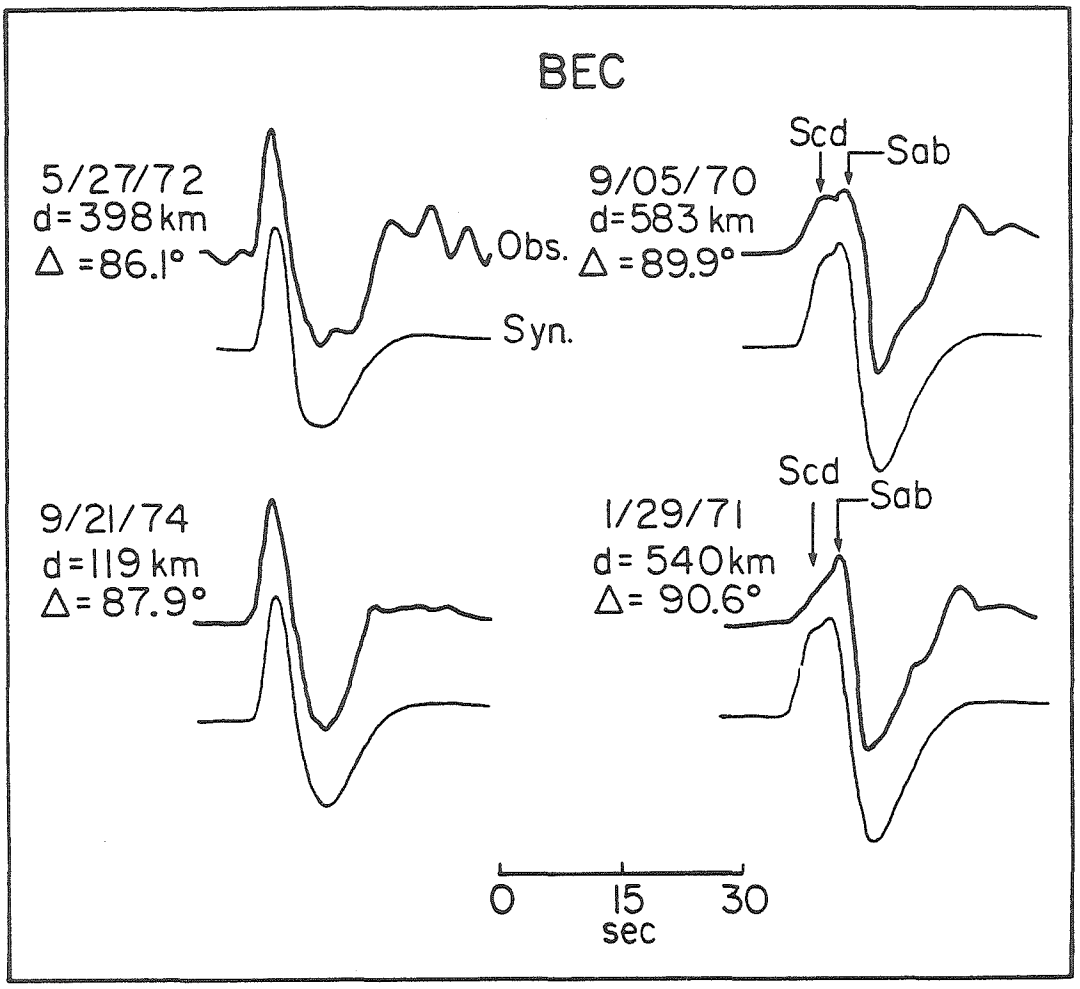

Figure I.1.16. Observations and synthetics of SH records at BEC for several Sea of Okhotsk events. As the distance increases from 86°, which is near crossover distance, to 90°, the interference between Scd and Sab becomes apparent. The synthetics are for model SLHO.

upswing to downswing amplitudes. This behavior is very consistent with the model SLHO, and the waveform distortion is unlike that observed in any of the direct S phases at closer distances.

Since the tests described above fail to explain Scd as a source region or receiver phase, and the data are very consistent with the predictions of a lower mantle discontinuity, it appears that model SLHO is an appropriate velocity structure for the lower mantle between the Sea of Okhotsk and North America. The waveform information places rather tight constraints on the permissible velocity model. The velocity discontinuity is constrained in depth to 278 $\pm$ 25 km above the CMB, and the velocity increase is 2.75 $\pm$ 0.25%. The observations near 90^{o} are particularly sensitive to the velocity contrast across the discontinuity. The direct Sab arrival has the same travel times as the direct S wave for the JB model to distances near 80^{o}, and becomes several seconds later than JB between 80^{o} and 89^{o}, as is observed in recent S wave travel time studies. The velocity gradient above the discontinuity in SLHO is probably somewhat steeper than necessary if the JB velocity structure were tapered off at shallower depth. This does not strongly affect the waveform modeling process. Beyond 100^{o} diffracted Sd becomes the only significant arrival.

In an attempt to constrain the velocity gradient below the discontinuity, we compared the amplitudes of ScS with direct SH in the distance range 40^{o} to 80^{o}. Mitchell and Helmberger (1973) suggested that the ScSH/SH amplitude ratio can be used to constrain the shear velocity gradient just above the core. We measured the peak-to-peak amplitude ratios for the Sea of Okhotsk observations, corrected them

for radiation pattern using the mechanisms in Table I.1.2, and plotted them as a function of distance as shown in Figure I.1.17. There is a fair amount of scatter, but the observations are numerous enough to define the mean amplitude ratio in each 5^{o} increment of distance. The amplitude ratios for SH synthetics for the JB model and SLHO are also shown in Figure I.1.17. Both models are in good agreement with the observations, indicating that smooth positive or near zero velocity gradients within D'' are consistent with the Sea of Okhotsk data. However, it turns out that the SH amplitude ratios are not particularly sensitive to the shear velocity gradient in D'', as discussed in Section I.2.

The sharpness of the velocity discontinuity is an important feature to resolve, but the long period records yield little constraint on this. The short period data are not easy to interpret, but we can an least make some consistency arguments for a rather sharp velocity discontinuity. Figure I.1.18 shows several variations of model SLHO where the velocity jump is replaced by transition zones of varying thickness. Long period synthetics throughout the triplication range are indistinguishable for these models, but short period synthetics on the near end of the triplication (near the C cusp) do show substantial differences. Figure I.1.19 compares a typical short period observation at 73.4^{o} with short period synthetics for SLHO and the transition zone models. Using the ratio of the amplitudes in the time window for Scd and ScS as a guide, it is clear that the data are compatible with a sharp increase. It is also apparent that a transition zone 45 km thick or thicker does not produce a large enough

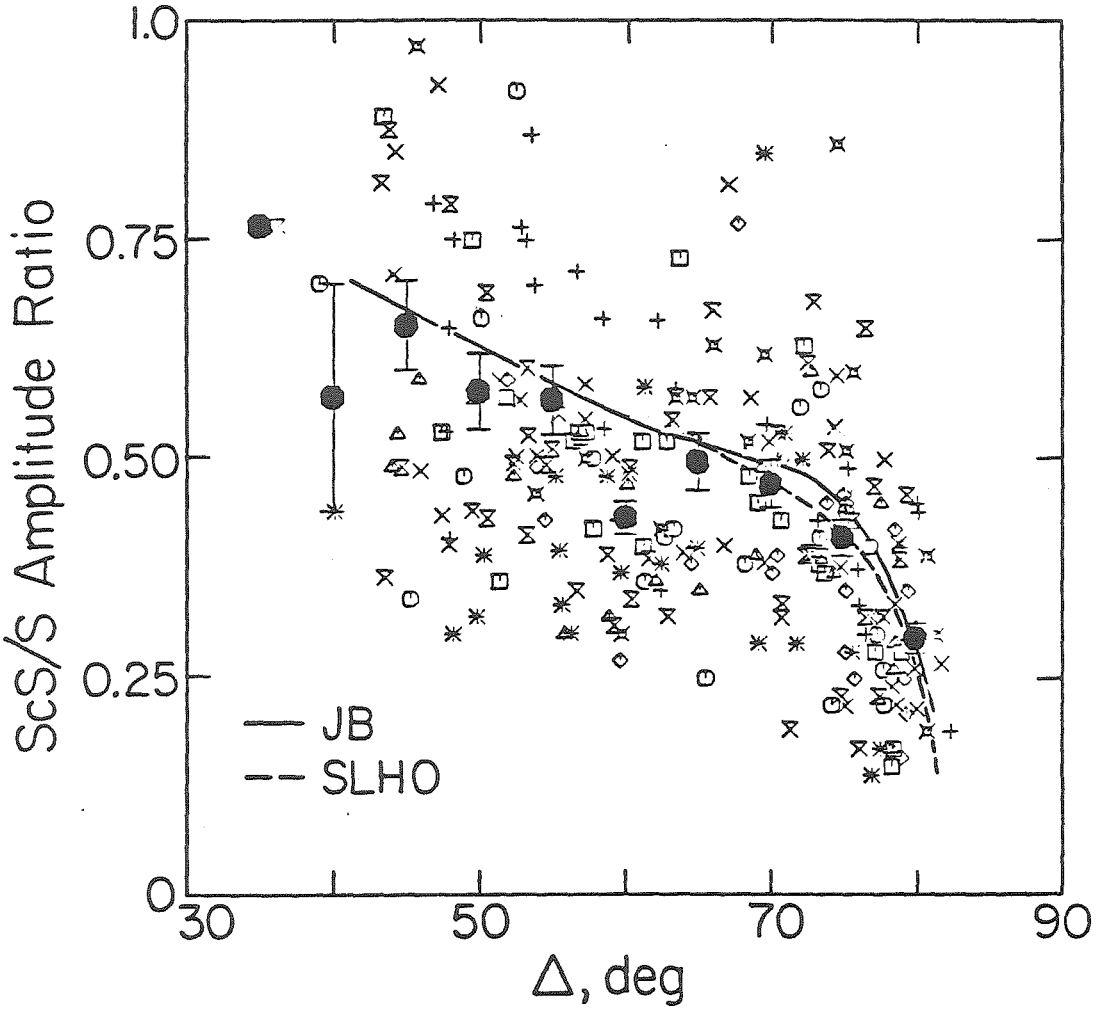

Figure I.1.17. The long period ScS/S amplitude ratio for Sea of Okhotsk observations in North America. Different symbols correspond to different events. The amplitudes are measured peak-to-peak for both data and models. The solid symbols give the mean and standard error of the observations in each 5^{o} increment of distance. At distances greater than 75^{o} the amplitude ratio is contaminated by interference between S and ScS.

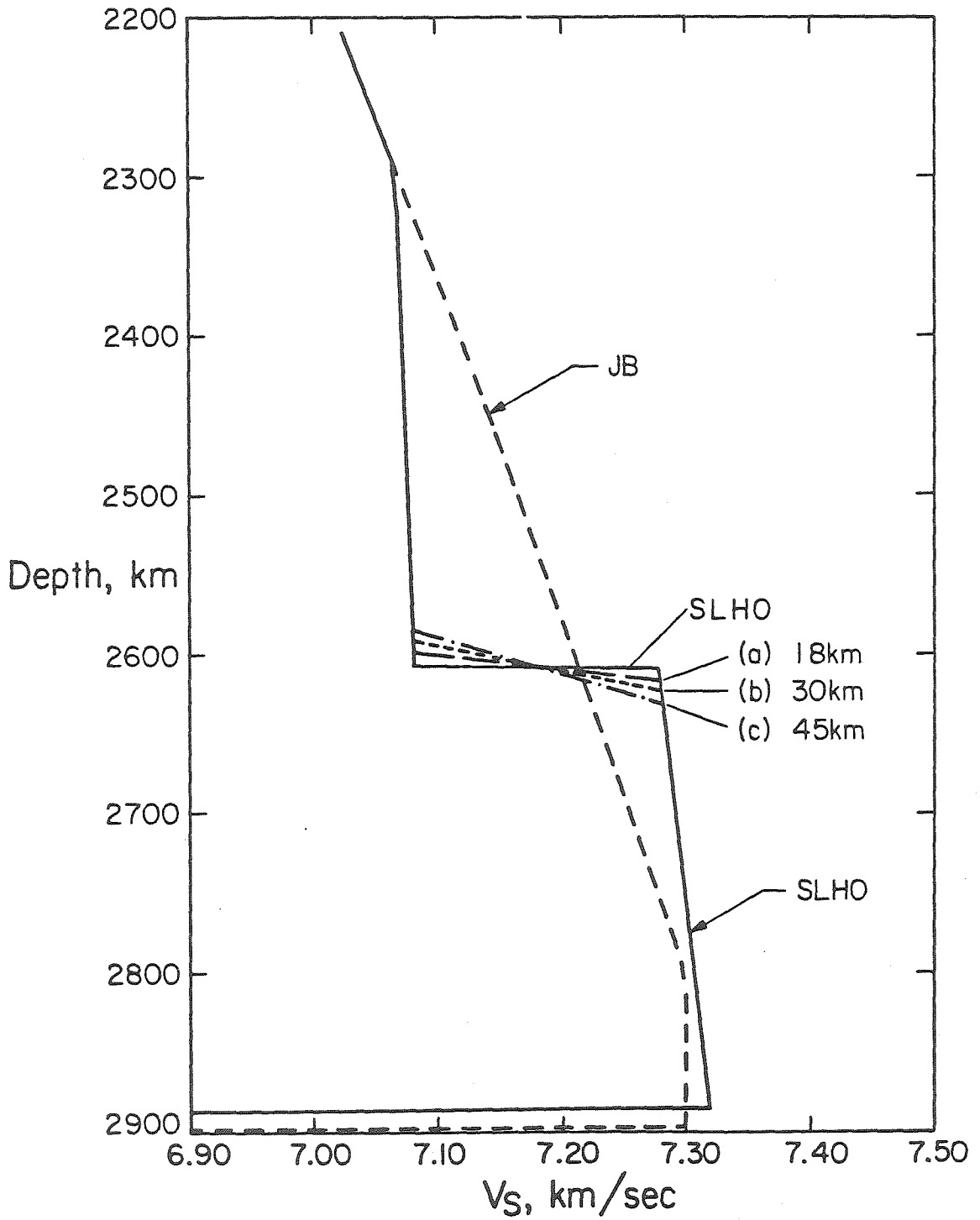

Figure I.1.18. Perturbations of model SLHO where the velocity discontinuity is replaced by transition zones of various thicknesses.

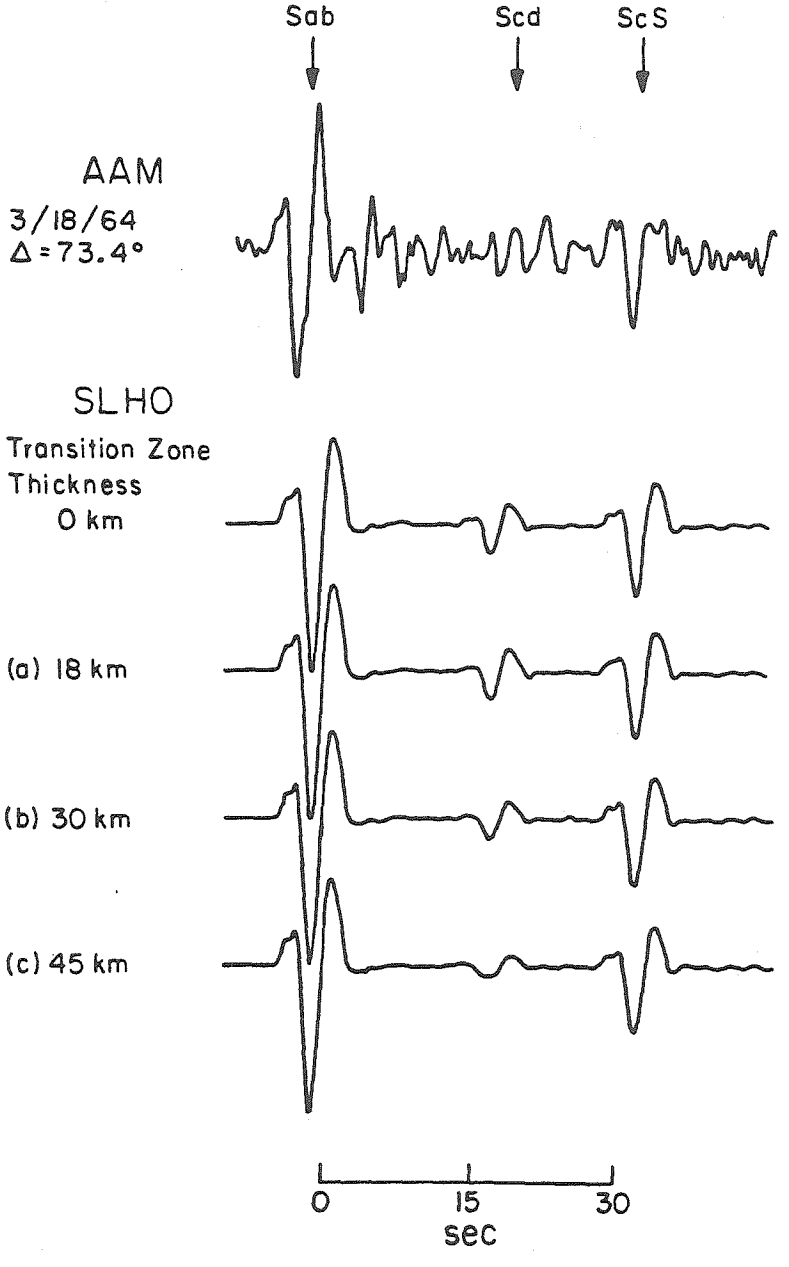

Figure I.1.19. Short period SH synthetics corresponding to the various models in Figure I.1.18. A typical observation on the near end of the triplication is shown at the top. Long period synthetics for the corresponding models are indistinguishable.

short period Scd arrival. Other short period data yield a similar conclusion.

The modeling procedure employed above does rely on rather subjective quality of fit assessment and it would be attractive to employ an inversion procedure that could more quantitatively span the model solution space. One of the major obstacles to applying a waveform inversion analysis to the SH data is that large travel time anomalies exist in the data, indicative of lateral variations in the mantle that are not easily incorporated in any automated modeling procedure. Examples of the azimuthal variations are shown in Figure I.1.20. The signals are recorded at the same distance from each event at stations separated by less than 20^{o} in azimuth. Note that with the traces aligned on the ScS arrival, the Scd arrivals are at the same relative time, but the relative timing of Sab can vary by 4.4 s. Such data indicate that the azimuthal variations affect the direct S waves more strongly. This could be due to either a near source anomaly, such as that proposed for the Sea of Okhotsk deep source region by Jordan (1977) or an anomaly along the Sab path in the mantle several hundred kilometers above the D" region, such as proposed for South American data in Chapter II. These large differential time anomalies clearly affect the nature of the Scd arrival at distances near 80^{o}, where it interferes with Sab, and this is difficult to allow for in any waveform inversion scheme. The stability of the ScS-Scd differential times suggests relative homogeneity of the lowermost 400 km of the mantle in the region sampled by the Okhotsk data.

Model SLHO is consistent with all of the Sea of Okhotsk SH data

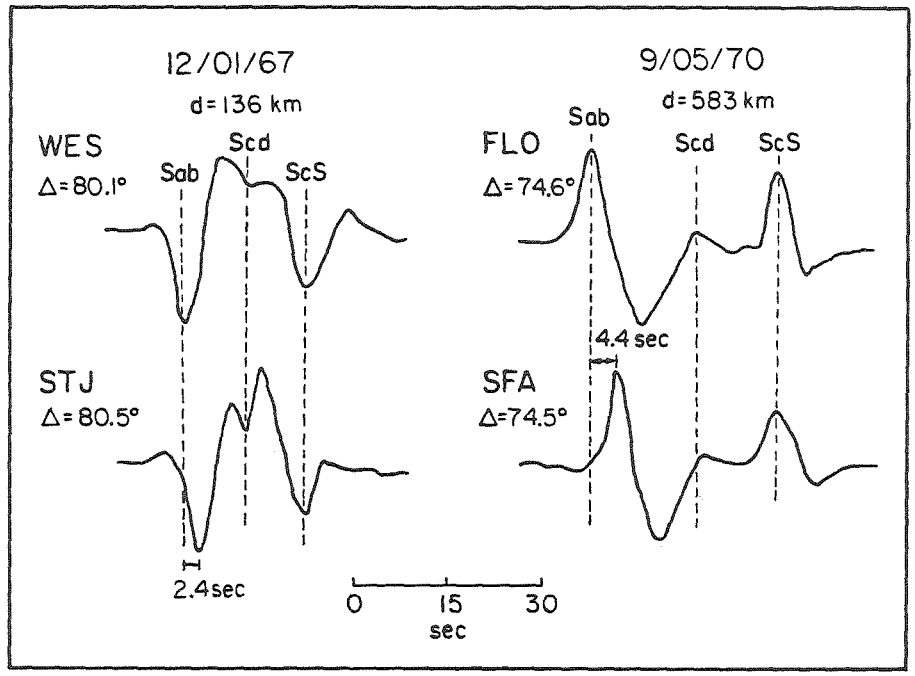

Figure I.1.20. Representative SH signals indicating the azimuthal travel time effects in the data. The ScS-S differential times at a given distance can vary by as much as 6 sec. The ScS-Scd times tend to vary less, though the nature of the Scd arrival at these distances is affected by the timing of Sab, as in the WES - STJ comparison. The azimuth differences are 10^{o} for WES and STJ and 17^{o} for FLO and SFA.

observed in North America, but the question arises as to whether the SV data are compatible with this model. SH waveform modeling alone cannot distinguish both shear velocity and density changes, so it is desirable to examine SV data in order to place any additional constraints on the density behavior across the D" discontinuity. The major problem with SV data is that if large amplitude, stable SV and ScSV pulses are observed, there will also be large SKS phases. This is demonstrated clearly by a profile of SV signals for the event of September 5, 1970 shown in Figure I.1.21. The SKS arrival is the strong upward pulse that sweeps through the SV signal, crossing over it near 81^{o}. Note that ScSV has opposite polarity to direct SV, while one would expect the SVcd arrival for model SLHO to have the same polarity as SVab in this distance range. While there is some hint of the SVcd arrival at FLO, MNT, and SCP, the SKS arrival crosses right through the time window of interest, making it practically impossible to look for the discontinuity in the SV data.

Since the model derived for the Okhotsk data involves a major earth structure feature, we have checked the SH synthetics generated by the Cagniard de Hoop method by comparing them with the reflectivity method as developed by Fuchs and Müller (1971) and Kind and Müller (1975). This was done to ensure that the partial ray sum used in the ray theory modeling does not introduce spurious features in models SLHO. A comparison of synthetic SH profiles for the two methods is shown in Figure I.1.22. The source depth is 580 km and no Q structure is included. A relatively high frequency source wavelet is used to enhance the waveform features. The reflectivity synthetics have a

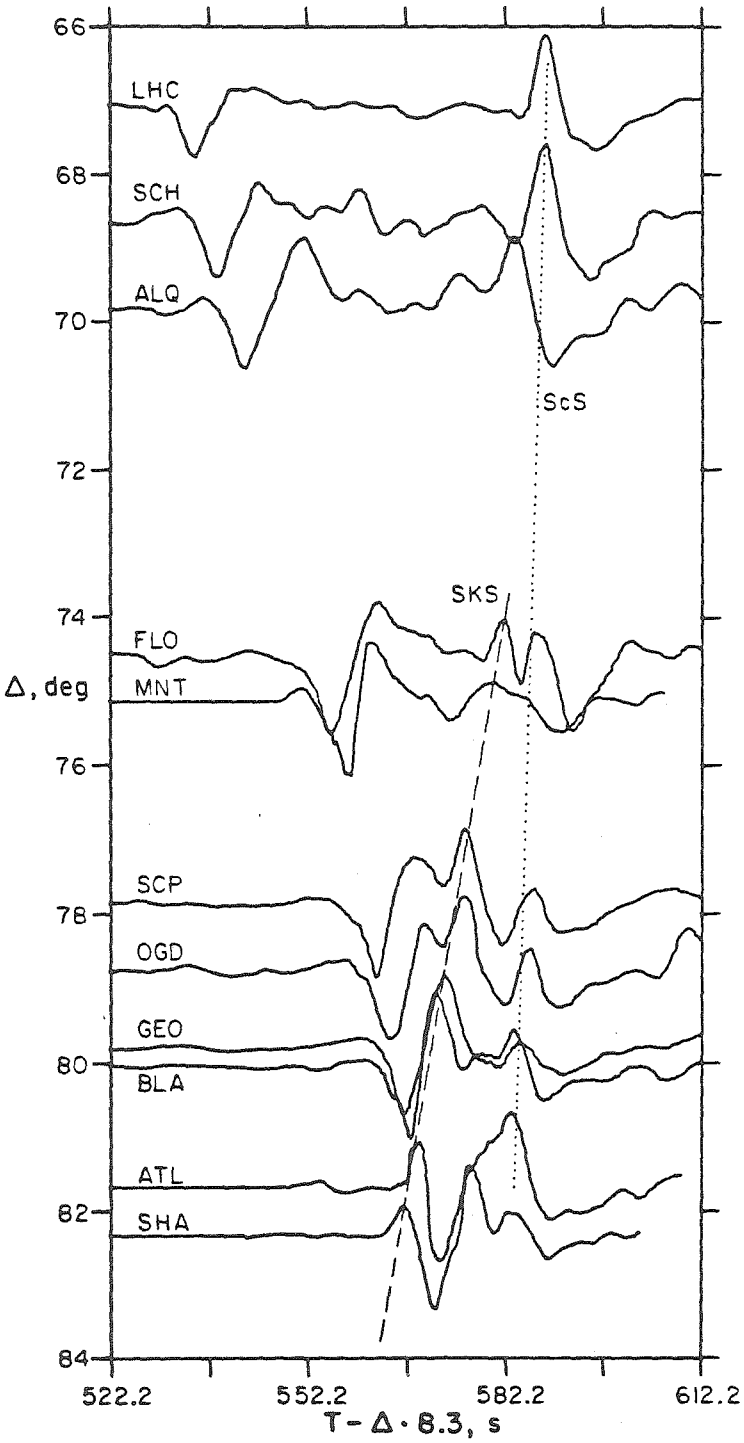

Figure I.1.21. Profile of long period radial component SV signals for the event of September 5, 1970 (d = 583 km). The corresponding SH seismograms are shown in Figure I.1.6. The JB station residuals have been removed from the data and the amplitudes are normalized. Note the reversal in polarity of the first arrival as SKS crosses the direct S arrival.

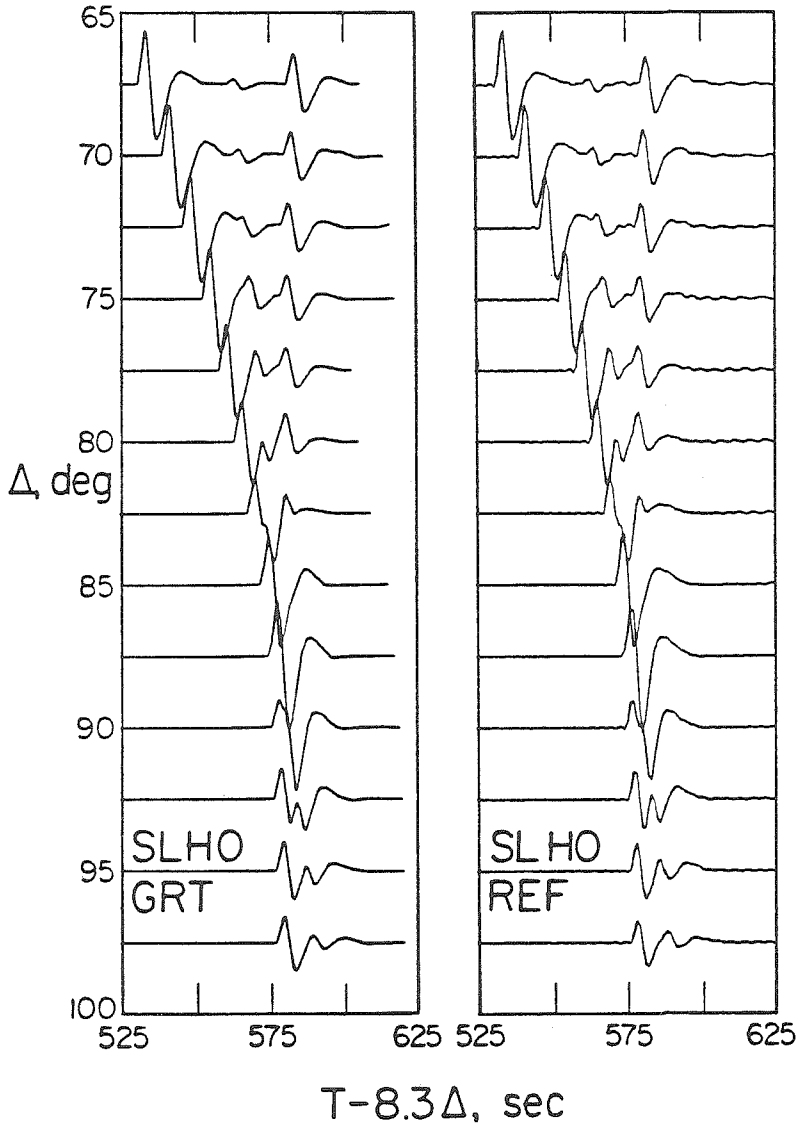

Figure I.1.22. SH synthetics computed with the Cagniard de Hoop generalized ray theory (GRT) technique and the reflectivity (REF) technique for the Sea of Okhotsk model. The agreement between these techniques throughout the entire range of the lower mantle triplication is clearly apparent.

very slight vertical radiation pattern in them. The generalized ray theory (GRT) and reflectivity synthetics for model SLHO are in excellent agreement throughout the triplication, with the synthetics at 92.5° showing the largest deviation, which is minor. From this test it appears that the ray theory waveform modeling is adequate for this application.

Using the reflectivity program, we have computed the effects of the proposed D" velocity structure on diffracted SH. A comparison of diffracted synthetics for the JB model and the Sea of Okhotsk model is shown in Figure I.1.23. The source wavelet has a dominant period of 20 s, which is comparable to long period diffracted SH observations at WWSSN stations. In the range 95° to 100° the Sab branch produces a secondary arrival which diminishes rather quickly. For model SLHO the amplitude decay into the core shadow is similar to that of the JB model. It is unlikely that diffracted S studies which have typically used data beyond 100° could distinguish between the SLHO and JB models, even in the absence of source and receiver noise. It may be possible to examine diffracted S traversing the same portion of D" as sampled by the Sea of Okhotsk data to seek the subtle differences between these velocity models, as well as to further constrain the overall velocity gradient within D".

Sea of Okhotsk Data Recorded in Europe

Having established the presence of the lower mantle S wave triplication in the Sea of Okhotsk data recorded in North America, it becomes of interest to examine other source region-receiver combinations to determine whether the discontinuity is global and what

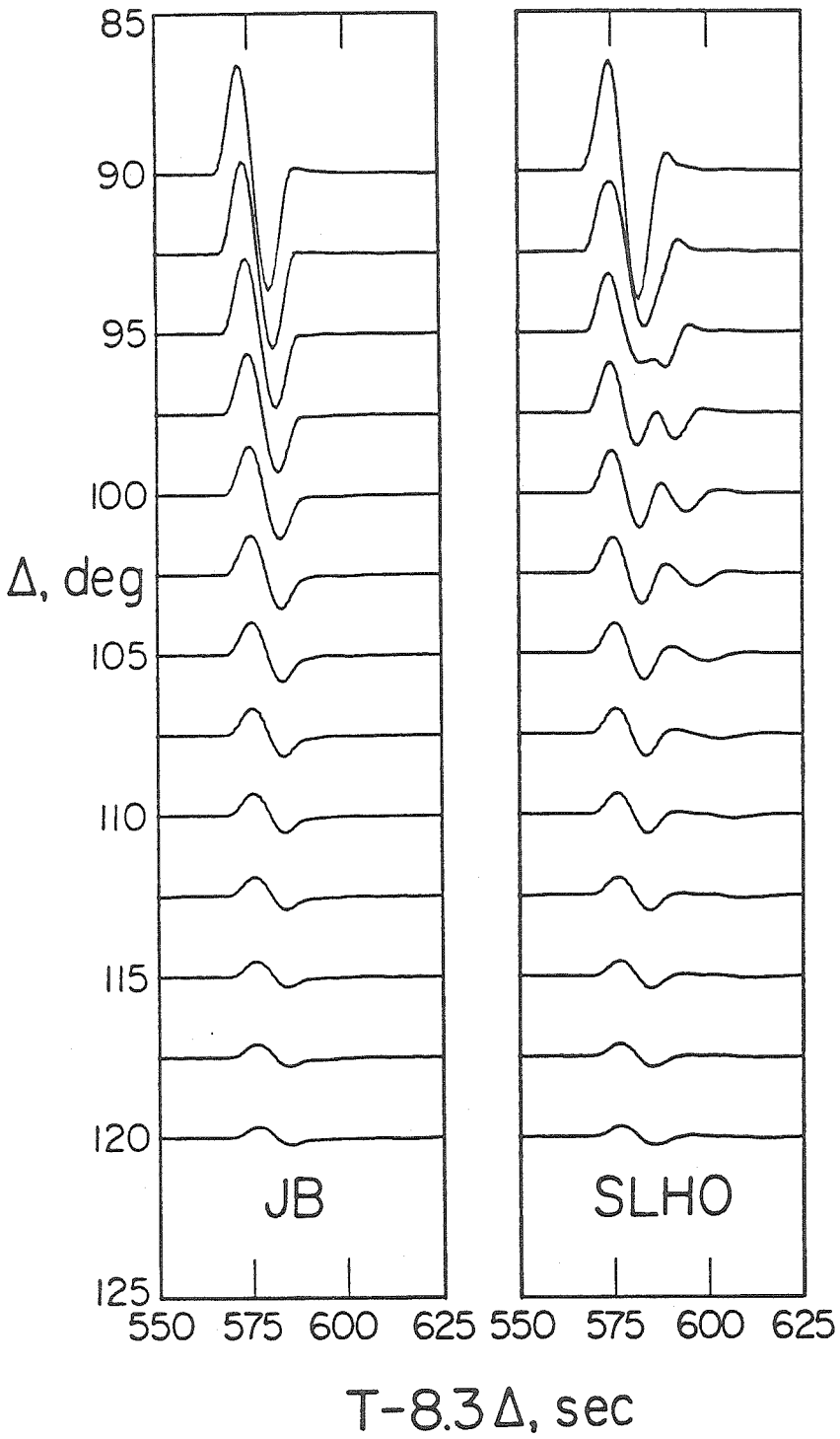

Figure I.1.23. SH synthetics for the JB and Sea of Okhotsk models shown in Figure I.1.2. The reflectivity technique was used to compute the signals. The amplitude scale is the same for both models. The presence of the receding Sab branch causes the distortion in the range 95^{o} to 100^{o} for models SLHO. The diffracted signals, beyond 105^{o}, are very similar for the two models, with little discernible difference in waveform character.

lateral variations may accompany it. The distribution of long period seismographs in North America is denser than anywhere else; however, a relatively dense array of WWSSN stations in Europe recorded the same Sea of Okhotsk events used above as well as other Sea of Japan events. Figure I.1.24 shows the epicenters and station distribution used for the European paths. A profile of SH seismograms across this array is shown in Figure I.1.25, for the event of September 5, 1970. Note the very simple signals and minimal receiver coda between S and ScS. This provides further evidence that this event, which was used extensively above, is not anomalous in its source complexity. Between 74^{o} and 76^{o} the Scd arrival appears to be present once again. The paths to these stations are very distinct from those to North America so this arrival appears to have a common lower mantle origin. Note that stations TOL and MAL near 90^{o} show distortion of the first pulse similar to that seen at BEC, with broadened first pulses and small upswing to downswing amplitude ratios.

Another profile of data is shown in Figure I.1.26, with very similar features. The observations at VAL and TRI show the clearest evidence for the triplication, though, once again, MAL shows a split first pulse. Comparisons of the SH recordings at VAL and TRI for several events are made in Figure I.1.27. In neither case can the apparent Scd arrivals be explained as receiver phases or source complexity. Thus, despite the sparseness of the data it appears that the European data are consistent with the North American results. However, close inspection of the traces shows that the waveforms are slightly shifted relative to those in North America.

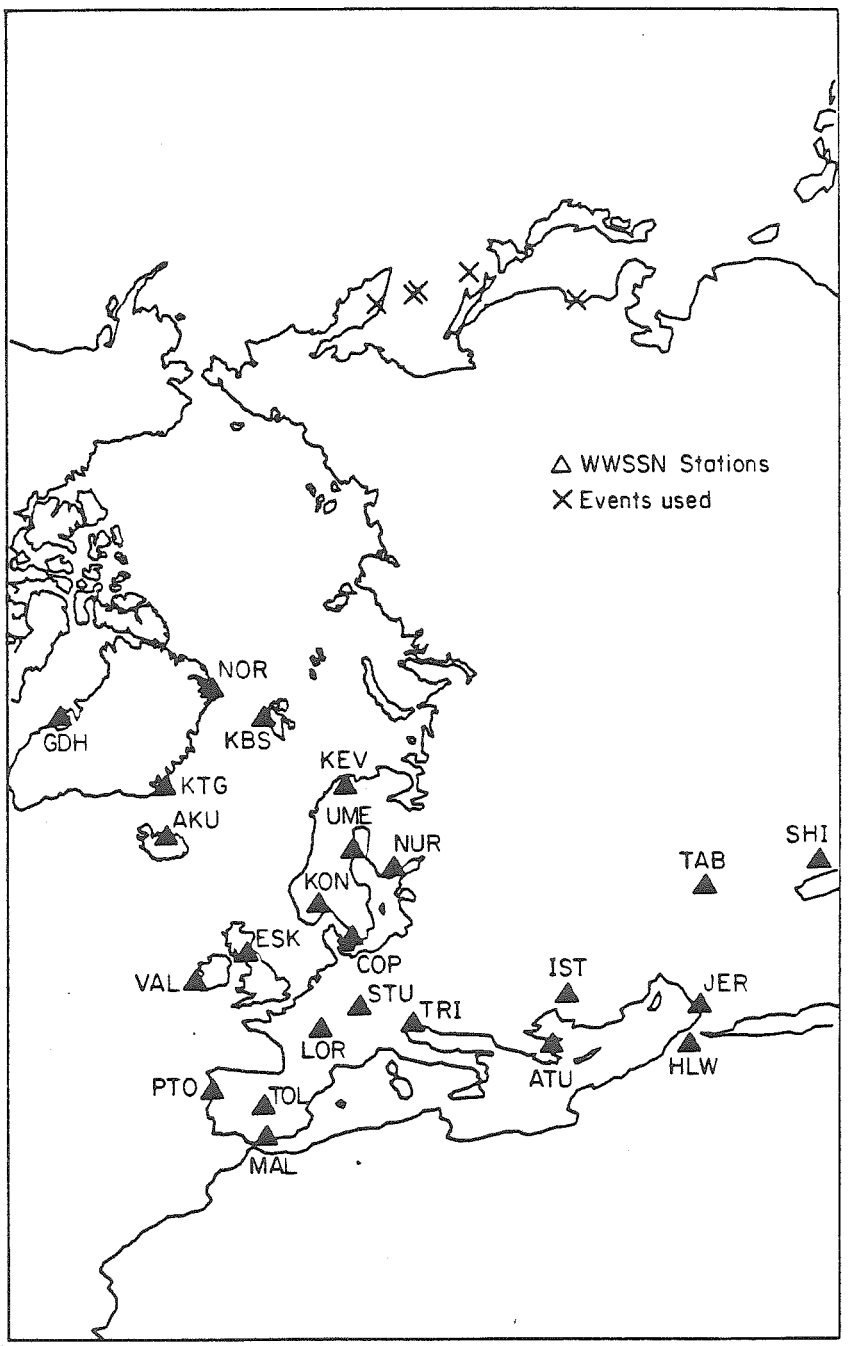

Figure I.1.24. Azimuthal equidistance projection showing the location of Sea of Okhotsk and Sea of Japan epicenters and European WWSSN stations used in this study.

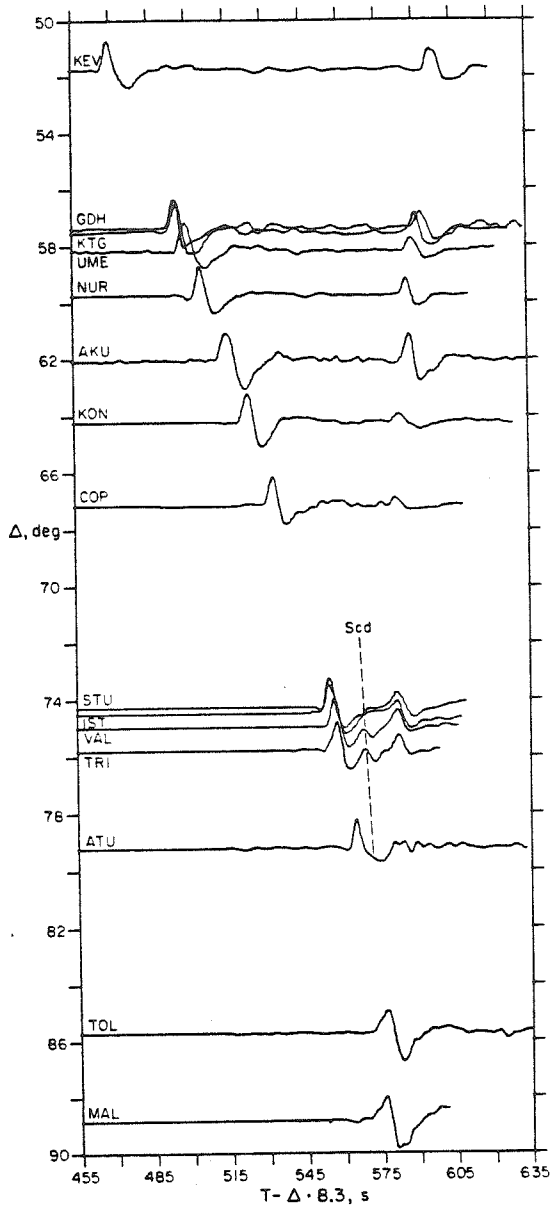

Figure I.1.25. Profile of tangential components of European stations for the September 5, 1970 Sea of Okhotsk event (d = 583 km). Note the simple pulses similar to those in Figures I.1.1 and I.1.6, and the arrival of Scd apparent near 75° and in the distortion of the first upswing at TOL and MAL.

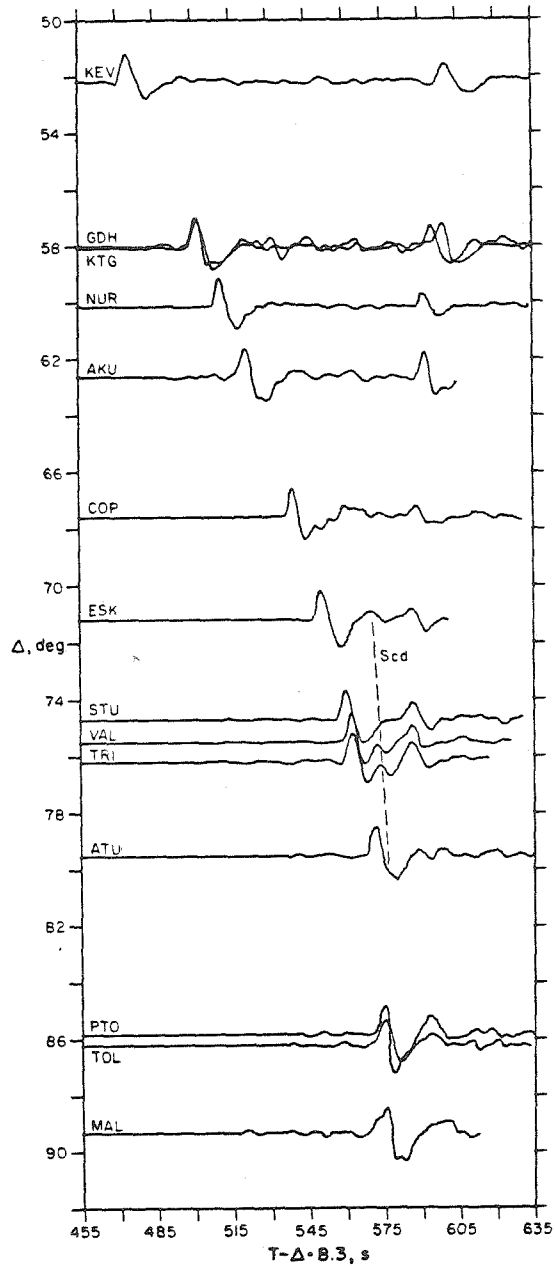

Figure I.1.26. Profile of tangential components at European stations for the Janauary 29, 1971 Sea of Okhotsk event (d = 540 km). Note the arrival of Scd near 75^{o} and the distortion of the first pulse at MAL.

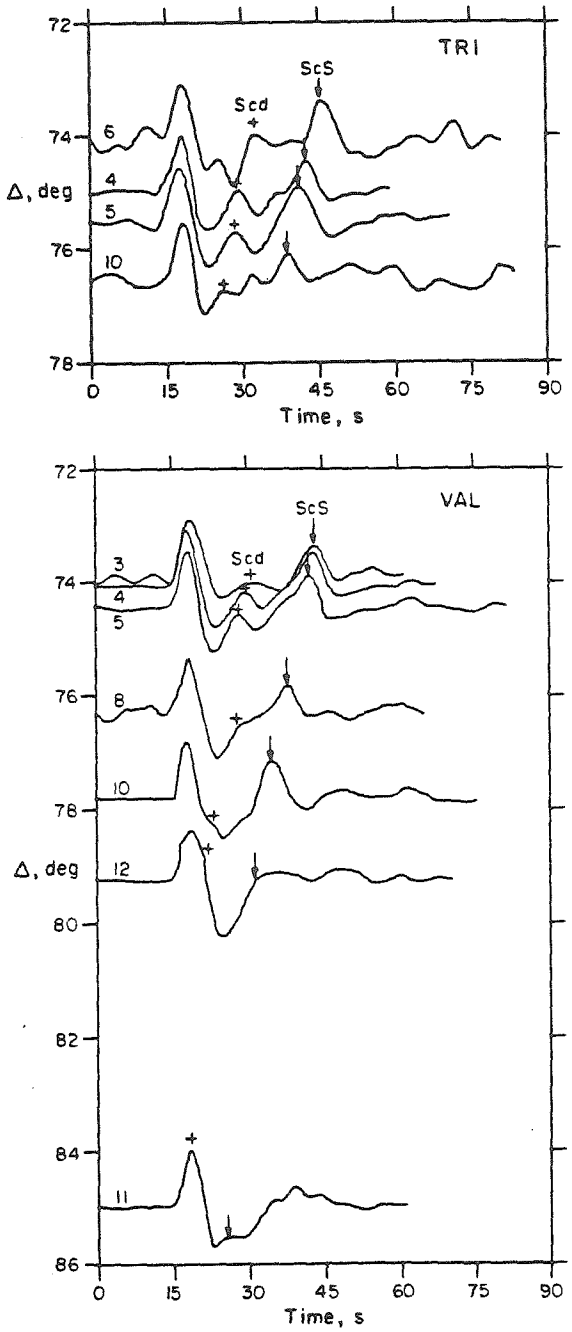

Figure I.1.27. Comparison of SH observations at VAL and TRI for several Sea of Okhotsk and Sea of Japan events. The numbers indicate the event in Table I.1.1 corresponding to each trace. The data are treated as in Figure I.1.15.

Observations near 75° in Canada, at stations SFA and MNT, are compared with the observation at VAL and TRI in Figure I.1.28. Synthetics for model SLHO are in close agreement with the Canadian observations as expected, but the Scd arrival is relatively late compared to the waveforms at VAL and TRI. This shift is several seconds and appears to be quite systematic. Moving the velocity discontinuity in SLHO upward by 40 km and keeping the same 2.75% velocity jump gives model SLHE, for which the ScS-Scd separation and Scd amplitude are in agreement with the European data. It is not possible to simply decrease the average D" velocity enough to produce the several second ScS-Scd travel time shift without having very strong negative velocity gradients. Thus, we feel that variation in the depth of discontinuity is the more reasonable explanation for this shift.

Argentine Events Recorded in North America

Deep focus Argentine earthquakes have suitable locations and mechanisms for examining the SH signals across North America. All short and long period SH seismograms recorded in North America were digitized and rotated for seven suitable deep focus events. No intermediate depth events with adequate location, size and orientation to seek the triplication were found in the data since 1963. The station distribution and epicenters are shown in Figure I.1.29. The azimuthal travel time anomalies in the Argentine data are particularly strong, with ScS-S residual variations of up to 8 s across the narrow azimuth range to North America. An attempt is made in Chapter II to isolate the cause of these azimuthal anomalies with the conclusion

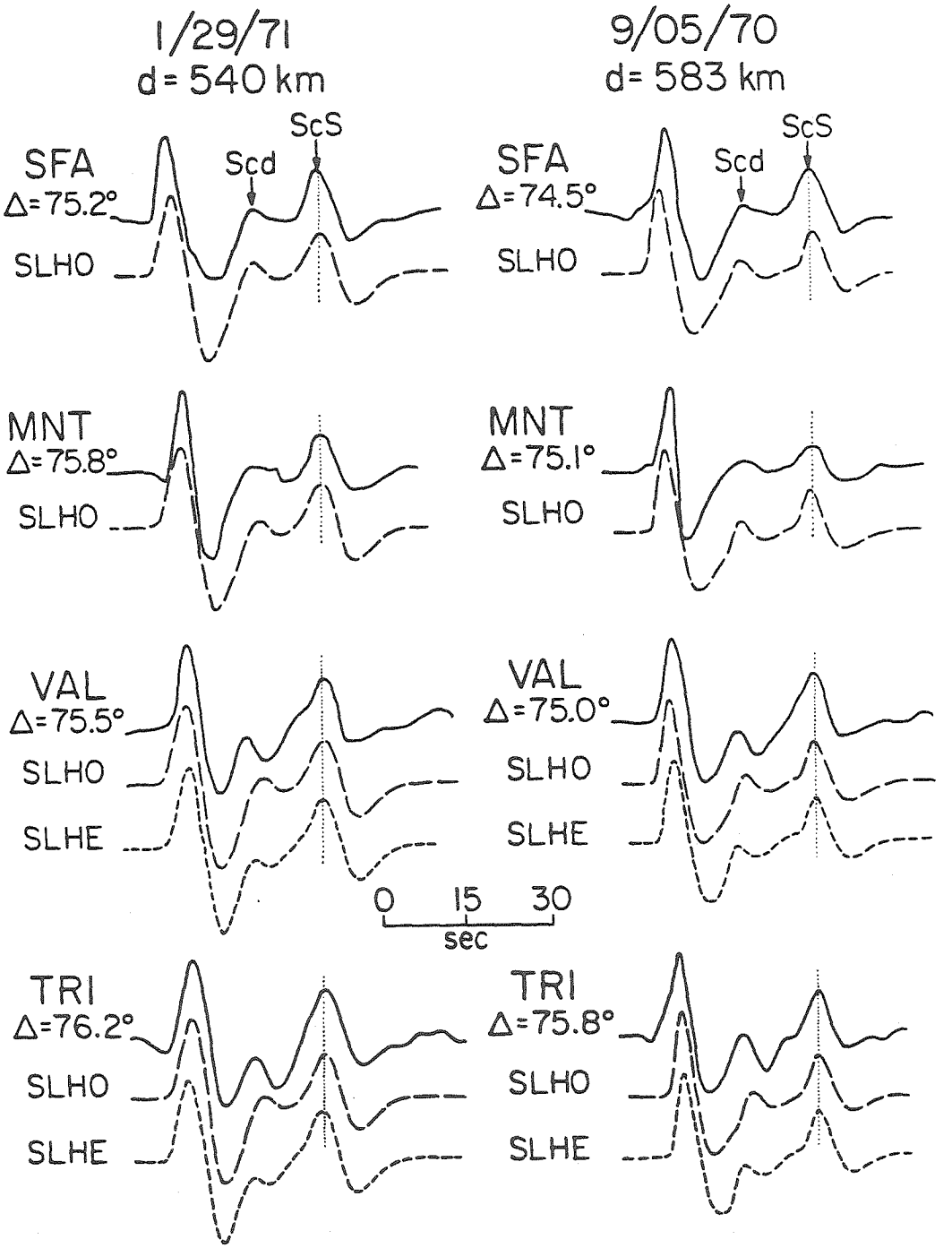

Figure I.1.28. Comparison of observations and synthetics for two deep focus Sea of Okhotsk events. SFA and MNT are Canadian stations, and hence are well modeled by SLHO (derived for paths to North America from the Sea of Okhotsk). VAL and TRI are European stations, so the paths to these sample distinct lower mantle. The Scd arrival is clearly visible at these stations, but arrives earlier than in the Canadian data or model SLHO. Model SLHE is similar to SLHO except that the major discontinuity is 40 km shallower.

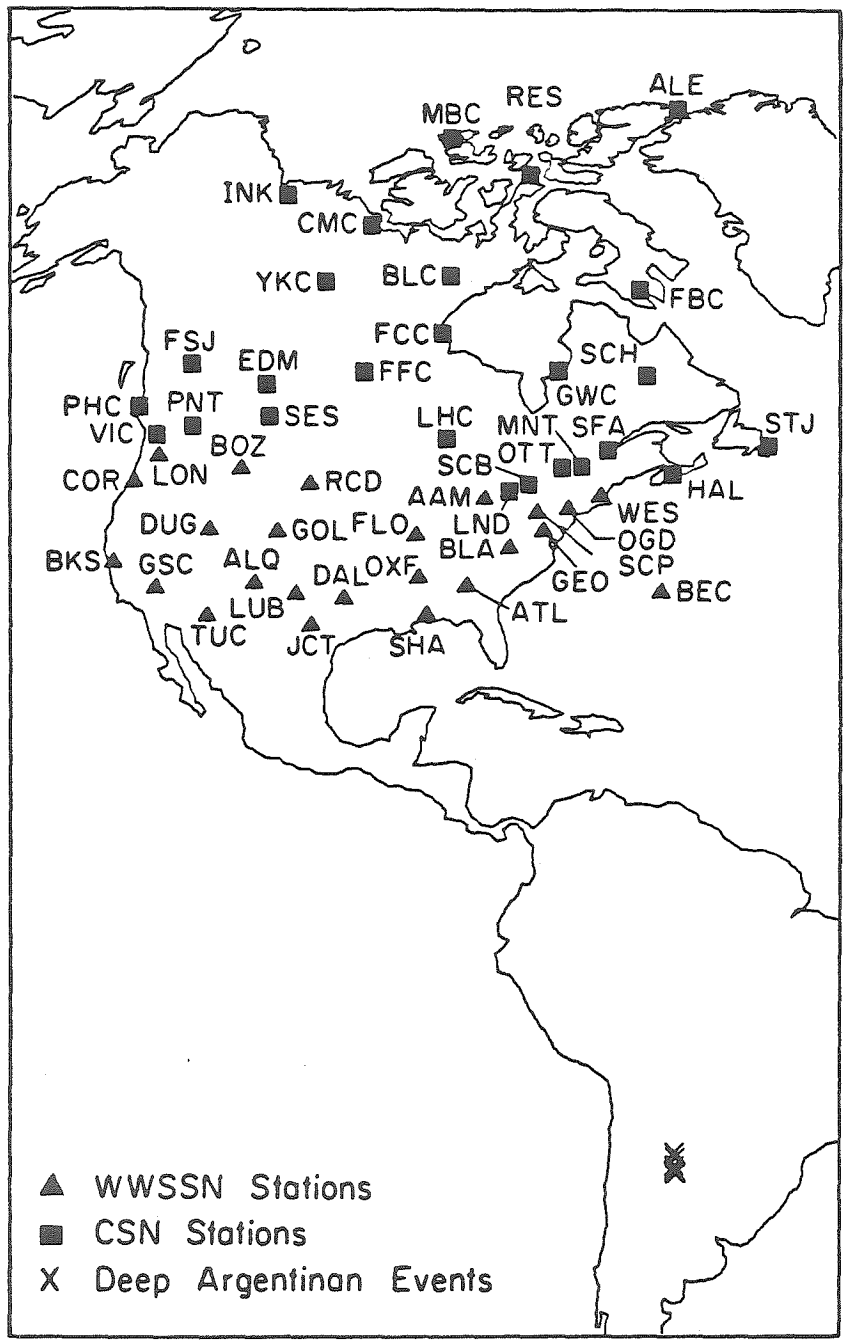

Figure I.1.29. Azimuthal equidistance projection showing the location of deep Argentine event epicenters and North American stations. GSC, RCD, and SCH are approximately 80° from the Argentine source region.

that the direct S phases encountered localized fast and slow regions in the mantle at depths of 1000 to 1900 km below the Caribbean and 1700 to 2700 km below Northern Brazil and Venezuela, respectively. If this interpretation is correct, the ScS-Scd differential times for any lower mantle triplication should show less variation than the ScS-Sab differential times. Thus, in plotting the data profiles from Argentina we align all the traces on the ScS arrival and seek the Scd branch.

Figure I.1.30 shows the SH seismograms for the event of January 17, 1967, which is known to be a simple event (Chapter III). It is clear that large ScS-S variations afflict the data, however, given the alignment of ScS it proves possible to pick the Scd arrival in the range 71^{o} to 81^{o}. Note the difference in ScS-Sab times at ALQ and SFA, but the consistency in ScS-Scd at these two stations. PAS and GSC show strong interference in the downswing that is consistent with the Scd arrival. GOL and DUG are very long period signals which show small Scd effects, but also comparably small ScS arrivals.

Another section aligned on the ScS arrival is shown in Figure I.1.31. The Scd branch can again be traced back to about 70^{o}. A third section is shown in Figure I.1.32, with strong Scd arrivals at SFA, STJ, LHC, and GSC. The other Argentine data profiles are similar, with fairly consistent Scd arrivals being apparent despite the large ScS-Sab travel time anomalies. These data are not as straightforward to model as the Okhotsk data, and not many stations lie in the range 75^{o} to 80^{o} where the Scd arrival should be strongest. However, the events have quite simple source character and high

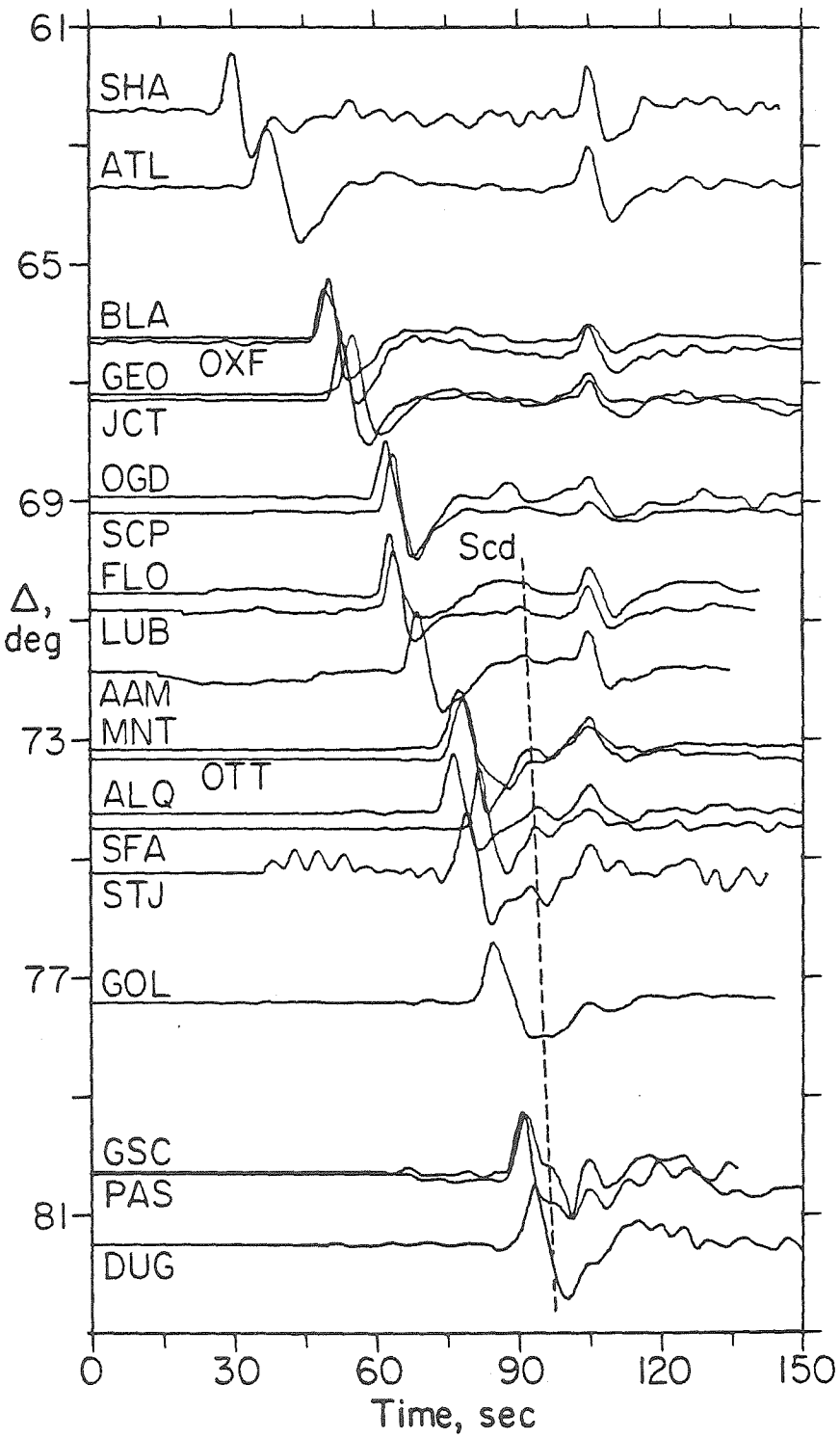

Figure I.1.30. Profile of tangential component observations for the Argentine event of January 17, 1967 (d = 588 km). The traces are aligned on the ScS arrival and the amplitudes are normalized.

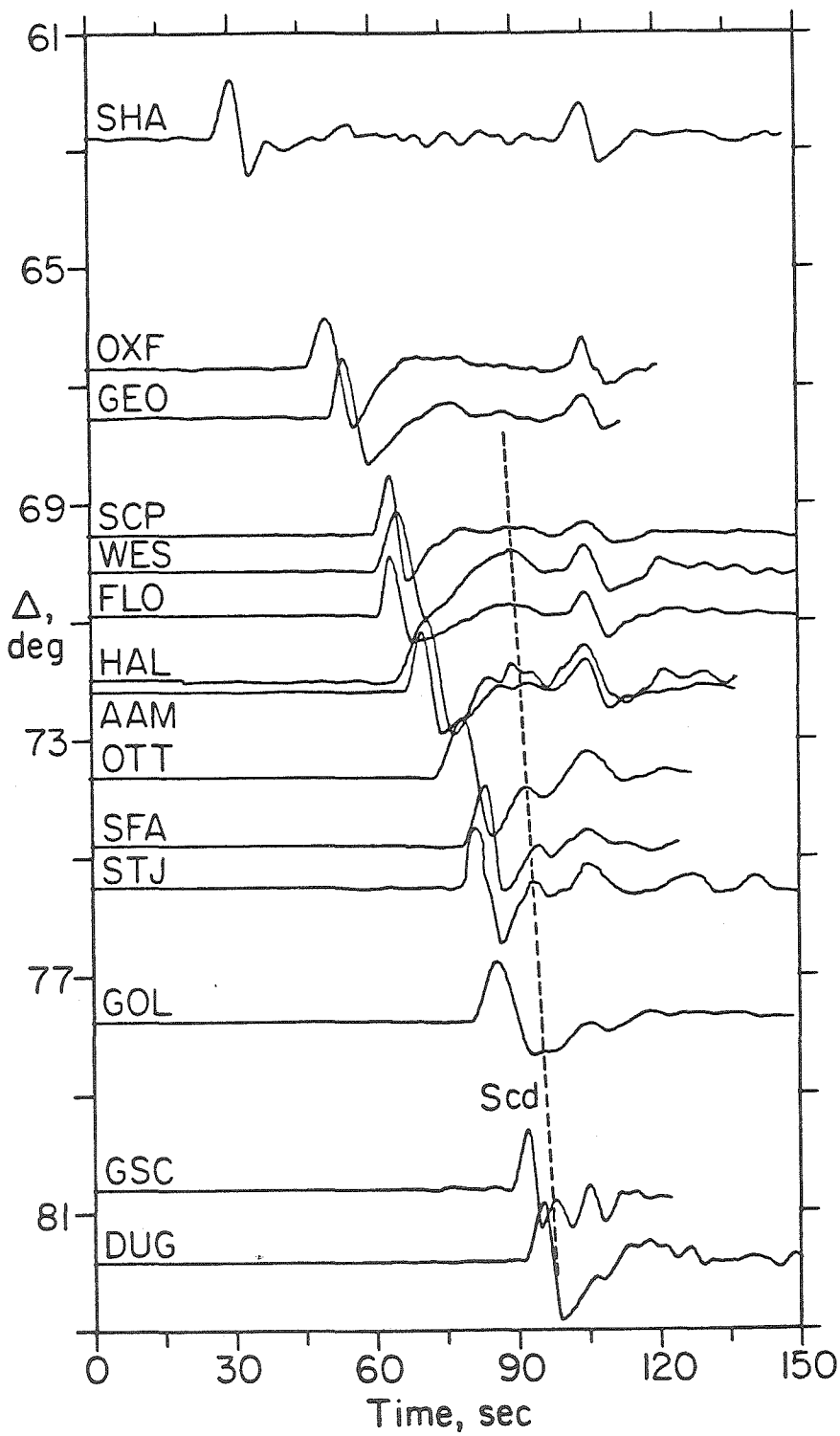

Figure I.1.31. Profile of tangential component observations for the Argentine event of September 9, 1967 (d = 578 km). The traces are aligned on the ScS arrival and the amplitudes are normalized.

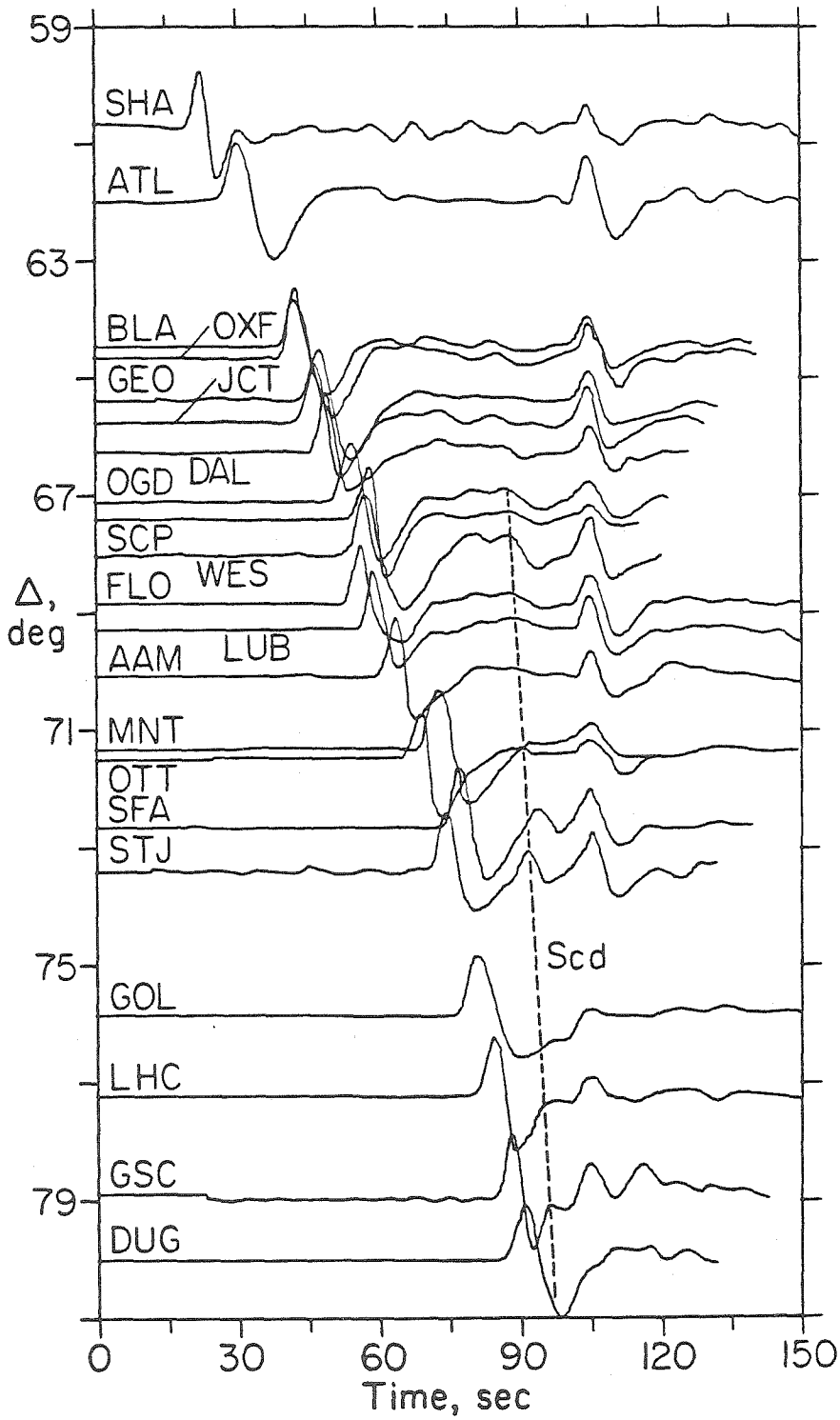

Figure I.1.32. Profile of tangential component observations for the Argentine event of July 25, 1969 (d = 579 km). The traces are aligned on the ScS arrival and the amplitudes are normalized.

signal-to-noise ratio.

As with the Okhotsk data, comparison of numerous recordings at a given station proves to be a powerful tool to eliminate misidentification of receiver phases and to increase the effective station density. The Argentine events are remarkably similar in location (Table I.1.1) and mechanism (Table I.1.2), so intercomparison of the events is straightforward. Four station comparisons are shown in Figure I.1.33. While the Scd arrival is small near 72^{o}, it is quite large near 80^{o}, which is consistent with the Sea of Okhotsk observations. Inspection of SH signals at stations such as GSC and PAS for closer events confirms that the Scd arrival is not a receiver phase. Several of the Canadian stations are near 90^{o}, and the waveforms at these show distinctive double arrivals in the first pulse that are generally consistent with the Scd and Sab interference seen in the Sea of Okhotsk data at similar distances. The better documented instances of this at stations FBC and EDM are shown in Figure I.1.34. It is interesting to note that the relative amplitude of the first and second arrivals is systematically different between the two stations. These two stations are relatively well separated in azimuth so it is possible that the change in Scd to Sab ratio is due to lateral variations in D" within the azimuth range spanned by the North American stations.

When all ScS-Scd differential travel time observations for Argentina are plotted as a function of distance, a clear Scd travel time branch is defined as shown in Figure I.1.35. While the scatter at a given distance can be as much as 4 s, in general it is about 2 s,

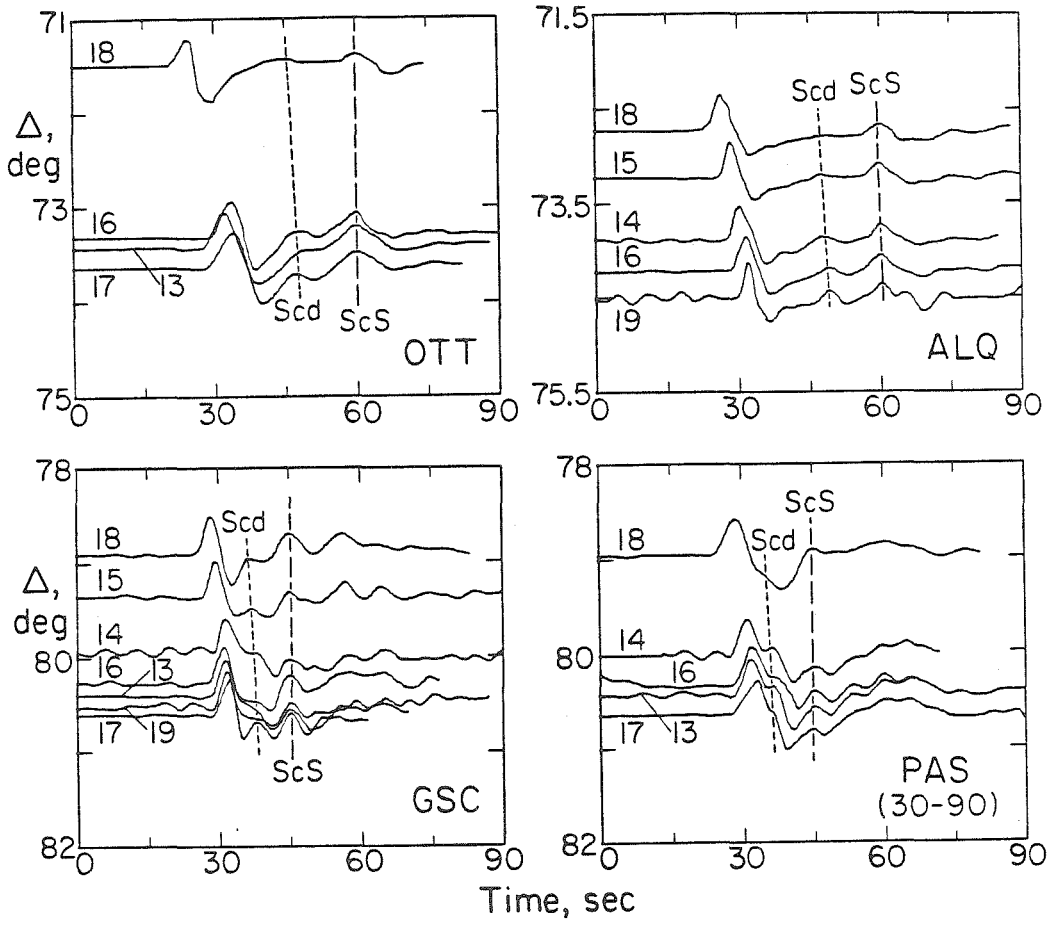

Figure I.1.33. Comparison of observations of several Argentine events at North American stations. The numbers indicate the corresponding events in Table I.1.1. The traces are aligned on the ScS arrival and the distances have been shifted as in Figure I.1.15. Note that the Scd arrival is very weak closer than 73°, but is very strong near 80°.

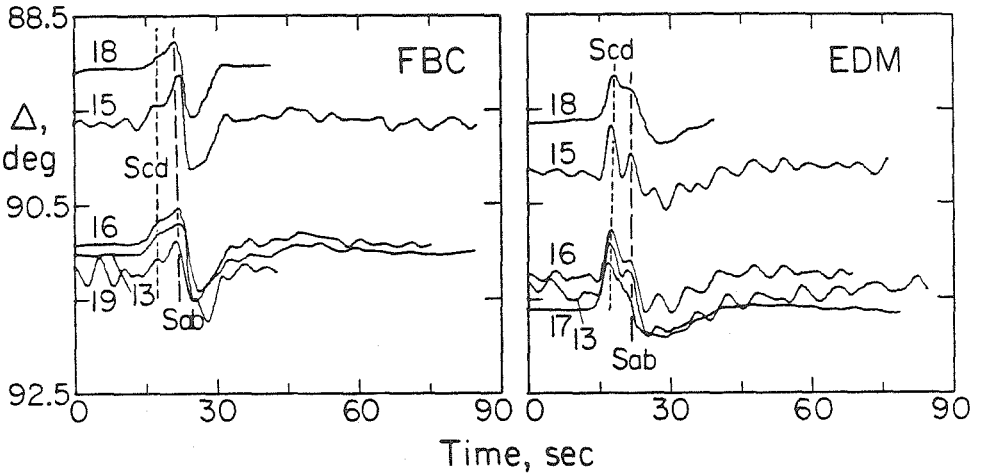

Figure I.1.34. Comparison of SH observations at two Canadian stations beyond crossover distance. The numbers indicate the corresponding events in Table I.1.1. The traces are aligned on the first arrival. Note the difference in relative amplitude of Scd and Sab.

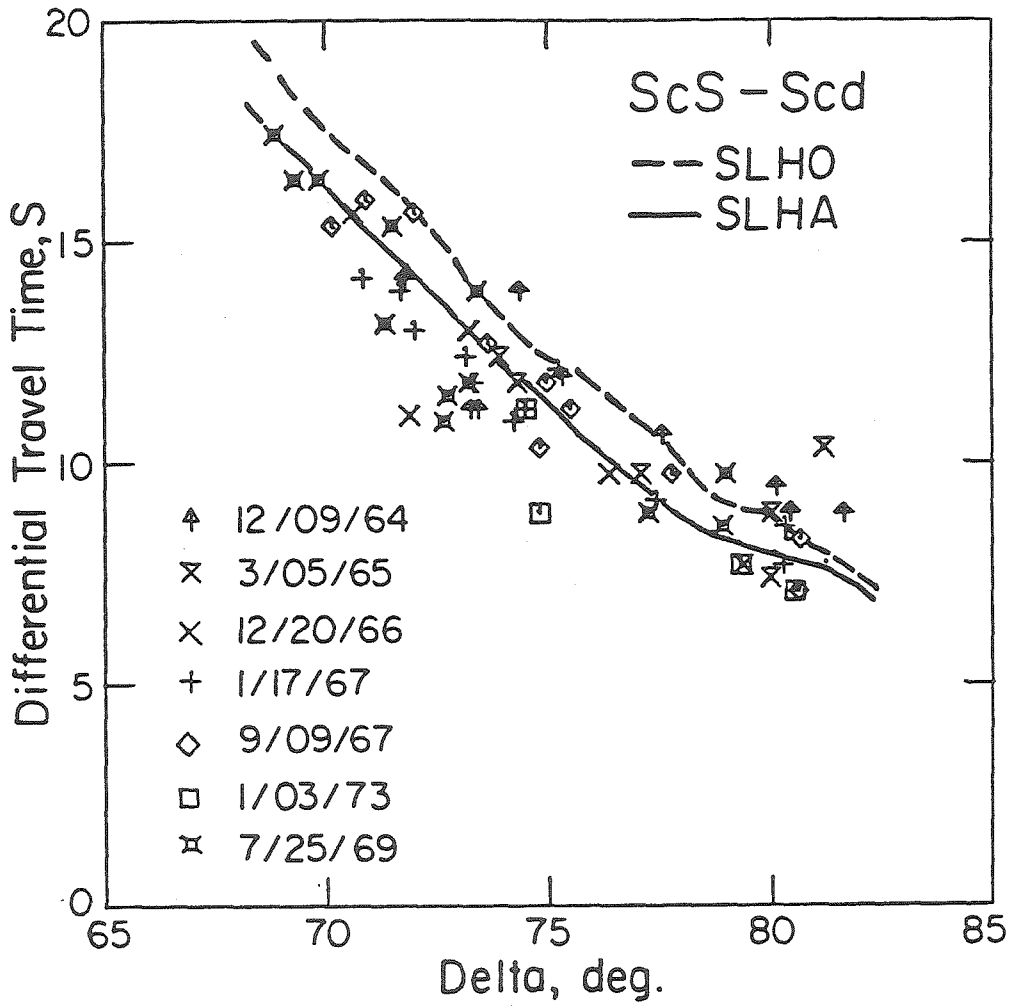

Figure I.1.35. The peak-to-peak differential times between ScS and Scd for all of the Argentine deep events. The corresponding times measured from synthetics for models SLHO and SLHA are also shown.

which is much less than the 8 s ScS-Sab variations. The time separation between ScS and Scd is slightly less than for model SLHO throughout the distance range 70^{o} to 82^{o}, which led us to determine model SLHA. This model has a velocity discontinuity of 2.75% at a depth 27 km deeper than in model SLHO. This modification reduces the travel time difference between ScS and the reflection off of the discontinuity and fits the Argentine data quite well in an average sense (Figure I.1.35). Synthetics for SLHA are compared with observations from several Argentine events in Figure I.1.36. The relative amplitude of the Scd branch throughout the range 73^{o} to 80^{o} is consistent with a velocity discontinuity the same size as in models SLHO and SLHE. The large azimuthal ScS-S anomalies in the Argentine data preclude the more complete waveform modeling performed for the Sea of Okhotsk observations in North America; however, SLHA provides a good average model for the Argentine paths.

Observations of the lower mantle triplication beyond crossover distance are particularly sensitive to the depth and size of the discontinuity. Thus, the observations at FBC and EDM near 90^{o} have also been modeled. These stations require localized modifications of model SLHA. Short and long period observations at these stations are compared in Figure I.1.37. The traces have the same start time, so it is apparent that at FBC there is a small short period precursor associated with the distortion of the long period upswing. At EDM, the first arrival is stronger on both the short and long period signals. These signals are generally consistent with the expected complexity near 90^{o} for the lower mantle triplication, with the first

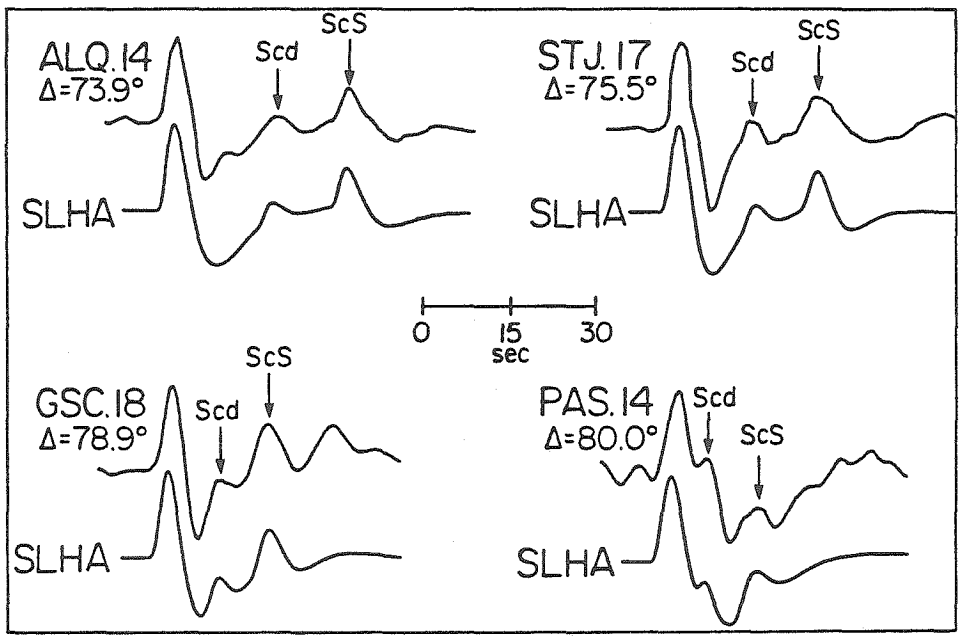

Figure I.1.36. Observed and synthetic long period SH waveforms for several Argentine events. The number after each station name indicates the corresponding event in Table I.1.1.

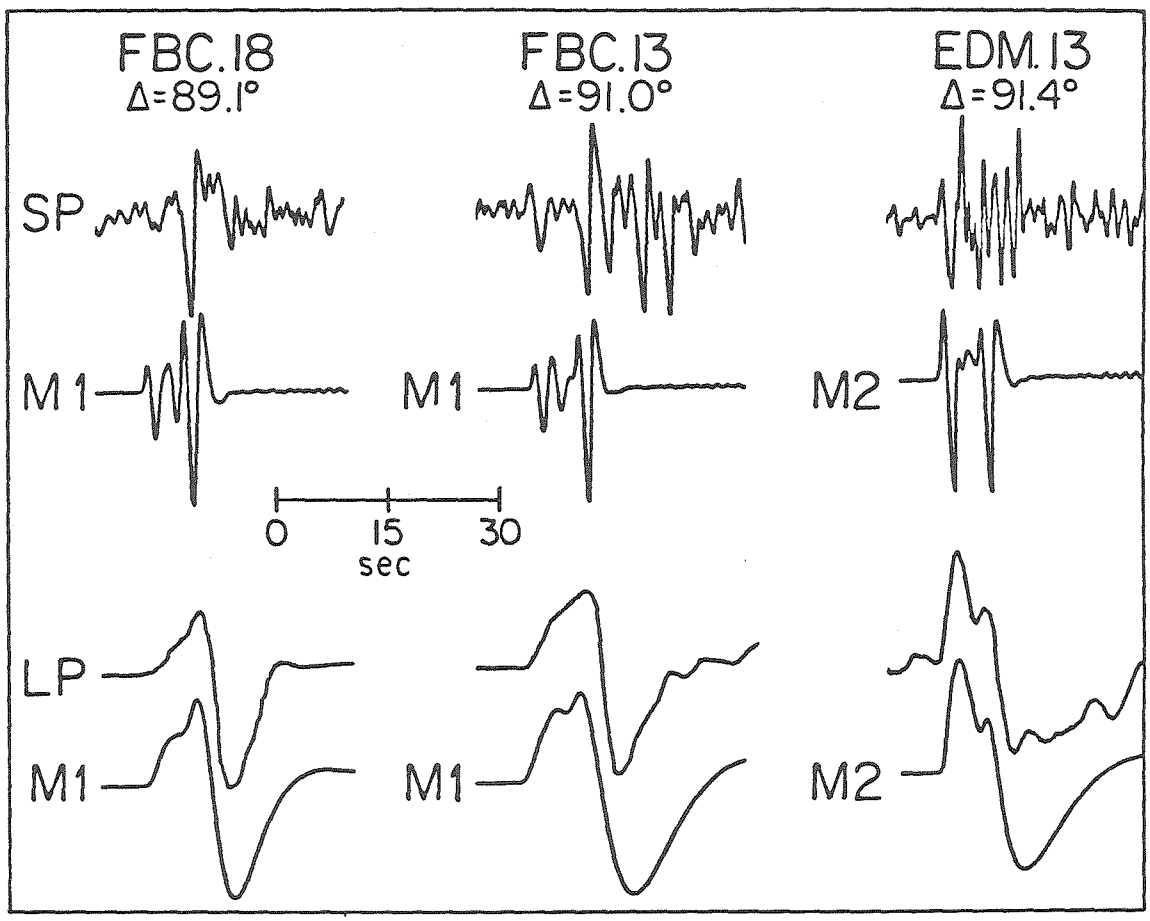

Figure I.1.37. Comparison between the short period and long period observations and synthetics for Argentine events in the distance range 89^{o} to 91.4^{o}. The start times of the short period and long period traces are the same. Note the small first arrival in the FBC data compared with the strong first arrival at EDM. These features can be modeled by perturbations of model SLHA. M1 has an increased velocity contrast across the discontinuity, while M2 has a transition zone 80 km thick rather than a sharp discontinuity. Details are given in the text.

arrival being Scd and the second arrival being Sab. However, for model SLHA, which fits the Argentine data in the range 70^{o} to 82^{o}, the Scd and Sab branches are not separated as much at 90^{o} as seen in the FBC observations. The relative amplitudes of Sab to Scd are also not quite consistent with either FBC, for which the predicted ratio is too small, or for EDM for which the predicted ratio is too big. Since these features do not appear to be receiver structure effects, we have searched for models which can satisfy these observations near 90^{o}.

To separate the Sab and Scd branches adequately to model the FBC observations, one can either move the discontinuity to shallower depths (which shifts the crossover distance toward the source) or one can increase the velocity contrast across the discontinuity (which increases the slope between the two branches). The discontinuity must be shifted upward by nearly 100 km compared with model SLHA if the first approach is adopted, or the velocity jump can be increased to 3.8% while keeping the discontinuity at a depth 280 km above the CMB. Moving the discontinuity shallower is inconsistent with the ScS-Scd times in the Argentine data at closer distances. The second approach yields model M1 for which synthetics are compared with FBC in Figure I.1.37. The time separation of the branches is in agreement with the data, though the relative amplitude of Scd to Sab is still somewhat too large. Introducing a mild negative gradient throughout D'' can diminish the Scd branch at this distance. For EDM, the time separation between Scd and Sab is fairly consistent with the prediction for model SLHA; however, the first arrival is much stronger than predicted. To decrease the Sab/Scd ratio the most

straightforward approach is to introduce a transition zone rather than a sharp discontinuity at the top of D". A transition zone 80 km thick with a 3% velocity increase centered 280 km above the CMB was introduced into Model M2. The synthetics for this model, which is similar to SLHA, but with a distributed velocity increase, are shown in Figure I.1.37.

While the Argentine data do not uniquely resolve the features of Models SLHA, M1, and M2, we feel that there is clear evidence for lateral variations in the lowermost 400 km of the mantle along the paths from Argentina to North America. The localized increase in velocity contrast in model M1 is very consistent with the results of Chapter II. There it is proposed that a localized region of the lower mantle just above D", centered below Venezuela, is about 2% slower than the surrounding mantle. The paths to FBC bottom in this vicinity, thus the total velocity contrast across the discontinuity might be expected to increase. The distinctive appearance of EDM and FBC clearly requires a rather substantial lateral variation in the nature of the discontinuity. Other stations in the 89^{o} to 92^{o} distance range such as COR, PNT, and VIC also show the split first pulse expected at this range, but the data are too sparse to map the lateral variations in detail.

Discussion

The data from all three source region-receiver combinations analyzed in this paper are consistent with the basic conclusion that a large shear velocity discontinuity exists about 280 km above the core. The models derived from the SH data for each sample of the D" region

are compared in Figure I.1.38. The basic feature of a 2.75 $\pm$ 0.25% velocity discontinuity is present for each of these distinct paths. We consider these to be the first order models, that satisfy nearly all of our SH observations. There appears to be lateral variation in the velocity increase and sharpness of the structure beneath northern South America represented by model SLHA; however, the basic character of the discontinuity is well established.

The similarity of the depth and size of the discontinuity in such distinct portions of the lower mantle as investigated here does suggest that the structure is a global feature. Additional source region-receiver combinations are presently being investigated, and a final conclusion on this point must await those results. The presence of a significant, observable lower mantle feature provides an exceptional tool for modeling lower mantle lateral variations. The differences in depth of the discontinuity for the three regions discussed here are fairly well resolved, though the depths can be modified if strong lateral velocity variations within D" are allowed. It appears more reasonable to allow some variation in the thickness of the D" layer (which we assume to extend upward to the discontinuity). Since we are unable to constrain the density contrasts with the SH data alone, we cannot make conclusive arguments about whether the relief in the discontinuity is dynamically supported.

Of the published lower mantle P velocity models, the only one similar to the shear velocity models obtained here, is the model of Wright and Lyons (1979, 1981). Their model contains a 1.2% P wave velocity increase 170 km above the CMB. Below this sharp

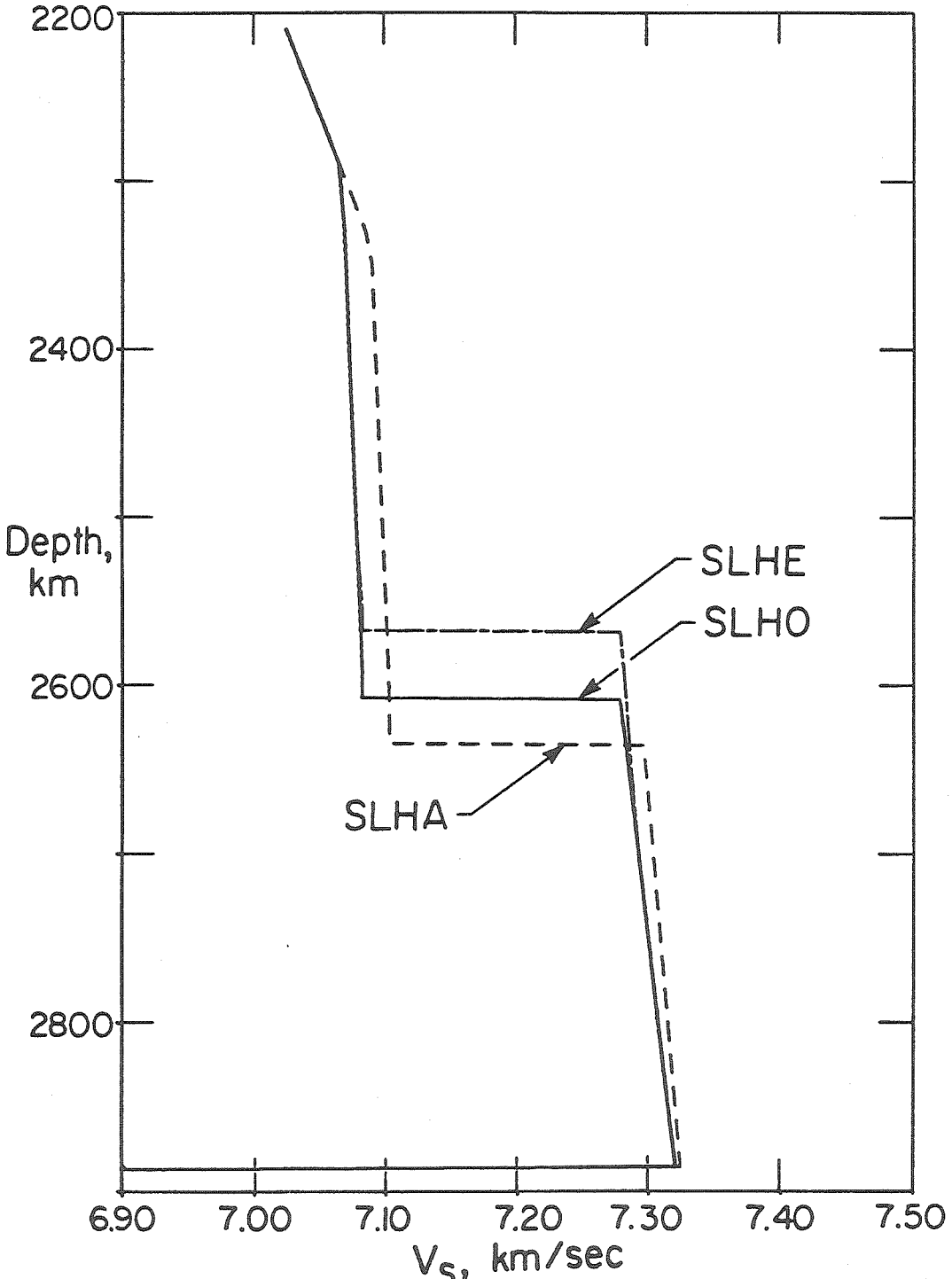

Figure I.1.38. Comparison of the preferred shear wave velocity models that are derived for the SH data for each of the three source region-receiver array combinations considered. The basic feature of a 2.75% velocity discontinuity about 280 km above the core is present in each case. The variations in thickness of the D" layer are clearly indicated by the data. There appear to be lateral variations in the sharpness and size of the discontinuity in model SLHA; however the simple model shown fits 90% of the data.

discontinuity is a strong negative velocity gradient. Most of their data are from South American events recorded at the Yellowknife (Western Canada) array. It may be possible to reconcile the difference in depth of the P and S wave discontinuities with lateral variations and intrinsic uncertainty in both models, and it may be possible to explain the difference in size of the discontinuities similarly or with compositional changes in Poisson ratio. However, at this point, the P wave models in the literature are simply too inconsistent with one another to justify strong conclusions based on P and S wave model comparisons. Further work on detailed P wave models is clearly required. Hopefully, this will also allow determination of the density structure of the D" region.

The S wave triplication and inferred velocity models constitute a major modification of existing lower mantle shear velocity models, but it is clear that most travel time or diffracted S wave studies would not have resolved the structure. It may be possible to detect the presence of the discontinuity in such studies if it is specifically sought. Detailed analysis of the differential times between the various branches of the triplication can be used to model lateral variations and detailed fine structure just as is done for upper mantle triplications. It is important to note that in this study, as well as in the corresponding travel time study of Chapter II, the major lateral variations affecting the signals appear to take place within the mantle between 600 and 2600 km depths. This is a different conclusion from previous studies which indicate that the D" is generally more heterogeneous than the central mantle.

The presence of a large discontinuity in the lower mantle is important for models of the Earth's thermal and compositional history, as well as for mantle dynamics. Without detailed knowledge of the density contrasts involved, it is impossible to discriminate between a phase change or a compositional change across the discontinuity. This issue is, of course, important to address, but has not been unambiguously resolved even for well known upper mantle discontinuities. At any rate, it is quite safe to conclude that the D" region is more complicated than a simple thermal boundary layer at the base of the mantle.

Conclusions

A large body of S wave data for three source region-receiver combinations indicates the presence of a 2.75 $\pm$ 0.25% shear velocity discontinuity about 280 km above the core. This discontinuity produces a triplication that can be directly observed in SH seismograms from intermediate and deep focus events in the range 70^{o} to 95^{o}. There appear to be lateral variations in the depth of the discontinuity of 40 to 50 km on a global scale; however, the triplication is quite similar for all three regions. Short period data are consistent with either a sharp discontinuity or one distributed over up to a 50 km thick transition zone. The presence of the discontinuity is best detected using direct S and ScS waveform information, rather than travel time or diffracted waves.

Section I.2 The Shear Velocity Gradient at the Base of the Mantle

Abstract

The relative amplitudes and travel times of ScS and S phases are utilized to place constraints on the shear-wave velocity gradient above the core-mantle boundary. A previously reported long-period ScSH/SH amplitude ratio minimum in the distance range 65^{o} to 70^{o} is shown to be a localized feature, apparently produced by an amplitude anomaly in the direct S phase, and therefore need not reflect the velocity gradient at the base of the mantle. The amplitude ratios that are free of this anomaly are consistent with calculations for the JB model or models with mild positive or negative velocity gradients in the lowermost 200 km of the mantle. ScSV arrivals are particularly sensitive to the shear velocity structure just above the core-mantle boundary. The apparent arrival time of ScSV is as much as 4 seconds greater than that of ScSH in the distance range 75^{o} to 80^{o} for Sea of Okhotsk events recorded in North America. This can be explained by interference effects produced by a localized high velocity layer or strong positive S wave velocity gradient in the lowermost 20 km of the mantle. A velocity increase of about 5% is required to explain the observed shift between ScSV and ScSH. This thin, high velocity layer varies laterally, as it is not observed in similar data from Argentine events. Refined estimates of the outermost core P velocity structure are obtained by modeling SKS signals in the distance range 75^{o} to 85^{o}.

Introduction

The nature of the shear-wave velocity structure at the base of the mantle has been a controversial subject for many years. Gross

earth models derived from travel times and free oscillations generally indicate smooth velocity gradients in the lower mantle, with slightly diminished gradients in the lowermost 200 km (D" region). These studies have little resolution of the detailed structure of the D" region. Early investigations of diffracted SH waves, relying on classical ray theory interpretations, indicated very low S-wave velocities at the core-mantle boundary (CMB), and attendant strong negative velocity gradients within D" (Cleary, et al., 1967, Cleary, 1969; Bolt et al, 1970; Hales and Roberts, 1970; Robinson and Kovach, 1972). Recent studies of diffracted SH incorporating more complete diffraction theory and synthetic modeling capabilities have proposed milder negative shear velocity gradients in D" (Mondt, 1977; Doornbos and Mondt, 1979) and near-zero or slightly positive gradients (Okal and Geller, 1979; Mula and Müller, 1980; Mula, 1981). These studies have been directed toward obtaining global averages, and the degree of lateral variation in D" properties remains an open question.

A conflicting result was found by Mitchell and Helmberger (1973), who utilized the relative amplitudes and timing of long-period ScS and S phases to constrain the S-wave velocity gradient in D". They found a minimum in the ScSH/SH amplitude ratio near 68^{o}, which was attributed to the ScS arrivals. Unable to explain this feature by models with negative or near-zero shear velocity gradients in D", they proposed models with positive S-wave velocity gradients above the CMB. These positive gradients extended over 40 to 70 km above the core, reaching velocities at the CMB as high as 7.6 to 7.8 km/sec. These models can explain the observed amplitude ratio behavior, as well as

an apparent difference observed in the arrival times of transversely and radially polarized ScS. Mitchell and Helmberger also proposed a low Q_β zone in D", or finite outer core rigidity, to explain the baseline of the ScSH/SH amplitude ratios. While the majority of their data was for deep South American events recorded in North America, they did analyze one deep Sea of Okhotsk event for which the radial and transverse ScS arrival times were not different, which suggested lateral variations in the D" velocity structure.

In this section we extend the analysis of ScS and S phases using an enlarged data set in order to understand the discrepancy between the diffracted S studies and the results of Mitchell and Helmberger (1973). A reinterpretation of the ScSH/SH amplitude ratio minimum indicates that this feature is more clearly associated with a localized amplitude anomaly in the direct S-waves rather than with D" structure. We find that the ScS amplitude behavior is consistent with the JB model for two distinct lower mantle regions and do not find evidence for a major low Q_β zone at the base of the mantle. ScSV and ScSH do show systematic timing differences for one of the regions, which can be well-modeled by introducing a thin, high velocity layer or strong positive velocity gradient above the core, but this thin zone varies laterally, and cannot be detected using the ScSH/SH amplitude ratios alone.

Amplitude Data

The S and ScS data analyzed in this paper are from 7 deep focus earthquakes in Argentina and 10 intermediate and deep focus events in the Sea of Okhotsk, recorded at long period WWSSN and Canadian Seismic

Network stations in North America. Figure I.2.1 shows the locations of the stations used for both source regions and the epicenters of the Argentine events. The source parameters for the events are given in Table I.1.1. All of the events were selected for their simple, impulsive waveforms and for their stable SH radiation patterns to the North American array. The horizontal components in the interval containing the S and ScS phases of all stations in the distance range 40^{o} to 80^{o} were digitized and rotated into radial and transverse polarizations. Numerous profiles of the SH and SV seismograms are presented in Section I.1.

In order to correct the observed amplitudes for radiation pattern, focal mechanisms determined from P-wave first motions and S-wave polarizations were extracted from the literature or newly determined. Then the long-period SV/SH amplitude ratio was used to refine the mechanisms or to select between various mechanisms in the literature proposed for a given event. This was done using a modification of a least squares inversion program written by Brian Mitchell. The final focal mechanisms adopted for the Argentine events, which are all consistent with both P-wave first motions and S-wave amplitudes, are listed in Table I.1.2. For the event of July 25, 1969, we could not determine a consistent mechanism. In only 4 of the 17 cases did we find solutions which significantly improved the SV/SH amplitude agreement over that for the starting mechanisms, and 2 of these cases involved only 5^{o} changes in dip. This is mainly due to the large scatter in the amplitude ratios.

For the Argentine events, the radiation pattern corrections

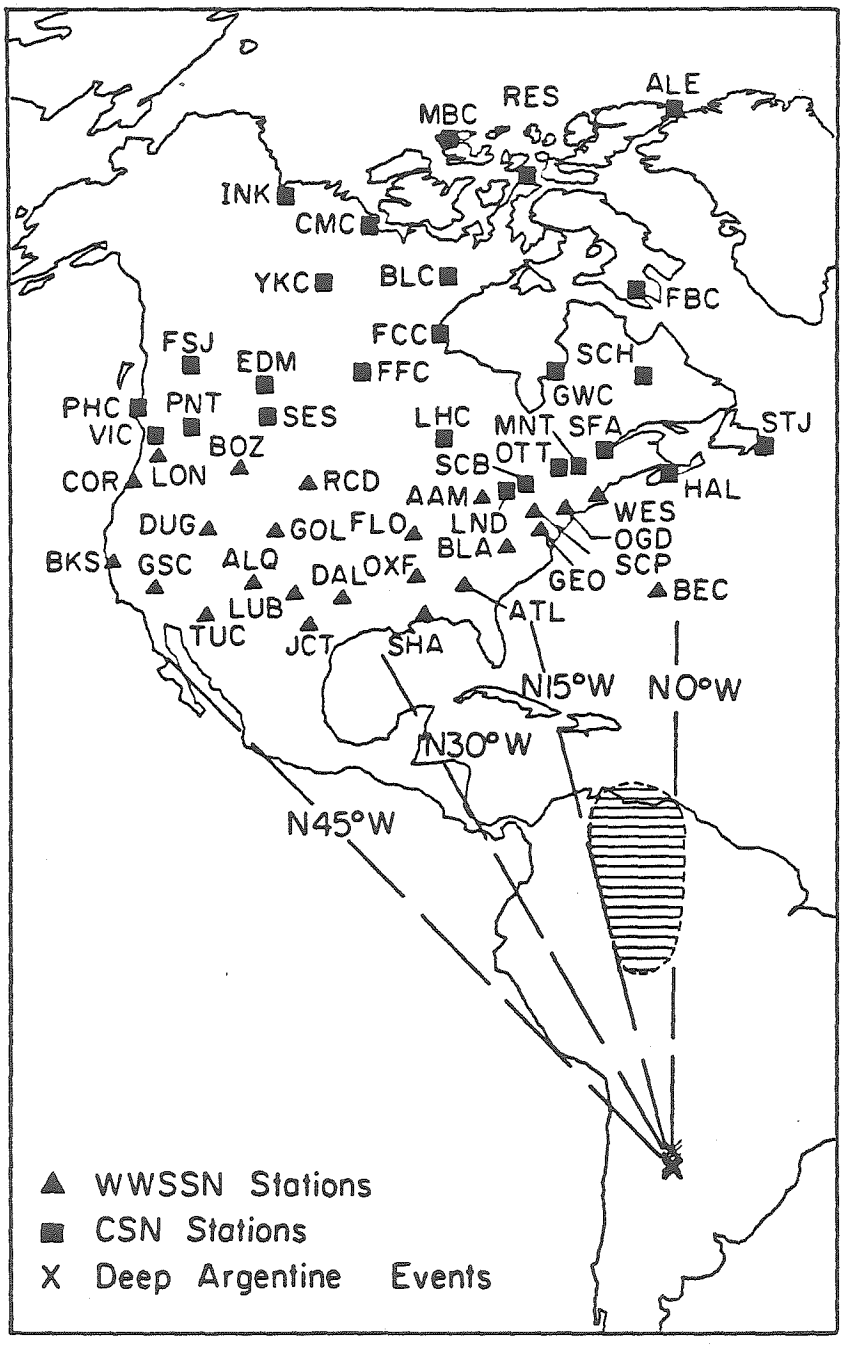

Figure I.2.1. Azimuthal equidistance projection showing the location of deep Argentine event epicenters and North American stations. GSC, RCD, and SCH are approximately 80° from the Argentine source region. The hatchured region is the map projection of the deep mantle low velocity anomaly proposed in Chapter II.

applied to the observed ScSH/SH amplitude ratios are all less than 12%, which reflects the stability of the SH radiation patterns to North American stations. Since these corrections are small, we include the uncorrected ratios for the event of July 25, 1969 below. Four of the Argentine events in our data set were used by Mitchell and Helmberger (1973). They applied radiation pattern corrections to their ScSH/SH amplitude ratios that were generally greater than 20% (Mitchell, personal communication). The focal mechanisms they used were also determined using SV/SH amplitudes, but in some cases were inconsistent with the P-wave first motions. The scatter in the amplitudes is substantial, and probably the larger size of our data sets for each event provides more reliable mechanisms.

The long-period peak-to-peak ScSH/SH amplitude ratios for the Argentine data are shown in Figure I.2.2. Radiation pattern corrections have been applied. In the distance range 55^{o} to 75^{o} the S and ScS arrivals are distinct phases for which the amplitudes can be accurately measured. Beyond 75^{o} ScS interferes with the instrument overshoot of the direct S arrival, and the apparent peak-to-peak amplitude of ScS diminishes rapidly. There is a factor of three scatter at each distance, which complicates the interpretation of the amplitude ratios. This scatter is primarily due to source and receiver structure complexity, as well as deep mantle structure.

Figure I.2.2 also shows the theoretical ScSH/SH amplitude ratio for a JB earth model. The curve was determined from long-period synthetics computed using the Cagniard de Hoop generalized ray theory technique (see Section I.1). The effective t_{β}^{*} is the same for S and

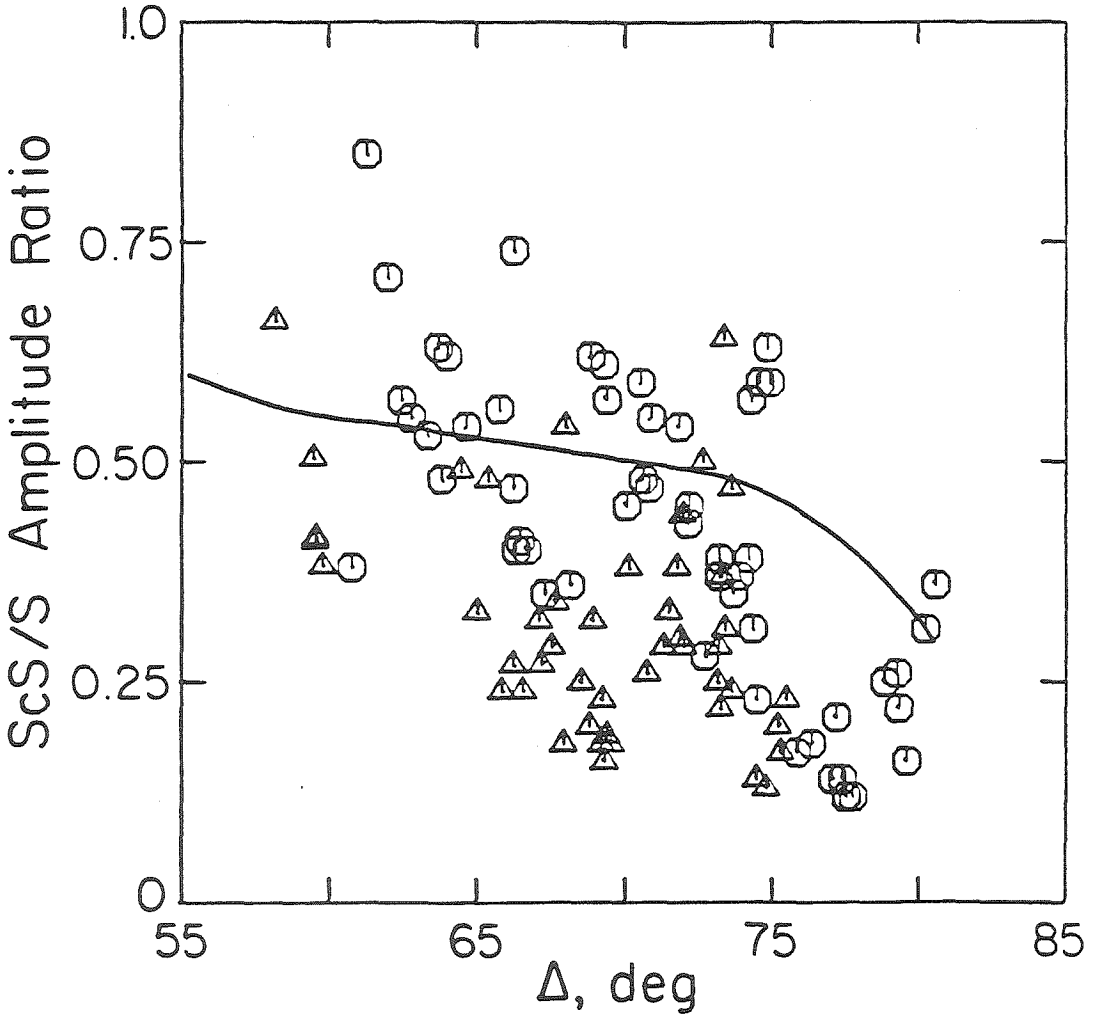

Figure I.2.2. The long period peak-to-peak ScSH/SH amplitude ratios for the Argentine events recorded in North America. Radiation pattern corrections for the focal mechanisms given in Table I.1.2 have been applied. The triangles are for data recorded at azimuths greater than 345^{o} from the source region. The curve shows the theoretical ratios measured from long-period synthetics for the JB model.

ScS for this and all other synthetic calculations presented here. For a lower mantle with a constant Q = 312 (e.g. the PREM model of Dziewonski and Anderson, (1981)) the difference in t^*_β for ScS and S varies from 0.2 to 0.0 sec in the distance range 55^o to 80^o, which produces an insignificant effect on the long-period amplitude ratios. However, for a model with a very low Q_β distribution near the CMB such as model SL8 (Anderson and Hart, 1978), the difference in t^*_β increases from 0.25 to 1.0 sec in the same distance range, which predicts a more rapid decay in the ScSH/SH amplitude ratios with distance than apparent in the theoretical curve in Figure I.2.2.

The data in Figure I.2.2 can be compared with that in Figure 6 of Mitchell and Helmberger (1973) if one omits their data points for Peruvian events and the Sea of Okhotsk event. Figure I.2.2 has twice as many data points for the Argentine source region. In the range 65^o to 70^o there is a cluster of low amplitude ratios, well below the JB model calculations, but there are observations in this range consistent with the JB model. At distances greater than 75^o the observed ratios drop off rapidly due to the interference between S and ScS, and the theoretical curve does also since the long-period synthetics have similar interference. As shown later, similar data from the Sea of Okhotsk source region do not show an amplitude minimum near 67^o, so this anomaly is investigated in detail below. It is also important to note that the amplitude ratios in Figure I.2.2 scatter in the range 0.2 to 0.75, which is significantly shifted relative to the range 0.1 to 0.5 spanned by the data in Mitchell and Helmberger (1973). This shift, which apparently results from the difference in

radiation pattern corrections applied, is important because the low average baseline of the data in the earlier study was cited as evidence for a low Q_β region at the base of the mantle.

A close inspection of the individual observations that define the amplitude ratio minimum near 67° in Figure I.2.2 and Figure 6 of Mitchell and Helmberger (1973) reveals that all of the stations involved lie on the East Coast of North America. In particular, SCP, OGD, BLA, GEO, LND, MNT, OTT and SFA (Figure I.2.1) repeatedly have low amplitude ratios. Stations at comparable distance such as OXF, FLO and LUB do not show low amplitude ratios. This indicates the anomaly is azimuthally restricted, and does not reflect radial earth structure. In Figure I.2.2 all of the observations at azimuths from the source region east of $N15^\circ W$ are plotted with triangles. There is relatively little overlap between the two populations for this azimuthal separation, and all of the anomalously low ratios are isolated to eastern observations.

The Argentine ScSH/SH amplitude ratios are plotted as a function of azimuth in Figure I.2.3. The sharp separation of the low ratios along an azimuth of $N15^\circ W$ indicates the localized nature of the amplitude anomaly. The event of July 25, 1969 shows some relatively large amplitude ratios at eastern stations, but these may be erroneous because radiation pattern corrections were not applied for that event. The data at an azimuth of 0° are for station BEC, which is near 55° distance. This station is isolated from the East Coast (Figure I.2.1) and appears to be free of the azimuthal anomaly.

The amplitude ratio minimum could result from either an S or ScS

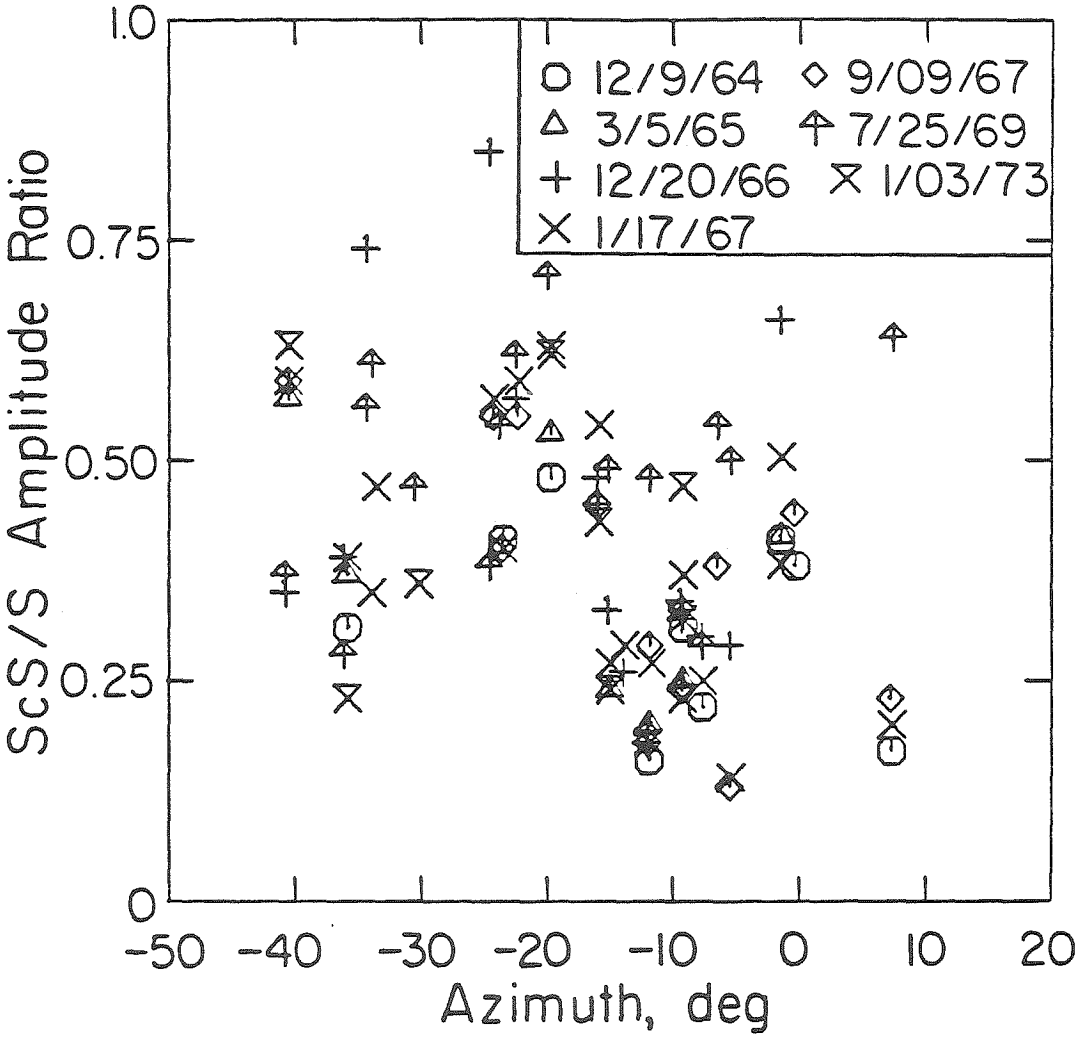

Figure I.2.3. The same data in Figure I.2.2 plotted as a function of azimuth from the source. Different symbols are used for each event. Only data in the distance range 55^{o} to 75^{o} are shown, because the expected distance dependence is small in this range.

amplitude anomaly. Mitchell and Helmberger (1973) inferred that the ScS phases were responsible based on the distance behavior of S and ScS amplitudes. In Figure I.2.4 the zero line-to-first peak amplitudes for S and ScS are plotted as a function of azimuth. Geometric spreading corrections determined from synthetics for a JB mantle have been applied, along with radiation pattern and event size corrections. The S-waves show an azimuthal pattern, with relatively high amplitudes recorded at East Coast stations. There is no corresponding trend in the ScS data. The factor of 2 to 3 enhancement of the S amplitudes in the East can account for the ScSH/SH amplitude anomaly. Chapter III presents a comparison of the long-period SH amplitude anomalies at North American stations for the Argentine and Sea of Okhotsk source regions. The Argentine data generally show relative enhancement of the SH amplitudes at East Coast stations, which indicates that the trend in Figure I.2.4 is not due to receiver structure.

Further evidence that the SH waves from Argentina are anomalous is given in Chapter II, which analyses the travel times from this data set. There it is shown that the SH-waves are 2 to 5 sec late at the East Coast stations, and that this is because they encounter an anomalously low velocity region in the lower mantle at depths of 1700 to 2700 km. The ScS times at these stations are not anomalous, nor are the S or ScS times at BEC. The map projection of this lower mantle anomaly is shown in Figure I.2.1.

Since the data recorded at East Coast stations appear to be contaminated by an anomaly in the direct S phase, we have removed the

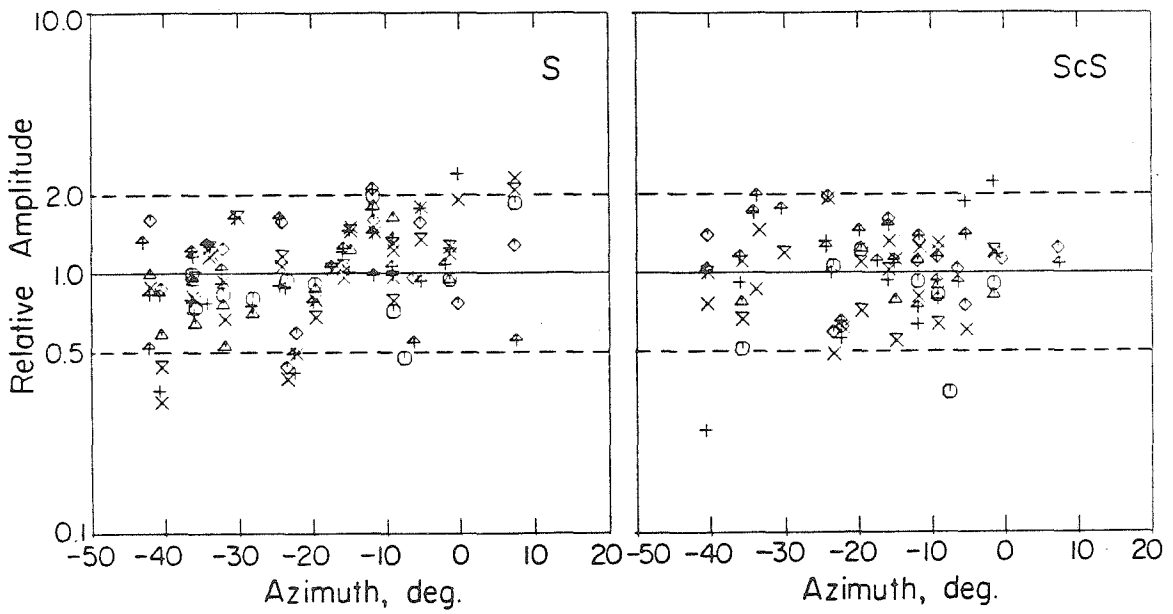

Figure I.2.4. The long period first peak SH (left) and ScSH (right) amplitudes from the Argentine events plotted as a function of azimuth from the source. Radiation pattern and geometrical spreading corrections have been applied as well as event size corrections. Note the relatively high S amplitudes recorded at East Coast station, whereas the ScS amplitudes at these stations are not enhanced. The symbols are the same as in Figure I.2.3. ScS amplitudes at distances greater than 75^{o} are not included.

East Coast observations from the Argentine data set in Figure I.2.5. The observations at BEC were retained since they are free of any obvious travel time or amplitude anomaly. As discussed in Chapter II there may be an additional S wave amplitude anomaly in the midwestern and southern stations, with diminished S amplitudes producing large ScS/S ratios. This is not as well-established as the East Coast anomaly, but it should be kept in mind that some of the larger values in Figure I.2.5 may be due to structure along the S-wave path. The JB model provides a reasonable fit to the average amplitude ratio behavior, throughout the range 55^{o} to 75^{o}, and there is no clear fine structure requiring lower mantle complexity. The average observed amplitude ratio level is generally compatible with the calculations for which t^{*}_{β} is the same for S and ScS, which indicates that no low Q_{β} zone at the base of the mantle is required by these data.

We have computed the theoretical ScSH/SH amplitude ratios as a function of distance for modified JB models with positive and negative linear velocity profiles in D". The dashed lines in Figure I.2.5 indicate the envelope of the theoretical ratios for all models with constant gradients over 20 to 200 km thick zones with velocities at the CMB ranging from 7.0 to 7.6 km/sec (7.3 km/sec for the JB model). Models with stronger velocity increases produce large ScS amplitudes around 75^{o} which are inconsistent with the data. Thin (<60 km) negative gradient transition zones reaching velocities less than 7.0 km/sec produce a precursor to ScS which is not observed, so these models can also be ruled out. The individual models produce fine structure in the ScSH/SH amplitude ratios not apparent in the JB model

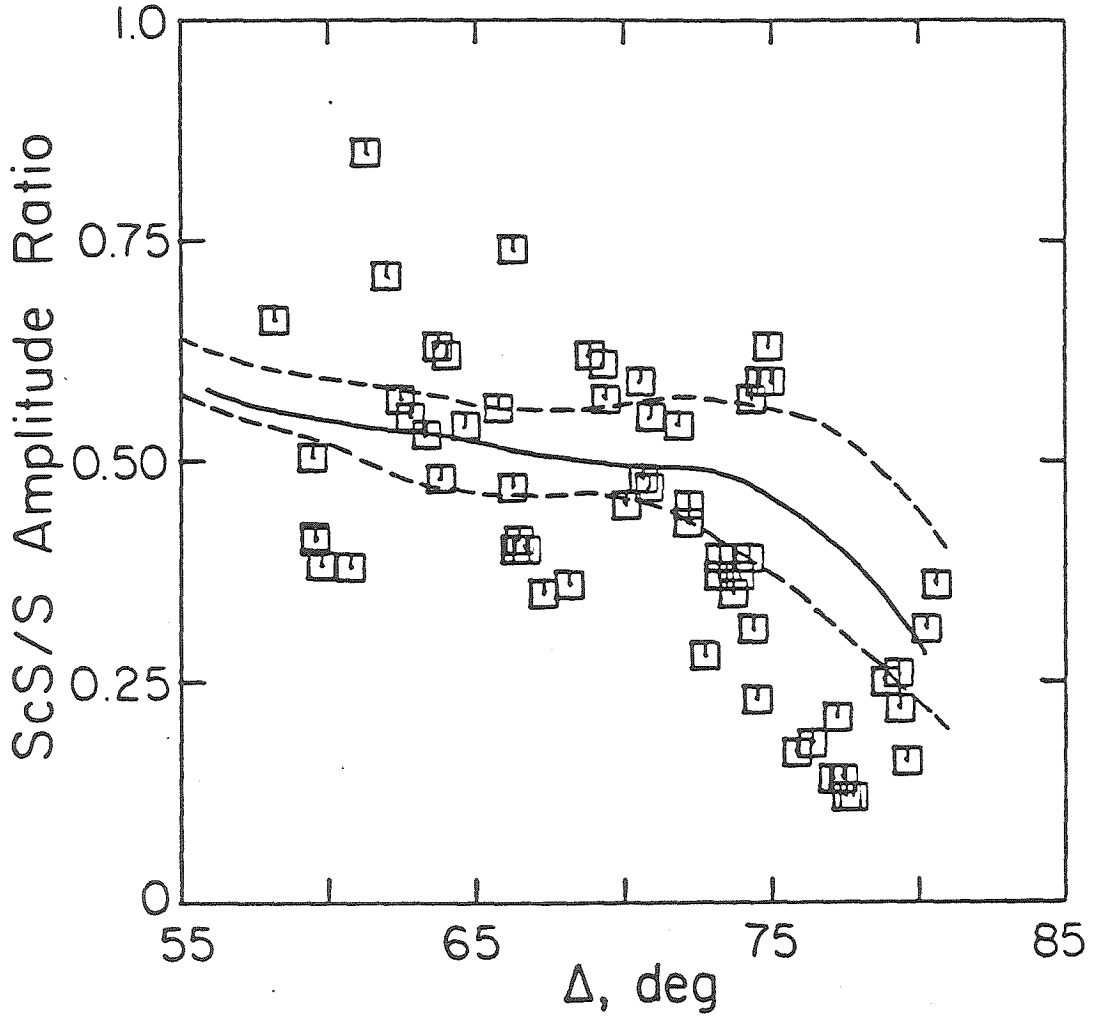

Figure I.2.5. The long-period peak-to-peak ScSH/SH amplitude ratios for the Argentine events recorded in North America at azimuths less than 345°, as well as at BEC. The solid curve shows the theoretical ratios for the JB model. The dashed curves indicate the envelope of amplitude ratios for models with mild positive and negative velocity gradients above the core. Details are given in the text.

calculations, but the data scatter too much to resolve any such features. At distances beyond 75° the theoretical computations scatter more because of the variable interference between S and ScS, and little constraint on the velocity structure can be inferred.

Section I.1 has shown that an S-wave triplication in the Argentine and Sea of Okhotsk data indicates the presence of a 2.75% shear-velocity discontinuity 250 to 280 km above the CMB. The presence of this structure does not strongly affect the ScSH/SH amplitude ratios, so the results found here using the JB model as a reference mantle structure apply to models with a discontinuity at the top of D" as well.

In Figure I.2.6 the long-period ScSH/SH amplitude ratios for the 10 Sea of Okhotsk events recorded in North America are shown as a function of distance. The amplitude ratios are corrected for radiation pattern. The source parameters and focal mechanisms for these events are given in Tables I.1.1 and I.1.2. The data appear to be largely free of trends due to azimuthal anomalies in the travel times or amplitudes, though there are large isolated fluctuations. The region of D" sampled lies below Alaska and western Canada. There is again a large amount of scatter, but the observations are numerous enough to compute meaningful averages in each 5° increment of distance, as shown. The data are reliable to a distance of 75°, beyond which the ScS phases interfere with the arrivals of the lower mantle triplication (Section I.1).

As for the Argentine data, the JB model produces a reasonable fit to the average ScSH/SH observations. The slight dip observed near 60°

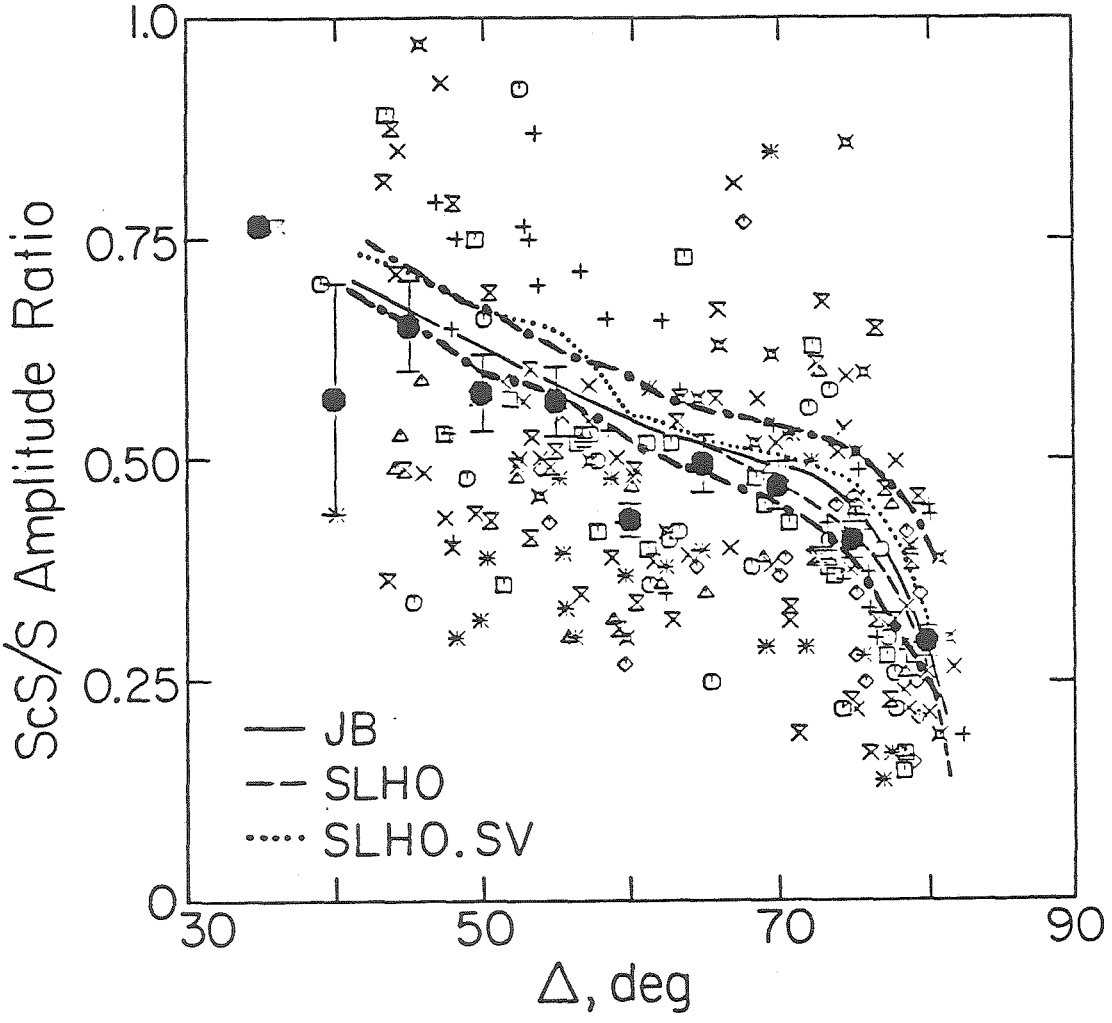

Figure I.2.6. The long period peak-to-peak ScS/S amplitude ratio for Sea of Okhotsk observations in North America. Different symbols correspond to different events. The solid symbols give the mean and standard error of the observations in each 5^{o} increment of distance. At distances greater than 75^{o} the amplitude ratio is comtaminated by interference between S and ScS. The labeled curves are theoretical ratios measured from synthetics for the models discussed in the text. The dash-dot curves indicate the envelope of theoretical ratios for the models with mild positive and negative linear gradients in D" discussed in the text.

may be resolvable, but is not a prominent feature. While many data points lie below the JB predictions, there is no compeling evidence for a low Q_β region in D" for this path. The dash-dot curves indicate the same range in theoretical amplitude ratios as shown in Figure I.2.5 and discussed above. These are consistent with the data averages in the range 40^o to 75^o. None of the constant gradient models investigated produce a localized minimum near 60^o. Model SLHO is a structure with a 2.75% S-wave velocity discontinuity 278 km above the CMB determined for this path in Section I.1. The velocity gradient in D" is slightly positive for this model, and the predicted ScSH/SH ratios are practically indistinguishable from those of the JB model. Model SLHO.SV, which is derived below, is similar to SLHO, but has a 20 km thick high velocity (7.6 km/sec) layer just above the core. This sharp velocity increase produces little effect on the long-period ScSH/SH ratios, which indicates the insensitivity of the SH phases to thin regions of high velocity gradient near the CMB. Clearly, the long-period ScSH/SH amplitude ratios do not uniquely constrain the shear-velocity gradient in D". The data are consistent with the JB model or with models with slightly positive or negative gradients in D".

ScSV-ScSH Travel Time Data

Mitchell and Helmberger (1973) suggested that comparison of the arrival time of long-period ScSV and ScSH can be used to determine the shear-velocity gradient just above the core. They found that in the range 60^o to 75^o the peak of ScSV arrives progressively later than the peak of ScSH for the Argentine data. This shift was attributed to an

interference effect produced by ScS precursors reflected from a positive velocity gradient at the base of D". Such a gradient produces a reflection in phase with ScSH and out of phase with ScSV, which causes a relative shift in the peak arrival of the core reflection on long-period records.

In this data set the SV signals are often nodal at the North American stations, but enough reliable observations could be made to test the relative ScS timing. If one compares the ScSH and ScSV arrivals for the Sea of Okhotsk data, it is found that beyond 75^{o}, the apparent ScSV arrival is late relative to ScSH. This is demonstrated in Figure I.2.7. Noting that the ScS arrival should have upward motion in the figure for both components, it is clear that the peak of the ScSV component is shifted by as much as 4 s relative to the peak of ScSH. The direct S pulses show no corresponding shift. Since the SKS arrival pulls ahead of ScSV beyond 70^{o}, as was seen in Figure I.1.21, one might attribute this shift to the interference between the downswing of the SKS arrival and the ScSV upswing. However, the ScSV shift is still observed at 80^{o} where SKS is relatively far ahead of ScSV. Furthermore, when we compute SV synthetics including the SKS arrival, no differential ScSV shift is observed, as shown below.

The peak-to-peak ScS-S differential times on the radial and tangential components were measured for all of the Sea of Okhotsk data for which the phases are fairly clear on both components at North American stations. The difference in these times is plotted against distance in Figure I.2.8, along with the average and standard error of the observations in each 5^{o} increment of distance. While on average

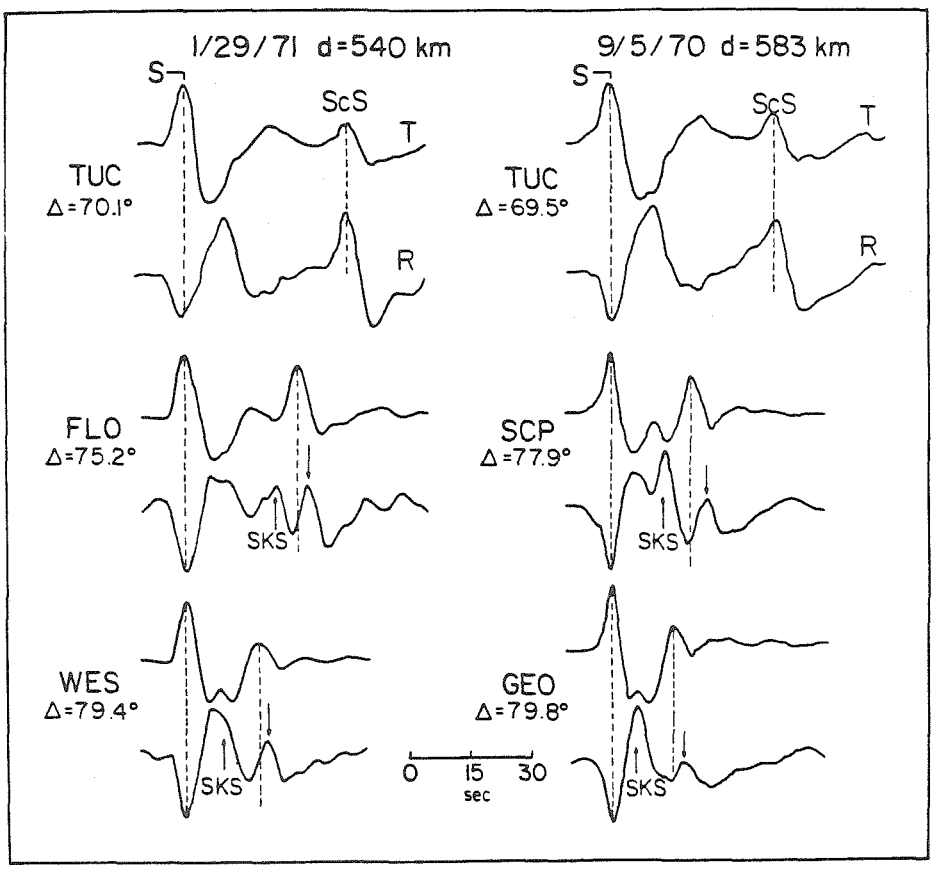

Figure I.2.7. Comparison of tangential (T) and radial (R) components of two deep focus Sea of Okhotsk events recorded in North America. The SH and SV peak amplitudes arrive at the same time at all distances. ScSV and ScSH arrive at the same time near 70°. Beyond 70°, the apparent ScSV arrival (↓) is shifted later than the ScSH arrival. This is not explained simply by the interference of SKS (↑) on the radial component.

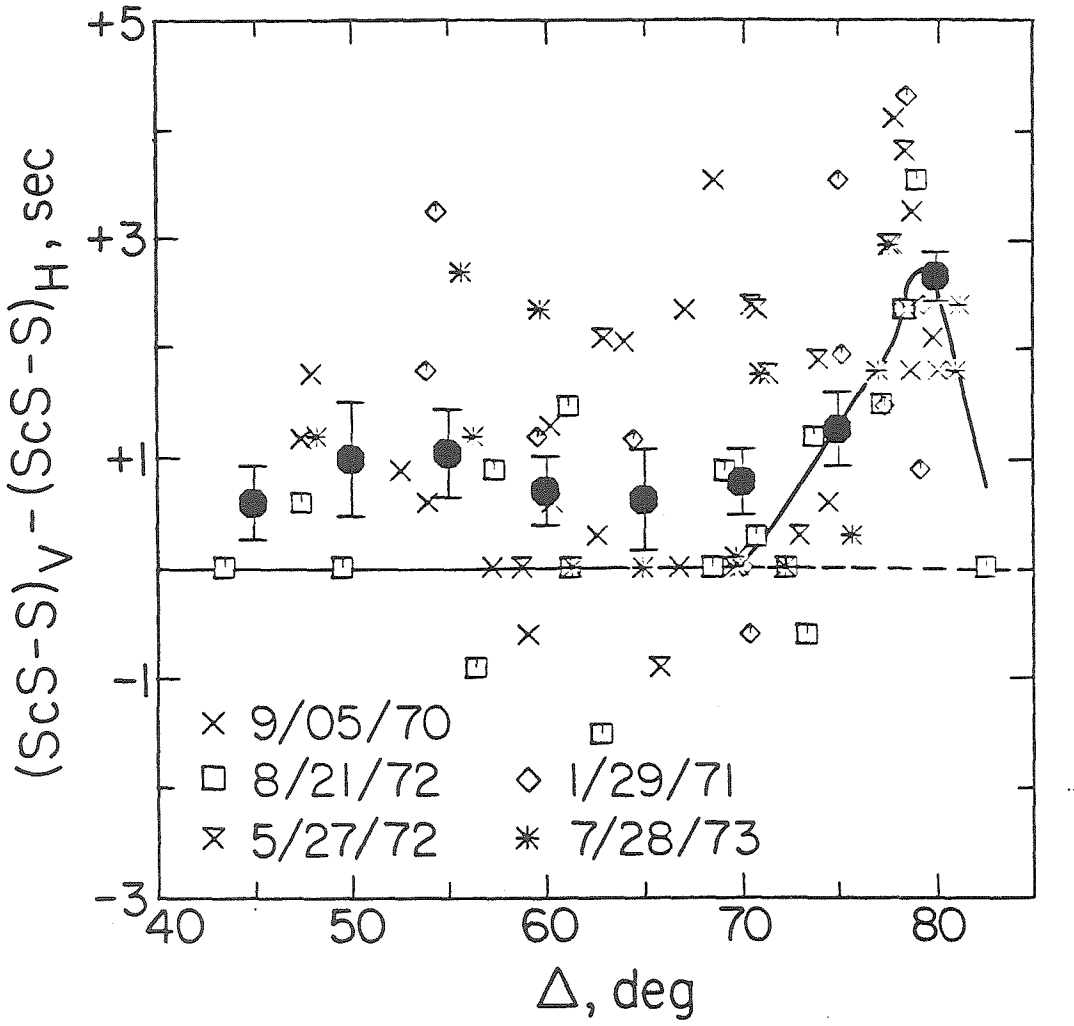

Figure I.2.8. Observed differences in ScS-S differential times measured peak-to-peak on the long period radial and tangential components for the Sea of Okhotsk observations in North America. The solid symbols give the mean and standard error of the observations in each 5^{o} increment in distance. The solid curve is for model SLHO.SV.

there is a slight positive residual at all distances, which is difficult to explain as a structural effect, there is a clear increase in the differential measurement beyond 70^{o}. Since the peaks of the direct arrivals are found to be at the same time in almost all cases, this difference is basically a measure of the ScSV-ScSH difference. The large number of observations indicates the robustness of this anomaly. The distance dependence of this observation suggests that it results from velocity structure rather than anisotropy or lateral variations in D". We have, therefore, sought to explain the observation by introducing fine velocity structure into the D" region. Following the reasoning of Mitchell and Helmberger (1973), it is possible to produce this apparent shift in ScSV relative to ScSH by producing an interfering arrival just ahead of the core reflection. To obtain the differential behavior, this precursor should have the same polarity as ScSH and opposite polarity to ScSV. A strong positive velocity gradient or discontinuity can accomplish this as suggested above.

Through trial-and-error waveform modeling we have obtained a modified SLHO model which satisfies both SH and SV observations from the Sea of Okhotsk recorded in North America. This model, SLHO.SV, is presented in Figure I.2.9. The major modification of SLHO is the introduction of a thin high velocity layer 20 km thick at the base of D". This layer produces a strong post-critical reflection which interferes with ScSH constructively, and a negative reflection which interferes with ScSV destructively producing a relative shift in the peak arrival time of ScSV. The velocity increase must be on the order

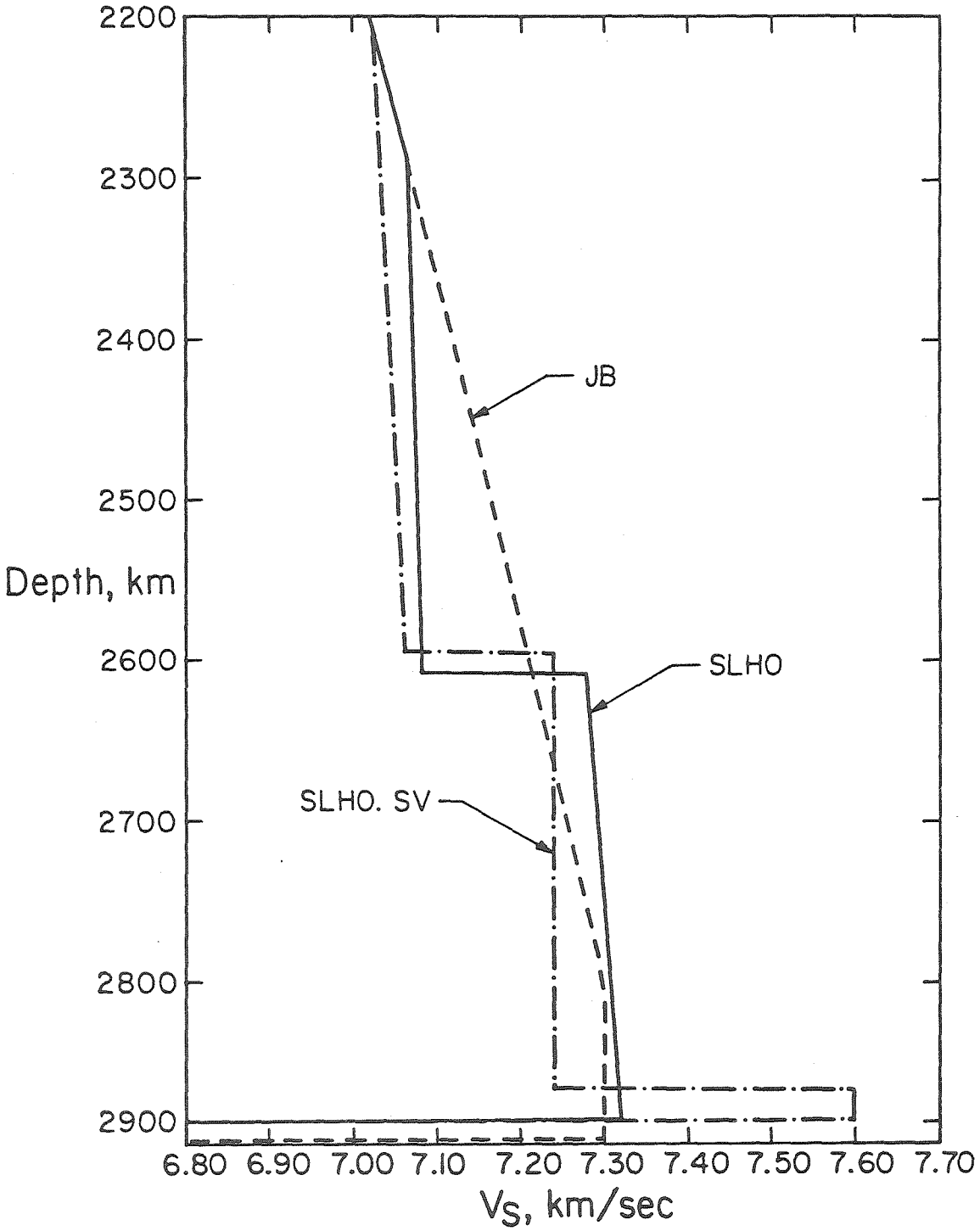

Figure I.2.9. Comparison of model SLHO and SLHO.SV. SLHO satisfies the SH data alone, and SLHO.SV satisfies both SH and SV for the Sea of Okhotsk events recorded in North America.

of 5% in order to produce as much as 3 s shifts in the peak of ScSV. The differential ScSV-ScSH travel times measured from synthetic seismograms for this model are plotted in Figure I.2.8. These fit the average data well, though the largest anomalies are a full second greater than even SLHO.SV predicts. Beyond 80^{o} the post-critical reflection weakens and the interference producing the ScSV shift diminishes.

In the course of modeling the SV seismograms it was necessary to adopt a core model that predicts the correct SKS timing and amplitude. We measured the differential times of SKS-Sab for all the Okhotsk observations and found that these times were on average 4 s greater than for the JB model, and only 1 s slower than for the Hales and Roberts (1971) model. Since the primary difference between these two models affecting SKS-S times is the lower velocities in the outermost core of the Hales and Roberts (HR) model, we adopted their core velocity structure as a starting model. Combining this model with SLHO produces excellent SKS-S travel time agreement with the data throughout the range 70^{o}-83^{o}. In determining the SLHO.SV model it was necessary to simultaneously adjust the core velocities in the outermost 100 km of the core. Figure I.2.10 shows the starting SLHO and HR model and the final SLHO.SV model. The depths at which SKS bottoms in the outer core for various distances are indicated. Note that the modified core model of SLHO.SV has a somewhat smoother gradient in the outer 300 km of the core than the Hales and Roberts model, which is consistent with most other core models. This change in gradient can be resolved in the data by comparison of ScSV and SKS

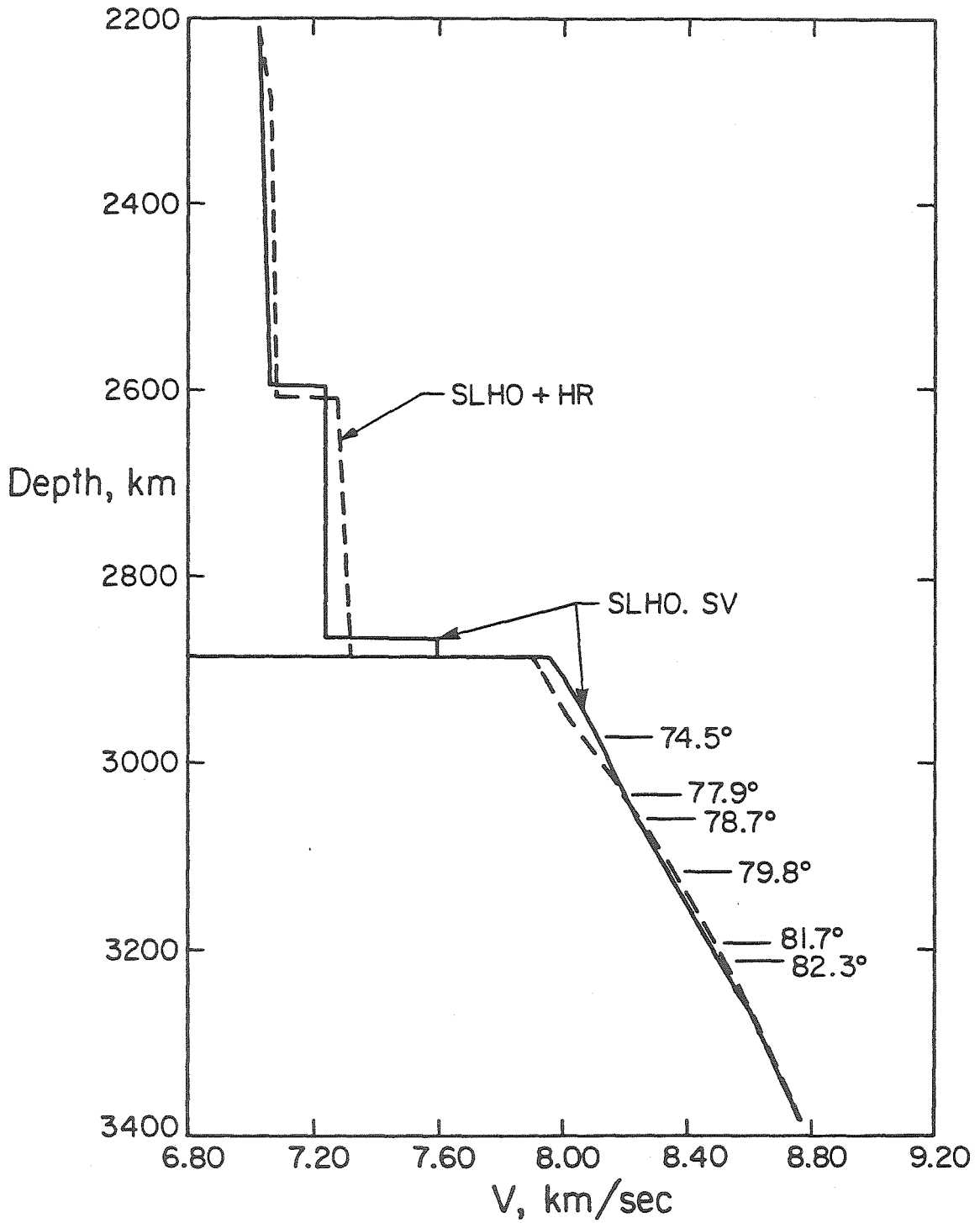

Figure I.2.10. Comparison of the starting (SLHO + HR) and final (SLHO.SV) models for the SV structure of the lower mantle and P wave structure of the outer core for paths from the Sea of Okhotsk to North America. The starting core model is from Hales and Roberts (1971). The bottoming depths for the SKS arrivals in the SLHO.SV synthetics in Figure I.2.11 are indicated by the distances.

at distances less than 75^{o}. Modeling additional direct SKS data in this distance range promises to yield exceptional resolution of the outermost core velocities, which can otherwise only be roughly obtained using SK_nS multiples.

Model SLHO.SV was determined not only by fitting the differential travel time of ScSV, but by fitting the entire SH and SV waveforms. In Figure I.2.11 observed SH and SV signals are compared with ray theory synthetics for the SLHO and HR model (top trace in each comparison). While SLHO fits all of the SH signal and the SV data are adequately modeled through the SKS arrival, at each station the peak ScSV signal is too early in all of the synthetics for this model. This proves true for any shear velocity model with flat gradients above the CMB. The synthetics for model SLHO.SV (bottom trace in each comparison) are equally good for the SH signals, with only slight discernible differences from the SLHO synthetics. However, now the entire SV waveform is well modeled, including the splitting of the SKS and ScSV signals at FLO and the long period ScSV coda at WES, GEO and SCP. In generating the synthetics for model SLHO.SV the first three multiple S bounces within the high velocity layer have been included. The lack of sensitivity of the SH data to a thin high velocity region is a bit surprising and indicates the insensitivity of the ScSH/SH amplitude ratio for modeling D'' velocity structure. The synthetic SH amplitude ratios for SLHO.SV are included in Figure I.2.6, which shows that the SH data are quite consistent with model SLHO.SV.

The synthetic SV waveform improvement is quite substantial for model SLHO.SV; however, we feel that additional data must be obtained

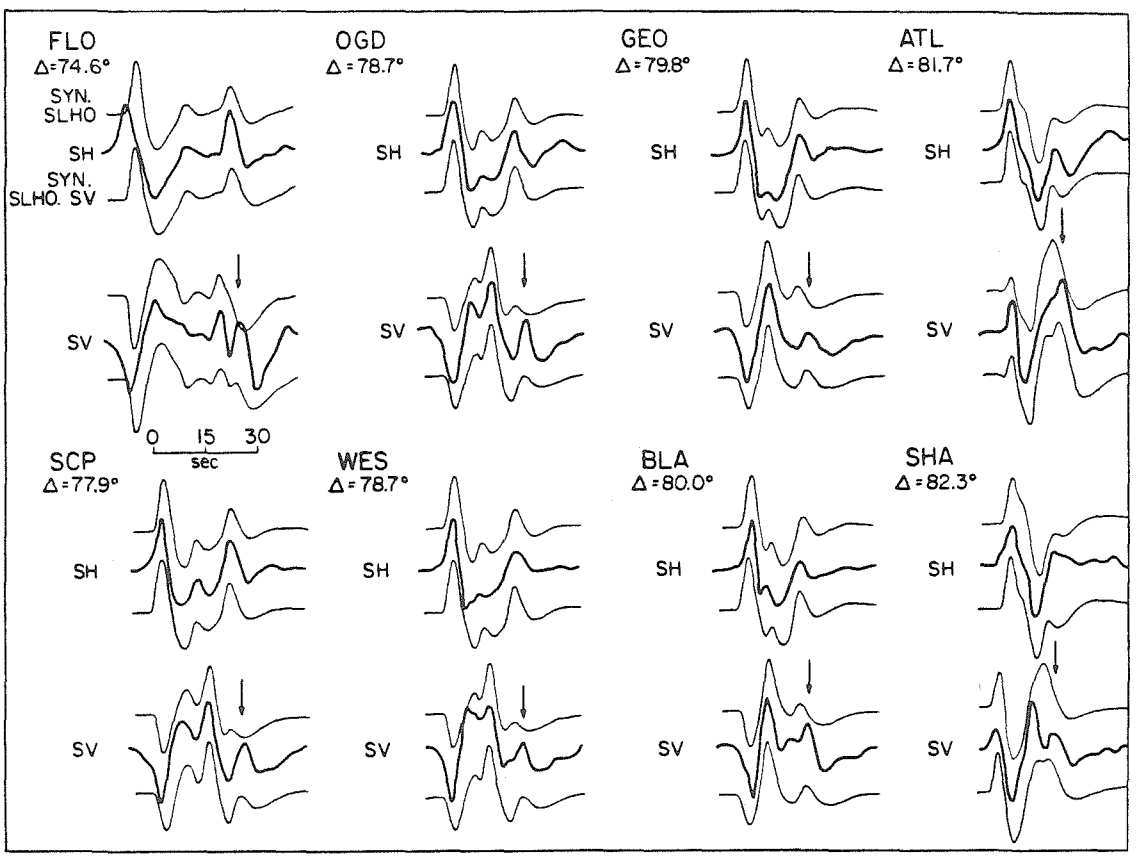

Figure I.2.11. Observed and synthetic SH and SV signals for the deep Sea of Okhotsk event of September 5, 1970. The top synthetic in each trace is for model SLHO overlying a Hales and Roberts (1971) core model. The lower synthetic is for model SLHO.SV (Figure I.2.10) overlying a modified core model. Both models fit the SH observations well, but for model SLHO the ScSV portion of the waveform (↓) is not accurately modeled. The interference caused by the high velocity layer in model SLHO.SV fits the entire SV waveform.

before a definitive model can be determined. In particular, the thickness and velocity contrast of the high velocity layer in model SLHO.SV are not uniquely constrained. The SV waveforms in the range 75^{o}-85^{o} represent a complicated interference pattern between SK_nS, SVab, SVcd, and ScSV, and one must be cautious in interpreting this complexity. However, it does appear that localized strong positive velocity gradients exist in the D" region.

For most of the Argentine events, the SV signals are very nodal, however there are enough observations with stable SH and SV signals to make a comparison of the ScSV and ScSH arrivals. Mitchell and Helmberger (1973) previously reported a systematic increase in the apparent ScSV-ScSH arrival time difference for the Argentine data in the range 65^{o} to 75^{o}. Our data set is shown in Figure I.2.12, with the number of Argentine observations being about twice that shown by Mitchell and Helmberger (1973). While there is a slight increase in the differential times near 75^{o}, there is no trend comparable to that in the Sea of Okhotsk data shown in Figure I.2.8. Near 75^{o} it is difficult to time ScSV because SKS arrives just a few seconds ahead, and near 80^{o} it is difficult to identify the ScS arrival, but there is no indication of an interference effect. We feel that these data do not indicate the presence of a strong positive velocity increase like that sampled by the path from the Sea of Okhotsk to North America. Therefore it appears that the high velocity layer producing the interference varies laterally.

As in Section I.1 it is desirable to check the SH synthetics generated by the Cagniard de Hoop method by comparing them with the

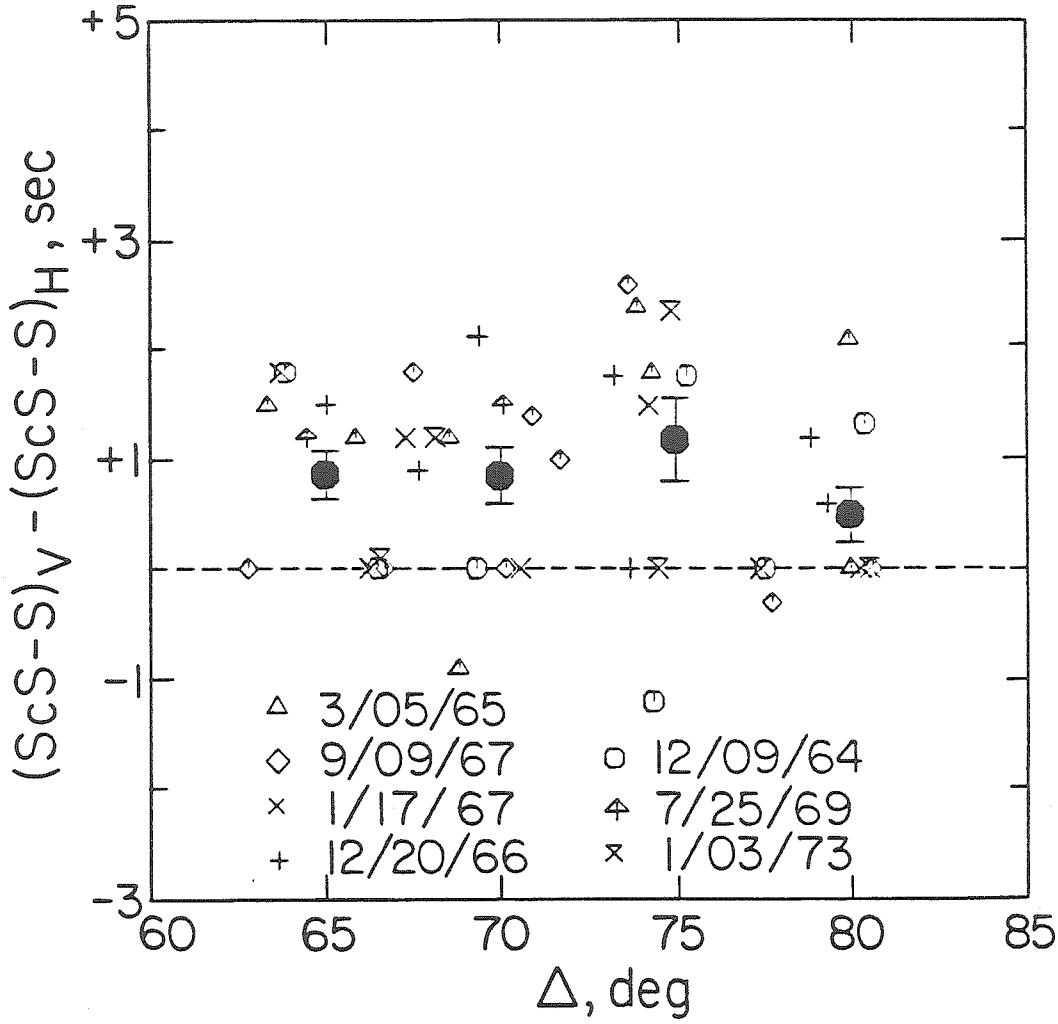

Figure I.2.12. Observed differences in ScS-S differential times measured peak-to-peak on the radial and tangential components for Argentine observations in North America. The solid symbols give the mean and standard error of the observations in each 5^{o} increment in distance.

reflectivity method developed by Fuchs and Müller (1971) and Kind and Müller (1975). The effect of multiple bounces within the high velocity layer in model SLHO.SV is particularly important to assess. Figure I.2.13 compares synthetic profiles for the two methods for a source depth of 580 km and no Q structure. The generalized ray theory (GRT) and reflectivity synthetics for model SLHO.SV are almost indistinguishable from those for model SLHO.

Figure I.2.14 shows reflectivity synthetics for diffracted SH for the JB model and the two Sea of Okhotsk models. The source wavelet has a dominant period of 20 sec, which is comparable to that of long period diffracted SH observations at WWSSN stations. In the range 95^{o} to 100^{o} the Sab branch produces a secondary arrival which diminishes rather quickly. For model SLHO.SV the amplitude decay into the shadow region is more rapid than for the JB and SLHO models. Depending on the extent of the high velocity layer, it may or may not be possible to detect this subtle difference by analyzing diffracted SH waves.

Discussion

The ScSH data presented in this section do not provide tight constraints on the D" shear-velocity structure, due to both the large amount of scatter in the amplitude data and the intrinsic lack of sensitivity to fine velocity structure of the long-period phases. However, the amplitude data do not clearly require major deviations from the smoothly varying velocity gradients in D" of the JB model. Analysis of diffracted phases and short period signals may provide higher resolution of the shear-velocity gradients above the core, however, future efforts must concentrate on regional variations more

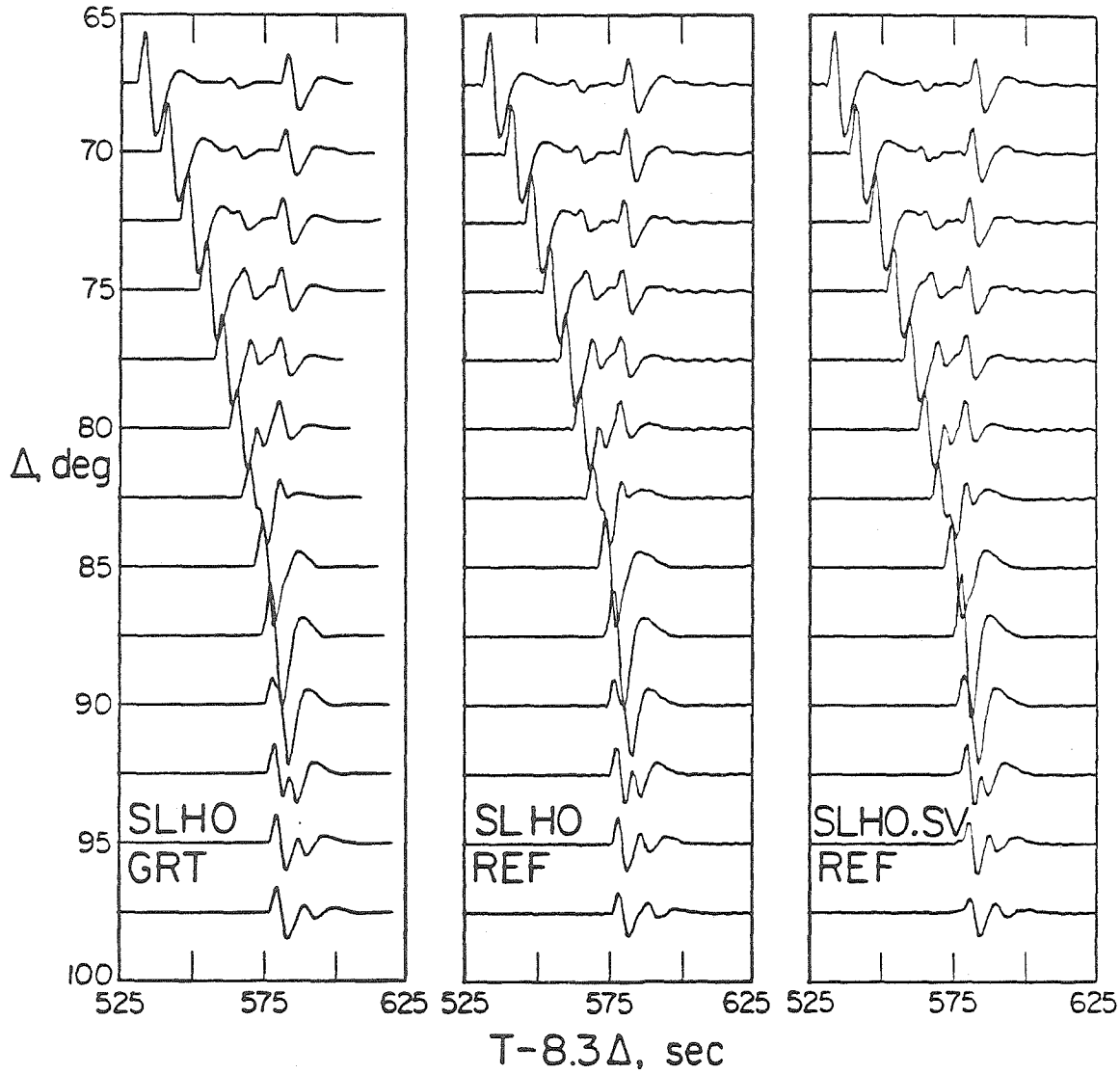

Figure I.2.13. SH synthetics computed with the Cagniard de Hoop generalized ray theory (GRT) technique and the reflectivity (REF) technique for the Sea of Okhotsk models. The agreement between these techniques throughout the entire range of the lower mantle triplication is clearly apparent. The introduction of the thin high velocity layer in model SLHO.SV does not strongly affect the SH signals.

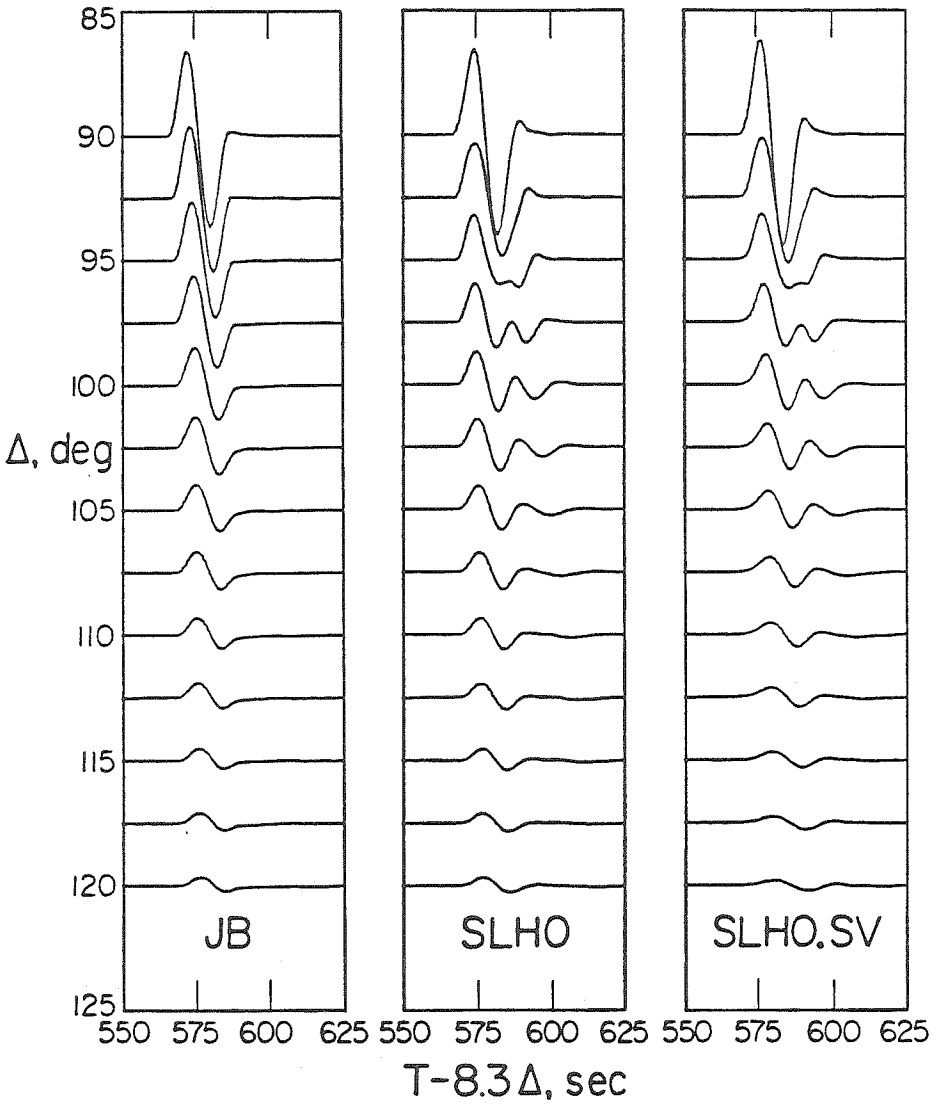

Figure I.2.14. SH synthetics for the JB and Sea of Okhotsk models shown in Figure I.2.9. The reflectivity technique was used to compute the signals. The amplitude scale is the same for all three models. The presence of the receding Sab branch causes the distortion in the range 95^{o} to 100^{o} for models SLHO and SLHO.SV. The diffracted signals, beyond 105^{o}, are very similar for the three models, with little discernible difference in waveform character. The high velocity layer in SLHO.SV causes a more rapid amplitude decay of diffracted S than in the other models.

than previous work. Future studies must also place greater emphasis on eliminating the spectral contamination due to complex receiver structures (Chapter III) before spectral analysis of diffracted waves and short periods will yield high resolution of lower mantle structure. Section I.1 showed that there are resolvable lateral variations in the velocity structure at the top of D". The ScSV-ScSH differential travel times shown here indicate lateral variations in the fine structure at the base of D" as well. The thin high velocity region at the base of the mantle detected in the Sea of Okhotsk data does appear to vary laterally, as might be expected for such a thin, anomalous layer. Possibly this layer represents a localized compositional heterogeneity. Such a feature may serve as the type of scatterer often attributed to the D" region (e.g. King et al., 1973; Haddon and Cleary, 1973).

While this section has reassessed the data and interpretations presented by Mitchell and Helmberger (1973), and yields very different results, their basic approach to the data remains sound. ScS phases sample very localized portions of the D" region, which provides an opportunity to study lateral variations in the region obscurred in travel time or diffracted wave studies. It is important to exercise caution when interpreting differential times and relative amplitudes because of the accumulating evidence for large velocity and amplitude anomalies produced by deep source region structure and localized anomalies in the central part of the lower mantle (Jordan, 1977; Chapter II).

Conclusions

An analysis of long-period ScS amplitude behavior indicates that the JB model or models with mild positive or negative velocity gradients above the core-mantle boundary are consistent with data for two distinct regions of D". An ScSH/SH amplitude ratio minimum reported by Mitchell and Helmberger (1973) appears to result from anomalous S amplitudes rather than from D" structure. The long-period ScS amplitudes do not give any clear indication of a very low Q_β zone at the base of the mantle. A systematic distance trend in the difference of the peak arrival times of ScSH and ScSV for paths below Alaska indicates the presence of a localized high velocity gradient just above the core. This structure appears to vary laterally, for data from South American earthquakes do not show a similar trend. A refined outer core P wave velocity model is determined by modeling SKS signals in the range 75^{o} to 85^{o}.

References

Anderson, D. L. and R. S. Hart (1976). An earth model based on free oscillations and body waves, J. Geophys. Res., 81, 1461-1475.

Anderson, D. L. and R. S. Hart (1978). Q of the Earth, J. Geophys. Res., 83, 5869-5882.

Bolt, B. A. M. Niazi and M. R. Somerville (1970)., Diffracted ScS and the shear velocity at the core boundary, Geophys. J. Roy. Astron. Soc., 19, 299-305.

Bullen, K. E. (1949). Compressibility-pressure hypothesis and the Earth's interior, Monthly Not. Roy. Astron. Soc., 5, 355-368.

Bullen, K. E. (1963). An Introduction to the Theory of Seismology, Cambridge Univ. Press, London, pp. 381.

Cleary, J. (1969). The S velocity at the core-mantle boundary, from observations of diffracted S, Bull. Seismol. Soc. Amer., 59, 1399-1405.

Cleary, J., K. Porra and L. Reed (1967). Diffracted S, Nature, 216, 905-906.

Doornbos, D. J. and J. C. Mondt (1979). P and S waves diffracted around the core and the velocity structure at the base of the mantle, Geophys. J. Roy. Astron. Soc., 57, 381-395.

Doyle, H. A. and A. L. Hales (1967). An analysis of the travel times of S waves to North American stations, in the distance range 28^{o} to 82^{o}, Bull. Seismol. Soc. Amer., 57, 761-771.

Dziewonski, A. M. and D. L. Anderson (1981). Preliminary reference Earth model, Phys. Earth Planet. Interiors, 25, 297-356.

Dziewonski, A. M. and R. A. W. Haddon (1974). The radius of the core

mantle boundary inferred from travel time and free oscillation data; a critical review, Phys. Earth Planet. Interiors, 9, 28-35.

Fuchs, K. and G. Müller (1971). Computation of synthetic seismograms with the reflectivity method and comparison with observations, Geophys. J. Roy. Astron. Soc., 23, 417-433.

Gilbert, F. and A. M. Dziewonski (1975). An application of normal mode theory to the retrieval of structural parameters and source mechanisms from seismic spectra, Phil. Trans. Roy. Soc. London, Ser. A, 278, 187-269.

Haddon, R. A. W. and J. R. Cleary (1973). Evidence for scattering of seismic PKP waves near the mantle-core boundary, Phys. Earth Planet. Inter., 8, 211-234.

Hales, A. L. and J. L. Roberts (1970). The travel times of S and SKS, Bull. Seismol. Soc. Amer., 60, 461-489.

Hales. A. L. and J. L. Roberts (1971). The velocities in the outer core, Bull. Seismol. Soc. Amer., 61, 1051-1059.

Helmberger, D. V. (1974). Generalized ray theory for shear dislocations, Bull. Seismol. Soc. Amer., 64, 45-64.

Jeffreys, H. and K. E. Bullen (1940). Seismological Tables, 55 pp., Brit. Assoc. Advancement of Sci., Gray-Milne Trust, London.

Jordan, T. H. (1977). Lithospheric slab penetration into the lower mantle beneath the Sea of Okhotsk, J. Geophysics, 43, 473-496.

Kind, R. and G. Müller (1975). Computations of SV waves in realistic earth models, J. Geophys., 41, 149-175.

King, D. W., R. A. W. Haddon and J. R. Cleary (1973). Evidence for

seismic wave scattering in the D" layer, Earth Planet. Sci. Letters, 20, 353-356.

Mitchell, B. J., and D. V. Helmberger (1973). Shear velocities at the base of the mantle from observations of S and ScS, J. Geophys. Res., 78, 6009-6020.

Mondt, J. C. (1977). SH waves: Theory and observations for epicentral distances greater than 90 degrees, Phys. Earth Planet. Interiors, 15, 46-59.

Mula, A. H. G. 1981. Amplitudes of diffracted long-period P and S waves and the velocities and Q structure at the base of the mantle, J. Geophys. Res., 86, 4999-5011.

Mula, A. H. and G. Müller (1980). Ray parameters of diffracted long period P and S waves and the velocities at the base of the mantle, Pageoph, 18, 1272-1292.

Okal, E. A. and R. J. Geller (1979). Shear-wave velocity at the base of the mantle from profiles of diffracted SH waves, Bull. Seismol. Soc. Amer., 69, 1039-1053.

Press, F. (1966). Seismic velocities in: Handbook of Physical Constants, ed. S. P. Clark, Jr., Geological Society of America, 587 pp., Memoir 97.

Randall, M. J. (1971). A revised travel time table for S, Geophys. J. R. Astron. Soc., 22, 229-234.

Robinson, R. and R. L. Kovach (1972). Shear wave velocities in the earth's mantle, Phys. Earth Planet. Interiors, 5, 30-44.

Ruff, L. and D. V. Helmberger (1982). The structure of the lowermost mantle determined by short period P wave amplitudes,

Geophys. J. R. Astron. Soc., 68, 95-119.

Sengupta, M. K. (1975). The structure of the earth's mantle from body wave observations, Sc.D. Thesis, 578 pp., Mass. Inst. of Technol., Cambridge.

Strelitz, R. (1975). The September 5, 1970 Sea of Okhotsk earthquake: a multiple event with evidence of triggering, Geophys. Res. Lett., 2, 124-127.

Veith, K. F. (1974). The relationship of island arc seismicity to plate tectonics. Ph.D. Thesis, S. Methodist Univ., Dallas.

Wright, C. and J. A. Lyons (1979). The identification of radical velocity anomalies in the lower mantle using an interference method, Phys. Earth Planet. Interiors, 18, 27-33.

Wright, C. and J. A. Lyons (1981). Further evidence for radial velocity anomalies in the lower mantle, Pageoph, 119, 137-162.

Appendices for Chapter I

Appendix I.1

Several additional profiles of data for the Sea of Okhotsk source region, along with synthetics for model SLHO, which was presented in Section I.1, are documented here. These data provide further confirmation of the robustness of the Scd arrival. Figures A.1.1 through A.1.4 show profiles for events at varying depths and distances from North America. The source parameters and focal mechanisms are listed in Tables I.1.1 and I.1.2. Figure A.1.5 presents differential travel time observations and theoretical curves for the September 21, 1974 event. The travel time data for the other events have been included in Figure I.1.13.

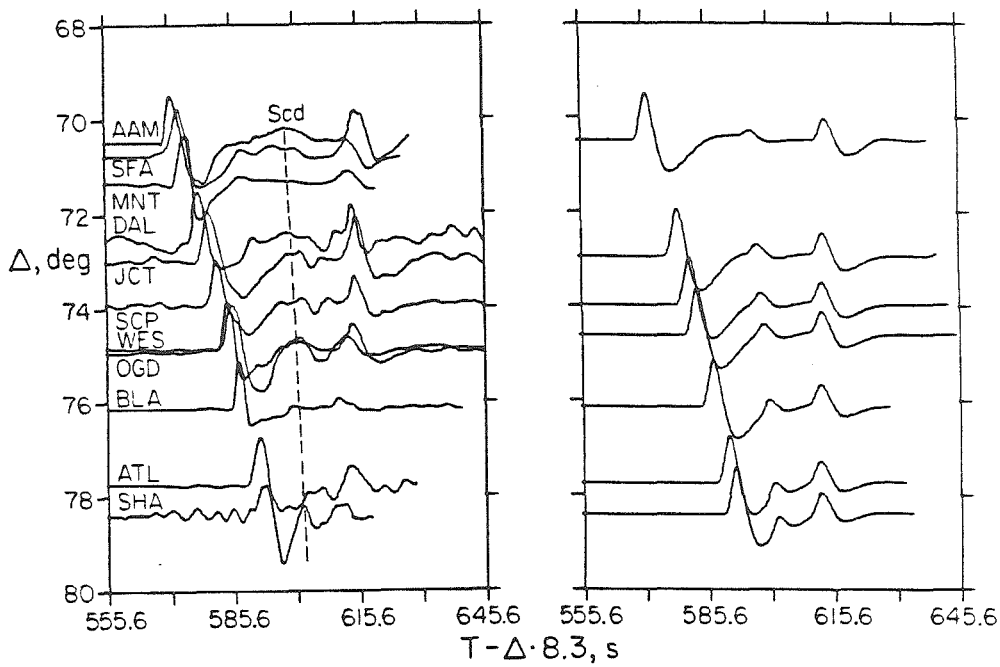

Figure A.1.1 Observed (left) and synthetic (right) profiles of long period SH seismograms for the event of May 27, 1972 (d = 397 km). The JB station residuals have been removed from the data, and the amplitudes are normalized. The synthetics are for model SLHO.

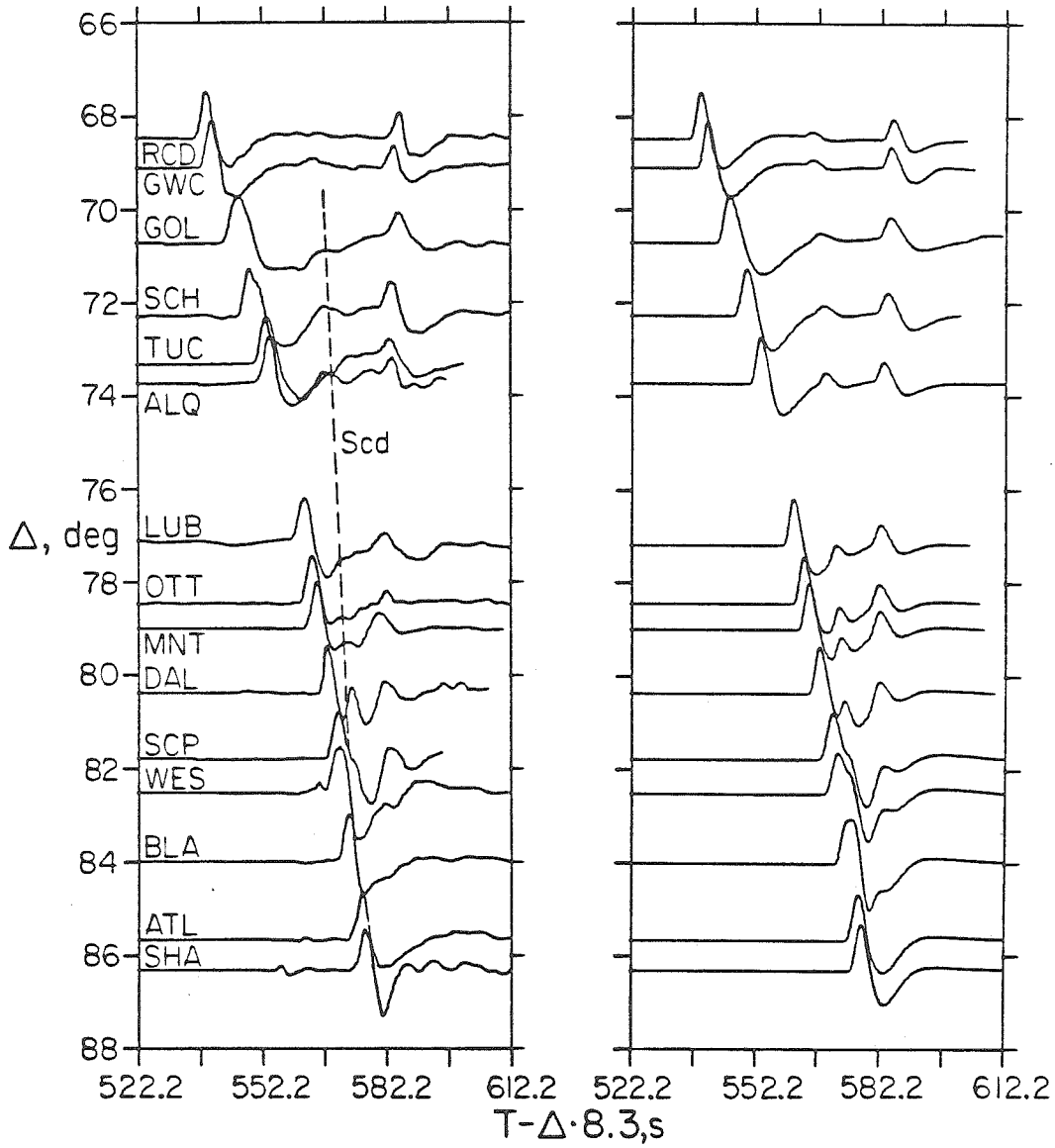

Figure A.1.2 Observed (left) and synthetic (right) profiles of long period SH seismograms for the event of August 21, 1972 (d = 573 km). The JB station residuals have been removed from the data, and the amplitudes are normalized. The synthetics are for model SLHO.

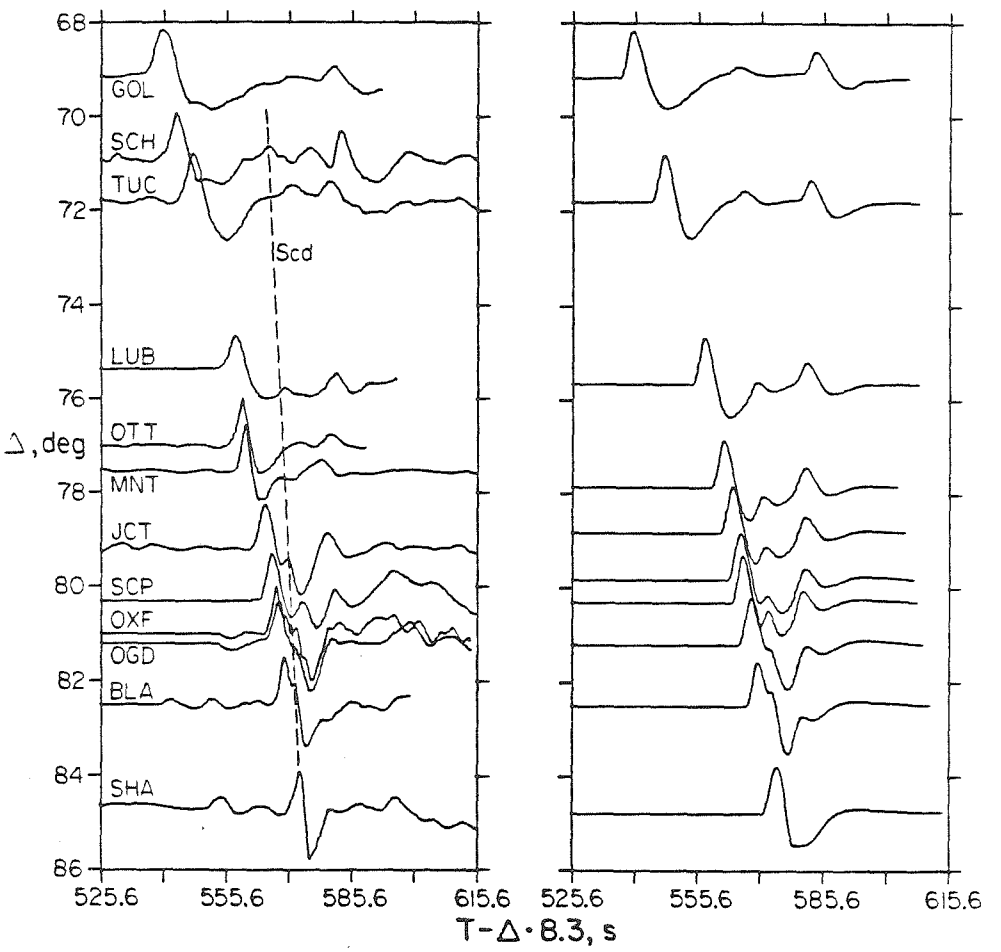

Figure A.1.3 Observed (left) and synthetic (right) profiles of long period SH seismograms for the event of July 28, 1973 (d = 585 km). The JB station residuals have been removed from the data, and the amplitudes are normalized. The synthetics are for model SLHO.

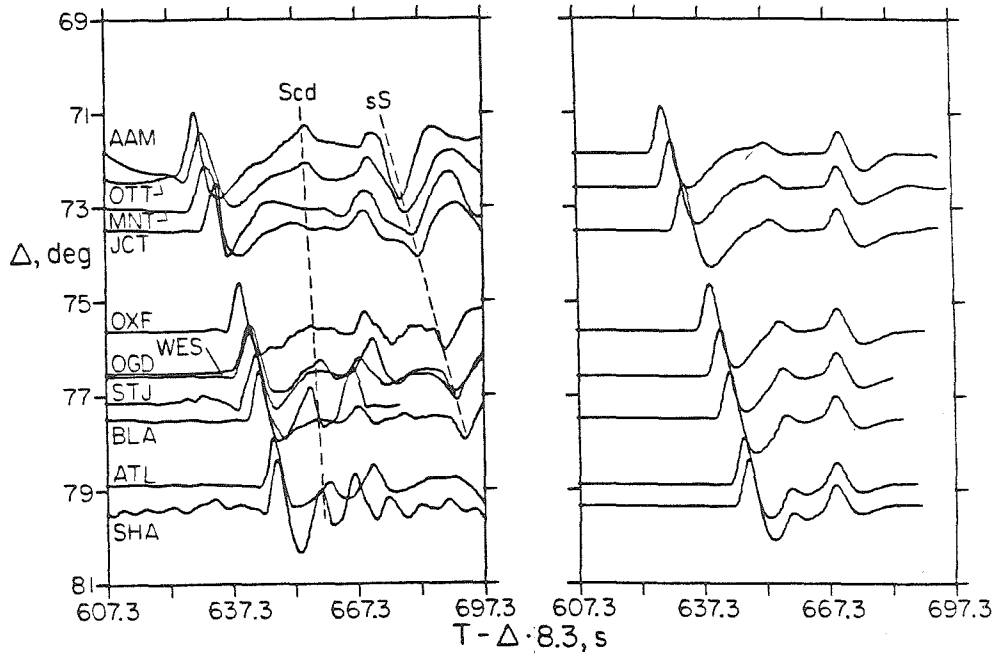

Figure A.1.4 Observed (left) and synthetic (right) profiles of long period SH seismograms for the event of September 21, 1974 (d = 119 km). The JB station residuals have been removed from the data, and the amplitudes are normalized. The synthetics are for model SLHO.

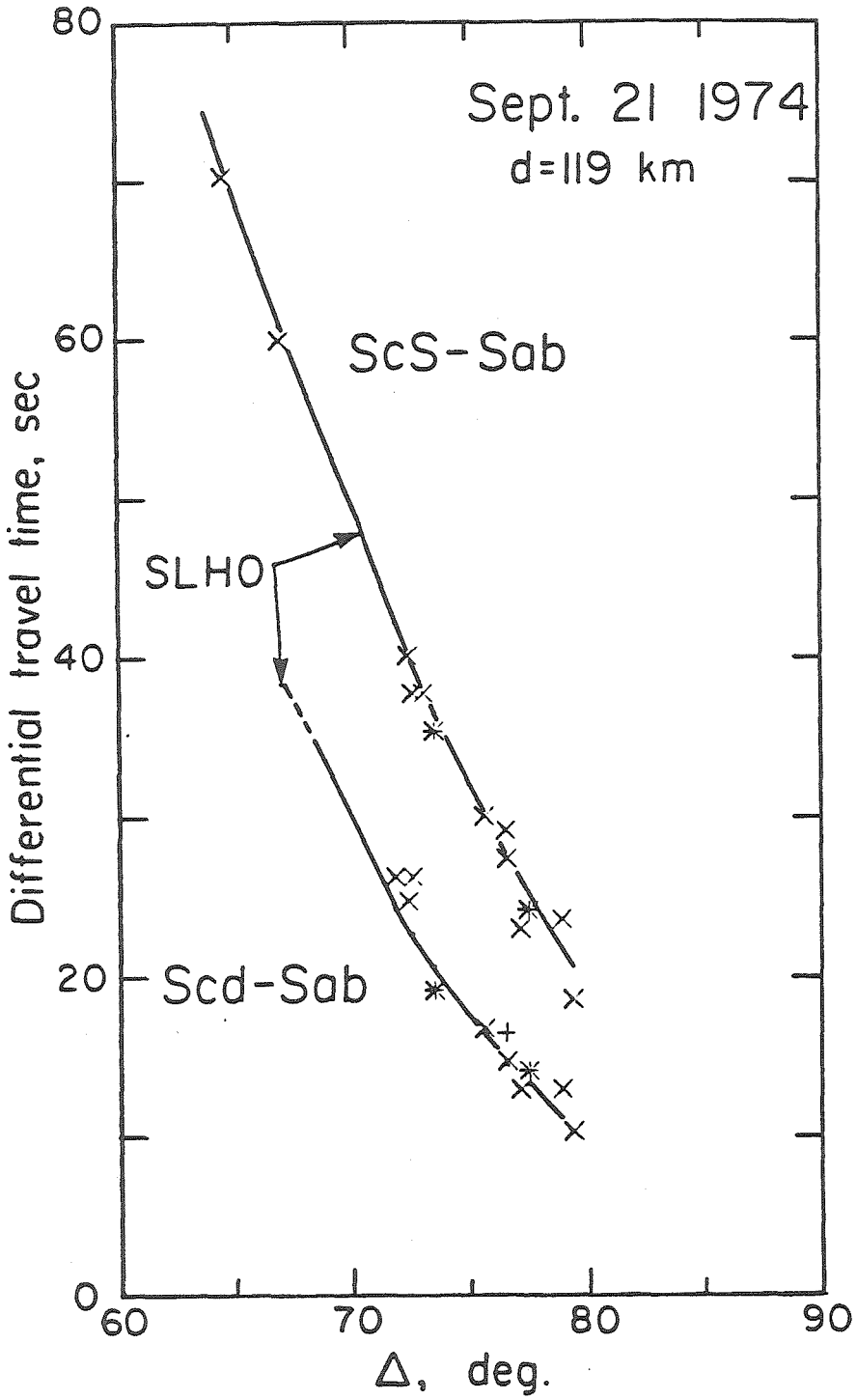

Figure A.1.5 Observed and theoretical differential travel times for the event of September 21, 1974 recorded in North America. The travel times are measured from peak-to-peak for both short period (+) and long period (x) observations. The theoretical times are similarly measured from the synthetic seismograms. The Scd branch has very low amplitude at distances less than 70°.

Appendix I.2

In order to supplement the ScSH/SH amplitude ratio data presented in Section I.2, an additional data set of European observations of the Sea of Okhotsk events is presented here. The data processing is the same as that described in Section I.2, with the source parameters and focal mechanisms being listed in Tables I.1.1 and I.1.2. Examples of the waveforms are shown in Figures I.1.25 and I.1.26. For the range in azimuth to the European stations the SH radiation for the Sea of Okhotsk events is less stable than it is toward North America. Therefore, the radiation corrections increase in size and uncertainty.

Figure A.2.1 shows the long period peak-to-peak ScSH/SH amplitude ratios observed at European stations plotted as functions of distance and azimuth from the sources. Note that relative to the JB model predictions, indicated by the solid line, the observations in the distance range 65^{o} to 70^{o} are low by a factor of two or more. This trend is similar to that observed in the Argentine data in the azimuth range -15^{o} to 0^{o}. However, in this instance there is no clear azimuthal separation of the anomalous ratios, and there are no 'normal' observations in the same distance range as the anomalously low ratios. It is also clear that the amplitude ratio minimum is not a receiver effect, because stations such as AKU and GDH record both large and small amplitude ratios for events at different distances.

The S and ScS amplitudes are plotted separately in Figure A.2.2. Geometric spreading, event size, and radiation pattern corrections have been applied. The amplitude scatter is substantial, and the uncertainty in the radiation pattern corrections is much greater for

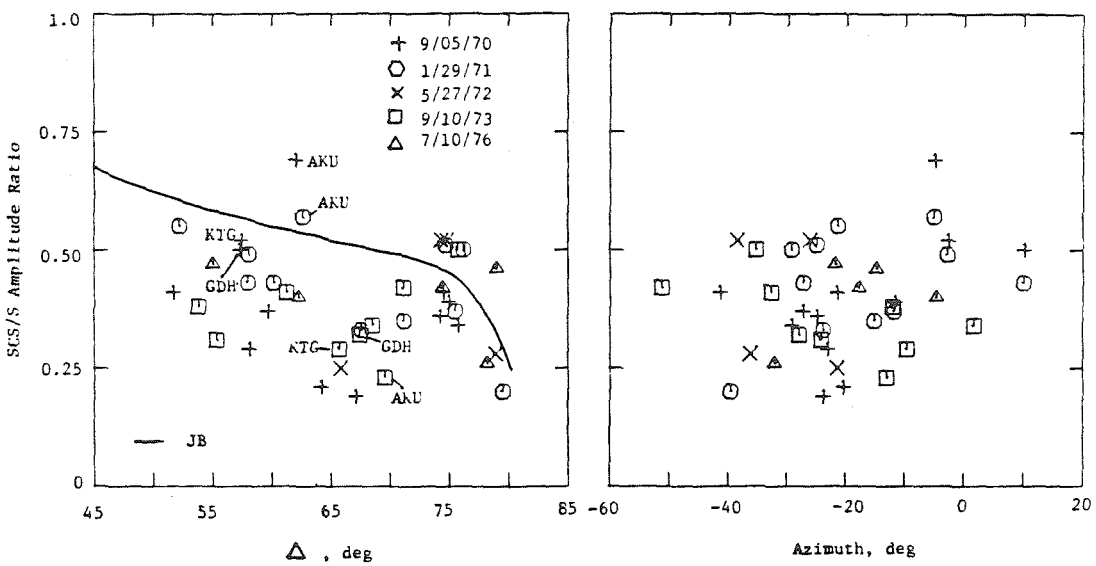

Figure A.2.1 The long period peak-to-peak ScSH/SH amplitude ratios for the Sea of Okhotsk events recorded in Europe, plotted as functions of distance (*left*) and *azimuth* (*right*) *from the source region*. The solid curve indicates the theoretical ratio computed for the JB model.

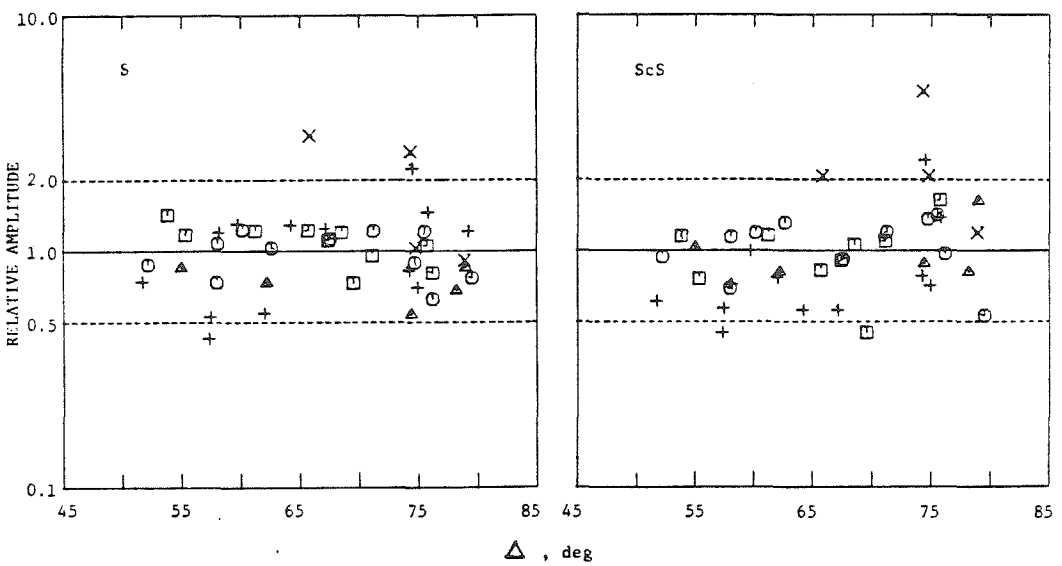

Figure A.2.2 The long period first peak SH (left) and ScSH (right) amplitudes from the Sea of Okhotsk events recorded in Europe, plotted as functions of distance from the sources. Radiation pattern and geometric spreading corrections have been applied as well as event size corrections. The symbols are the same as in Figure A.2.1.

these individual phases than for the ScS/S ratios. In the distance range 65^{o} to 70^{o} the ScS amplitudes tend to be slightly lower than the overall average, and the S amplitudes are slightly higher than the overall average, but neither phase has a clear minimum or maximum to which to attribute the ratio anomaly. It appears that a larger data set is needed (all suitable events presently available have been included here) if these data are to be confidently interpreted. The results of Section I.2 and Chapter II suggest that much caution should be taken when interpreting the relative amplitude of phases which both traverse the lower mantle.

Chapter II

Localized Velocity Anomalies in the Lower Mantle

Abstract

Two localized regions of velocity heterogeneity in the lower mantle with scale lengths of 1000 to 2000 km and 2% velocity contrasts are detected and isolated through comparison of S, ScS, P and PcP travel times and amplitudes from deep earthquakes in Peru, Bolivia, Argentina and the Sea of Okhotsk. Comparison of the relative patterns of ScS-S differential travel time and S travel time residuals across North American WWSSN and CSN stations for the different source regions provides baselines for interpreting which phases have anomalous times. A region of low S and P velocities is located beneath Northern Brazil and Venezuela at depths of 1700-2700 km. This region produces S wave delays of up to 4 s for signals from deep Argentine events recorded at eastern North American stations. The localized nature of the anomaly is indicated by the narrow bounds in azimuth (15^{o}) and take-off angle (13^{o}) of the arrivals affected by it. The long period S waves encountering this anomaly generally show 30 to 100% amplitude enhancement, while the short period amplitudes show no obvious effect. The second anomaly is a high velocity region beneath the Caribbean originally detected by Jordan & Lynn (1974), who used travel times from deep Peruvian events. The data from Argentine and Bolivian events presented here constrain the location of the anomaly quite well, and indicate a possible short and long period S wave amplitude diminution associated with it. When the travel time data are corrected for the estimated effects of these two anomalies, a systematic regional variation in ScS-S station residuals is apparent between stations east of and west of the Rocky Mountains. One

possible explanation of this is a long wavelength lateral variation in the shear velocity structure of the lower mantle at depths greater than 2000 km beneath North America.

Introduction

Numerous approaches to the problem of mapping lateral heterogeneity in the lower mantle are currently being pursued. Among these techniques are included array studies (e.g. Chinnery, 1969; Davies and Sheppard, 1972; Kanasewich et al. , 1973; Wright and Cleary, 1972; Powell, 1975); inversion of global travel time data (Julian and Sengupta, 1973; Sengupta and Toksoz, 1976; Dziewonski et al. , 1977; Sengupta et al. , 1981); and studies using differential travel times of phases at a given station to remove upper mantle effects (Jordan and Lynn, 1974; Pillet, 1979). This problem is also being addressed using high quality digital recordings of long period surface waves and free oscillations, though such techniques are not fully developed for resolving lower mantle variations. Most of the studies reported to date have utilized P waves rather than S waves, since the S wave data sets available from arrays or earthquake bulletins are small and frequently contain large errors. Jordan and Lynn (1974) demonstrated the advantages of carefully read S wave travel times, particularly the differential time ScS-S, for detecting lower mantle heterogeneities. The large amplitude of the S wave travel time anomalies, which may be 3 s or larger, enables the use of relatively small data sets for lower mantle studies. There is, however, a corresponding increase in the effects of upper mantle variations on S wave travel times, which requires additional care in

interpreting the S wave anomalies.

Hales and Roberts (1970a) and Jordan and Anderson (1974) have presented numerous observations of ScS-S differential travel time residuals from shallow and deep focus events. These differential times show a large amount of scatter, of up to 10 s, which is comparable to the scatter in direct S residuals. The insensitivity of ScS-S residuals to event mislocation and upper mantle and crustal receiver structure, particularly for deep events, indicates that large and numerous lower mantle heterogeneities produce the range in observed ScS-S times (Jordan and Anderson, 1974; Jordan, 1975).

Jordan and Lynn (1974) demonstrated that in some cases the ScS-S residuals have systematic patterns which can be used to infer the location of the anomalies producing them. Figure II.1 shows the ScS-S and PcP-P JB residuals at North American stations for the two deep Peruvian events they analyzed. The data are plotted against azimuth from the source region. In the limited azimuth range from -15^{o} to -22^{o} the residuals are anomalously positive, indicating that either the direct S waves are early or the ScS arrivals are late. Since a strong negative correlation between the direct S residuals and the ScS-S residuals was found, they concluded that the direct S waves encountered a high velocity region over a limited range in azimuth. The location of this anomalous region could not be well constrained using these data alone, but Jordan and Lynn (1974) suggested that it may be localized beneath the Caribbean at depths of 600 to at least 1400 km. It is clear in Figure II.1 that the P waves show a similar pattern, but with anomalies that are 3 to 4 times smaller than in the

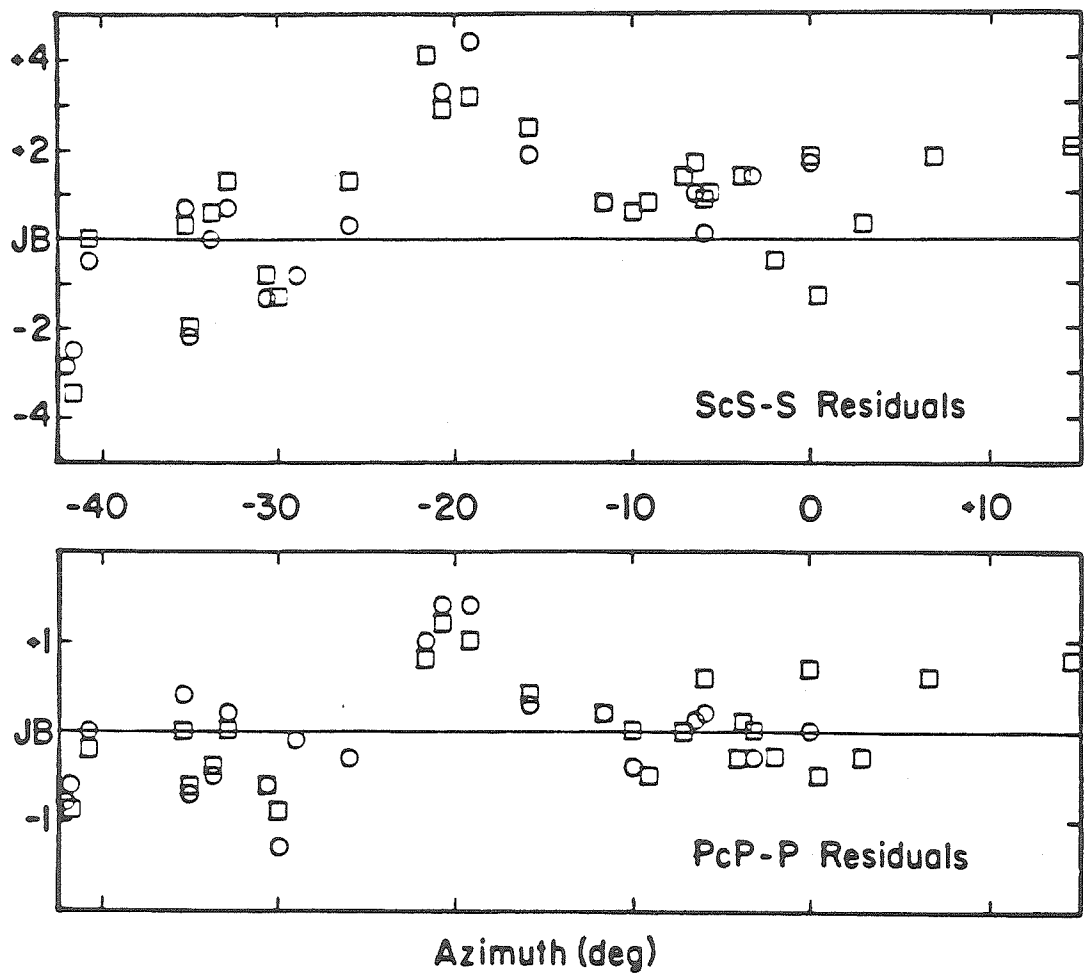

Figure II.1. ScS-S residuals (top) and PcP-P residuals (bottom) from two deep Peruvian events plotted as a function of azimuth from the source. Note that the vertical scales are not equal (From Jordan and Lynn, 1974)

S wave data.

In this chapter, a large data set of S and ScS-S travel times read from rotated SH signals from 17 deep and intermediate depth events in the Sea of Okhotsk and Argentina is used to isolate two lower mantle heterogeneities. These data are supplemented by S, ScS-S and PcP-P times read from records of two deep Bolivian events, as well as the data presented for two deep Peruvian earthquakes by Jordan and Lynn (1974). Since numerous studies have elaborated the upper mantle velocity structure beneath North America, the travel times have been read at North American stations for all four source regions. Independent knowledge of the regional variations in the upper mantle structure beneath the stations allows us to detect anomalous S residuals and to estimate the upper mantle effects on the differential times. The relative amplitude behavior of short and long period SH and ScSH phases are also investigated to examine the effects of the proposed lower mantle heterogeneities on teleseismic amplitudes.

Data

The short and long period horizontal components of all available North American WWSSN and Canadian Seismic Network (CSN) stations have been digitized and rotated for 7 deep earthquakes in Argentina and 10 deep and intermediate depth events in the Sea of Okhotsk. The events from these regions were selected for their simple, impulsive signal character. The source parameters of all the events used are listed in Table II.1. The absolute S wave travel times and ScS-S differential times were read from the rotated tangential components, and residuals relative to the Jeffreys and Bullen (1940) tables were determined.

Table II.1 Source Parameters for Events Used in This Study.

Region	Date	Origin Time	Latitude	Longitude	Depth, km	Reference
Peru	3 Nov. 1965	01:39:03.2 ± 0.09	9.04° ± 0.022°S	71.32° ± 0.032°W	587 ± 4.4	ISC
	15 Feb. 1967	16:11:11.8 ± 0.25	9.05° ± 0.020°S	71.34° ± 0.024°W	598 ± 3.6	ISC
Bolivia	23 Aug. 1968	22:36:49.8 ± 0.34	21.95° ± 0.024°S	63.64° ± 0.033°W	513 ± 4.2	ISC
	25 Oct. 1973	14:08:58.5 ± 0.29	21.96° ± 0.018°S	63.65° ± 0.025°W	517 ± 3.6	ISC
Argentina	9 Dec. 1964	13:35:42.4	27.5°S	63.2°W	586	NOAA
	5 Mar. 1965	14:32:19.2	27.0°S	63.3°W	573	NOAA
	20 Dec. 1966	12:26:54.6	26.1°S	63.2°W	586	NOAA
	17 Jan. 1967	01:07:54.3	27.4°S	63.3°W	588	NOAA
	9 Sep. 1967	10:06:44.1	27.7°S	63.1°W	578	NOAA
	25 Jul. 1969	06:06:42.4	25.6°S	63.3°W	579	NOAA
	3 Jan. 1973	02:58:16.7	27.7°S	63.3°W	563	NOAA
Sea of Okhotsk	18 Mar. 1964	04:37:25.7 ± 0.08	52.56° ± 0.022°N	153.67° ± 0.030°E	424 ± 4.2	ISC
	12 Oct. 1967	12:53:45.9 ± 0.21	52.15° ± 0.018°N	152.57° ± 0.025°E	466 ± 2.7	ISC
	1 Dec. 1967	13:57:02.4	49.5°N	154.4°E	136	NOAA
	5 Sep. 1970	07:52:32.4	52.32°N	151.46°E	583	Strelitz (1975)
	29 Jan. 1971	21:58:06.7	51.72° ± 0.032°N	151.04° ± 0.024°E	540 ± 5.7	Veith (1974)
	27 May 1972	04:06:49.6 ± 0.25	54.97° ± 0.013°N	156.33° ± 0.020°E	397 ± 2.8	ISC
	21 Aug. 1972	06:23:48.6 ± 0.16	49.47° ± 0.012°N	147.08° ± 0.019°E	573 ± 2.2	ISC
	28 Jul. 1973	20:06:35.4 ± 0.15	50.45° ± 0.013°N	148.92° ± 0.022°E	585 ± 2.1	ISC
	21 Sep. 1974	15:54:59.1 ± 0.37	52.19° ± 0.016°N	157.44° ± 0.023°E	119 ± 3.5	ISC
	10 Jul. 1976	11:37:14.0 ± 0.14	47.31° ± 0.011°N	145.75° ± 0.018°E	402 ± 1.7	ISC

Station elevation corrections and source depth dependent ellipticity corrections (Dziewonski and Gilbert, 1976) were applied to the travel time residuals.

Figure II.2 shows an azimuthal, equidistance projection centered on the Argentine epicenters. The distribution of North American stations that are used is shown. S and ScS-S times for the Argentine events were read from the long period records at all stations closer than 78^{o} and from the short period records at all stations closer than 80^{o}. This distance range is roughly defined by the arc through GSC, RCD and SCH. Direct S travel times were read at all other North American stations out to 110^{o}. The epicenters of the four deep Bolivian and Peruvian earthquakes are also shown in Figure II.2. Due to their size and complexity most of the S waves from these events were not digitized. The S wave travel times for the Bolivian events were read from the unrotated records and the raw travel times for Peru were taken from Jordan and Lynn (1974) and corrections for ellipticity and station elevation were applied to the JB residuals.

The S waves from Peru and Bolivia are dominated by SV energy, and large Sp precursors introduce some uncertainty in the travel time measurements (Jordan and Lynn, 1974; Jordan and Frazer, 1975). Careful analysis of the particle motion was made to reduce the timing error due to these precursors. For the Argentine and Sea of Okhotsk events, the rotation of the S waves, and the fact that for 75% of the events the SV radiation to North America was nodal, considerably reduced the errors in travel time measurement. The Bolivian events are treated separately from the Argentine data because the mechanisms

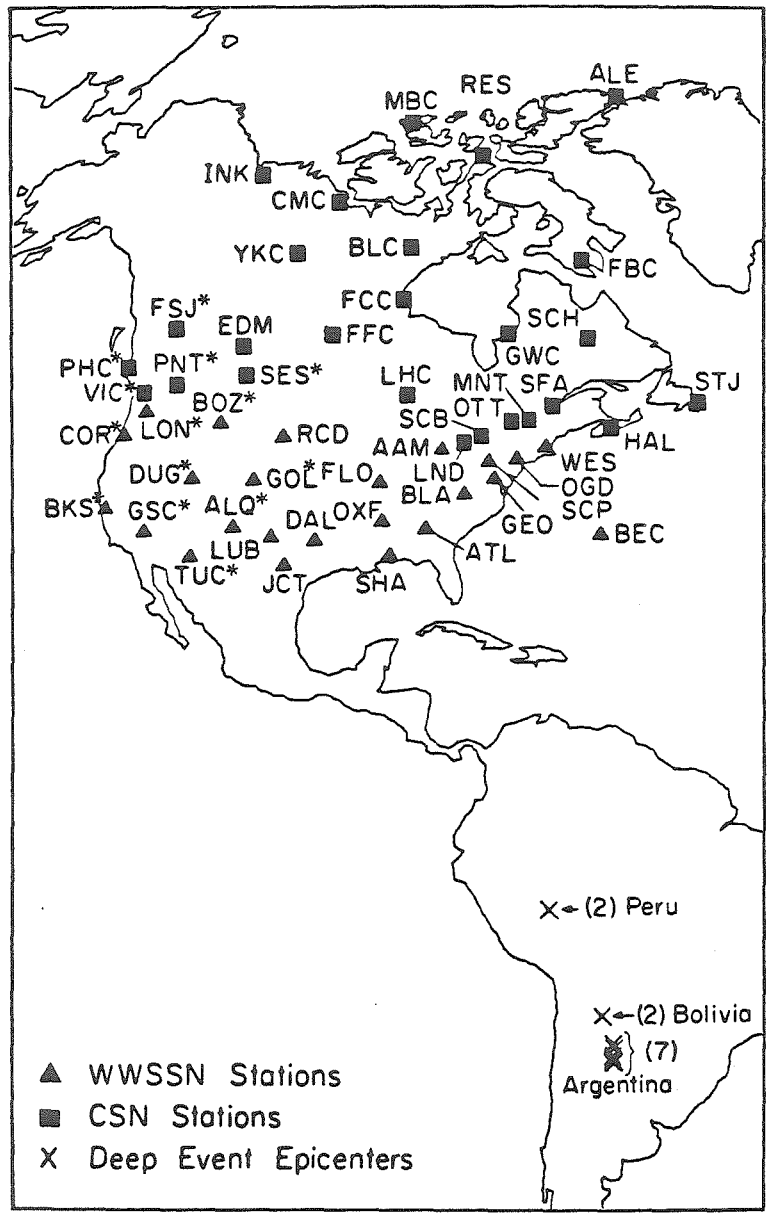

Figure II.2. An azimuthal equidistance projection centered on the Argentina source region. The location of the deep South American event epicenters and recording stations used in this study are shown. The stations with an asterisk are included in the western array discussed in the text. GSC, RCD and SCH are approximately 80° from the Argentina source region.

and depths are quite different between these two source regions. In Figure II.2 it is clear that the range in azimuth to North America is very similar for the three South American source regions, but Peru is 20^{o} closer, and Bolivia 4^{o} closer to the stations than Argentina.

Only one of the Argentine events could be used to measure PcP-P times in North America due to the large distances and nodal P wave radiation patterns of this source region. The PcP-P times were read from the vertical components of the long period records for the event on September 9, 1967, as well as for the two Bolivian events. The Peruvian PcP-P times were obtained from Jordan and Lynn (1974), corrected for station elevation and ellipticity, and used to determine JB residuals. Direct P wave residuals were determined from the short and long period records of the Bolivian events, and from travel times reported in the ISC bulletins for the Peruvian and Argentine events.

Figure II.3 shows another map projection centered on the Okhotsk source region. The WWSSN station SHA ranges from 78^{o} to 88^{o} in distance from the events used. There were no obvious systematic variations in the focal mechanisms or relative travel time residuals between events along the trench warranting subdivision of this source region. It is interesting to note in Figures II.2 and II.3 that the four source regions used lie along a great circle which bisects North America along the Rocky Mountain Range. The expected dips of the deep seismic zones are all transverse to this great circle, which, combined with known upper mantle variations across the Rocky Mountains, introduces the potential of some systematic bias common to each source region. Since no other deep source regions are suitably located

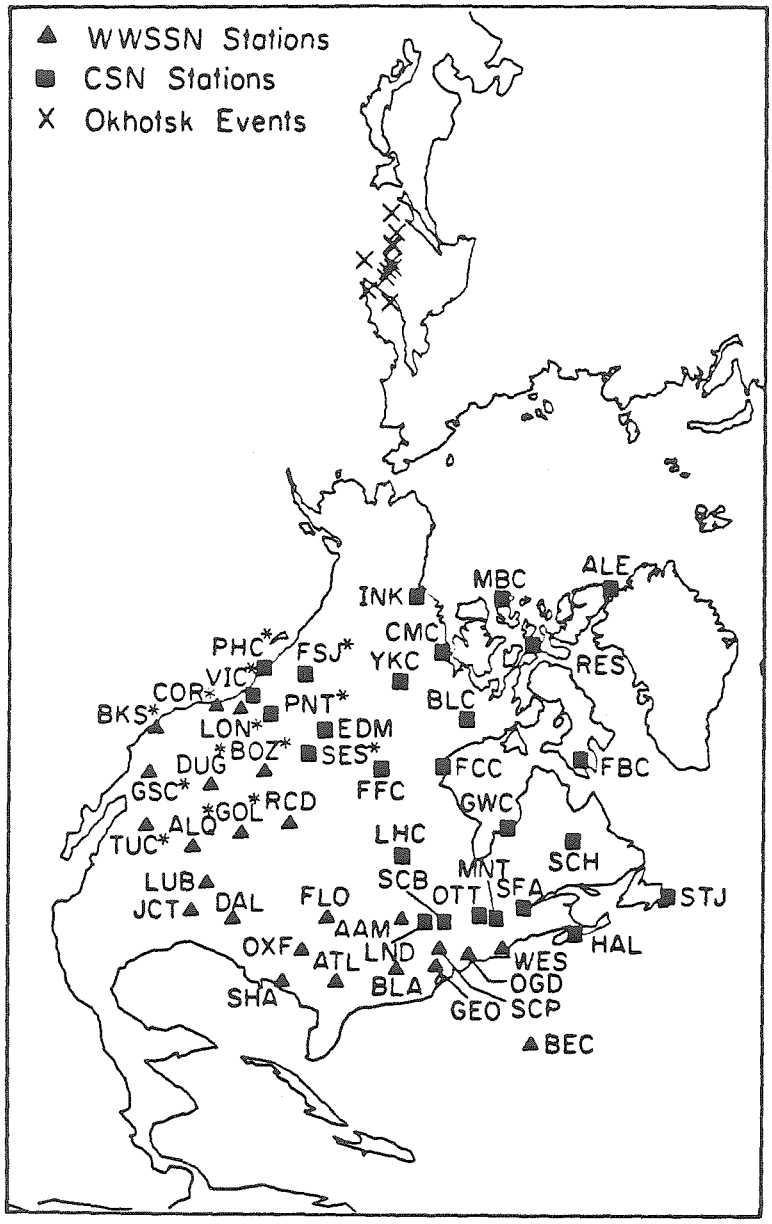

Figure II.3. An azimuthal equidistance projection centered on the Sea of Okhotsk source region. The location of the intermediate and deep focus event epicenters and recording stations used in this study are shown. The stations with an asterisk are included in the western array discussed in the text. SHA ranges from 78^{o} to 88^{o} from the events used.

relative to North America, this cannot be avoided.

A representative profile of long period SH components for the Argentine event of January 17, 1967 is shown in Figure II.4. The peak trace amplitudes have been normalized to unity, but no travel time corrections have been applied. Note that there are large variations in the S and ScS-S travel times and that the amplitude ratio ScS/S varies substantially. Additional short and long period S waves from the Argentine events are shown in Chapter III. The impulsive nature of the signals and the good time resolution of the corresponding short period data indicate that the absolute and differential travel times can be read with an accuracy of better than 1 s for the rotated Argentine and Sea of Okhotsk data.

The results of the SH and ScSH amplitude analysis described in Section I.2 are drawn upon to consider the association between travel time and amplitude anomalies in this data set.

Travel Time Residual Patterns

The deep events used in this study are quite well located, as indicated by the small errors in the ISC locations and the agreement between ISC or NOAA locations with relocations such as performed by Veith (1974). Jordan and Lynn (1974) estimated that for these deep, well located events, a reasonable upper bound on the error due to mislocation on ScS-S times is 0.5 s. This is supported by the small scatter in these differential times at a given station between events in each source region. There may be substantially greater errors in the absolute timing, affecting direct S or P residuals and the travel time baselines between source regions. Since we are analyzing the

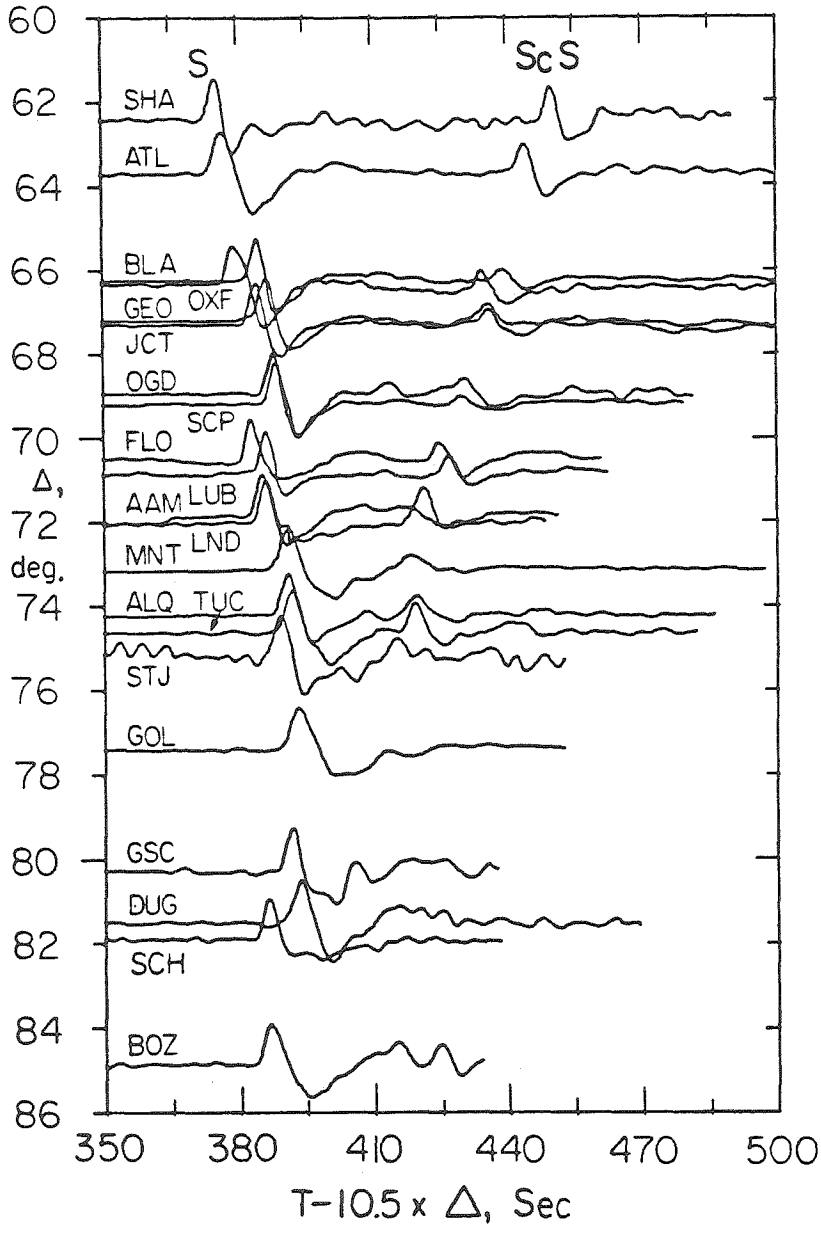

Figure II.4. Profile of the long period SH components recorded from the deep Argentine event on January 17, 1967. The peak trace amplitudes have been normalized to unity, but no time corrections have been applied.

travel times over a limited range in azimuth from each event, we have determined event corrections by minimizing the scatter at each station between events. This was done using an L1 norm to determine the additive constant which minimizes the scatter relative to a reference event. This procedure allowed us to determine station residuals for each source region for the direct S or ScS phases.

For the Argentine S wave data, the event on January 17, 1967 was selected as the reference event. The relative event corrections ranged from -1.6 to 1.2 s. Applying these corrections removes the first order effects due to relative origin time and depth errors, which appear to be small. The Argentine S wave JB residuals, with these event corrections applied, are shown in Figure II.5 where the stations are ordered in azimuth from the source. The short period times have been treated as independent readings from the long period times to remove any baseline shifts due to measuring different frequency onsets or differential instrument group delay. The event corrections determined for short and long periods from a given event all differed by less than 1 s, with larger magnitude events having the largest differences. The scatter about the mean residual at each station was slightly reduced by this procedure, and an alternative procedure which is commonly employed of simply removing the average residual from each event produced nearly identical relative residuals.

It is indicated by Figure II.5 that the first order features in the data for a given source region can be analyzed using the average residual at each station. The small changes in distance and azimuth of each station between events in a given source region permit this.

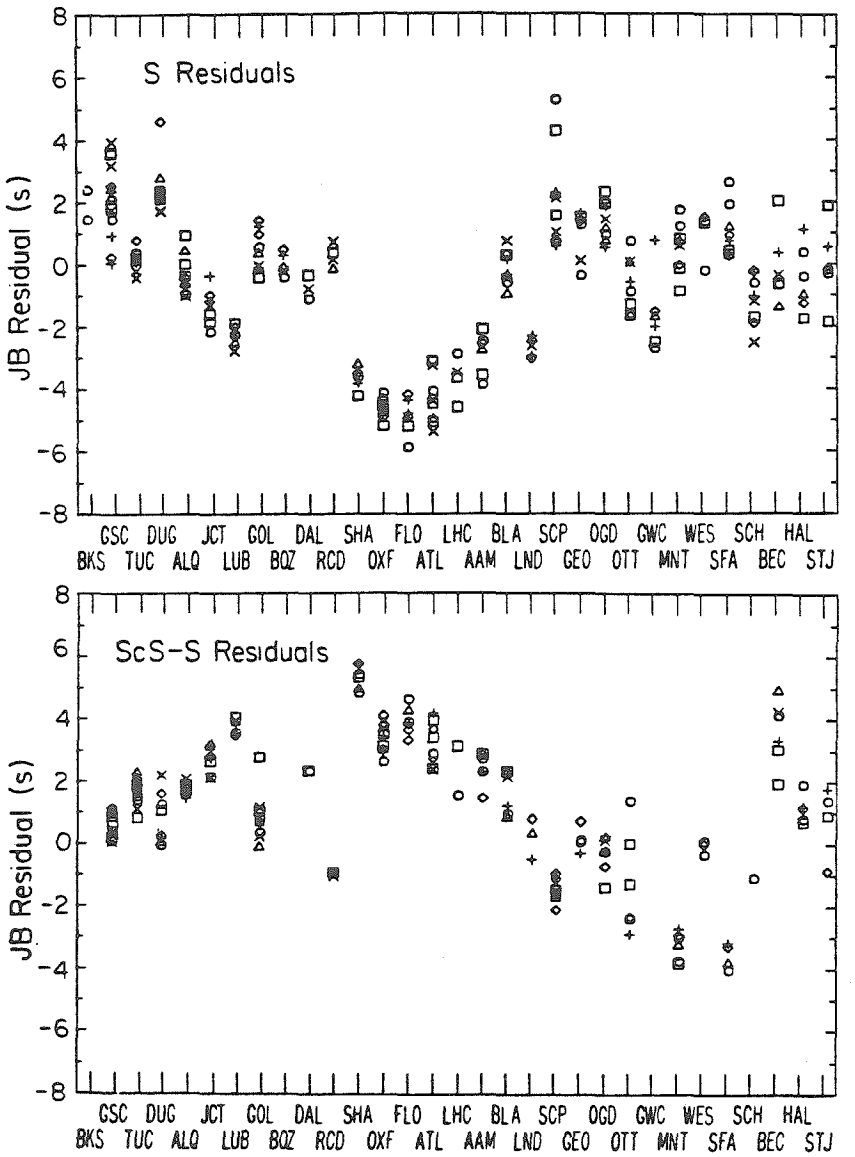

Figure II.5. Short and long period S and ScS-S JB residuals from the Argentine source region at North American stations. The stations are ordered in azimuth from the source region. The event corrections described in the text have been applied to the S wave data.

For the Okhotsk data, the variation in source to station distance is as much as 10^{o}, though usually less, so utilizing station averages may smooth out some trends with distance. The scatter observed in the S residuals at individual stations for the Okhotsk data is only slightly greater than in Figure II.5, indicating that such trends are minor. This averaging process helps to suppress anomalous readings, gives greater confidence in the robustness of the residual pattern for a given source region, and enables us to compare the different source regions.

The ScS-S residuals for the Argentine events are also shown in Figure II.5. Again, the scatter at each station is much smaller than the variation between stations, indicating that the differential time pattern is well characterized by the station means. Systematic baseline shifts in ScS-S residuals between events from a given region were sought by minimizing the scatter at each station. For the Argentine data these shifts were all less than 0.5 s with only a 0.17 s average, so no corrections were applied to the data. This indicates that any bias in the differential times due to source mislocation or source region velocity structure are common to all events in each source region. It is clear in Figure II.5 that there are large variations in both S and ScS-S residuals of nearly 10 sec, as has been reported by Hales and Roberts (1970b) and Jordan and Anderson (1974). Neither the rotation of the S wave data nor the selection of well located deep focus events has reduced this total range in variation; however, there are some systematic features in the data indicating the origins of these variations. The most readily apparent of these is

the general negative correlation of S and ScS-S residuals.

The mean and standard error of the mean of the S and ScS-S residuals at each station were computed for the Argentine data and are plotted against azimuth from the source in Figure II.6. As indicated above, the averaging procedure simplifies the data display without altering the pattern apparent when all of the data are plotted. The S residuals show a clear azimuthal pattern, with early arrivals at azimuths from -15^{o} to -27^{o}. Stations in the Eastern United States (EUS) and Eastern Canada have residuals similar to those in the Western United States (WUS) and Texas. The ScS-S residuals show a few relatively large positive values at azimuths from -20^{o} to -27^{o}, similar to those in the Peruvian data in Figure II.1. However, unlike the Peruvian data, the residuals are negative in the azimuth range 0^{o} to -15^{o}. These trends separate much more clearly when the data are plotted against azimuth as in Figure II.6, than when they are plotted against distance, although there is a general tendency for the ScS-S residuals to decrease with distance as is true for the Peruvian data (Jordan and Lynn, 1974). The azimuthal separation of the residuals indicates that most of the anomalies result from lateral rather than radial variations. It has been found in numerous studies that in the distance range 60^{o} to 80^{o} systematic departures of global S and ScS-S times from the JB times have little trend, of 1 s or less, justifying the use of the JB model as a reference (Doyle and Hales, 1967; Hales and Roberts, 1970a; Jordan and Anderson, 1974; Sengupta, 1975; Dziewonski and Anderson, 1981).

Interpretation of the residual patterns in Figure II.6 is not a

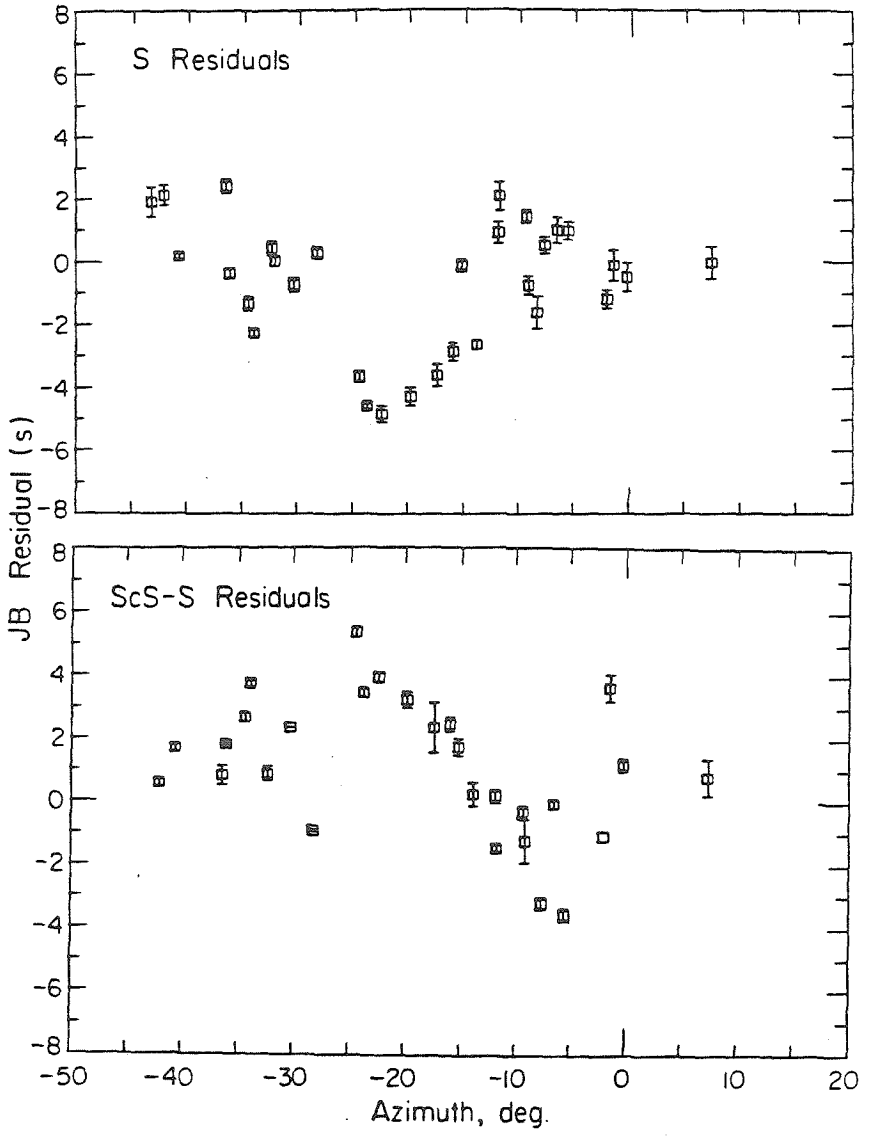

Figure II.6. The mean and standard error of the mean of the Argentine S and ScS-S residuals at each station in Figure II.5 plotted as a function of azimuth from the source. Note the difference in the pattern of the ScS-S residuals at azimuths from 0^{o} to -15^{o} from that for Peru shown in Figure II.1.

simple procedure. The effects of systematic bias due to an inadequate reference earth model, azimuthal source region anomalies, and systematic receiver variations must be considered before lower mantle anomalies can be confidently isolated. Each of these problems is assessed in this paper through comparison of the residual patterns from the different source regions considered.

One approach to identifying the source of differential time anomalies is to correlate the direct travel times of the phases involved with their differential times. The correlations of the Argentine S and ScS residuals with ScS-S residuals are shown in Figure II.7. The correlation coefficient of S and ScS-S is $r_S = -0.62$, whereas for ScS and ScS-S the correlation coefficient is $r_{ScS} = 0.33$. The data in Figure II.7 were subdivided into two provinces, separated along an azimuth of -15° from the source, which show distinct behavior. The western province has $r_S = -0.75$ and $r_{ScS} = -0.25$, and the eastern province has $r_S = -0.33$ and $r_{ScS} = 0.77$. For the Peruvian data, using all of the stations, Jordan and Lynn (1974) found $r_S = -0.86$ and $r_{ScS} = -0.11$. This procedure highlights the azimuthal separation of the ScS-S anomalies in the Argentine data shown in Figure II.6, particularly relative to the Peruvian data, but unlike Jordan and Lynn (1974) we do not feel that these correlations are necessarily reliable indicators of the anomalous phase. Part of the ambiguity in this procedure is that the azimuthal trends apparent in Figures II.1 and II.6 indicate relatively localized anomalies, but large correlation coefficients result from trends in the entire data set. Another problem is that the effect of an anomaly may be to

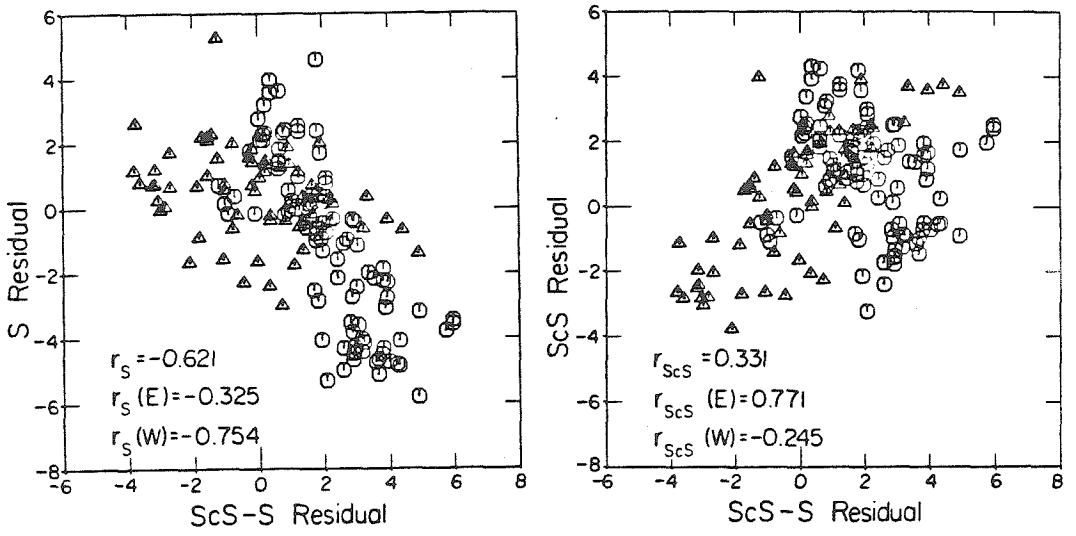

Figure II.7. Correlation plots of S versus ScS-S residuals (left) and ScS versus ScS-S residuals (right) for the Argentina data. The sample correlation coefficients r_S and r_{ScS} are given for the entire data sets and for a subdivision of the stations along an azimuth of -15^o from the source. Data from stations to the west of this azimuth are indicated by octogons, while data from stations to the east of this azimuth are indicated by triangles.

produce residuals which seem reasonable rather than anomalous. This appears to be the case for the S residuals from Argentina in the EUS, where the residuals are near zero or slightly positive when independent lines of evidence indicate that they should be negative.

An alternative procedure for isolating the anomalous phases is adopted here. This involves comparison of the relative behavior of the absolute and differential travel time residuals with independent data sets. Such comparisons are not free of uncertainty, for a given source region may have unique azimuthal and distance biases producing systematic differences from the data used to establish a reference baseline. However, the use of deep earthquake travel times somewhat reduces the likelihood that source region effects dominate the data. We have processed the P and S data from Peru, Bolivia, and the Sea of Okhotsk in the same manner as for the Argentine data above, providing residual patterns for S, ScS-S, ScS and PcP-P across North America. S wave station anomalies from other studies are also used to establish the S residual pattern produced by upper mantle variations alone. By comparing these data sets and allowing for reasonable systematic trends due to source and receiver variations, the lower mantle contributions to the residual patterns can be identified and to a certain degree, isolated.

Source Region Comparisons

In order to compare the average S residual patterns across North America from each source region, it is necessary to determine source region baseline corrections. These shifts are similar in nature to the event corrections applied in each region, and partially offset

systematic differences in source region velocity structure and regional mislocations or origin time errors. Since we are interested in the relative station residual behavior between source regions we have used a subset of WUS and Texas stations to determine the source region corrections. In Figure II.8, the S residuals are compared for stations at which both S and ScS could be observed from all four source regions. The scatter at the first 11 stations from the left was minimized to determine the baseline shifts, all of which were less than 1.5 s. This procedure simplifies the comparison of the residual patterns between source regions, since the residual patterns show coherent regional variations. The Sea of Okhotsk S residuals clearly show a systematically larger variation between the WUS and East Coast than do the South American data. These relative differences are of course independent of the baseline shifts. The Argentine data show the least variation between the East Coast and WUS, with Bolivia being intermediate between Argentina and Peru. While some of the differences in relative residuals for northwestern and southern azimuths may be due to upper mantle lateral variations, such near receiver variations cannot explain the relative east to west trend between Peru and Argentina. It is interesting that FLO, ATL, AAM, BLA, BEC and STJ do not show strong azimuthal variations. Using the western stations, which are the slowest from all azimuths, to determine the relative baselines should maximize the differences at these stations. This suggests the possibility that the baseline corrections that have been applied, which are all small, are close to the true corrections, and that the differences between source regions

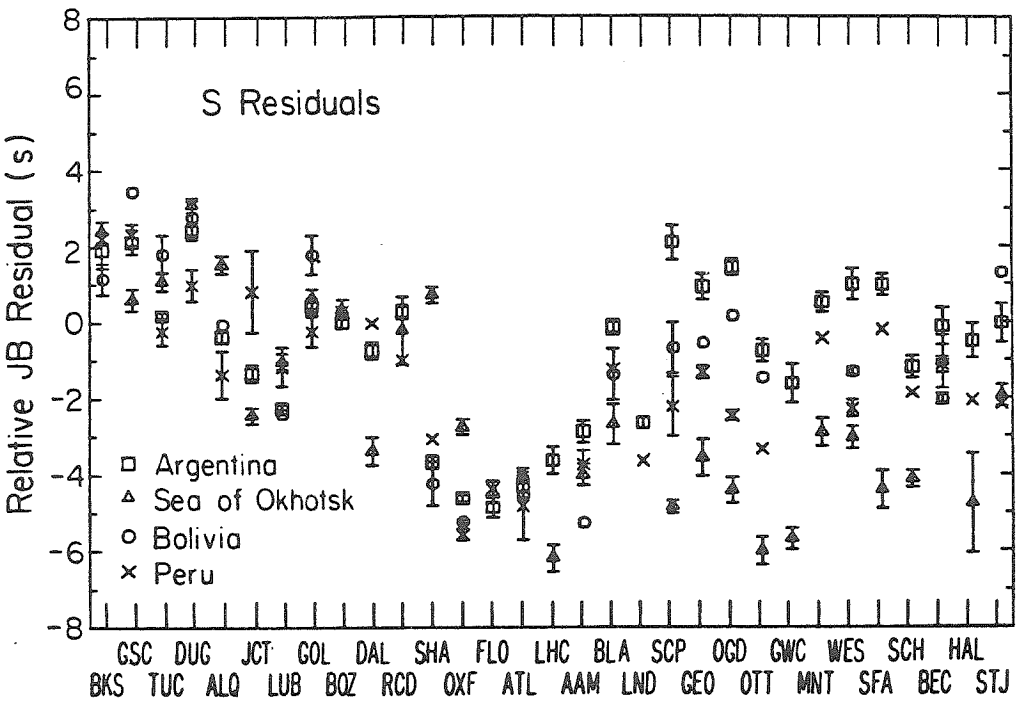

Figure II.8. The mean and standard error of the mean of the S wave JB residuals at North American stations for the four source regions studied. Only those stations at which S and ScS could both be observed from each source region are shown. Source region corrections have been determined using the western U.S. and Texas stations which are the first 11 from the left.

affect the East Coast stations preferentially. By referring to Figures II.2 and II.3 it is clear that the stations with the largest relative residual variations, SCP, GEO, OGD, WES, OTT, GWC, SFA, SCH and HAL are closely grouped in azimuth from each source region, whereas those with little azimuthal variation are widely distributed.

The S residual data for Peru, Argentina and Okhotsk are compared with previous determinations of North American S wave station anomalies in Figure II.9. In order to again emphasize the relative residual variations, the data sets have all been shifted to minimize the scatter at the first 11 stations from the left. The S station anomalies used for comparison have been determined from studies of the ISC catalogue (Romanowicz, 1979; Poupinet, 1977); from shallow event data (Hales and Roberts, 1970a); from intermediate and deep events recorded in Canada (Wickens and Buchbinder, 1980); and from deep events recorded in the U.S. (Sengupta, 1975). Generally, these studies have involved substantial azimuthal averaging in the data processing, and thus provide estimates of the upper mantle shear velocity variations under North America.

In Figure II.9 the error estimates have been omitted for clarity, but these are given in Table II.2. The baseline for the Canadian data of Wickens and Buchbinder (1980) was chosen by fixing the value at LHC to be the same as for Argentina since their residuals do not overlap the western stations. The Argentina S times to East Coast stations are clearly slow relative to all other determinations. The consistency between the residuals from Argentina and the other data sources at BEC, BLA, AAM, FLO and ATL relative to the western stations

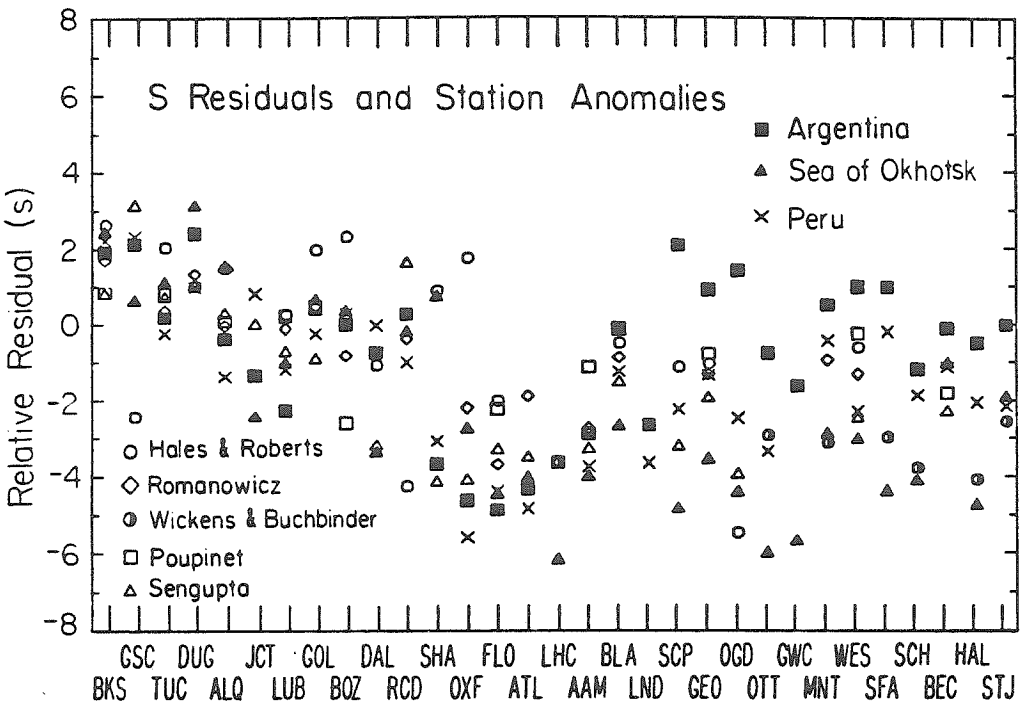

Figure II.9. Comparison of the mean S wave JB residuals for the Peru, Argentina, and Sea of Okhotsk source regions and the station anomalies from previous studies. Baseline corrections have been determined using the first 11 stations from the left in order to emphasize the differences in regional variations between the data sets. The error estimates for each station anomaly are given in Table II.2.

Table II.2 Relative S Wave Station Anomalies.*

Sta	Peru	Bolivia	Argentina	Okhotsk	Hales & Roberts	Romanowicz	Wickens & Buchbinder	Poupinet	Sengupta
BKS	2.69 ± 0.00	0.86 ± 0.40	1.92 ± 0.47	3.53 ± 0.27	2.26	1.92 ± 0.31	-	3.54 ± 0.12	1.78 ± 0.83
GSC	2.78 ± 0.28	3.15 ± 0.00	2.13 ± 0.32	1.73 ± 0.28	-2.80	-	-	-	4.08 ± 0.94
TUC	0.24 ± 0.35	1.50 ± 0.50	0.18 ± 0.09	2.21 ± 0.24	1.67	0.59 ± 0.26	-	3.52 ± 0.13	1.68 ± 0.47
DUG	1.45 ± 0.41	2.46 ± 0.44	2.40 ± 0.22	4.21 ± 0.18	0.65	1.56 ± 0.56	-	-	2.01 ± 0.79
ALQ	-0.89 ± 0.63	-0.36 ± 0.00	-0.37 ± 0.17	2.62 ± 0.23	1.11	0.19 ± 0.35	-	2.78 ± 0.20	1.25 ± 0.63
JCT	1.28 ± 1.07	-	-1.33 ± 0.22	-1.32 ± 0.20	-	-	-	-	0.98 ± 0.83
LUB	-0.70 ± 0.50	-2.69 ± 0.00	-2.25 ± 0.11	0.10 ± 0.20	-0.10	0.12 ± 0.33	-	2.90 ± 0.20	0.26 ± 1.03
GOL	0.23 ± 0.39	1.47 ± 0.50	0.42 ± 0.22	1.75 ± 0.25	1.60	0.71 ± 0.37	-	3.19 ± 0.13	0.07 ± 1.01
BOZ	0.76 ± 0.00	-	0.01 ± 0.16	1.46 ± 0.25	1.94	-0.58 ± 0.64	-	0.12 ± 0.41	-
DAL	0.44 ± 0.00	-	-0.73 ± 0.22	-2.22 ± 0.35	-1.42	-	-	-	-2.19 ± 0.41
RCD	-0.51 ± 0.00	-	0.27 ± 0.18	0.92 ± 0.88	-4.57	-0.14 ± 0.65	-	-	2.58 ± 0.69
SHA	-2.57 ± 0.00	-4.50 ± 0.58	-3.63 ± 0.17	1.84 ± 0.21	0.53	-	-	-	-3.12 ± 0.20
OXF	-5.06 ± 0.15	-5.48 ± 0.41	-4.58 ± 0.09	-1.61 ± 0.20	1.38	-1.95 ± 0.60	-	-	-3.08 ± 0.30
FLO	-3.86 ± 0.21	-	-4.82 ± 0.24	-3.30 ± 0.28	-2.35	-3.42 ± 0.90	-	0.49 ± 0.30	-2.30 ± 0.59
ATL	-4.31 ± 0.88	-4.80 ± 0.00	-4.28 ± 0.29	-2.88 ± 0.20	-	-1.65 ± 0.68	-	-	-2.49 ± 0.13
LHC	-	-	-3.60 ± 0.35	-5.02 ± 0.35	-	-	-0.07 ± 0.39	-	-
AAM	-3.23 ± 0.35	-5.52 ± 0.00	-2.85 ± 0.28	-2.85 ± 0.28	-3.21	-2.49 ± 0.50	-	1.58 ± 0.22	-2.27 ± 1.13
BLA	-0.75 ± 0.00	-1.67 ± 0.66	-0.14 ± 0.18	-1.53 ± 0.52	-0.84	-0.63 ± 0.31	-	2.58 ± 0.17	-0.52 ± 0.88
LND	-3.14 ± 0.00	-	-2.63 ± 0.14	-	-	-	-	-	-
SCP	-1.75 ± 0.78	-0.98 ± 0.66	2.07 ± 0.45	-3.69 ± 0.17	-1.47	-	-	-	-2.20 ± 0.66
GEO	-0.85 ± 0.16	-0.85 ± 0.00	0.90 ± 0.34	-2.41 ± 0.48	-1.38	-1.07 ± 0.45	-	1.93 ± 0.23	-0.95 ± 0.75
OGD	-1.99 ± 0.11	-0.15 ± 0.00	1.41 ± 0.21	-3.27 ± 0.34	-5.78	-	-	-	-2.94 ± 2.30
OTT	-2.85 ± 0.00	-1.76 ± 0.00	-0.75 ± 0.29	-4.85 ± 0.36	-	-	0.63 ± 0.35	-	-
GWC	-	-	-1.61 ± 0.50	-4.54 ± 0.27	-	-	-	-	-
MNT	0.04 ± 0.00	-	0.50 ± 0.26	-1.77 ± 0.36	-	-0.71 ± 0.95	0.42 ± 0.58	-	-
WES	-1.81 ± 0.22	-1.61 ± 0.10	0.98 ± 0.40	-1.91 ± 0.29	-0.97	-1.08 ± 0.57	-	2.44 ± 0.27	-1.48 ± 1.72
SFA	0.27 ± 0.00	-	0.96 ± 0.27	-3.26 ± 0.49	-	-	0.56 ± 0.66	-	-
SCH	-1.40 ± 0.01	-	-1.19 ± 0.29	-3.00 ± 0.22	-	-	-0.24 ± 0.41	-	-
BEC	-0.67 ± 0.20	-2.33 ± 0.14	-0.12 ± 0.48	0.07 ± 0.70	-	-	-	0.88 ± 0.27	-1.32 ± 0.00
HAL	-1.60 ± 0.00	-	-0.49 ± 0.44	-3.64 ± 1.30	-	-	-0.55 ± 1.22	-	-
STJ	-1.70 ± 0.00	1.00 ± 0.00	-0.02 ± 0.50	-0.81 ± 0.28	-	-	0.97 ± 0.84	-	-

*All error estimates are standard error of the mean, and all units are s.

indicates that the Argentina S waves to the East Coast are anomalously late. A similar argument would suggest that the Okhotsk travel times to the East Coast are slightly (1-2 s) fast. The Peruvian S residual variations are similar to those of the upper mantle station anomalies. Figure II.9 demonstrates that lateral variations in upper mantle structure beneath North America produce at least 6 or 7 sec S wave travel time variations.

Inspecting Figure II.9 alone would not necessarily lead one to conclude that the South American S travel times to SHA, OXF and FLO are anomalously fast. Sengupta's station residuals are very similar for these stations relative to the WUS, but this stems from his data for these stations being dominated by deep South American events. If the Romanowicz (1979) or Sea of Okhotsk anomalies are chosen as better estimates of the upper mantle correction, one can estimate the path anomalies for the South American data at these stations to be 4.5 s at SHA, 1.5 to 2.5 s at OXF, and 0.5 to 1.5 s at FLO. These estimates can be compared with the anomalies estimated from the relative ScS-S residuals as discussed later. The strong gradient in the shear wave velocity between SHA and stations farther north apparent in the Okhotsk data is supported by the P residual patterns presented by Hales and Herrin (1972) and by the relatively slow SS velocities observed for paths in the Gulf of Mexico (Steve Grand, personal communication). The relative variations in the S wave station anomaly estimates from previous work are so large that no one set is adopted to remove the receiver effects from the data.

The direct S residuals from Argentina and Okhotsk are compared at

all of the Canadian stations in Figure II.10. The station residuals from Wickens and Buchbinder (1979) are included. The source region shifts applied to the data were determined by minimizing the scatter at stations in Western Canada, which are the first 13 from the left in Figure II.10. This group of stations was selected because they are separated in azimuth from Argentina along the azimuth of -15^{o} which appears to delimit the East Coast S and ScS-S anomalies from Argentina. The relative residual patterns are similar to those across the U. S.. The Okhotsk data are faster to eastern Canadian stations relative to the western stations than the azimuthally averaged values of Wickens and Buchbinder (1980), while the Argentina data are slower. The Okhotsk and Argentina data across Canada do span significantly different distance ranges from the source regions, so these comparisons are subject to uncertainty in the JB model, but it is clear that azimuthal patterns are more important than distance trends in this data.

While interpreting the relative S wave residual patterns is subject to ambiguity, a consistent and simple scenario to explain the data is that the S times from Argentina and Boliva are slow in the azimuth range -5^{o} to -15^{o} and in the distance range 60^{o} to 110^{o}. Stations further to the east such as BEC, SCH, HAL, FBC and STJ show less azimuthal variation, while stations west of the -15^{o} azimuth show an abrupt return to normal relative behavior, indicating that this trend is not a mislocation artifact. The azimuthal variation in travel times due to epicenter mislocation vary with the cosine of the difference in azimuths of the stations. For these well located events

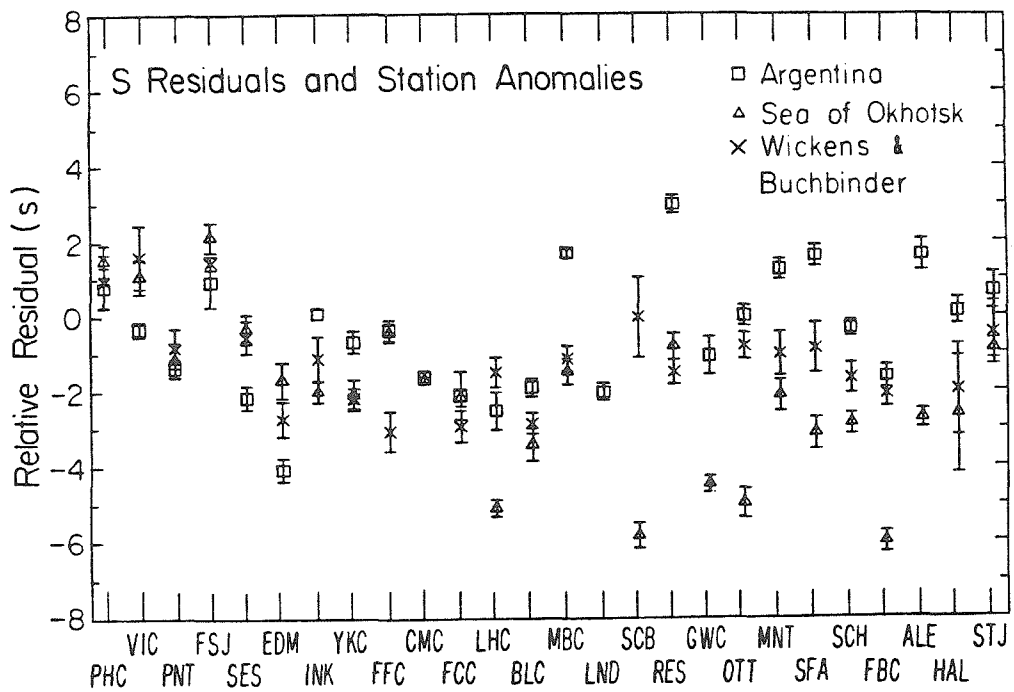

Figure II.10. Comparison of the Canadian station S wave JB residuals for the Argentina and Sea of Okhotsk data and the station anomalies from Wickens and Buchbinder (1980). Baseline corrections were determined using the first 13 stations from the left, which are to the west of the -15° azimuth from Argentina.

less than a 0.5 s variation over the whole azimuth range would be expected, and this would be a smooth feature (Jordan and Lynn, 1974). Note that identifying the S phases to the East Coast as anomalously late could not be done directly from Figure II.5 alone, nor is this obvious in the S versus ScS-S correlations. The Okhotsk S times appear to be fast to stations in the Northeastern U. S. and Eastern Canada. These interpretations are tested against the ScS-S residual patterns below.

The P wave residuals for the South American events are compared in Figure II.11. The western stations were used to determine source region corrections. The range in residuals is much smaller than in the S wave data, but the Argentine data along the East Coast are systematically later than for Bolivia and Peru. SHA, OXF and FLO recorded slightly fast arrivals from each source region. Because the P residual variations are much smaller than the S residual variations, and since the Argentina events produced nodal P waves radiation to North America, we do not emphasize the P wave data in this paper.

The average ScS residuals are compared in Figure II.12. Again, the first 11 stations from the left were used to determine the baseline shifts. It is quite clear that the ScS residuals show less regional variation from each source region and less evidence for azimuthal variation than the S residuals. The decrease in total range of the station residuals is greater than would be expected due to the difference in upper mantle raypath between ScS and S. The reduced scatter in Figure II.12 indicates that the S phases are more strongly affected by source and mantle velocity variations, but there also

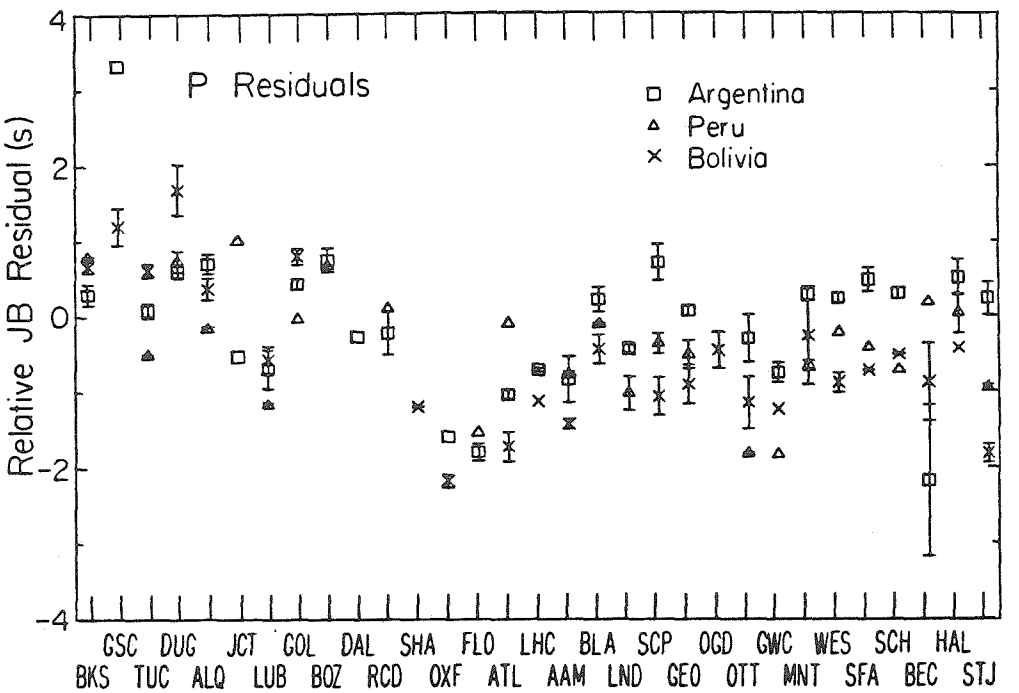

Figure II.11. Comparison of the P wave station residuals for the South American source regions. The residuals for Bolivia were determined from the original records, whereas the residuals for Argentina and Peru were determined using travel times reported in the ISC catalogue. The first 11 stations from the left were used to determine source region corrections.

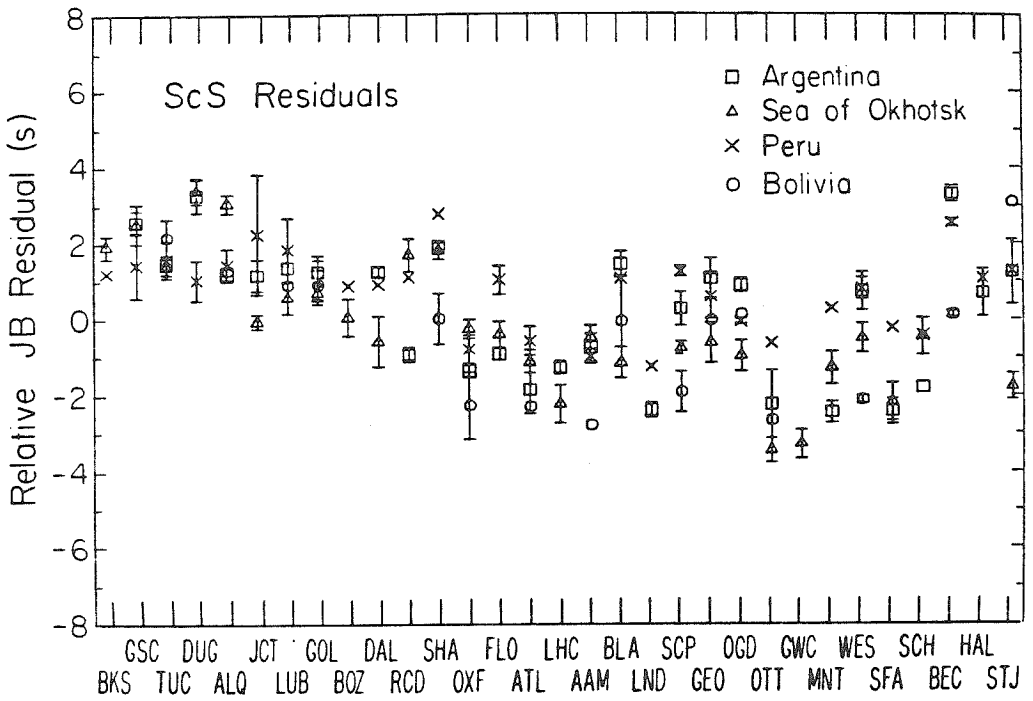

Figure II.12. Comparison of the ScS station residuals for the four source regions studied. The first 11 stations from the left were used to determine source region corrections. Note the reduced scatter and diminished total range of the data relative to the S residuals in Figure II.8.

appears to be a systematic effect suppressing the total range in ScS residuals which is common to all 4 source regions.

The ScS-S station residuals are shown in Figure II.13. In this case, no baseline shifts have been applied, since the differential times presumably cancel out source region and receiver variations. However, baseline differences may in fact exist if for any of the source regions the S or ScS phases encounter anomalous velocity structure affecting all of the arrivals in the azimuth range covered by the North American stations. Since the ScS phases span a much narrower cone of rays near the source, and since the ScS paths traverse the D" region which is suspected to have global variations, one might expect these phases to be more susceptible to such baseline shifts. One of the most intriguing features in Figure II.13 is the tendency for the differential time residuals from Peru and Okhotsk to track quite closely at most stations, with the exceptions being GSC, STJ, SHA and OXF. The residuals from Bolivia track those from Argentina closely as well, but with a systematic 1 s offset. The latter two regions show an east to west trend relative to the pattern defined by the Peruvian and Okhotsk data.

The South American data all show large positive ScS-S residuals in the South-Central U. S., with SHA and OXF showing the largest azimuthal variation. In Figure II.8 it was apparent that the S residuals at these stations are relative negative (i.e. fast S) in both an absolute sense and relative to the Okhotsk data. The ScS residuals in Figure II.12 do not show a similar pattern. From this it appears that the interpretation advanced by Jordan and Lynn (1974) of

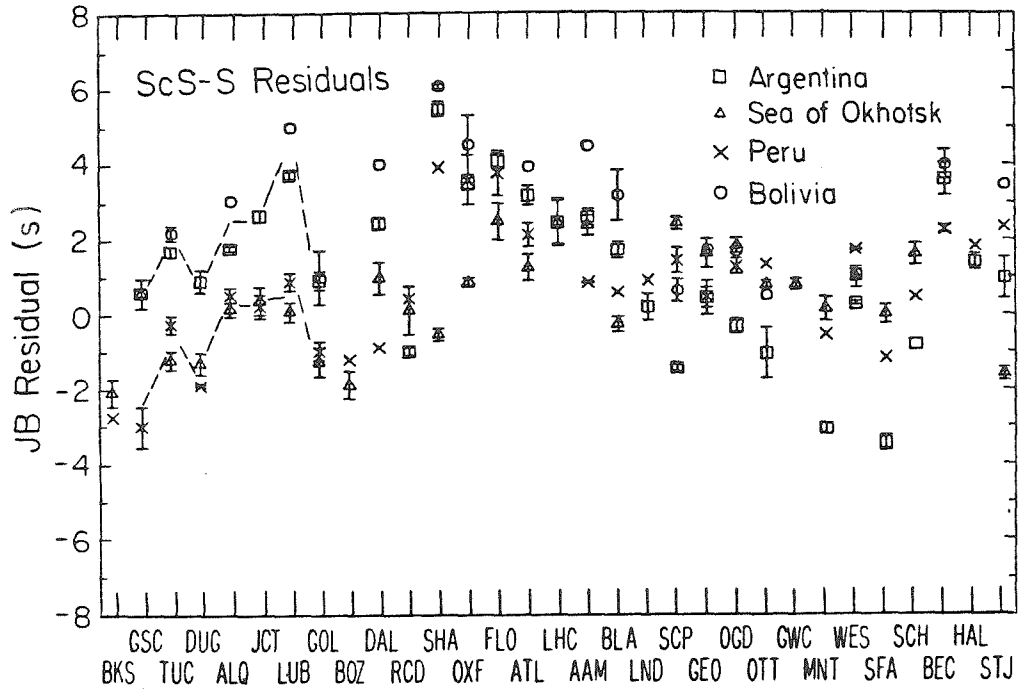

Figure II.13. Comparison of the ScS-S station residuals for the four source regions studied. No corrections have been applied to the data. The Peruvian and Sea of Okhotsk residuals track closely except at stations in the South-Central U.S.. The Bolivian data track the Argentine residuals, but have a 1 s relative offset. The dotted lines indicate the tendency for all the residuals from all four regions to follow the same relative patterns at the western and Texas stations.

a localized fast velocity anomaly in the direct S waves applies not only to Peru but also to Bolivia and Argentina. The size of the anomalies involved can be estimated by using the relative ScS-S residual variations as a baseline as long as any systematic biases in the relative residual patterns are removed.

Careful inspection of the ScS-S residuals from Okhotsk and Peru (Figure II.13) reveals a systematic regional variation. In general, there is a 2 to 3 s west to east increase in the residuals from these two source regions, and this trend is more closely associated with geographical provinces of the stations than with simple azimuthal variations from each source. Raytracing through realistic models of the upper mantle under North America indicates that shear velocity variations consistent with the 5 to 6 s regional variations in S wave station anomalies permit little more than a 0.5 s systematic regional variation in ScS-S differential times. Thus, it appears that source or lower mantle variations affect the data from Peru and Okhotsk in a similar way. The departure of the Argentine and Bolivian data from this trend partially results from the ScS-S anomaly apparent at the East Coast stations in Figure II.6, which Bolivia also appears to show. Note that the relative pattern of ScS-S residuals between WUS and Texas stations is similar for all four source regions. The fact that such stable relative behavior persists even though the overall patterns deviate, indicates that baseline shifts do in fact exist in the differential times, though it is not yet clear whether these are uniform shifts only or azimuthally or distance dependent trends.

The relative residual comparisons are completed with the

comparison of the PcP-P times shown in Figure II.14. The data are rather sparse, but it can be seen that the Argentine events show systematically more negative residuals at East Coast stations. The Bolivian residuals are intermediate between Peru and Argentina for the more distant East Coast stations such as OTT, MNT and WES. This is also apparent in the P residuals at OTT, MNT and GWC in Figure II.11. It is interesting that while SHA shows large positive PcP-P residuals from all three source regions, this is not true at OXF and FLO, where only the Peruvian residuals are clearly anomalous. This suggests that the P wave paths differ from the S wave paths by at least enough to miss the anomaly, except for the paths to SHA. There is no clear evidence for a baseline shift in the PcP-P times, though the data in the WUS are particularly sparse.

Tests for Systematic Biases

The ScS-S differential time residuals hold the most promise for isolating any lower mantle anomalies and for finding common anomalies in the data from different source regions, providing the source region comparisons can be used to give estimates of the baselines and intrinsic scatter in the data. In order to interpret the residual patterns with confidence, it is necessary to determine whether strong azimuthal or distance trends exist in the ScS-S residuals, particularly whether they contribute to the relative patterns in Figure II.13. The Sea of Okhotsk ScS-S residuals are plotted against distance and azimuth from the sources in Figure II.15. The short and long period readings from a given event have been averaged at each station to give each data point. The mean and standard error of the

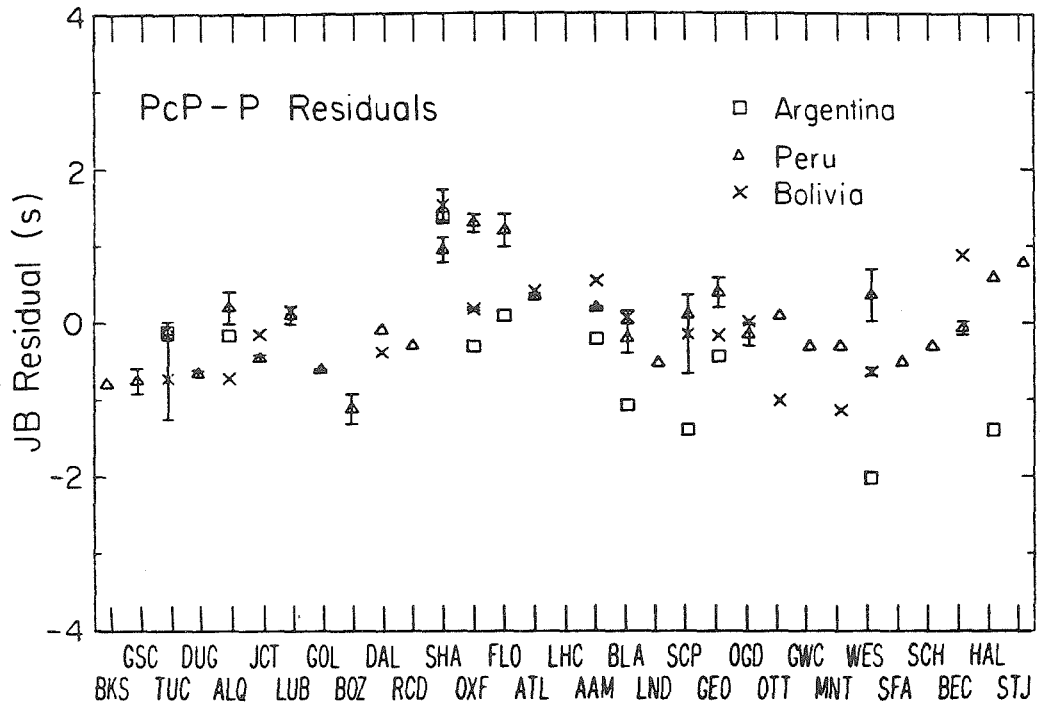

Figure II.14. Comparison of the PcP-P residuals for the South American source regions.

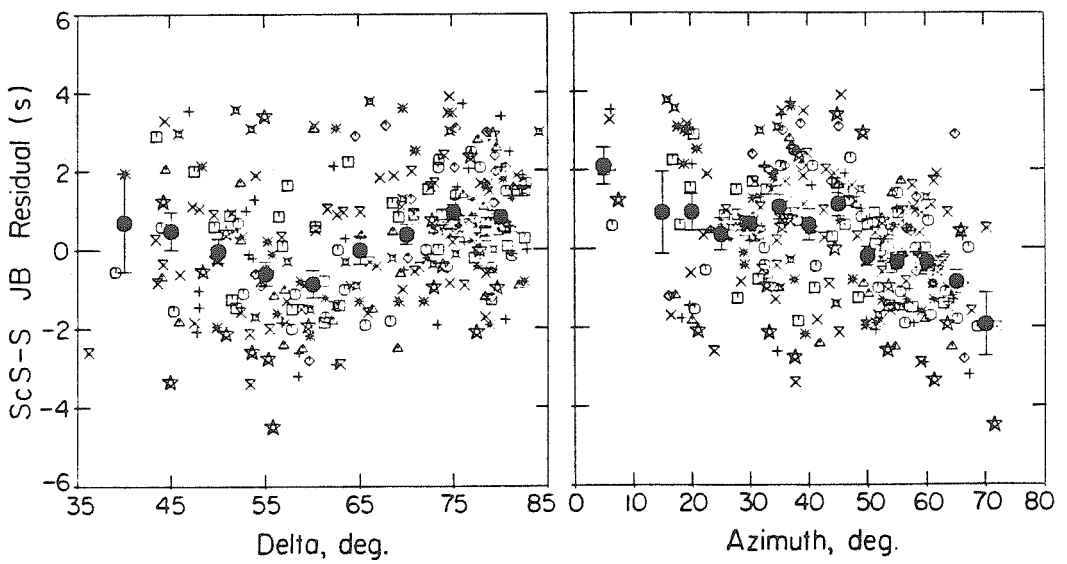

Figure II.15. Plots of the ScS-S residuals at North American stations from the Sea of Okhotsk events as a function of distance (left) and azimuth (right). The mean and standard error of the data in each 5^{o} increment of distance or azimuth are superimposed on the data. Each data point represents the average of the short and long period residuals at each station for each event. Different symbols are used for each event.

mean in each 5^{o} increment in distance or azimuth are superimposed on the data. A minimum in the residuals near 60^{o} suggests a distance trend. However, this minimum is defined mainly by western Canadian and WUS stations, and thus shows up as a clear azimuthal trend as well. These data alone cannot resolve whether this feature is due to a large scale radial or lateral departure from the JB model. A uniform change in core radius would produce a linear trend with distance in the residuals (Hales and Roberts, 1970b), which is not apparent in these data or in the data presented by Jordan and Anderson (1974) which have a global distribution.

By combining the ScS-S data from Peru and Argentina a corresponding range in distance from South America can be obtained, as shown in Figure II.16. None of the suspected anomalous times have been omitted. The means and standard errors for the Peruvian and Argentine data in each 5^{o} distance increment have been computed separately and for the combined data. It is clear that there are very similar trends with distance between the two source regions, which only partially results from the large positive anomalies at the South-Central U. S. stations. The WUS recordings from Peru do define a minimum near 60^{o}, which could be interpreted as additional evidence for a systematic distance trend, but if this is a purely radial effect the positive anomalies for the Argentine data in this distance range are made all that much more anomalous.

An additional test was made by combining the Okhotsk, Peru and Argentine residuals, and subdividing them into western and eastern arrays. The stations included in the western array are indicated in

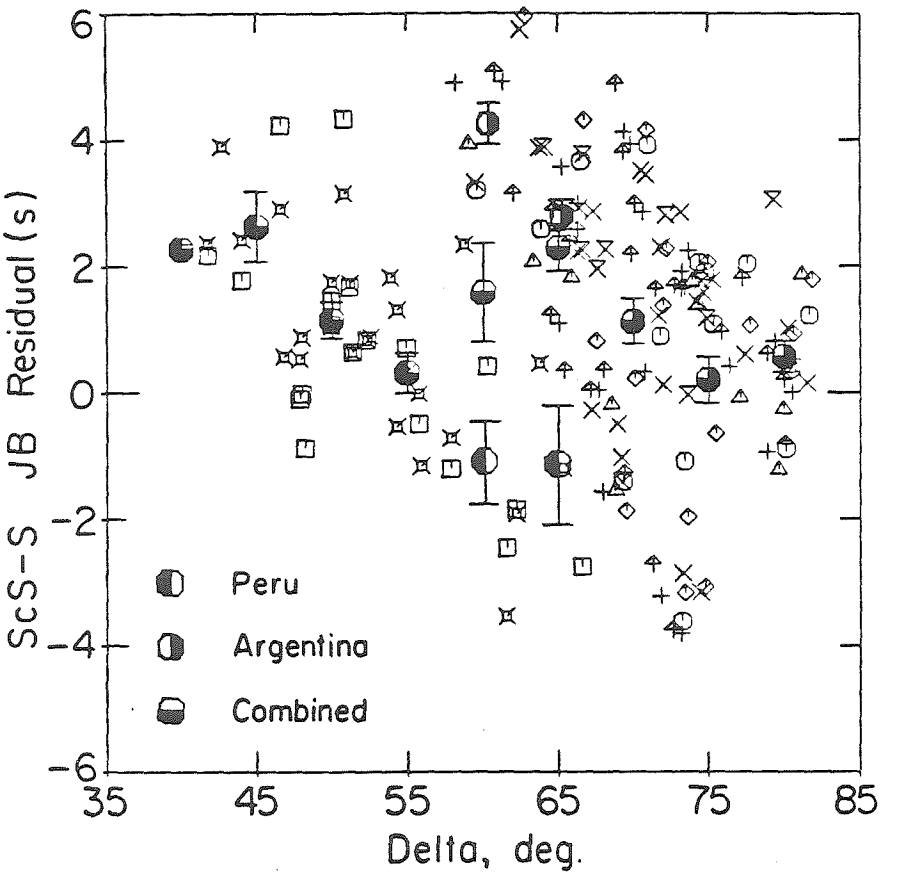

Figure II.16. The ScS-S residuals from Peru and Argentina plotted as a function of distance. The mean and standard error of the mean of the data in each 5^{o} increment of distance are shown for the two regions separately and for the combined data set. Each data point represents the average of the short and long period residuals at each station from each event. Different symbols are used for each event.

Figure II.2. The residuals from these two subgroups are plotted against distance in Figure II.17. In the distance range 45^{o} to 70^{o} the subgroups are well separated. Beyond 70^{o} the western array is dominated by observations from Argentina, which may differ from the other source regions due to a distance trend restricted to the WUS, or due to a baseline shift between the source regions as suggested above. The lack of a pervasive distance trend in the entire data set and the regional variations in behavior indicate that the differential time residuals are free of a systematic radial earth structure bias.

The possibility that there may be strong azimuthal trends in the differential time residuals from deep events is suggested by the study of Jordan (1977). He proposed a deep vertical extension of the Sea of Okhotsk slab, penetrating to 1000 km, well below the maximum depth of seismicity. The size and geometry of this deep slab could produce strong velocity gradients between S and ScS paths. The smoothed source anomaly he determined using the S and ScS times from the deep event on January 29, 1971 is shown in Figure II.18. Interpreting this pattern as a source anomaly is subject to uncertainty in the station anomalies and other path anomalies in the data. The deep focus Sea of Okhotsk data employed in the present study have S and ScS projections that would lie in the northeastern quadrant of the projection in Figure II.18, if the source anomaly does not change along the strike of the subduction zone. The large velocity contrasts (5%) and long S and ScS path lengths (400 to 500 km) associated with the proposed deep slab anomaly (which are needed to explain the pattern in Figure II.18 as a source anomaly) would predict a systematic azimuthal pattern in

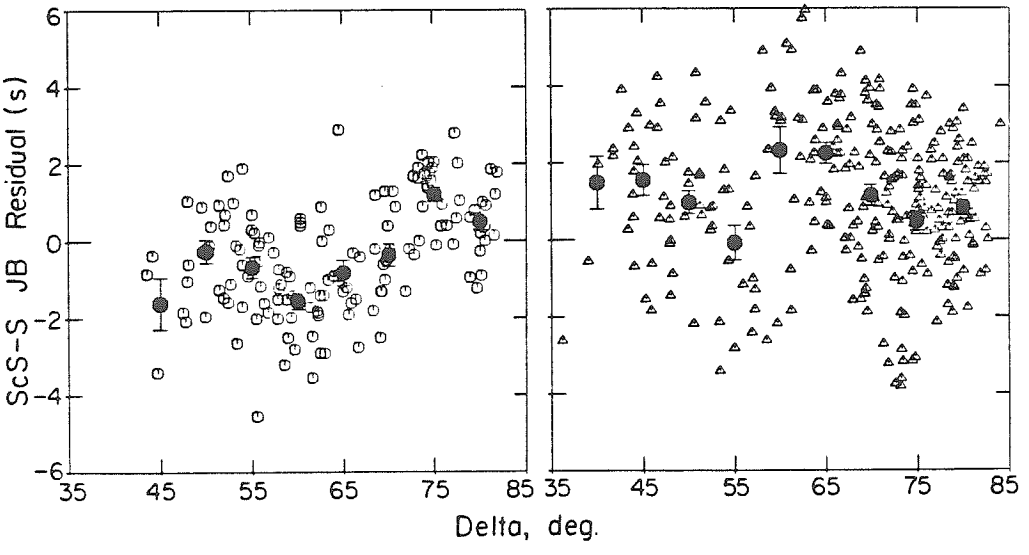

Figure II.17. Comparison of the ScS-S residual dependence on distance for the western array stations (left) and all other North American stations (right). All data from Peru, Argentina and the Sea of Okhotsk are shown. Note that the populations are distinct throughout the range 40-70°. The data from the western array for distance greater than 70° are dominated by the Argentine observations, which may have a baseline shift relative to the other source regions.

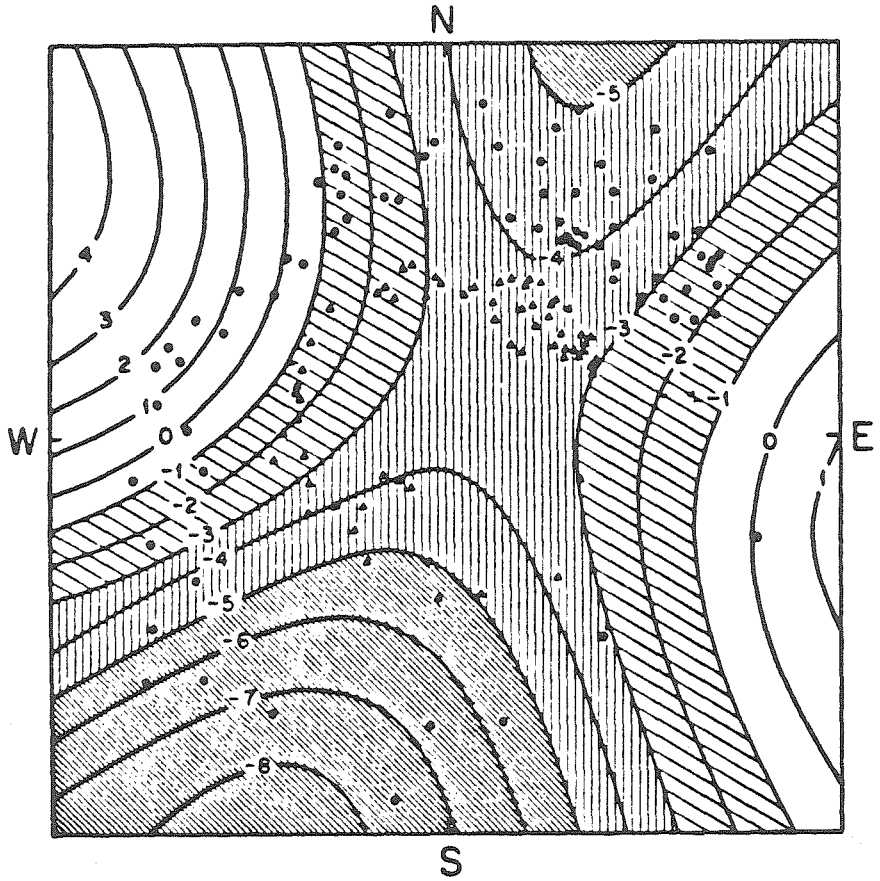

Figure II.18. Stereographic projection of a portion of the lower focal hemisphere showing the smoothed source anomaly contours for the deep Sea of Okhotsk event of January 29, 1971, as determined by Jordan (1977). The contour interval is 1 s. The triangles represent ScS observations and the circles represent S observations. The data in the northeastern quadrant are from North American stations.

ScS-S residuals similar to that in Figure II.15. This involves up to a 2 s decreasing trend between the eastern and western stations in North America. In addition, the direct S times would be 2 s faster to eastern and northern stations than to western stations, while ScS would show less azimuthal variation. This is qualitatively consistent with the trends in Figures II.9, II.10 and II.12. However, there is a major problem with attributing the patterns observed in our data to such a deep slab anomaly. This is that the relative S and ScS-S variations in the Okhotsk data do not change systematically with source depth, between depths of 100 and 583 km.

In Figure II.19 the azimuthal distribution of the Sea of Okhotsk ScS-S residuals for events in the depth ranges 100 to 150 km, 400 to 470 km, and 540 to 590 km are shown separately. The azimuthal pattern for events with shallower source depths is not diminished relative to that for deeper events, as one would expect if a deep slab anomaly is the only cause of the azimuthal patterns. Near 100 km depth the slab dips at about 50^{o}, in a direction transverse to the azimuth toward North America. Thus, the shallow events are displaced from the proposed vertical deep slab extension by several hundred km, and both the S and ScS rays should exit the slab quickly. Given the azimuthal distribution of the stations relative to the slab orientation, one might expect some azimuthal variation in both S and ScS residuals affecting all source depths, independent of any deep slab extension. This could explain the relatively fast S and ScS arrivals in eastern North America, but little ScS-S anomaly would be accumulated near the sources without some dramatic feature such as proposed by Jordan

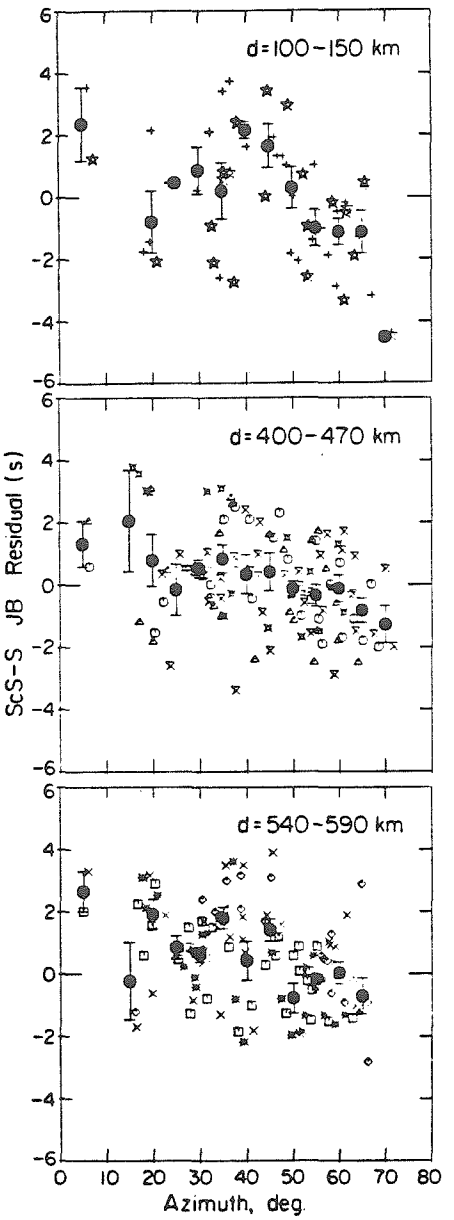

Figure II.19. Comparison of the ScS-S residual azimuthal pattern for Sea of Okhotsk events in the depth range 100-150 km (top), 400-470 km (middle) and 540-590 km (bottom). The mean and standard error of the data in each 5^{o} increment of azimuth are shown.

(1977). We do not claim that these data disprove Jordan's model, much more complete azimuthal coverage would be needed to do that, but it seems reasonable that the persistence of the azimuthal pattern in ScS-S residuals for all source depths indicates a lateral velocity anomaly removed from the source region.

The ScS-S residuals from Peru indicate a similar anomaly to that in the Okhotsk data, given the tendency for the residuals from these two source regions to follow very similar regional patterns. The presumed orientation of the subducting slab in Peru relative to the North American network is similar to that in the Sea of Okhotsk, so a deep slab anomaly in Peru could possibly produce a similar pattern in ScS-S residuals to that from Okhotsk. If this is the case, it is surprising that the regional variations in the S residuals from Peru show no trend relative to the estimated station anomalies in Figure II.9. It would also seem unlikely that the orientation and velocity contrasts of a deep slab anomaly in Peru would produce such good agreement in the regional and inter-station variations of ScS-S residuals with the Okhotsk data. Any deep slab anomalies affecting Argentina and Bolivia would appear to have substantially different orientations from those in Peru and Okhotsk, unless the other anomalies in the data obscure the source region trends.

Interpretation

Since we have not found compelling evidence for distance or near-source systematic biases in the ScS-S residuals from the different source regions, it is possible to use the data in Figure II.13 to estimate the size of the lower mantle anomalies and to

determine which regions have anomalies in common. Several lines of evidence cited above indicate that there are baseline shifts in the differential times, so we have applied uniform corrections to the Argentine and Bolivian ScS-S residuals of -1.5 and -2.5 s respectively. These shifts were determined from the difference in the baseline shifts for S and ScS residuals applied in Figures II.8 and II.12. The resulting relative residuals are shown in Figure II.20. As expected, the scatter at stations in the WUS and Texas is very small, but now the scatter is also very small at ATL, AAM, BLA and BEC. These stations show no strong evidence for azimuthal variations in the direct S and ScS residuals. The ScS-S anomaly in the East Coast is readily apparent for both the Argentine and Bolivian data.

The implication of the baseline shifts is that the S or ScS phases from Argentina and Bolivia encounter different average mantle structure from the other source regions. The studies of Julian and Sengupta (1973), Greenfield and Sheppard (1969) and Burdick and Powell (1980) indicate that such variations do exist along South America and between South America and the Sea of Okhotsk. Pillet (1979) contoured the global differences in station residuals determined using PKIKP and P phases separately. The differential residuals, PKIKP-P are larger below Bolivia and southern Peru than anywhere else in the world, with the more vertically traveling waves (PKIKP) being slower than the P waves. If the S velocities have corresponding behavior, one would expect the ScS phases from Argentina and Bolivia to be slowed down relative to S, producing a positive shift in the ScS-S residuals. The region covered by the PKIKP-P anomaly found by Pillet (1979) is shown

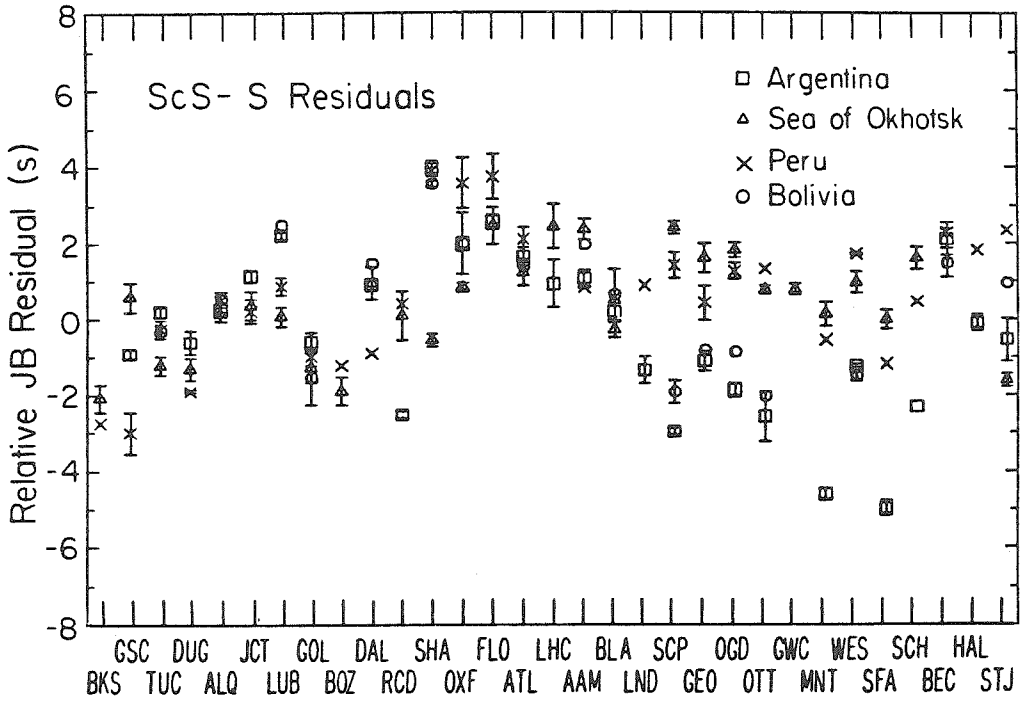

Figure II.20. The ScS-S station residuals with baseline corrections of -1.5 s and -2.5 s applied to the Argentine and Bolivian data respectively. Application of these shifts isolates the East Coast and South-Central U.S. anomalies in the South American data, while reducing the variations at all other stations.

in Figure II.23, and appears to span the range in azimuth from Argentina to North America, thus the ScS phases may be uniformly affected. It should be emphasized that the baseline shifts do not affect the presence of the South-Central U.S. or East Coast anomalies in the South American data, for these are clearly defined in Figures II.1 and II.6, but the shifts do appear to provide a stable baseline (i.e. the Peru and Okhotsk patterns) from which to estimate the size of the anomalies, and to determine to what degree different source regions sample the same anomaly. Other possible explanations for the relative trends in ScS-S residuals between the source regions can of course be proposed, but these invariably lead to rather complex and fortuitous distributions of lower mantle and source anomalies.

Using the relative ScS-S patterns in Figure II.20 and assuming that the patterns would track very closely if no anomalies were present, one can estimate the travel time anomalies. The estimated travel time anomalies for the East Coast stations and for the South-Central U.S. stations are listed in Table II.3. It is important to note that AAM, BLA, BEC and possibly STJ show no relative anomaly, or at least a deviation from the general East Coast azimuthal pattern. A comparison of the ScS-S anomalies in Table II.3 with the relative S residual patterns in Figures II.8, II.9 and II.10 indicates that the anomalies can almost entirely be attributed to the late S arrivals along the East Coast for Argentina and Bolivia, and to early S arrivals at SHA, OXF and FLO for all the South American data. For example, SCP is 4 to 5 s slow in a relative sense in Figure II.9, which corresponds to the -4 to -5 s ScS-S anomaly in Figure II.20.

Table II.3 Estimated ScS-S Anomalies.*

Station	Peru	Bolivia	Argentina
SHA	4.5	4.5	4.5
OXF	2.7	1.1	1.1
FLO	1.2	-	0.0
LND	0.0	-	-2.2
SCP	0.0	-3.9	-5.0
GEO	0.0	-1.9	-2.1
OGD	0.0	-2.5	-3.4
OTT	0.0	-3.1	-3.7
MNT	0.0	-	-4.4
WES	0.0	-2.7	-2.7
SFA	0.0	-	-4.5
SCH	0.0	-	-3.4

*Units are s.

The estimates of the S anomalies at SHA, OXF and FLO made earlier are in good agreement with the values in Table II.3.

If the data are corrected for the estimated anomalies in Table II.3, the ScS-S residual pattern is relatively simple, as shown in Figure II.21. The corrected differential times show little azimuthal variation and small scatter at each station except GSC, LUB, RCD and STJ. With the exception of ALQ, stations in the WUS are systematically slower than stations east of the Rocky Mountains. This is not a purely azimuthal pattern relative to each source region, as can be seen from Figures II.2 and II.3, and is at least 1.5 s greater than can be explained with upper mantle S wave velocity variations. The consistency of the relative station behavior in the WUS indicates that all four source regions sample the same WUS anomaly, which in turn suggests that the regional variation is not an artifact of the baseline shifts. The western anomaly appears to be localized beneath the WUS, at depths great enough to produce differential time variations. A deep seated, large scale region of slightly high S velocity would preferentially affect the ScS arrivals from all four source regions, producing slightly negative residuals. The global average for ScS-S residuals for the distances covered by our data is about 1 s (Jordan and Anderson, 1974), which is consistent with the averages for stations east of the Rocky Mountains. If deep slab anomalies exist for all four source regions, with orientations such as to produce similar azimuthal ScS-S patterns across North America, some of the regional variation in Figure II.21 could be reduced, but this would be a rather fortuitous situation which cannot be isolated in

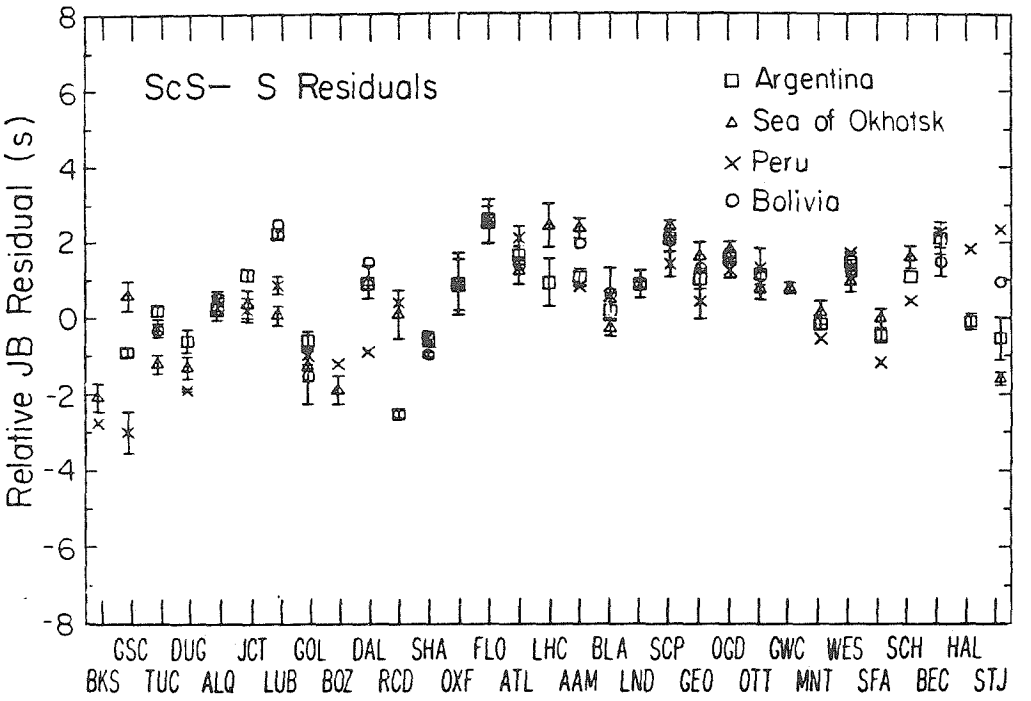

Figure II.21. The ScS-S station residuals with baseline corrections after the estimated anomalies in Table II.3 are removed. Note the distinct baseline of all WUS stations except ALQ for all four source regions.

these data.

The relative travel time residual comparisons indicate the following localized anomalies. The Argentine and Bolivian S waves in the azimuth range of 0^{o} to -15^{o} encounter a lower mantle velocity anomaly producing from 1 to 4 s delays. This anomaly may affect the S waves observed at the large distances to northern Canada as well, but does not appear to affect the ScS times to stations in this azimuth range. The P wave travel times also appear to be slow to these stations, by up to 1 s. The Bolivian data show somewhat less pronounced anomalies. All three South American source regions indicate fast S arrivals at SHA, OXF and FLO, with the anomalies being the largest at SHA (4 s) and decreasing with distance. The same trend is observed in the P waves, though the anomalies are only 1 s or less. A third anomaly appears to produce early ScS travel times to WUS stations, with about 1.5 s anomalies. All four source regions appear to sample this anomaly. There is also some evidence for short wavelength variations in the upper mantle beneath stations involving strong velocity gradients which produce distinctive station character in the ScS-S residuals.

Having identified the phases with anomalous travel times, it becomes possible to locate the anomalies. We first attempt to constrain the location of the anomaly affecting SHA, OXF and FLO for the South American events. The fact that all three source regions sample the anomaly indicates that it is not near any of the source regions. Since the ScS arrivals from each source region miss the anomaly, some lateral constraints on the anomaly's location can be

determined. In Figure II.22, the raypaths for S and ScS waves in a mantle with a JB velocity structure are shown for geometries corresponding to the Peru and Argentina source regions. Since the azimuths involved are similar, it is possible to identify the portion of the mantle that the S wave from both regions sample. This zone is the hatchured area. If we utilize the fact that the travel time anomalies appear to decrease with distance from OXF and FLO for both P and S waves, the raypath of the direct S wave to FLO from Argentina provides an approximate lower depth limit to the anomaly of 1900 km. The fact that the residuals at SHA are similar for the three source regions indicates that the anomaly does not extend farther south at shallow depths than the hatchured region. The anomaly must extend upward to within 1000 km of the surface, but the upper boundary of the anomaly cannot be determined using these data.

When the azimuthal and lateral bounds on the anomaly are projected onto a map, as in Figure II.23, it is clear that the anomaly is centered on the Caribbean as was proposed by Jordan and Lynn (1974). Estimates of the velocity structure under the Caribbean from ScS_2 anomalies indicate that the upper mantle is moderately slow (Sipkin and Jordan, 1976), so the anomaly probably does not project vertically upward to depths above 600 km. The scale length of the anomaly appears to be about 1000 km. Jordan and Lynn (1974) pointed out that the location of this anomaly may be related to the observations by Davies and Capon (1972) of body wave multipathing for a northern Columbian event recorded at the LASA. The velocity contrasts indicated by the 4 s S wave anomalies and 1000 km path

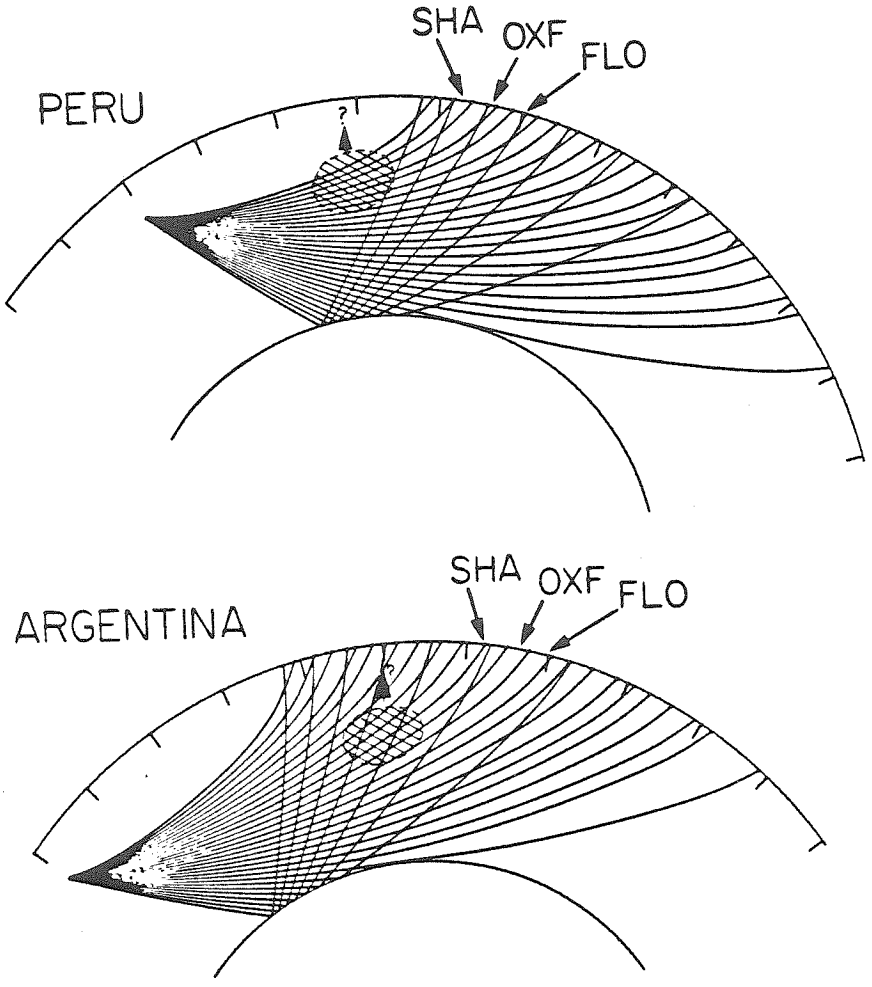

Figure II.22. S and ScS rays traced through a mantle with a JB shear velocity distribution. the source depths are 585 km in each case, and the relative geometries correspond to the Argentina and Peru source regions. The hatchured zone covers the anomalous mantle sampled by S waves to SHA, OXF and FLO from each source region. The constraints on this zone are discussed in the text.

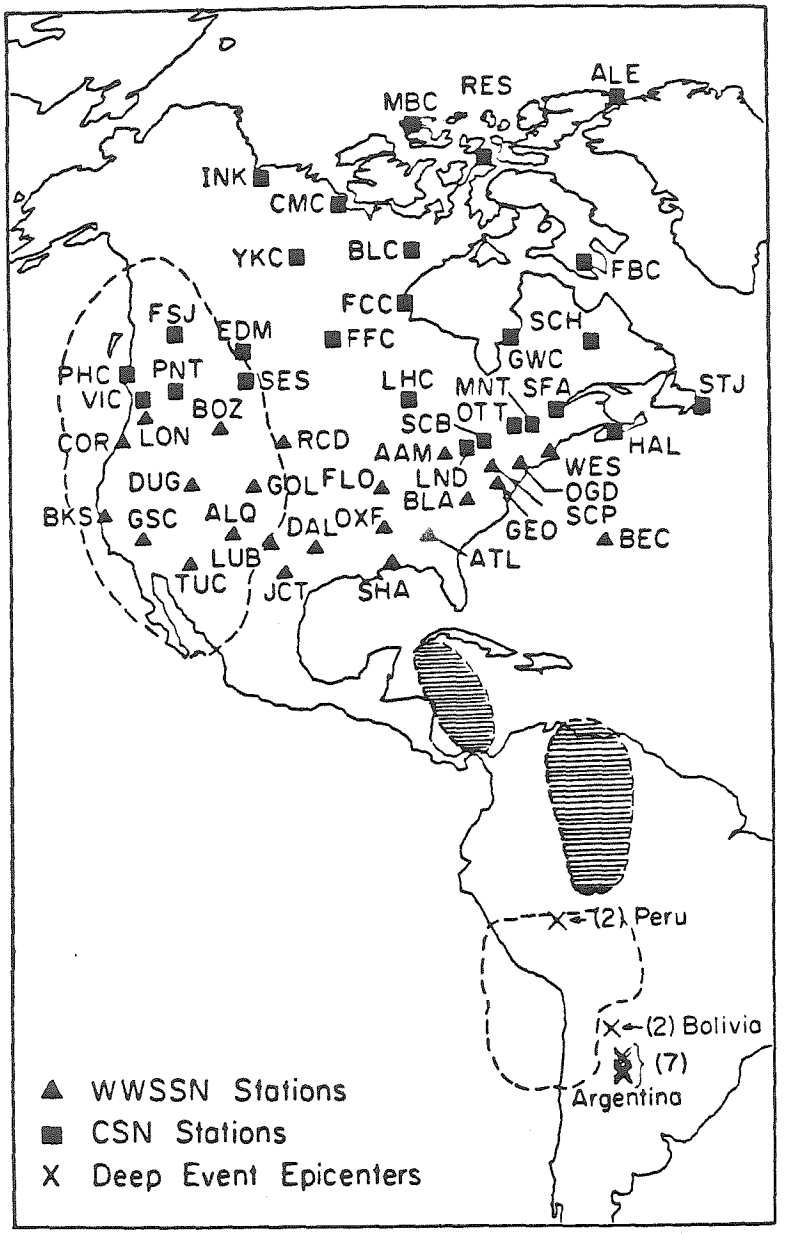

Figure II.23. Map showing the lateral position of the deep mantle anomalies. The fast anomaly beneath the Caribbean is at depths of 1000 to 1900 km; the slow region beneath Northern Brazil is at depths of 1700 to 2700 km; and the large region beneath the western U.S. is the proposed fast S wave velocity zone at depths greater than 2000 km. The dotted line near the Bolivian and Argentine epicenters indicates the range of the PKIKP-P anomaly detected by Pillet (1979). The exact depth range and lateral extent of the anomalous region is not known.

lengths are of the order of 2%.

The anomaly affecting the Bolivian and Argentine S waves in the East Coast cannot be as tightly constrained in location, but is still quite localized. The raypaths for the two source regions are compared in Figure II.24. The region in which the anomaly can reasonably be placed is indicated in the figure. The important constraints on its location are the lack of S or ScS anomalies at BEC, STJ and BLA; the late S times at northern Canadian stations; the normal times for ScS in the azimuth range of the anomaly; and the slightly smaller anomalies in the Bolivian data which are a few degrees closer to the stations. These factors constrain the anomalous region to a zone from 20^{o} to 40^{o} to the north of Argentina, at depths from 1700 to 2700 km. The northern limit of the anomaly is not well constrained, but the fact that the ScS-S residuals at BEC from Peru are not anomalous suggests that the anomaly does not extend north of Venezuela. The likely bounds on the anomaly are projected on the map in Figure II.23. It is possible that the relatively positive ScS-S residual for Peruvian events at STJ (Figure II.20) results from the ScS phase being slowed down by the anomaly. For path lengths of 1000 to 1500 km through the anomalous region the velocity contrasts necessary to produce 4 s S wave delays are about 2%.

If one adopts the hypothesis that the WUS ScS arrivals travel through a deep-seated, relatively fast velocity region for all four source regions, some estimate of the depth range of the anomaly can be made. The high velocity anomaly would have to extend over a broad region beneath the WUS at depths of greater than 2000 km. Isolating

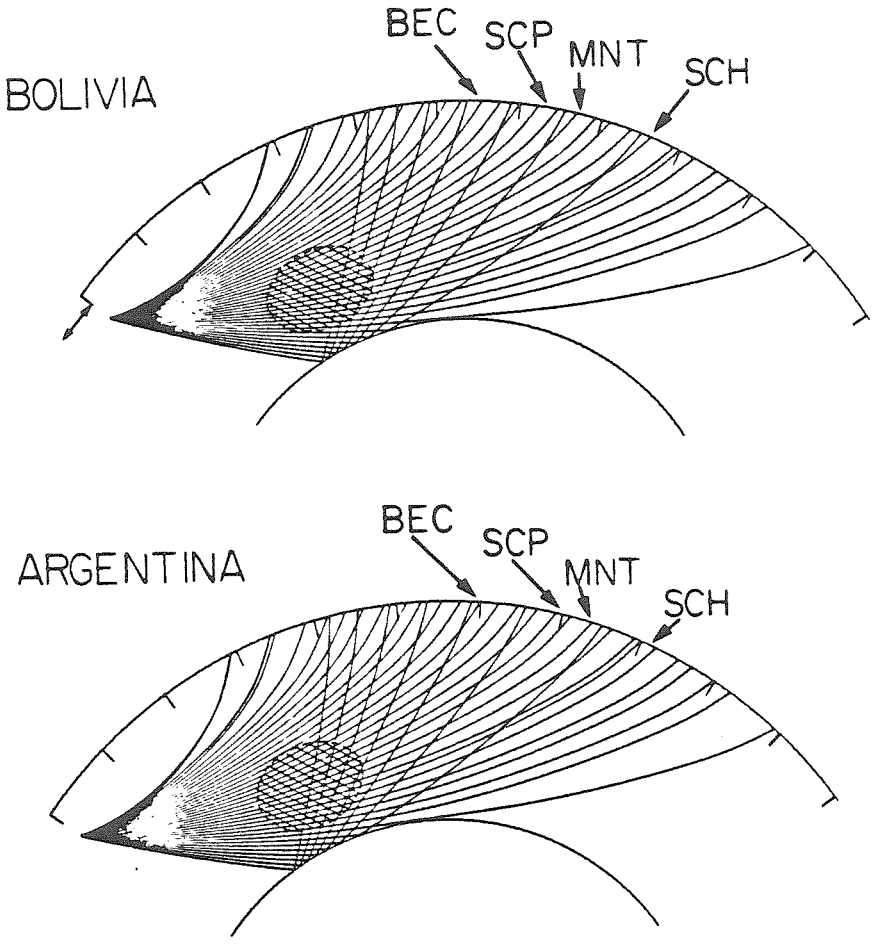

Figure II.24. S and ScS rays similar to those in Figure II.22, but for the relative geometry of the Bolivian and Argentine source regions. The hatchured zone covers the possible range of the lower mantle anomaly affecting the East Coast data, as discussed in the text.

such a deep seated anomaly is difficult because as the distance from the receivers increases, the direct S may start to sample the region also, reducing the diagnostic differential travel time anomaly. One could appeal to such a distance effect to explain some of the ScS-S residual differences between Argentina and Peru at WUS stations, rather than a baseline shift. The nature of the WUS anomaly cannot be resolved unambiguously with our data, since the velocity anomaly is only 1 to 1.5 s, and any source region baseline shifts or distance trends may offset one another. Since the upper mantle shear velocity in the WUS is very slow, it is even harder to find the subtle trends that such a deep, fast region would produce. The approximate lateral extent of this proposed deep anomaly is shown in Figure II.23. Independent evidence for this anomaly has been presented in a P wave travel time study by Kogan (1981). He showed that the mantle beneath the WUS at depths near 2400 km is anomalously fast by 0.7%. P waves traversing the region have anomalies of -0.44 ± 0.21 s.

Amplitude Patterns

Having constrained the position of the localized lower mantle anomalies, it is of obvious interest to determine whether any amplitude anomalies are associated with the travel time anomalies. The SH and ScSH amplitudes, with radiation pattern corrections, for the Sea of Okhotsk and Argentina data are compared in this section. The data processing is described in Section I.2. In Figure II.25, the long period amplitude ratio of ScS/S is plotted as a function of azimuth from Argentina. These ratios have not been corrected for distance, but the expected trend with distance in the range 55^{o} to 75^{o}

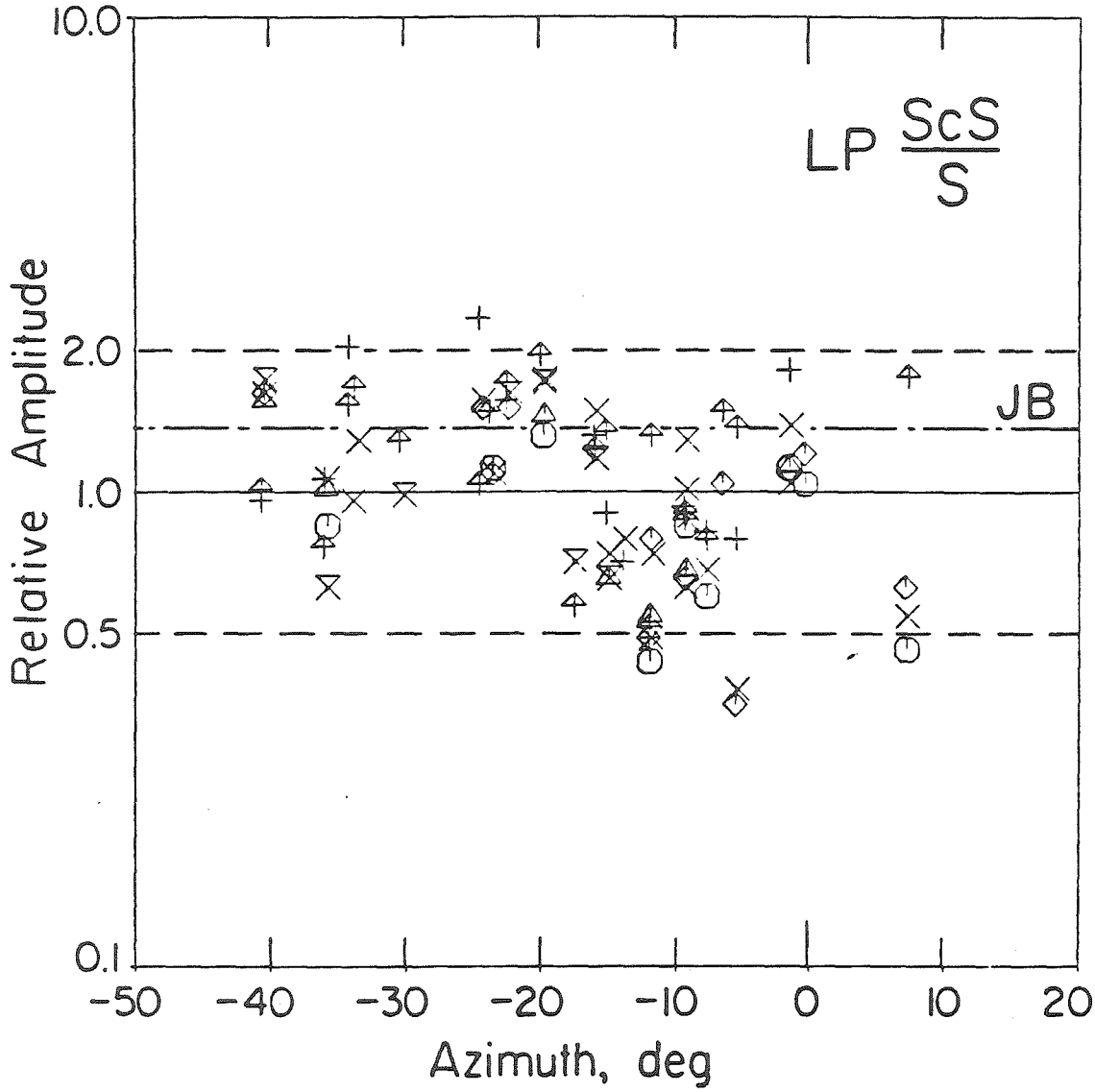

Figure II.25. The long period peak-to-peak amplitude ratio ScSH/SH for the Argentine data plotted as a function of azimuth from the source. Radiation pattern corrections have been applied, but no spreading corrections are included. The East Coast stations in the range -5^{o} to -18^{o} show relatively low ratios. The theoretical ratio for a JB earth model at a distance of 60^{o} is shown for reference.

spanned by the data is small for a JB earth model (Section I.2; Mitchell and Helmberger, 1973). Note that in the azimuth range -5^{o} to -18^{o} the amplitude ratios are relatively small, while there is a slight enhancement of the ratios in the range -20^{o} to -25^{o}. The expected ratio for a JB earth model is indicated in the figure. This trend separates much better when the data are plotted against azimuth than when they are plotted against distance (see Figure I.2.2).

This ScS/S amplitude anomaly was investigated in detail in Section I.2. In order to determine whether the S or ScS phases are anomalous, the radiation pattern corrected amplitudes of each were plotted in Figure I.2.4. Geometric spreading corrections determined from generalized ray theory synthetics for a JB mantle were also applied to the amplitudes. It was found in Section I.2 that the direct S waves show an azimuthal pattern, with relatively high amplitudes recorded at East Coast stations, whereas the ScS phases show no corresponding trend. This suggests that the S waves, which have anomalously late arrival times, are also enhanced in long period amplitude. To test whether this is the case, an independent estimate of the expected amplitude variations across North America is needed.

To provide a reference baseline, the amplitude data from Argentina and Okhotsk were used to determine station amplitude anomalies as is described in detail in Chapter III. The average station amplitude anomalies for the Argentine data show larger relative variations than the Okhotsk data, of a factor of 4, which is suprisingly large for 20 s period signals (see Figure III.2.11). The effects of regional variations in attenuation cannot reasonably

explain the total range in long period amplitudes (Chapter III), though receiver function effects may be important if rather severe three dimensional structures exist beneath the stations. To illustrate the relative behavior, the ratios of the Argentina to Okhotsk stations amplitude anomalies are shown in Figure II.26. Note that the ratios at SCP, GEO, OGD, SCH, SFA and HAL are relatively large, indicating that the Argentina S wave data at the East Coast stations are enhanced by as much as a factor of 2. This is consistent with the S versus ScS behavior shown above. OTT and WES do not show this enhancement, though WES is known to have a relatively complicated SH receiver function unlike the other East Coast stations which are essentially transparent (Chapter III). Another interesting feature in Figure II.26 is the group of low ratios at SHA, OXF, FLO, RCD and BOZ. The latter two stations do not appear to sample the Caribbean travel time anomaly, though RCD is along the same azimuth. DAL, which is close in distance and azimuth to SHA, has a very high amplitude ratio, perhaps suggesting a scattering type interference effect associated with the diminished amplitudes at SHA, OXF and FLO. While the amplitude data cannot be unambiguously interpreted, and amplitude and travel time effects could be totally decoupled, there is a clear coincidence of enhanced amplitudes being associated with the late arrivals and diminished amplitudes being associated with the early arrivals.

For completeness, a similar comparison of the short period SH wave signals was made. In Figure II.27 the ScS/S amplitude ratios are plotted against azimuth from Argentina. There is no general pattern

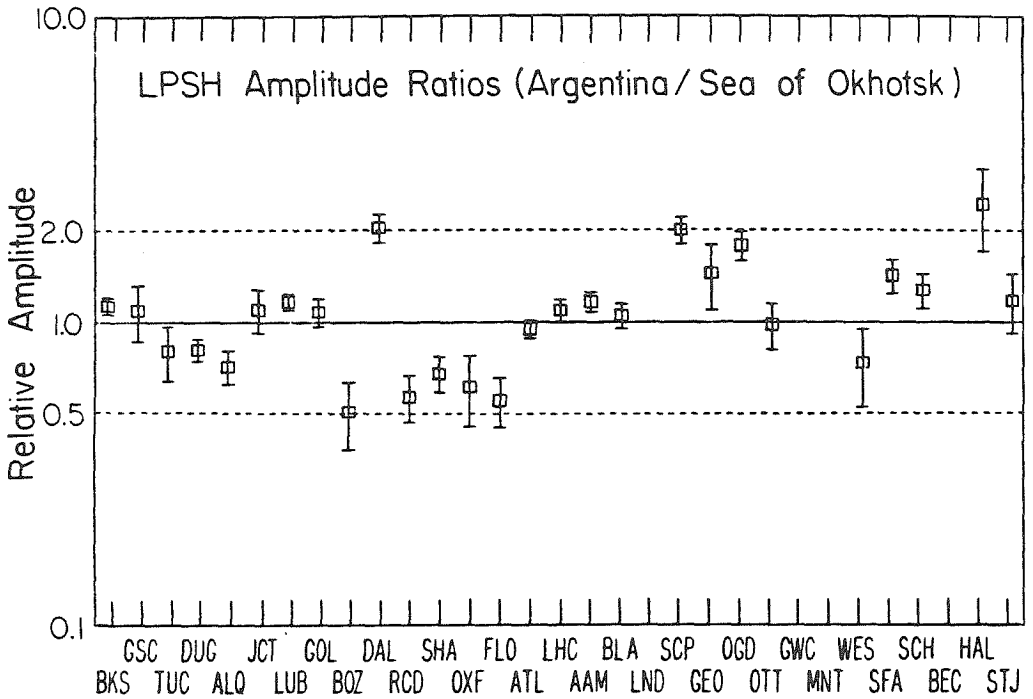

Figure II.26. Ratios of the long period SH station anomalies for Argentina over those for the Sea of Okhotsk. The East Coast stations for the Argentine data are relatively enhanced, whereas SHA, OXF and FLO are relatively low amplitude.

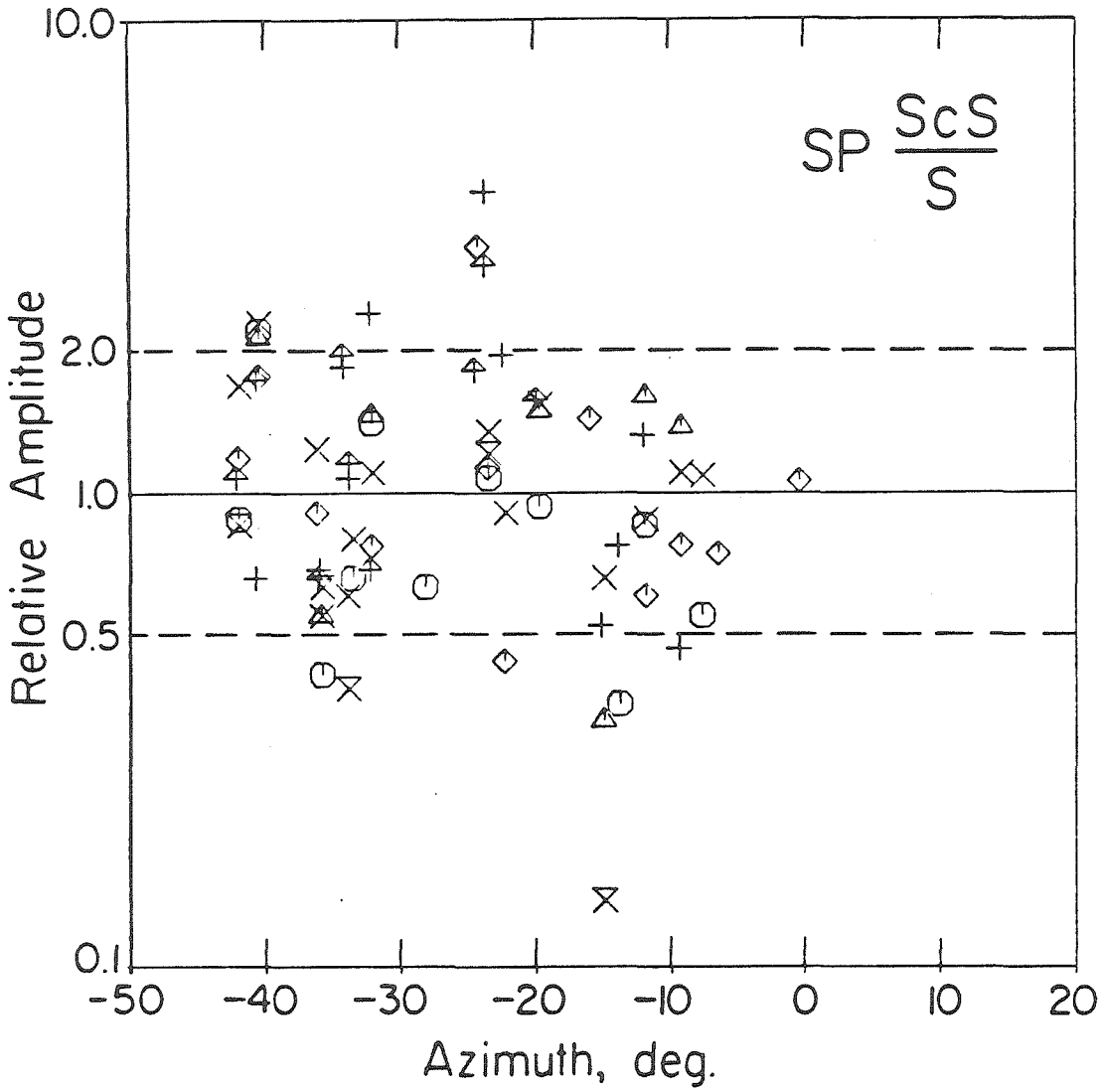

Figure II.27. The short period peak-to-peak amplitude ratio ScSH/SH for the Argentine data plotted as a function of azimuth from the source. Radiation pattern corrections have been applied, but no spreading corrections are included. Note the absence of any East Coast anomaly compared with Figure II.25.

corresponding to the East Coast anomaly in Figure II.25, however the ratios in the range -20^{o} to -25^{o} again tend to be slightly high. The short period S wave amplitude station anomalies determined in Chapter II for the Sea of Okhotsk and Argentina azimuths show larger overall variations than the long periods (see Figure III.2.13), and the amplitude ratios (Figure II.28) indicate greater azimuthal variations, as might be expected for these shorter period (2 to 5 s) signals. The Argentina S waves in the East Coast do not appear to be enhanced relative to the pattern for the northwestern azimuth, but the short period signals at SHA and OXF are a bit low. The most enhanced amplitudes from Argentina are found at the Texas stations which are in the same distance range and fairly close in azimuth to SHA and OXF, but do not show velocity anomalies. Again, this may reflect a defocusing or multipathing effect associated with the lower mantle anomaly rather than merely indicating independent behavior of the travel times and amplitudes.

Discussion

The existence of lateral variations in the lower mantle has many implications for the dynamic behavior and geochemical evolution of the earth. Localized blobs of fast or slow material with scale lengths of 1000 km are intrinsically fascinating phenomena, which lead to important questions about their origins and composition. The fast Caribbean anomaly is at least superficially associated with an upper mantle subduction zone, and may indicate deep mantle penetration as speculated by Jordan and Lynn (1974). However, the slow Northern Brazil anomaly is not clearly associated with upper mantle processes.

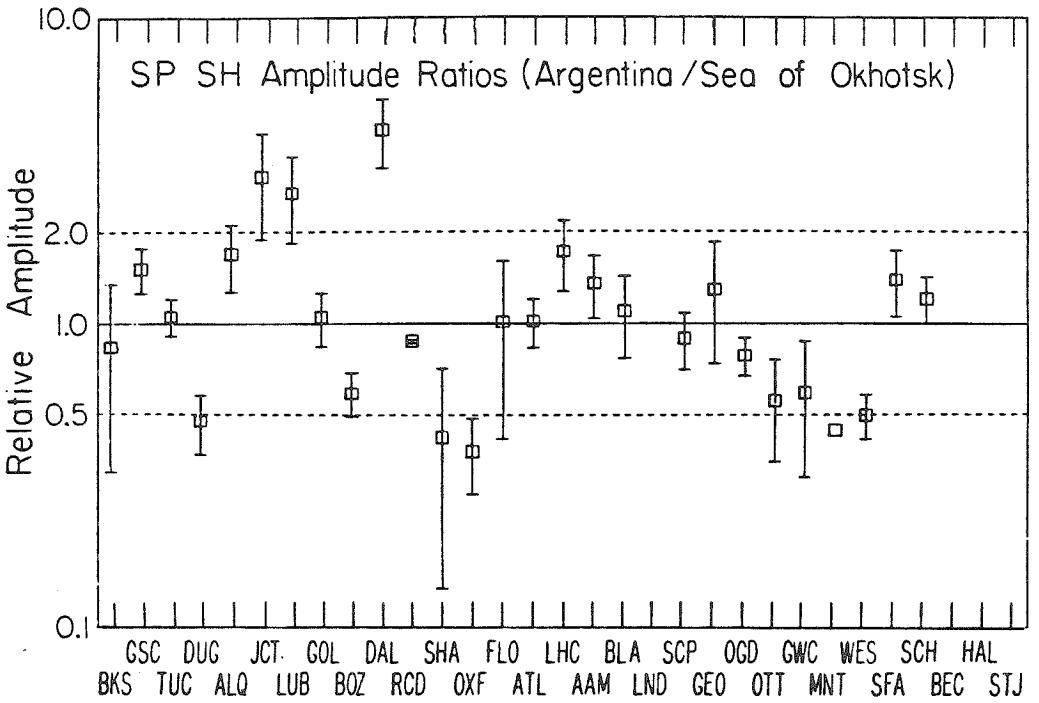

Figure II.28. Ratios of the short period SH station anomalies for Argentina over those for the Sea of Okhotsk. SHA and OXF are slightly diminished from Argentina, and the Texas stations are enhanced. No East Coast anomaly is apparent.

It is not possible to fully characterize the properties of these anomalies with our data, other than to say that 2% velocity contrasts are involved as well as 1000 km scale lengths. The anomalies also appear to have rather abrupt boundaries, given the sharp azimuthal separation of the anomalous times. If the results of this study are representative of the general degree of lower mantle heterogeneity, attaining a complete understanding of mantle composition and dynamics will clearly be a formidable task.

Identifying lower mantle anomalies producing several second velocity variations is important for many different studies, ranging from location of earthquakes to mapping upper mantle or slab velocity structure. The indications of a systematic amplitude effect due to these lower mantle structures is particularly exciting. In many earthquake or explosion source modeling efforts, there is a pervasive scatter in amplitude misfit that is unexplained. The data in Figure II.26 indicate that for long period body waves this scatter may be as much as a factor of 4, even over the limited range in azimuth and for the very simple, stable waveforms of our data. One could speculatively attribute the majority of this amplitude variation to the effects of the lower mantle anomalies. The absence of clear short period amplitude effects associated with the travel time anomalies may result from the large amplitude scatter introduced by receiver structure and lateral variations in attenuation, or it may reflect the physical properties of the lower mantle anomalies. The regions of anomalous velocity may have anomalous attenuation properties that negate any geometric effects on the short period signals, or the

'roughness' of the anomalous region may be such that geometric focusing is less efficient for 5 s periods than for 20 s periods. Through further analysis of the broadband frequency content of the S wave data from Argentina it should be possible to test the hypothesis that major focusing or defocusing effects are produced by the lower mantle velocity anomalies.

The data presented in this paper also indicate the presence of larger scale lateral variations in the lower mantle. The apparent baseline shifts in differential times between source regions is one indication of this, as is the regional pattern of ScS-S residuals in the WUS. The latter anomaly warrants further examination because it is the type of feature which could be mistakenly attributed to near source anomalies. The study of Mitchell and Helmberger (1974) interpreted the long period ScS/S amplitude ratio anomalies in the Argentine data as resulting from high velocity gradients at the base of the mantle. Our data indicate that the S phases are anomalous rather than the ScS phases, and that mid mantle structure produces the anomalies. This result indicates that care must be taken when amplitude ratios or differential times are used to interpret mantle structure.

Conclusions

Through comparison of absolute and differential time residuals from deep events recorded at North American stations two localized lower mantle velocity anomalies have been identified and located. A region of low S and P velocities exists beneath northern Brazil at depths of 1700 to 2700 km. The lateral dimension of the region is

from 1000 to 2000 km, and the velocity contrasts involved are about 2%. The long period S waves that have travel time delays due to this anomaly also show 30 to 100% amplitude enhancement, suggesting a geometric focusing effect. The short period S amplitudes at the same stations do not show an obvious amplitude effect. The second lower mantle anomaly is a fast region located at depths of 1000 to 1900 km beneath the Caribbean. This region has dimensions of about 1000 km, and also involves 2% velocity contrasts. Both short and long period S waves from Argentine events traveling through the fast velocity region show diminished amplitudes. A third region, which could not be well constrained, may exist in the lower mantle below 2000 km deep beneath the western United States. This region appears to produce ScS travel times that are fast by about 1.5 s.

References

Burdick, L. J. and C. Powell (1980). Apparent velocity measurements for the lower mantle from a wide aperture array, J. Geophys. Res., 85, 3845-3856.

Chinnery, M. A. (1969). Velocity anomalies in the lower mantle, Phys. Earth Planet. Interiors, 2, 1-10.

Davies, D. and J. Capon (1972). Body wave multipathing, Seismic Discrimination SATS, pp. 39-40. Lincoln Lab., Mass. Inst. Technol., Cambridge.

Davies, D. and R. M. Sheppard (1972). Lateral heterogeneity in the earth's mantle, Nature, 239, 318-323.

Doyle, H. A. and A. L. Hales (1967). An analysis of the travel times of S waves to North American stations, in the distance range 28^{o} to 82^{o}, Bull. Seismol. Soc. Amer., 57, 761-771.

Dziewonski, A. M. and D. L. Anderson (1981). Preliminary reference earth model, Phys. Earth Planet. Interiors, 25, 297-356.

Dziewonski, A. M. and F. Gilbert (1976). The effect of small, aspherical perturbations on travel times and a re-examination of the corrections for ellipticity, Geophys. J. Roy. Astron. Soc., 44, 7-17.

Dziewonski, A. M., B. H. Hager and R. J. O'Connell (1977). Large-scale heterogeneities in the lower mantle, J. Geophys. Res., 82, 239-255.

Greenfield, R. J. and R. M. Sheppard (1969). The moho depth variations under the LASA and their effect of $dT/d\Delta$ measurements,

Bull. Seismol. Soc. Amer., 59, 409-420.

Hales, A. L. and E. Herrin (1972). Travel times of seismic waves, The Nature of the Solid Earth, New York, McGraw-Hill, 172-215.

Hales, A. L. and J. L. Roberts (1970a). The travel times of S and SKS, Bull. Seismol. Soc. Amer., 60, 461-489.

Hales, A. L. and A. L. Roberts (1970b). Shear velocities in the lower mantle and the radius of the core, Bull. Seismol. Soc. Amer., 60, 1427-1436.

Jeffreys, H. and K. E. Bullen (1940). Seismological Tables, 55 pp., Brit. Assoc. Advancement of Sci., Gray-Milne Trust, London.

Jordan, T. H. (1975). Lateral heterogeneity and mantle dynamics, Nature, 257, 745-750.

Jordan, T. H. (1977). Lithospheric slab penetration into the lower mantle beneath the Sea of Okhotsk, J. Geophysics, 43, 473-496.

Jordan, T. H. and D. L. Anderson (1974). Earth structure from free oscillations and travel times, Geophys. J. Roy. Astron. Soc., 36, 411-459.

Jordan, T. H. and L. N. Frazer (1975). Crustal and upper mantle structure from Sp phases. J. Geophys. Res., 80, 1504-1518.

Jordan, T. H. and W. S. Lynn (1974). A velocity anomaly in the lower mantle, J. Geophys. Res., 79, 2679-2685.

Julian, B. R. and M. K. Sengupta (1973). Seismic travel time evidence for lateral inhomogeneity in the deep mantle, Nature, 242, 443-447.

Kanasewich, E. R., R. M. Ellis, C. H. Chapman and P. K.

Gutowski (1973). Seismic array evidence of a core boundary source for the Hawaiian linear volcanic chain, J. Geophys. Res., 78 1361-1371.

Kogan, S. D. (1981). Anisotropy and large scale lateral inhomogeneity of the upper mantle, Phys. Earth Planet. Interiors, 26, 171-178.

Mitchell, B. J. and D. V. Helmberger (1973). Shear velocities at the base of the mantle from observations of S and ScS, J. Geophys. Res., 78, 6009-6020.

Pillet, R. (1979). Anomalies de propagation des ondes sismiques du manteau inférieur et du noyau terrestres, Thèse d'État, Grenoble, France.

Poupinet, G. (1977). Hétérogéneités du manteau terrestre déduites de la propagation des ondes de volume-implication géodynamique, Thèse d'État, Grenoble, France.

Powell, C. A. (1975). Evidence for mantle heterogeneity from two large seismic arrays, Nature, 254, 40-42.

Romanowicz, B. A. (1979). Seismic structure of the upper mantle beneath the United States by three-dimensional inversion of body wave arrival times, Geophys. J. R. Astron. Soc., 57, 479-506.

Sengupta, M. K. (1975). The Structure of the Earth's Mantle from Body Wave Observations. Sc.D. Thesis, 578 pp., Mass. Inst. of Technol., Cambridge.

Sengupta, M. K., R. E. Hassel and R. W. Ward (1981). Three dimensional seismic velocity structure of the earth's mantle using body wave travel times from intra-plate and deep-focus

earthquakes, J. Geophys. Res., 86, 3913-3934.

Sengupta, M. K. and M. N. Toksoz (1976). Three dimensional model of seismic velocity variation in the earth's mantle, Geophys. Res. Lett., 3, 84-86.

Sipkin, S. A. and T. H. Jordan (1976). Lateral heterogeneity of the upper mantle determined from the travel times of multiple ScS, J. Geophys. Res., 81, 6307-6320.

Strelitz, R. (1975). The September 5, 1970 Sea of Okhotsk earthquake: a multiple event with evidence of triggering, Geophys. Res. Lett., 2, 124-127.

Veith, K. F. (1974). The Relationship of Island Arc Seismicity to Plate Tectonics. Ph.D. Thesis, S. Methodist Univ.

Wickens, A. J. and G. G. R. Buchbinder (1980). S wave residuals in Canada, Bull. Seismol. Soc. Amer., 70, 809-822.

Wright, C. and J. Cleary (1972). P wave travel time gradient measurements for the Warramunga seismic array and lower mantle structure, Phys. Earth Planet. Interiors, 5, 213-230.

Chapter III

Variations in Attenuation and Shear Velocity Beneath North America

Section III.1 Body Wave Amplitude Patterns Across North America

Abstract

A broad band amplitude study of P and SH waves from deep South American events recorded at WWSSN stations in the United States provides constraints on upper mantle variations in attenuation. The events were selected to minimize contamination due to source complexity, radiation pattern, and source structure. The prevalent feature in the short period and long period bands is that the SH amplitudes show the same regional variations as the P amplitudes, with the regional variations of short periods being similar, but enhanced relative to the variations at long periods. The amplitudes show some systematic regional difference between the East Coast and Rocky Mountain provinces, and both short and long periods are enhanced at the Gulf Coast and midwestern stations, probably due to thick sedimentary bed receiver structure. Since detailed receiver structures for individual stations are poorly known, we used the working hypothesis that the regional amplitude patterns are caused by lateral variations in upper mantle attenuation. Both a constant Q and a frequency dependent attenuation operator were considered, with the relative amplitudes and waveforms in short period and long period bands used to estimate the acceptable range of Δt^* in the constant Q model, or the acceptable range of the parameter τ_m, which describes the high frequency roll-off of the absorption band in the frequency dependent model. Time domain modeling indicates that the short period P and SH amplitudes and waveforms in the 1 to 10 sec period range do not unambiguously demand frequency dependent attenuation, allowing for

the uncertainty in source frequency content and long period absorption band amplitude. The short period P amplitudes can be fit with a range in $\Delta t^*_\alpha = 0.5$ sec or a range in τ_m from 0.001-0.25 sec, with either single parameter variation consistent with the general short period SH amplitude behavior. A technique for determining the absolute value of t^* and possible τ_m values appropriate for the 5-20 sec band was applied to selected data. A value of $t^* = 0.8$ sec and small τ_m were found for travel paths from the deep events to North America, and lower t^* or large τ_m values were found for paths to southern African stations. Long period amplitude variations cannot be explained by frequency dependent models with only a single high frequency roll-off of the absorption band, but values of Δt^*_β determined from the long period SH amplitudes do exceedingly well in predicting the long period P amplitudes under the assumptions of constant Q and $t^*_\beta/t^*_\alpha = 4.0$. The total range in long period Δt^*_β is about 3 to 4 sec. Though receiver effects may cause some of this variation between stations, the data make it clear that such effects must produce amplitude behavior similar to that caused by regional variations in attenuation. It is shown that the Δt^*_β values determined from the long periods do not predict the short period amplitudes in detail, but the predictions are not prohibitively outside the range of the short period amplitude variations, as long as the larger long period anomalies are excluded. Spectral analysis of the long period SH waves was also performed, yielding a slightly greater range of Δt^*_β than the time domain results, but the resulting values of Δt^*_β do not predict the amplitude variations well, indicating significant effects of long period

receiver functions on both the amplitude and spectral behavior.

Introduction

This study examines the regional amplitude behavior of body waves over a range of periods from one to 20 seconds. The short period and long period WWSSN seismographs in the contiguous United States serve as a broad array for this purpose. Short and long period P and SH wave amplitudes from deep South American events in Peru and Argentina provide a large data set, which has been carefully screened to minimize factors such as source complexity, trends due to radiation pattern, and source structure. Present knowledge of the receiver structure under each WWSSN station is inadequate for removing receiver effects from the amplitude data, which precludes direct interpretation of the amplitude behavior in terms of upper mantle scattering or attenuation. The general impact of receiver effects is to increase the total range in relative amplitude behavior, particularly between amplitudes recorded at receivers on thick sedimentary layers and amplitudes recorded at stations in tectonically active or shield regions. Bearing this in mind, we sought to determine the bounds on the possible range of lateral variations in attenuation under the United States by finding attenuation models which reproduce the waveforms and amplitudes of the data. The range in period of the data, as well as the simultaneous use of P and SH phases, provides constraints on the attenuation models. Both constant Q and frequency dependent attenuation models have been examined, and time domain and frequency domain methods applied.

Numerous studies have indicated systematic regional differences

in body wave amplitudes and frequency content between the eastern and western United States. The amplitude studies include measurement of short period P wave amplitudes (Cleary 1967; Evernden and Clark 1970; Butler and Ruff 1980); short period and long period P wave m_b (Booth, Marshall and Young 1974); m_b versus M_s (Ward and Toksöz 1971; Evernden and Filson 1971; Marshall, Springer and Rodean 1979); and short period P and S amplitudes (Der, Masse, and Gurski 1975). The majority of amplitude studies have utilized LRSM stations, and these yield a general tendency for body wave magnitudes to be .26 magnitude units larger in the East relative to the West. Spectral analysis of short period P waves (e.g. Der and McElfresh 1977) and of short period S waves (Der, Smart and Chaplin 1980) has produced evidence for lateral variations in upper mantle attenuation with average Δt^*_α = .25 sec and Δt^*_β = .67 sec between the East and West Coasts. Such lateral variations of attenuation, combined with receiver effects, may account for much of the m_b variations at LRSM stations (Der, McElfresh and Mrazek 1979).

The amplitude studies utilizing WWSSN data of Butler and Ruff (1980) and Burdick (1978) failed to detect significant east to west differences in amplitudes, though individual stations showed distinctive amplitude patterns and some regional trends. These studies were more selective in choosing simple, coherent nuclear explosion and earthquake data than most previous studies. This selectivity is necessary for analysis of amplitude trends in the time domain, as it minimizes the effects of source complexity and radiation pattern, which can otherwise only be limited by utilizing very large

data sets. Analysis of long period WWSSN body wave spectra indicates regional variations in attenuation of Δt^*_β = 7.0 sec (Solomon and Toksöz 1970; Mikumo and Kurita 1968; Teng 1968). The resulting Δt^* values differ from, and exceed, those determined at short periods. This last point has been asserted as evidence for frequency dependence of attenuation, since the long period values of t^* would prevent observation of 2-4 Hz energy in short period P and S waves.

The amplitude data gathered in this study do not clearly indicate a simple east to west regional amplitude variation in the short period band. The major amplitude anomaly is in the Great Plains and Gulf Coast regions, for both short period and long period waves, consistent with the results of Butler and Ruff (1980) and Der et al. (1979). As shown in this paper, the amplitude variations are grossly consistent with regional variations in upper mantle attenuation, and this consistency argues against dismissing the amplitude behavior as being purely the result of varying receiver structure until further constraints are placed on the regional variations. Section III.2 will present data from other azimuths and a more detailed assessment of the individual receiver structures.

The evidence for lateral variations in attenuation from spectral studies has principally been gathered from data in the .5-10 Hz band (Der et al., 1980). The relatively high energy levels observed at frequencies greater than 1 Hz are inconsistent with frequency independent t^* values of around 1 sec that are often adopted in the long period body wave band (10-30 sec). This indicates that either t^* is frequency dependent within the body wave band, or the long period

body wave t^* values are inappropriate. There are large uncertainties in the absolute t^* levels throughout the body wave band, though the t^* values for periods shorter than one second must be low enough to allow the high frequency energy to be observed. Because of this uncertainty it is not obvious at what periods frequency dependent effects may be apparent. In this section we analyze the amplitude and waveform behavior of the WWSSN body waves in terms of their implications for either frequency independent or frequency dependent attenuation in the period range 1 to 20 sec. We first consider frequency independent, but laterally varying, t^* models to check the consistency of such models with the data in this period range. In this analysis, due to the tradeoffs between source time function and attenuation, the absolute levels of t^* chosen for the time domain models are unimportant. The results indicate that the WWSSN body waves are fairly consistent with frequency independent attenuation assuming $t^*_\beta = 4t^*_\alpha$, as long as significant lateral variations in t^* are permitted. This result follows from the pervasive tendency for the amplitude variations of P and SH to track one another in the 1-20 sec band.

In order to accommodate the possilility that t^* does vary with frequency in this period range, we also adopt a frequency dependent Q model after Minster (1978a,1978b). This model introduces a roll-off in the absorption band so that short period signals are less attenuated than long periods compared with the constant Q model. We find that such models can be consistent with the WWSSN data, but the data do not clearly demand frequency dependence. This procedure is somewhat sensitive to the choice of t^*, but both the waveform modeling

and absolute t^* determinations that are performed indicate that we have chosen appropriate long period t^* values. The presence of the absorption band roll-off ensures that these models are not inconsistent with the observations of significant energy at frequencies greater than 1 Hz. Since we lack detailed receiver corrections we cannot determine reliable station dependent attenuation parameters, rather the principal gain from this modeling is in demonstrating the consistency of the WWSSN amplitudes and waveforms with laterally varying attenuation of either frequency dependent or frequency independent models.

Data

Twenty five WWSSN stations in the United States have been operating over at least several years since the establishment of the network in 1962-1963. After 1965, all stations have been operating with uniform instrumentation, with short periods peaked at 0.70 second and long periods peaked at 15 seconds, except for the station at Golden, GOL, which has continued to operate its long period instrument with a response peaked at 30 seconds. The gain settings vary widely for both short period and long period instruments, ranging from x6250 to x400000 and from x750 to x6000 respectively. Thus, there is considerable variation in the amplitude of recorded body wave phases and in the reliability with which they may be measured and digitized. The data selection process has been such as to only accept data with good signal-to-noise ratio, resulting in fairly uniform data quality.

Since this study is concerned with upper mantle and receiver variations, the earthquake data have been carefully screened to

minimize source complications. Because of presumed large upper mantle attenuation, only deep earthquakes have been analyzed, so as to clearly observe short period SH phases. We selected deep South American events because the resulting range in azimuth to North American stations is relatively small, spanning 32^{o} from Argentina and 50^{o} from Peru, ensuring that the deep mantle paths are similar for a given event. The two clusters of deep earthquake activity in Peru and Argentina range in distance across the United States from 42^{o} to 71^{o} and 60^{o} to 90^{o} respectively. Typically, the data collected for a particular event span smaller ranges in azimuth and delta since the event may not be recorded at all stations, and due to omitting any SH data contaminated by SKS or ScS, which interfere beyond 80^{o}.

In selecting the data, several criteria were imposed. Most importantly, we considered only simple, impulsive events with clear body wave arrivals. We also required adequate coverage of a particular event to measure amplitudes at eastern and western stations. Another basic constraint was that first motions had to be consistent across the "array", with demonstrable phase coherence. These criteria were imposed with the intention of maximizing the reliability of the amplitude behavior for this relatively small data set by limiting source effects. Several events with focal mechanisms determined by other researchers were included in the data, and the first motions at all WWSSN stations were checked for comparison with events for which published mechanisms were not available. It was found that the source orientations are naturally divided between Peru and Argentina, with deep events in Peru favoring stable P wave

radiation across North America, and events in Argentina favoring stable SH wave radiation. All deep events recorded since 1964 with $m_b \geq 4.9$ were examined, utilizing the combined WWSSN film libraries of Caltech, Menlo Park, and UCLA. Table III.1.1 provides a listing of NOAA catalog hypocenters of acceptable events and the phases selected for examination. Figure III.1.1 shows a gnomonic projection of the WWSSN stations used and the earthquake epicenters. All of the events for which long period SH waves were obtained (m_b = 5.5 - 5.8) were used in the short period SH analysis. The events for which long period P waves were large enough to measure reliably (m_b = 5.5 - 6.2) generally had few measurable short period amplitudes. The short period P waves were collected from events with m_b = 5.0 - 5.3, and were all confined to the Peruvian zone.

Focal mechanisms of eight of the 19 events used in this study were available. The P and SH mechanisms for six of the events, as determined by Stauder (1973) using first motion and S wave polarization, are shown in Figure III.1.2. In each lower hemisphere nodal projection, the take-off directions of stations at the extremes in azimuth and distance used for that particular event are shown. With the exception of the 1968 event, the mechanisms are all for Argentinan events used in the SH analysis. It is clear that for these normal-faulting events, the conditions producing favorable SH radiation are the proximity of one of the P nodal planes to the projection of stations on the western continental margin. Only one event, that of July 25, 1969, of the eight events used in the SH analysis has a P nodal plane that actually intersects the array.

Table III.1.1 Earthquake Data Set

Date	Origin Time	Lat.,°S	Lon.,°W	Depth,km	m_b	Phase
9 Dec. 1964	13:35:42.4	27.5	63.2	586.	5.9	SH(sp)
22 Dec. 1964	00:24:48.7	9.5	71.3	614.	5.3	P(sp)
18 Feb. 1965	22:32:19.6	9.9	71.2	594.	5.2	P(sp)
5 Mar. 1965	14:32:19.2	27.0	63.3	573.	5.5	SH(sp,lp)
3 Nov. 1965	01:39:03.1	9.1	71.4	593.	6.2	P(lp)
20 Dec. 1966	12:26:54.6	26.1	63.2	586.	5.7	SH(sp,lp)
17 Jan. 1967	01:07:54.3	27.4	63.3	588.	5.6	SH(sp,lp)
27 Mar. 1967	08:26:34.6	8.9	71.4	605.	5.3	P(sp)
9 Sep. 1967	10:06:44.1	27.7	63.1	578.	5.8	SH(sp,lp)
11 Oct. 1967	20:28:10.2	10.3	71.2	585.	5.0	P(sp)
23 Aug. 1968	22:36:51.3	22.0	63.5	537.	5.8	P(lp)
25 Jul. 1969	06:06:42.4	25.6	63.3	579.	5.5	SH(sp,lp)
13 Dec. 1971	16:19:00.1	8.9	71.6	614.	5.3	P(sp)
12 Jan. 1972	09:59:10.3	6.9	71.8	580.	5.9	P(lp)
21 Jan. 1972	19:18:57.2	6.7	71.9	562.	5.6	P(lp)
3 Jan. 1973	02:58:16.7	27.7	63.3	563.	5.6	SH(sp,lp)
25 Oct. 1973	14:08:59.5	22.0	63.7	529.	6.1	P(lp)
11 Feb. 1975	21:56:49.5	20.7	62.9	562.	5.3	SH(sp)
9 Apr. 1977	04:04:12.5	10.0	71.2	564.	5.5	P(lp)

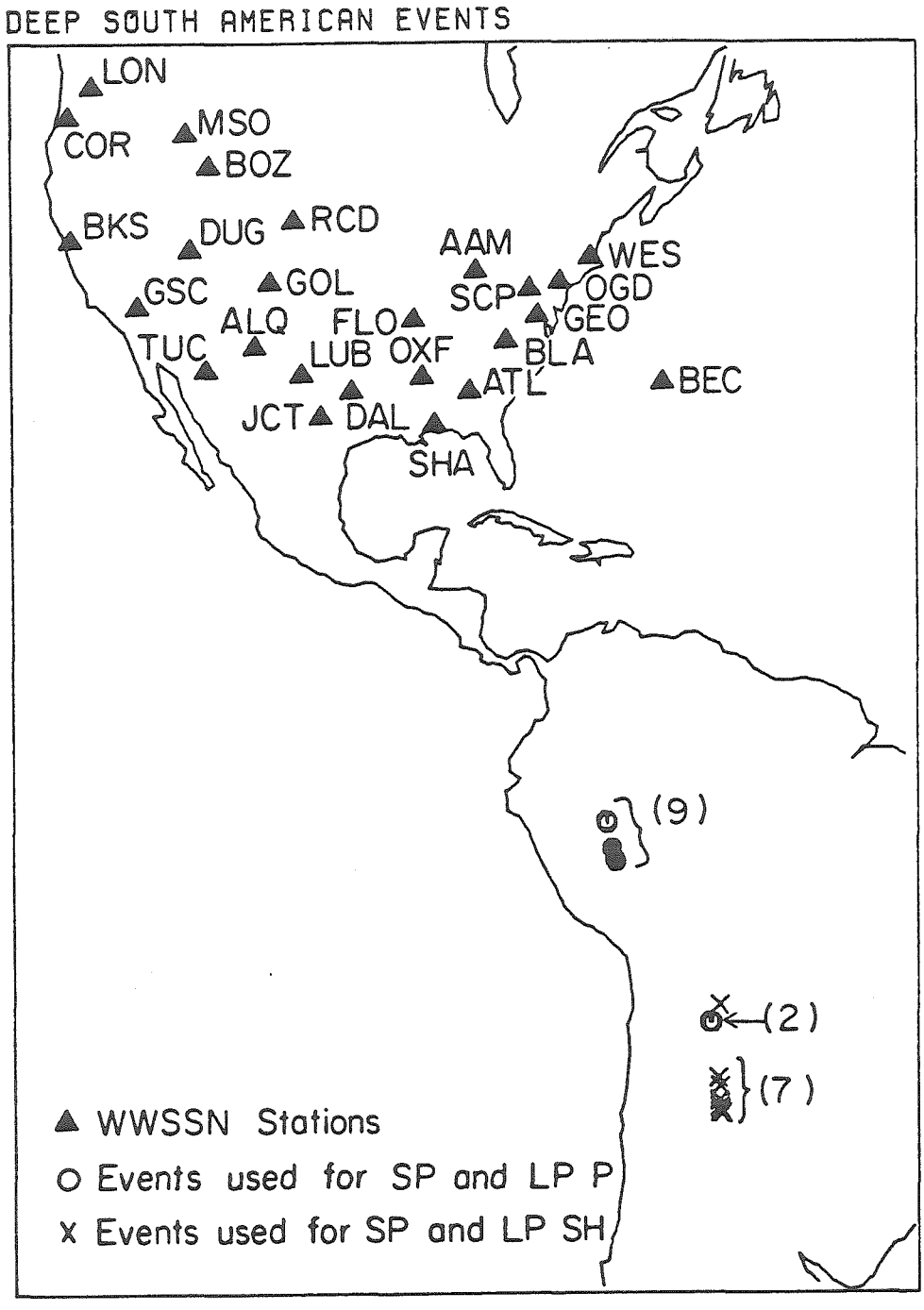

Figure III.1.1. A gnomonic projection (all great circles are straight lines) showing the epicenters of the deep events in Peru and Argentina and the location of WWSSN stations used in this study.

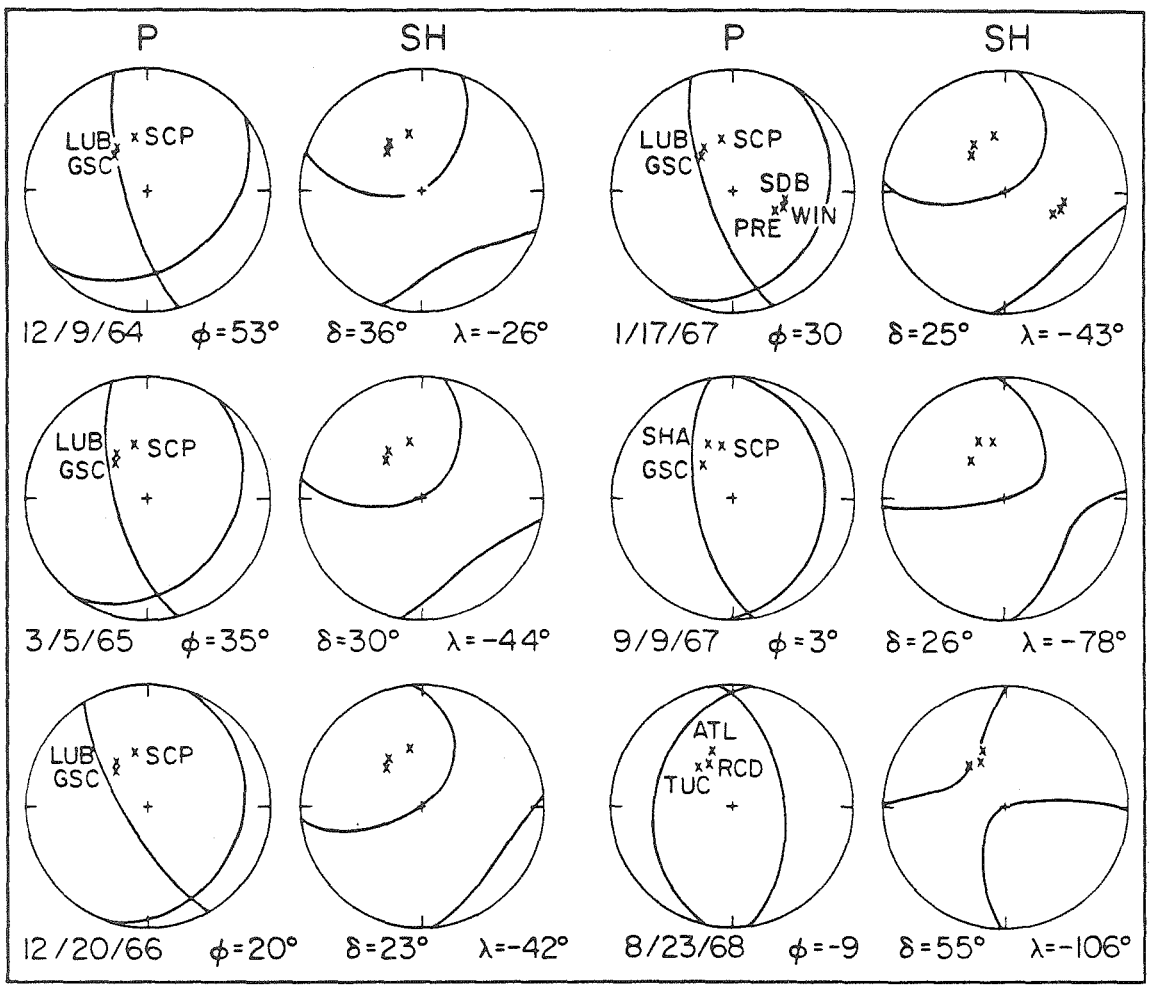

Figure III.1.2. P and SH equal area nodal projections in the lower hemisphere for some of the events used in this study. For each event, projections of stations at the extremes of azimuth and distance for the data from that event are shown.

Thus, any high frequency directivity effects caused by rupture along the nodal plane should be confined to the westernmost stations. The 1968 event occurred in northern Argentina and has a focal mechanism similar to the Peruvian events used in the P wave analysis, (Stauder 1975). For instance, the focal mechanism of the November 3, 1965 event was given by Khattri (1969) as $\phi = -9^{o}$, $\delta = 52^{o}$, $\lambda = -88^{o}$. Focal mechanisms for the same events shown in Figure III.1.2 were given by Isacks and Molnar (1971), with most solutions being very similar and the least constraint being on the northeast trending P wave nodal plane, which does not affect the location of the SH radiation nodes significantly.

Of all the data collected, the short period P waves were from the events for which the focal mechanisms were least constrained. To circumvent this, only events in Peru, for which the larger events are known to have favorable P radiation patterns, were used. The short period P amplitudes from four Argentinan events, including the events of January 17, 1967 and December 20, 1966, were measured and compared with the pattern from the Peruvian events. These amplitudes all showed a stable east to west decreasing trend relative to the Peruvian amplitudes, consistent with the known nodal proximity of the Argentinan P waves. This indicates that the Peruvian amplitudes are indeed free of such bias. This comparison was also done for the long period P data with similar results. Synthetics computed with the focal mechanisms shown in Figure III.1.2 indicate that the range in amplitude variation caused by radiation pattern should be less than 25% for any given event, for all phases used in this study. Use of

several events probably reduces this source of error considerably.

In the course of measuring amplitudes, the calibration pulse and calibration current recorded on the seismograms were checked to ensure correct gain setting. Though the only viable test of this was by amplitude measurement of the calibration pulse, the results give some confidence in the stability of the WWSSN instruments over the sixteen years spanned by the data set. Generally, short period calibration pulse amplitudes fluctuated by about 5% with rare fluctuations as large as 30%. The long period fluctuations were generally on the order of 10% with occasional deviations of up to 30%. Data with exceptionally bad calibration amplitudes were excluded.

The only detailed study of short period SH phases across North America has been performed by Der et al. (1980), who rotated LRSM recordings into SV and SH. They then fit lines to the log amplitude spectra to infer Δt^*_β variations. The LRSM instruments are responsive to slightly higher frequencies than the WWSSN short period instruments, but the major difference is in the faster recording speed of the LRSM instrument, which allows for more accurate digitization and rotation of the SH component. For WWSSN data, this stage of processing is undoubtedly the source of some amplitude and waveform error, though the relatively long period nature of the SH observations offsets this somewhat. We selected events with adequate signal-to-noise ratio to enable accurate digitization. The East Coast stations recorded SH predominantly on the EW component for the events used, and required little rotation, but western stations required greater rotation. Fortunately, the very low background noise level of

western stations and the high gains that they operate at, permit good confidence in the resulting rotated phases. The SH data collected for this study constitute an important new data set of high quality and are discussed below.

Figures III.1.3 through III.1.10 present plots of the rotated short period and long period SH phases. Station data are not presented when film records could not be located; the event was not recorded; the trace was too faint to reliably digitize; or long period transients obscure the arrival. For the 1964 and 1965 events, most WWSSN stations were operating with long period instruments peaked at 30 seconds, and few long period arrivals were recoverable. The amplitudes in all of these figures have been normalized to unit peak amplitude in order to better portray differences in complexity and frequency content.

In Figure III.1.3 only short period waveforms are shown. A five second leader ahead of the SH arrival indicates the signal-to-noise ratio. The length of digitized signal may vary due to location on the seismogram and omission of later ScS arrivals. This event has the largest body wave magnitude of those used for the SH analysis, yet has simple, high frequency pulses which are rather coherent from station to station. Note the strong second arrival at BEC, a feature that occurs frequently in this data set and represents a receiver effect. Note also that ATL, LUB, OXF and RCD have the highest frequency SH waves. GOL, ALQ, TUC and GSC appear somewhat lower in frequency content, consistent with the observations of Der et al. (1980). ScS phases are present in the coda of some western stations, but are

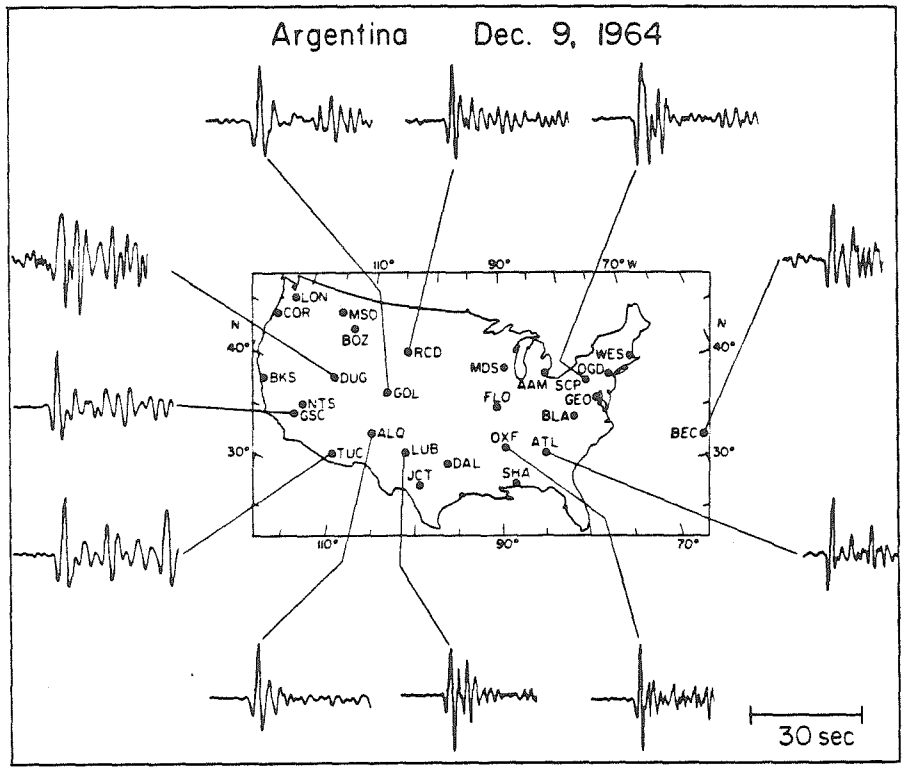

Figure III.1.3. Rotated short period SH components of the December 9, 1964 event recorded at WWSSN stations in the United States. Peak amplitudes are normalized to unit amplitude.

always at least several seconds after the SH phase. The receiver structure at DUG is exceedingly complicated judging from the ringing nature of the coda, but this ringing is somewhat enhanced by the arrival of the strong second pulse which may be ScS. The amplitude ratio of SH to SV varies from about one in the West to more than two in the East for this event. The radiation patterns for SV indicate rapid amplitude variations across the array for this and the other Argentine events, thus no attempt has been made to incorporate SV data in this study other than to note the greater complexity of the SV signals, which presumably results from receiver structure.

The data in Figure III.1.4 includes a few long period SH signals, but only ALQ and TUC had changed the peak response to 15 seconds at this date. The similarity of signals between instruments peaked at 30 and at 15 seconds is due to the similarity in response over the 10 to 20 second band, which spans the dominant periods of these long period SH signals. The amplification difference over this range averages only 20%. The numbers shown are the gain corrected amplitude ratios of the short period to long period signals. The amplitudes measured were the zero line-to-peak of the first half cycle of the long period SH, which was chosen to avoid receiver structure complexity later in the signal, and the peak-to-peak measurement of the first 1 1/2 cycles of the short period signal. This latter amplitude was measured rather than the first peak-to-trough amplitude because it was subject to less scatter between events. Note that the short period to long period amplitude ratio can vary by a factor of three, even between closely adjacent stations such as SCP and OGD or TUC and ALQ. The strong

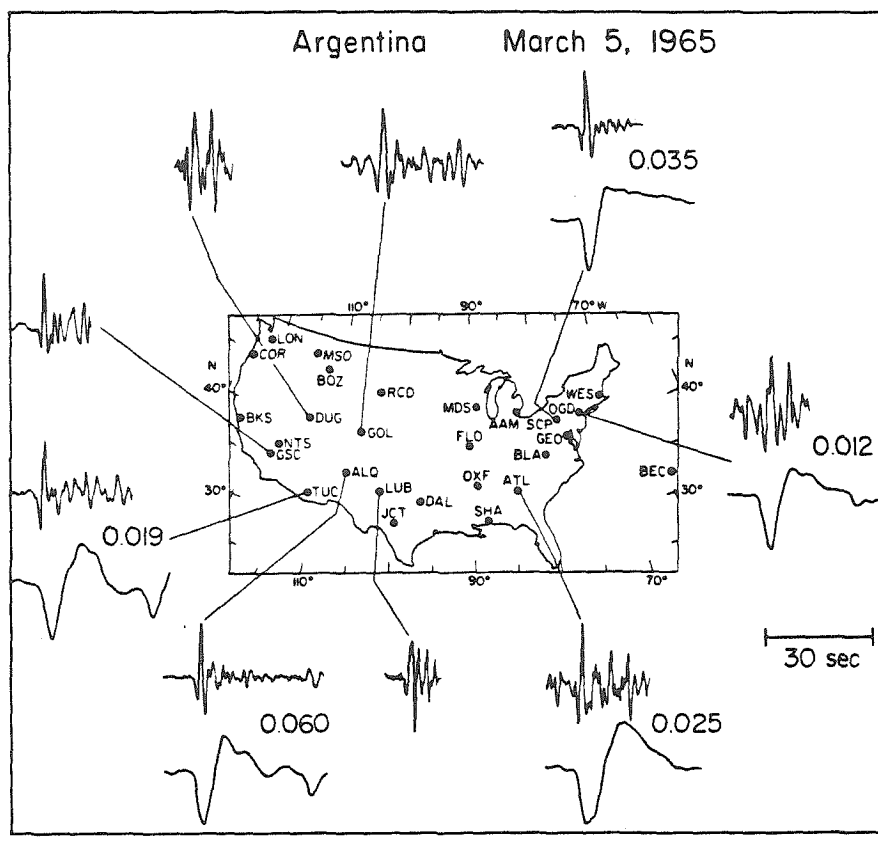

Figure III.1.4. Short period and long period SH components of the March 5, 1965 event. Only stations ALQ and TUC have long period response peaked at 15 seconds, the rest are peaked at 30 seconds. The numbers given are the gain corrected short period to long period amplitude ratios.

second arrival at OGD is not present at SCP, thus some of the short period amplitudes may be diminished by scattering at OGD. There is evidence that such is the case at TUC also, where both the long periods and short periods show strong arrivals about 10 seconds after SH. As proves true for all of the events, ATL and LUB have very high frequency signals. The strong second arrival at DUG is either a receiver phase or ScS.

More complete long period and short period SH data sets are shown in Figures III.1.5 through III.1.9. The data in Figures III.1.5 and III.1.6 indicate that these were very similar events as suggested by the focal mechanisms of Figure III.1.2. Of particular interest are the high frequency content and large short period to long period ratios for stations OXF, FLO, JCT and LUB. Strong second arrivals are apparent at BEC, SHA and TUC. ScS arrives in the SH overshoot at BOZ, GSC, DUG, and RCD, but is sufficiently delayed to reliably measure the first half cycle of SH. There is no obvious distinction in frequency content between the Rocky Mountain stations and East Coast stations; the only signals with consistently different frequency content being those recorded by the midwestern and Gulf Coast stations which are known to overlie sedimentary structures (Butler and Ruff 1980).

These figures show that the long period waveforms at OXF and ATL stand out as being exceptionally long period. Signals at GOL were recorded with a peak instrument response of 30 seconds, so they too are broadened. Burdick (1978) found large amplitude ratio anomalies associated with ATL and OXF, and his data included the events in Figures III.1.6 and III.1.7. He correctly attributed some of the OXF

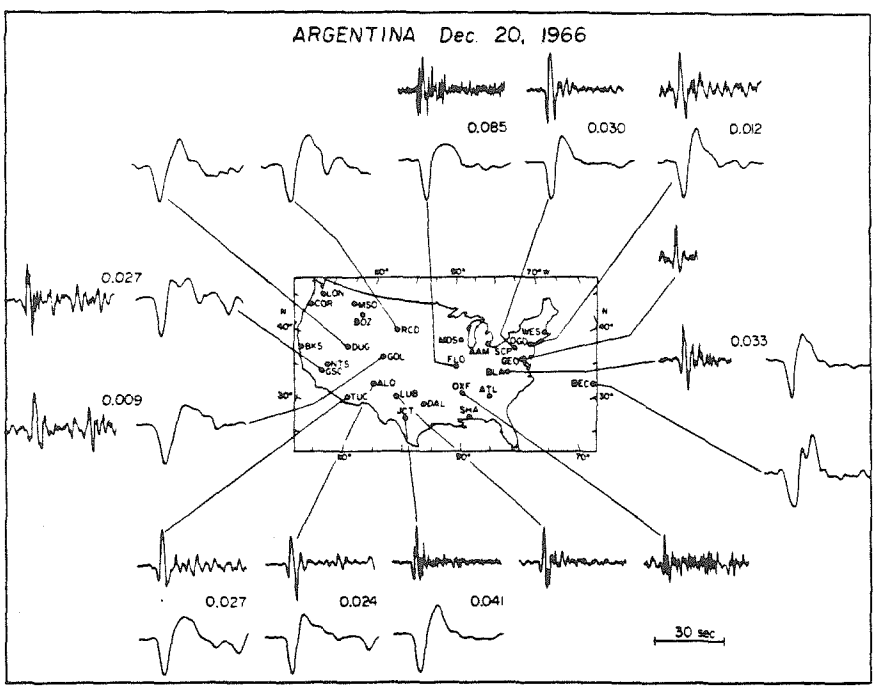

Figure III.1.5. Short period and long period SH components and amplitude ratios of the December 20, 1966 event. All stations except GOL have long period response peaked at 15 seconds for this and the following figures.

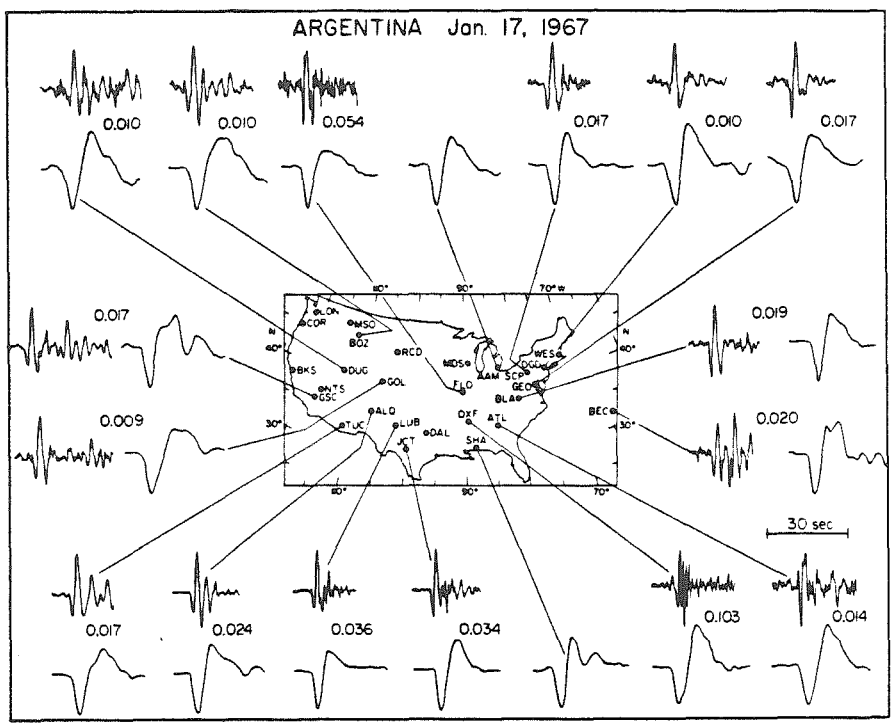

Figure III.1.6. Short period and long period SH components and amplitude ratios of the January 17, 1967 event.

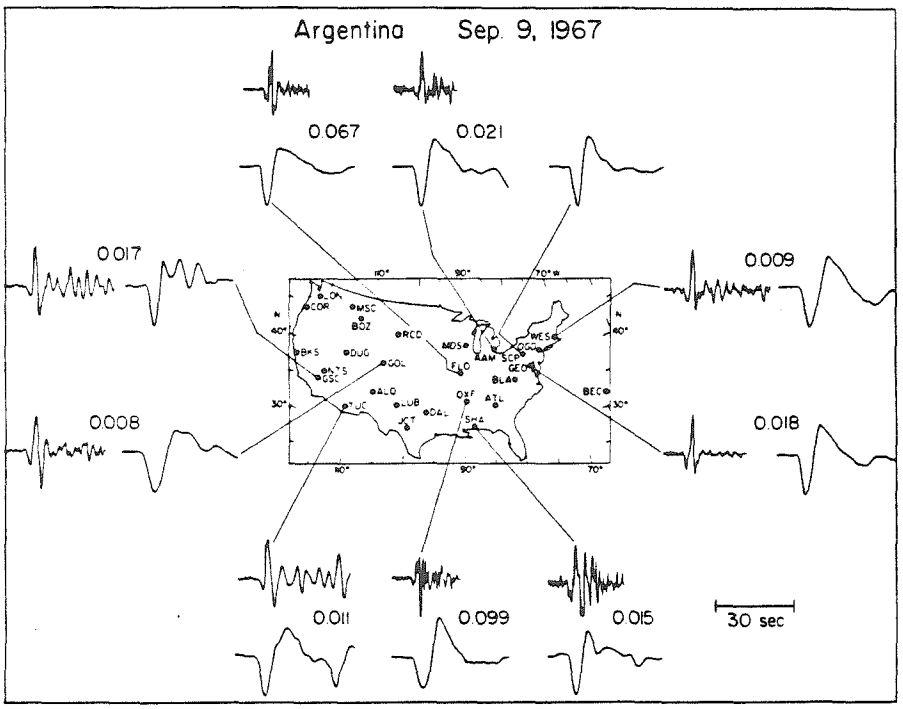

Figure III.1.7. Short period and long period SH components and amplitude ratios of the September 9, 1967 event.

anomaly to a substantial drop in long period amplitude relative to adjacent stations, presumably a strong receiver effect. The high frequency arrivals at OXF are also associated with relatively high short period amplitudes. In these data ATL does not show anomalous amplitude ratios, only very broad long period waveforms.

The event of July 25, 1969, shown in Figure III.1.8, has very complete coverage, but slightly greater SH wave complexity. This complexity is not manifested in the long period signals, but is rather clear in the short periods. There appears to be a second pulse in the short period waveforms, smaller than the first and a few seconds later. Despite this, the waveforms are still rather coherent, and demonstrate the same characteristics as the other events. For this event, the P nodal plane appears to trend north through JCT, but it is difficult to discern any obvious effects of having the nodal plane actually segment the array.

The focal mechanism for the event in Figure III.1.9 was not well constrained by first motions. However, a comparison with Figure III.1.3 shows that the short period waveforms at common stations ATL, GSC, TUC and ALQ are virtually identical, and thus, the mechanism is probably much the same as for the 1964 event shown in Figure III.1.2. The distinctive feature in Figure III.1.9 is the very large amplitude ratio at DAL. This value is the only one determined for DAL, a station with an erratic recording history, and is thus somewhat suspect. The high frequency of these simple SH pulses, relative to the other events, does tend to enhance any visual difference between the East and West Coast stations. This may be consistent with Der et

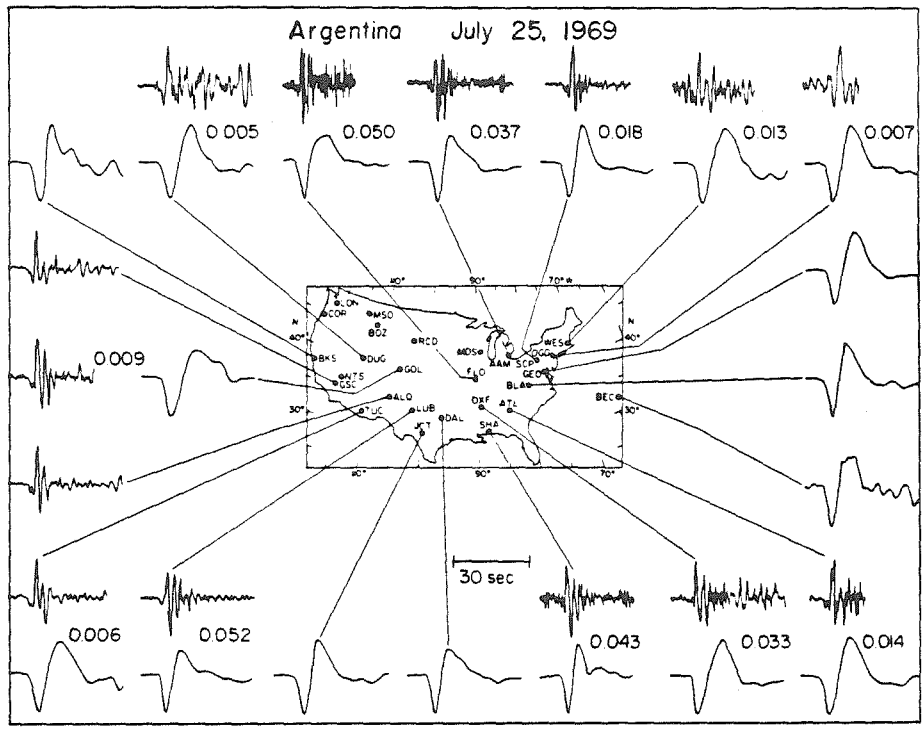

Figure III.1.8. Short period and long period SH components and amplitude ratios of the July 25, 1969 event.

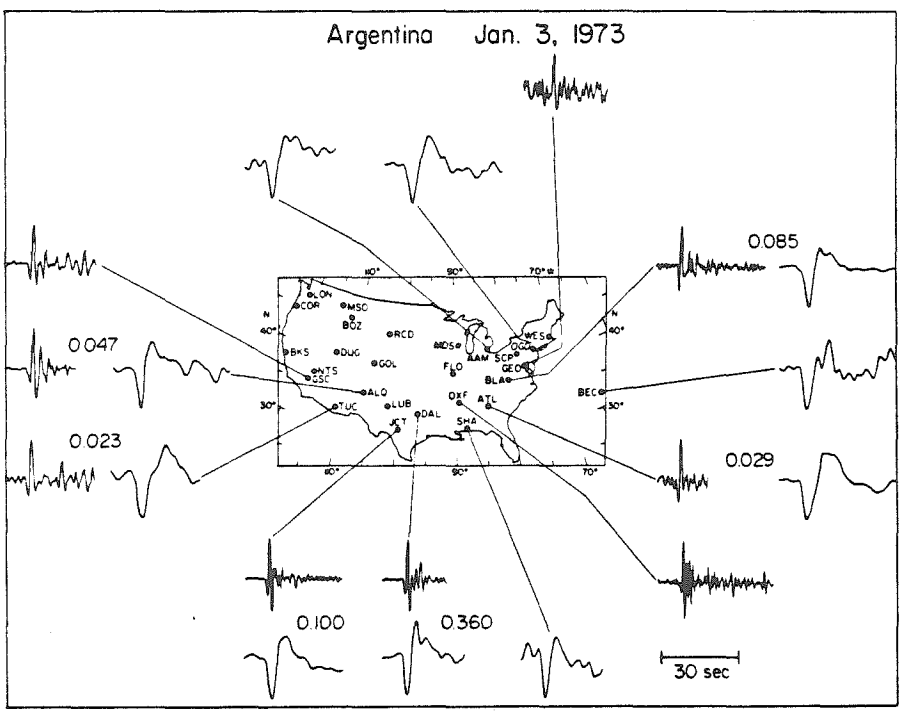

Figure III.1.9. Short period and long period SH components and amplitude ratios of the January 3, 1973 event.

al.'s (1980) assertion that higher frequency sources seem to show more dramatic differences in East versus West Coast signals.

The last event included in the SH data set (Figure III.1.10) is a small event that was located slightly north of the other events. The signal-to-noise ratio is substantially lower due to the small size of the event and no long period signals were retrievable. Though the waveforms are not quite as stable as desired, it is of interest to determine whether there is resolvable source region bias in the data, which will be discussed later. The basic constraint on the focal mechanism of this event was that the western P waves were close to being nodal, as was the case for the other events used to obtain SH phases.

The amplitude data set for long period P consists of six events, four located in Peru, and two located in northern Argentina, as shown in Figure III.1.1 and Table III.1.1. All events were checked for consistency with favorable P-wave radiation patterns, which was facilitated by three published focal mechanisms of events used. The gain setting of WWSSN instruments required examination of slightly larger magnitude events than for the other phases, but all long period waveforms were selected to be as simple and as impulsive as possible. An example of the P wave data is shown in Figure 2 of Mikumo and Kurita (1968). Stations at all azimuths from 30^{o} to 90^{o} were checked to ensure similarity in P and S waveforms in order to avoid excessive source complexity. Several of the events had relatively strong second arrivals about ten seconds after P, which may indicate some source complexity, but this did not contaminate the amplitude measurements,

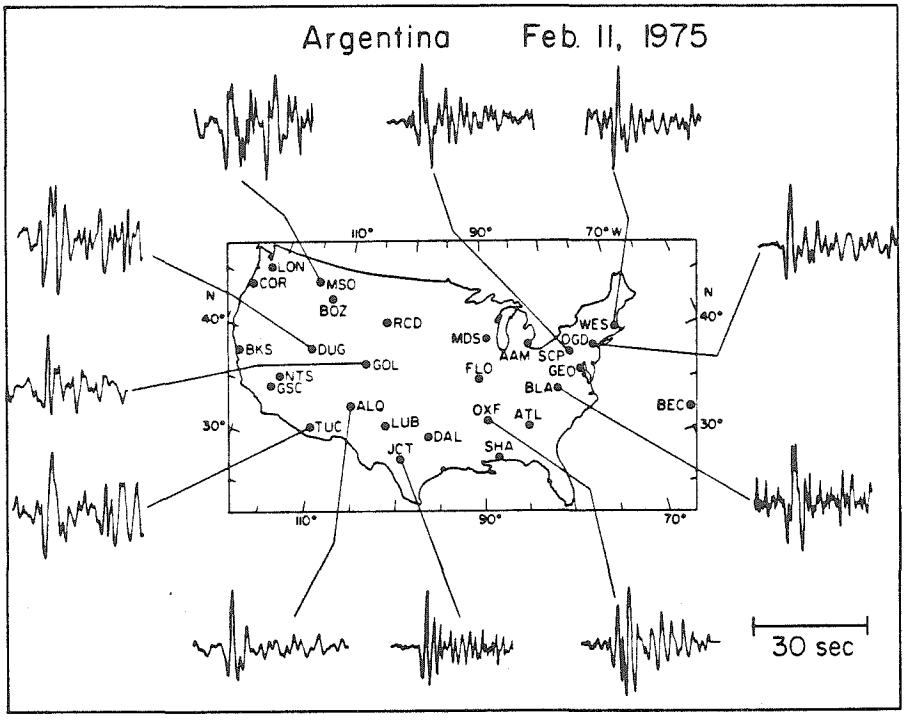

Figure III.1.10. Short period SH components of the February 11, 1975 event.

which were of the peak of the first half cycle of the P arrival. Measurement of this peak minimized crustal and multiple source effects. The events had very good signal-to-noise ratio and thus amplitudes could be accurately measured with an error of approximately 10%. The short period amplitudes of these events were generally too large to measure, however, they were systematically checked for evidence of excessive source complexity. As would be expected based on the relative magnitudes, the short period signals of the events used for long period P wave amplitudes were more complicated than those of the data used for short period P wave amplitudes. However, they were far less complicated than for larger deep events which were excluded from any measurement.

The short period P amplitudes from deep events constitute a somewhat sparse data set. The focal mechanism and source complexity constraints limited the number of acceptable events to only five. However, the much larger data set of carefully selected P waves from shallow events in South America presented by Butler and Ruff (1980) and Butler et al. (1979) provides a useful comparison and supplement. In the analysis decribed below, the deep and shallow data sets were treated separately and the results compared to verify that the small data set from deep focus events does not introduce systematic errors. Butler and Hart (1979) show many of the shallow P wave waveforms employed in the shallow source analysis. Our P waves from deep sources were generally of significantly higher frequency content and few could be reliably digitized, though amplitudes could be measured with an accuracy of 10-20%. The amplitude measured was the peak of

the first half cycle to first trough measurement which was found to be most stable and free of receiver effects by Butler and Ruff (1980). All of the new short period P data were from closely clustered hypocenters in Peru. The high frequency nature of the data precludes any general observation of frequency differences between the eastern and western stations, though again, the midwestern and Gulf Coast stations tend to be higher frequency.

Relative Amplitudes

The amplitude data were normalized to a common gain and then amplitudes from Argentina events were corrected for geometric spreading to a distance of 70^{o}, while those from Peru were corrected to 60^{o}. This amounted to no more than a 15% correction for most stations, using the expressions of Kanamori and Stewart (1976). We then employed the technique described by Butler and Ruff (1980) to normalize each data set. In this procedure we took the set of observations of a particular phase, O_{ij}, for I events and J stations, and from the I events chose a reference event k. Scale factors α_i were found to minimize the least squares error for each event $i \neq k$:

$$\min \Sigma \left| \alpha_i O_{ij} - O_{kj} \right|^2.$$

Let β_k be the average amplitude of the master event k:

$$\beta_k = J^{-1} \Sigma_j O_{kj}.$$

The total error for all events I in the source region is then:

$$\beta_k^{-1} \Sigma_i \Sigma_j \left| \alpha_i O_{ij} - O_{kj} \right|^2. \qquad (1)$$

By iteratively allowing each event i to be the master event k, factors α_i were found which best minimized the total error (1).

The short period P amplitudes are shown in Figure III.1.11. For

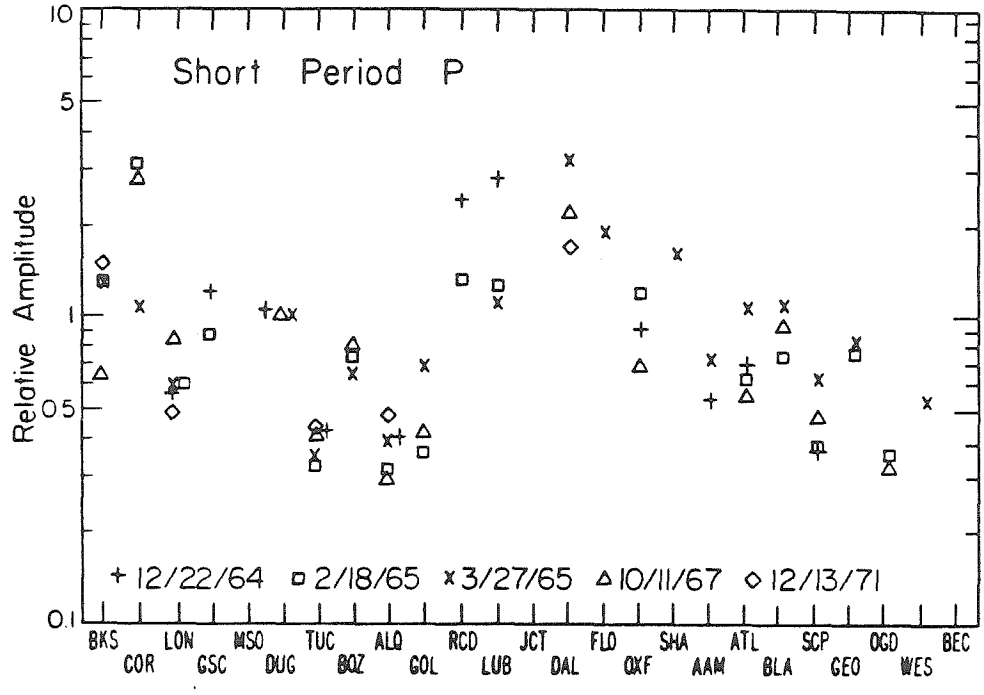

Figure III.1.11. Relative amplitudes of short period P waves from deep events in Peru recorded at WWSSN stations across the United States.

this and all similar figures, the ordinate is a log scale indicating relative amplitude, and stations are ordered in a west to east arrangement as viewed from the South American azimuth. The scatter in amplitudes at each station is relatively small, less than a factor of 1.5 around the mean, and individual events do not appear to have significant trends across the array relative to the station means. The lowest signal amplitudes are observed at TUC, ALQ and OGD, with GOL and SCP being relatively low. High amplitudes are concentrated in the Texas stations LUB and DAL as well as at FLO, RCD and COR. The midwestern and Gulf Coast stations tend to record the highest amplitudes, with the East Coast and West Coast stations scattering around the same level. This general pattern is consistent with the results presented by Butler and Ruff (1980). The total range in mean amplitudes between stations is a factor of six.

A similar basic pattern, but one containing a greater total range in variation of a factor of 10, is shown by the short period SH amplitudes in Figure III.1.12. With the exception of ALQ, the Rocky Mountain stations record relatively low amplitudes, though the eastern stations ATL, OGD and WES are similarly low. Again, midwestern and Gulf Coast stations are generally enhanced. The contact between stations recording high amplitudes and stations recording lower amplitudes is more abrupt along the Rocky Mountain front than in the East, as is the case for the P waves. The 1975 event in northern Argentina which was located north of the other epicenters may have a slight east to west amplitude trend relative to the other events, but this is not sufficiently outside the scatter of the data, nor is the

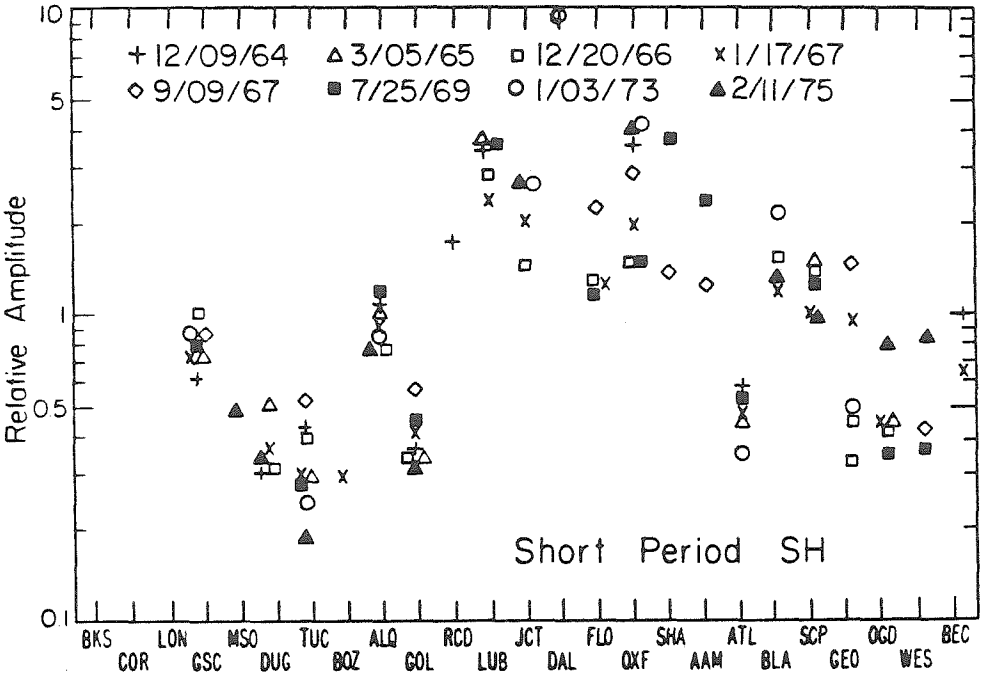

Figure III.1.12. Relative amplitudes of short period SH waves from deep events in Argentina recorded at WWSSN stations across the United States.

focal mechanism well enough constrained, to detect significant source region bias in the amplitudes. The scatter at stations OXF, GEO and SHA tends to be greater than for most stations, and there is a single, very high amplitude observation at DAL. This scatter and anomalously high amplitude may indicate strong receiver effects that are acutely sensitive to incidence angle.

The long period data are presented in Figures III.1.13 and III.1.14. As is expected for these longer period waves, the amplitudes demonstrate less overall variation between stations and less individual station scatter. The striking features of the long period P data in Figure III.1.13 are the very low amplitudes of OXF, which deviate from the regional trend, and the enhancement of DAL, FLO, COR and DUG. The total range in amplitude variation is only a factor of two, which indicates remarkable stability of the WWSSN long periods over the 12 years spanned by the data, and the relative insensitivity of long period P to receiver or attenuation variations. The long period SH amplitude pattern (Figure III.1.14) has larger variation between stations, with very low amplitudes at TUC, FLO, OXF and WES, and slight amplitude enhancement at LUB and JCT. The anomalously low long period amplitudes of OXF produce much of the amplitude ratio anomaly noted by Burdick (1978).

To facilitate comparison of the data sets, the mean and standard error of the mean were computed for each station and the P and SH observations plotted together. The relative mean values are given in Table III.1.2. The short period data are shown in Figure III.1.15. The two data sets have been linearly scaled to minimize the separation

Table III.1.2 Relative Mean Amplitudes

Station	spP			spSH			lpP			lpSH		
	Mean	S.E.M.	N	Mean	S.E.M.	N	Mean	S.E.M.	N	Mean	S.E.M.	N
BKS	1.13	0.18	4	-	-	0	1.12	0.03	6	1.11	0.00	1
COR	2.17	0.58	3	-	-	0	1.39	0.10	5	-	-	0
LON	0.60	0.06	5	-	-	0	0.98	0.07	4	-	-	0
GSC	1.00	0.16	2	0.51	0.03	7	0.88	0.11	4	1.03	0.10	4
MSO	-	-	0	0.31	0.00	1	-	-	0	-	-	0
DUG	0.98	0.01	3	0.24	0.02	5	1.24	0.06	6	1.04	0.07	3
TUC	0.38	0.02	5	0.21	0.02	8	0.76	0.09	6	0.60	0.05	6
BOZ	0.71	0.04	3	0.19	0.00	1	0.82	0.08	2	0.69	0.00	1
ALQ	0.37	0.03	5	0.60	0.04	7	0.89	0.06	5	1.09	0.09	4
GOL	0.48	0.10	3	0.26	0.02	7	1.04	0.06	5	1.02	0.07	4
RCD	1.76	0.49	2	1.09	0.00	1	1.13	0.00	1	1.00	0.00	1
LUB	1.64	0.50	3	1.99	0.16	4	0.97	0.08	4	1.30	0.18	2
JCT	-	-	0	1.39	0.19	4	1.06	0.02	4	1.30	0.18	4
DAL	2.22	0.41	3	6.07	0.00	1	1.52	0.10	3	1.56	0.18	2
FLO	1.79	0.00	1	0.94	0.16	4	1.42	0.00	1	0.47	0.03	4
OXF	0.90	0.14	3	1.76	0.27	7	0.62	0.04	5	0.52	0.11	3
SHA	1.53	0.00	1	1.60	0.74	2	1.03	0.02	6	1.26	0.06	4
AAM	0.62	0.09	2	1.13	0.34	2	1.00	0.11	3	0.97	0.08	4
ATL	0.72	0.11	4	0.31	0.02	5	0.84	0.05	5	0.85	0.12	4
BLA	0.90	0.09	3	0.91	0.14	4	1.06	0.08	6	1.35	0.18	4
SCP	0.46	0.06	4	0.75	0.06	6	1.03	0.06	6	1.44	0.07	5
GEO	0.78	0.04	2	0.47	0.13	5	0.98	0.14	3	1.09	0.15	3
OGD	0.34	0.04	2	0.32	0.05	5	0.72	0.09	4	1.07	0.09	5
WES	0.53	0.00	1	0.34	0.09	3	0.79	0.06	5	0.56	0.07	2
BEC	-	-	0	0.53	0.11	2	0.73	0.01	4	0.69	0.15	4

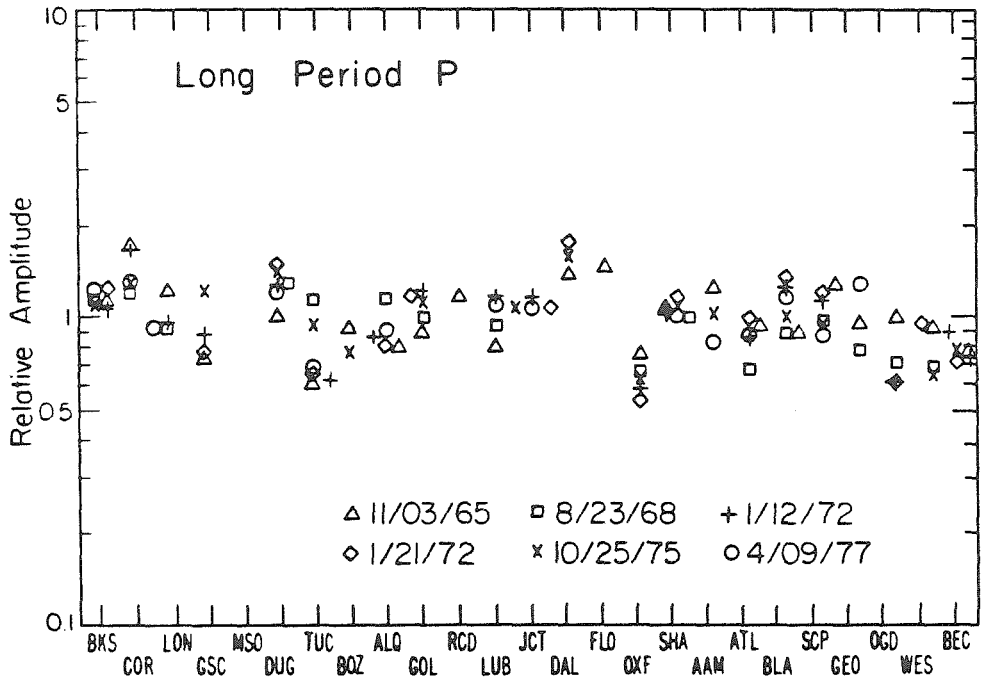

Figure III.1.13. Relative amplitudes of long period P waves from deep events in Peru and Argentina recorded at WWSSN stations across the United States.

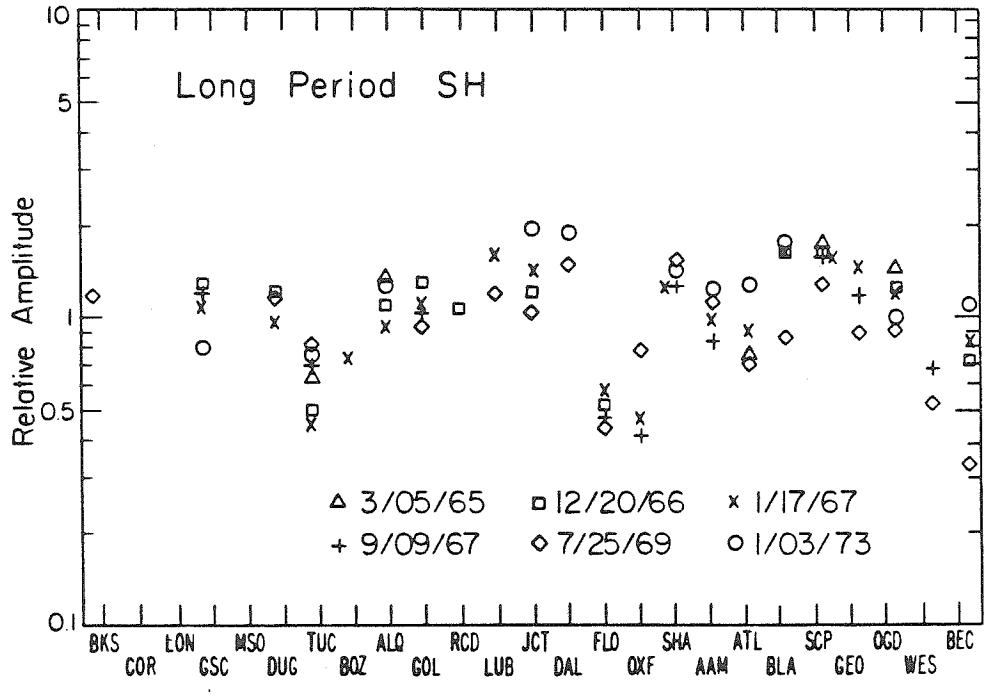

Figure III.1.14. Relative amplitudes of long period SH waves from deep events in Argentina recorded at WWSSN stations across the United States.

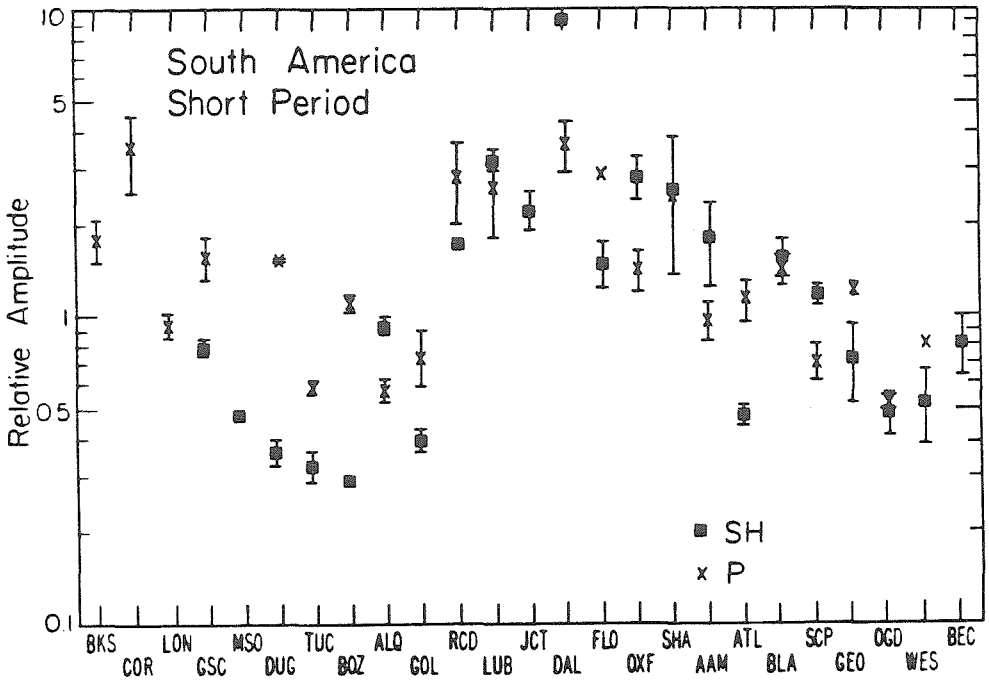

Figure III.1.15. The mean and standard error of the mean of the short period P and SH amplitudes from South America recorded at WWSSN stations across the United States.

between them. The first order feature apparent in the data is that the short periods track one another well, with high amplitudes in the central states and fairly similar behavior in the eastern stations. In the West, the amplitudes of SH are consistently lower than the P waves relative to the rest of the pattern, with the notable exception of ALQ. The western station SH waves are the lowest in the SH pattern, though GSC appears to record higher amplitudes than the Rocky Mountain stations. The stations DUG and BOZ show the greatest discrepancy between P and SH behavior, though there is only a single SH data point at BOZ.

The long periods are plotted in Figure III.1.16, and again the outstanding feature is the degree to which they track. The largest deviation in behavior occurs at FLO, where the SH waves are much lower amplitude, but there is only a single P measurement. Comparing the short period and long period P variations shows that the patterns track closely though LUB, JCT and RCD do not show long period enhancement. The short periods at GSC, BOZ, SCP and OGD do not track the long period trends very closely either, but the rest of the stations do. The SH data also show strong correlation between short and long period behavior except for FLO, OXF, OGD and ALQ.

The tendency of the amplitudes of the various phases to track one another is the type behavior expected for attenuation controlled amplitude variations. The more highly attenuated SH phases have larger regional variations than the P waves, consistent with the commonly accepted notion that attenuation is dominated by losses in shear. There are clearly substantial amplitude variations introduced

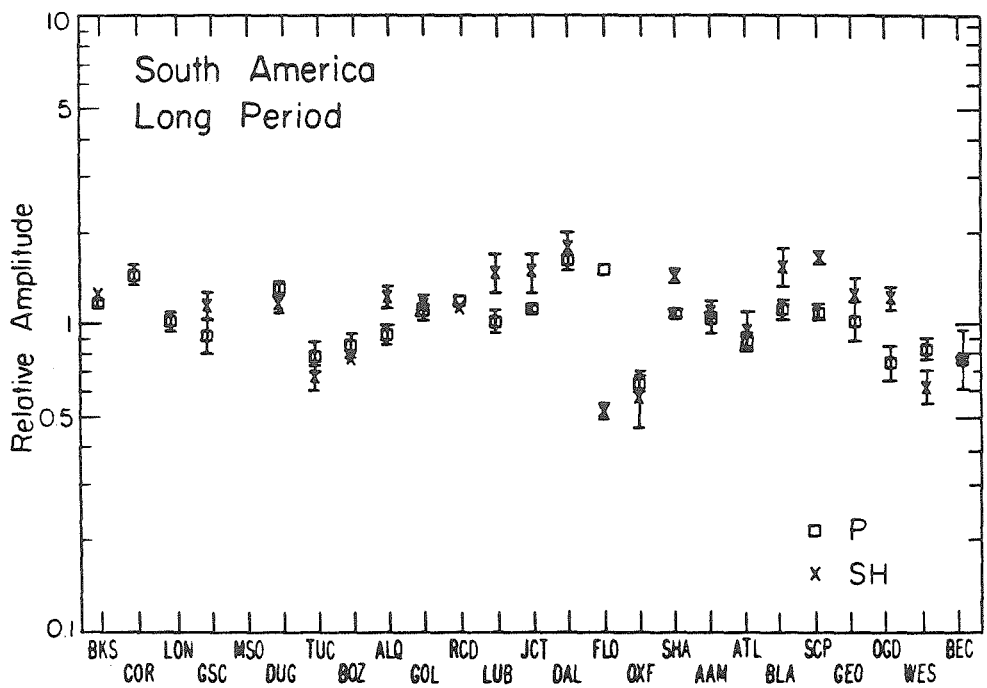

Figure III.1.16. The mean and standard error of the mean of the long period P and SH amplitudes from South America recorded at WWSSN stations across the United States.

by receiver structure, and the order of magnitude of these variations may actually exceed the scatter between some stations. Consider the short period high amplitudes recorded at midwestern and southern stations, or the long period behavior of FLO and OXF, both of which are such large effects that they dominate the amplitude patterns. Butler and Ruff (1980) examined various receiver structure induced amplifications for short period P waves and concluded that a factor of two amplification due to horizontal sedimentary layer receiver structures is reasonable. This may account for much of the midwestern short period anomaly, but cannot explain all of the other variations. The long period variations at OXF are very large, and it is difficult to assess what type of receiver structure may be responsible, though it must clearly have three-dimensional structure. The fact that the short periods are relatively enhanced and have complicated high frequency codas, indicates that this anomaly is no conventional attenuation effect. The azimuthal behavior of this anomaly will be considered in the following section, but it should be noted here that the occurrence of the anomaly at adjacent stations FLO and OXF in the Mississippi Valley indicates that this is not the result of faulty instrument emplacement. The studies of Burdick and Langston (1977); Langston and Blume (1977); and Langston (1977,1978) have detected the presence of dipping structures beneath the stations LON and COR utilizing long period body waves. Due to their distance from Argentina these stations were not used in the SH analysis, but COR does show slight long period and short period P enhancement, while LON does not.

Source variations

The similarity of focal mechanism and earthquake location of the data presented above requires some consideration of possible systematic variations in amplitudes that are not due to attenuation in the upper mantle. Though we can fairly well rule out systematic trends due to focal mechanism based on the tests mentioned above, there remains a question about bias introduced by comparing Peruvian and Argentine sources, and in utilizing data from a narrow range in depth. The selection of deep events for analysis helps reduce potential bias due to source region slab heterogeneities that could cause azimuthal variations. In Figure III.1.17 we compare the short period P wave data collected in this study with the results compiled by Butler et al. (1979), which includes 15 shallow and intermediate depth South American events, the majority of which were located in Argentina, well south of the deep data epicenters. The amplitude behavior is very similar at the eastern and central stations. OXF shows greater enhancement for the shallow events, and the single shallow source reading for BOZ is low relative to the three readings from deep events, which may be due to receiver effects. Taking the ratio of the mean values shows that there is at most a factor of two total range in relative amplitude behavior for stations for which there are adequate data. The only systematic trend in the ratios is a tendency for BKS, COR, LON and GSC to record slightly larger amplitudes from deep sources, but this is not a robust feature, and of little import for this work as these stations were generally too distant to obtain SH data, with the exception of GSC. There is

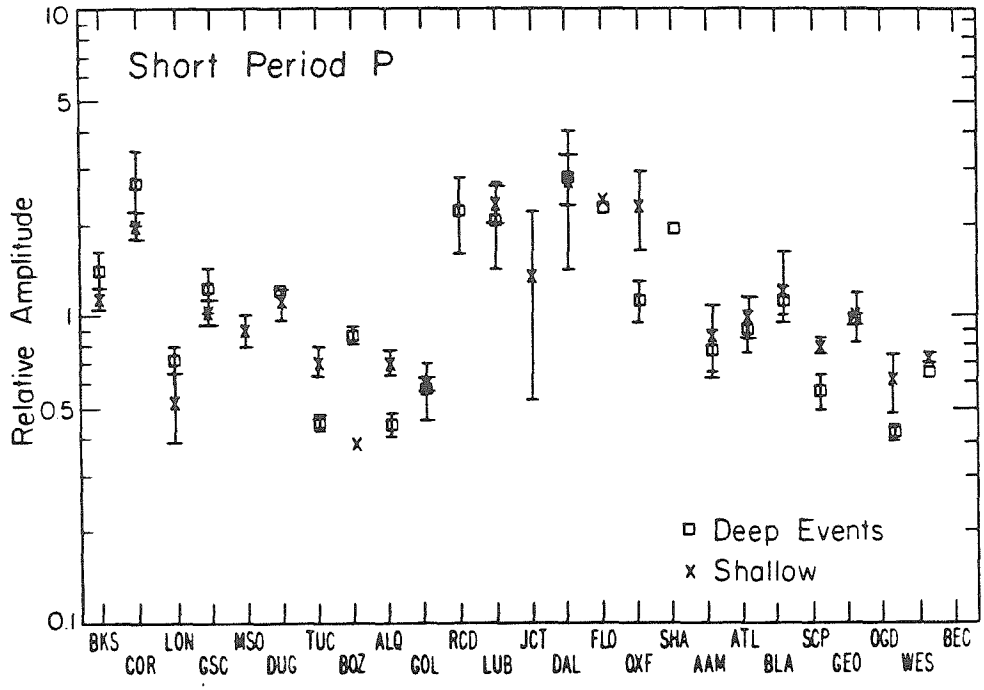

Figure III.1.17. Comparison of the means and standard errors of amplitudes of short period P waves from deep and shallow earthquakes in South America recorded at WWSSN stations across the United States. The shallow source amplitude data are from Butler et al. (1979).

certainly no obvious systematic source bias such as that found between the much closer together test sites in southern and northern Novaya Zemlya by Butler and Ruff (1980).

As another test, we divided the long period P data set into Peruvian and Argentine subsets, and checked for systematic source effects. The data are shown in Figure III.1.18, and though the statistical samples are small in this case, there is again no systematic source region effect apparent in the data. The amplitude ratios show no resolvable trends and a total range in variation of two, though much less variation for the majority of stations. The similarity between patterns from different depths and source regions allows some confidence in comparison of the amplitude patterns in this section.

In the foregoing discussion of the amplitude data set, several instances of probable receiver dominated effects have been mentioned. Comparison of the amplitude patterns with data from other azimuths identifies stations with rapidly varying behavior, which is more likely due to near receiver effects. Section III.2 presents an analysis of the azimuthal variations of the SH phases. These variations are very large at some stations for both short and long periods, and some of the larger amplitude variations are associated with the travel time anomalies discussed in Chapter II. However, many of the general features apparent in the S wave amplitude patterns are not strongly dependent on azimuth. Butler et al. (1979) have considered the azimuthal sensitivity of short period P waves, and their conclusions indicate substantial azimuthal receiver effects at

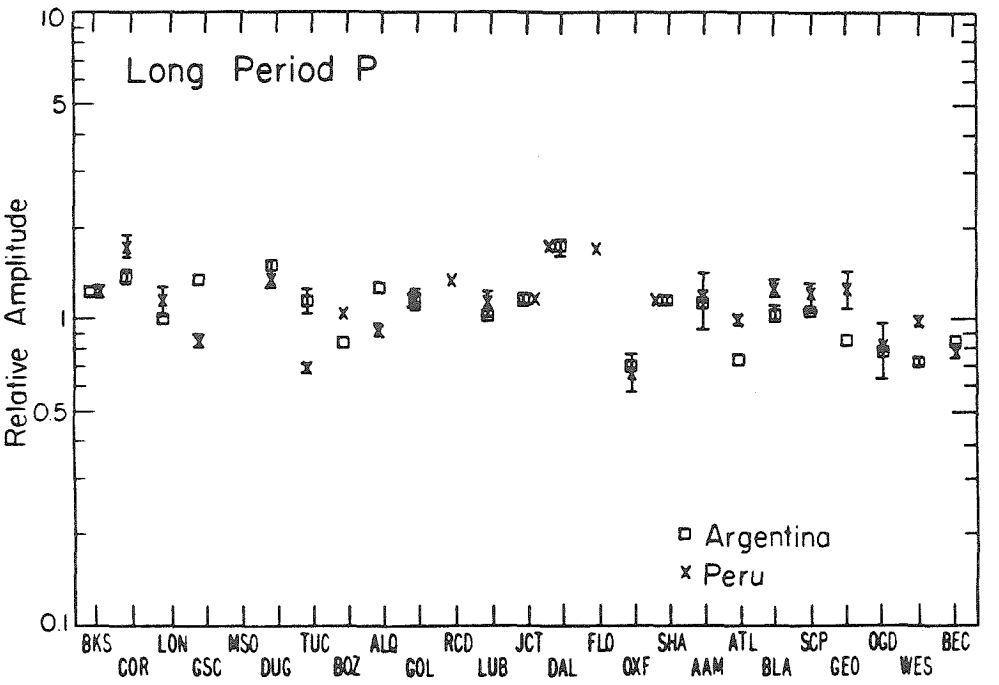

Figure III.1.18. Comparison of the means and standard errors of amplitudes of long period P waves from deep events in Peru and Argentina.

LON and BOZ, and lesser variations at most other stations. However, the general pattern of short period amplification in the central states is common to all azimuths, as is the lack of strong east to west amplitude differences. It should be noted that Butler and Ruff (1980) found that scattering, as reflected in the horizontal components of the P waves, does not appear to be responsible for the short period P amplitude pattern.

Attenuation models

The question of upper mantle regional variations and frequency dependence of attenuation is a controversial and fundamental problem in seismology. Most studies have failed to overcome the uncertainties in source frequency content, receiver and propagational effects, and instrumental band width to present unambiguous conclusions. In this study we primarily sought to test compatibility and consistency of a range of attenuation variations with the South American body wave data set, rather than to make absolute attenuation determinations that require complete knowledge of the source and receiver. In order to accommodate the tradeoffs between source time function and attenuation, a broad range in source frequency content was considered, as was a broad range in long period absorption band amplitudes, in the time domain modeling. Comparison with the observed short period and long period data places bounds on these variables, however there is inevitably an uncertainty in reference baseline selection. To partially circumvent this, we utilized results from the literature as well as performing an absolute t^* determination, to minimize arbitrariness in baseline selection. Spectral ratio techniques were

also employed and compared with the time domain models.

Two basic attenuation models have been considered, with only single parameters varied in each. These are the constant Q, Futterman model (Futterman 1962) parameterized by

$$t^* = \int_{\text{Ray path}} Q^{-1}(s)V^{-1}(s)ds,$$

and a frequency dependent model parameterized by a high frequency roll-off of the relaxation spectrum given by τ_m^{-1} (Minster 1978a,b). In the latter model, for small attenuation, Q is given by

$$Q^{-1}(f) = 2/(Q_m) \tan^{-1}(2\pi f(\tau_M - \tau_m)/(1+(2\pi f)^2\tau_M\tau_m)) \qquad (2)$$

Q_m is the quality factor in the absorption band. The points at which Q^{-1} is half of its maximum value occur for $f = (2\pi\tau_M)^{-1}$ and $(2\pi\tau_m)^{-1}$. We fix τ_M at 1000 sec, well outside the body wave pass band of our data in all of the models. The constant Q model has frequently been adopted in time domain modeling of body waves at frequencies lower than 1 Hz, and we tested how well this model agrees with our broad band data. The motivation for considering the frequency dependent model are the numerous observations of body wave frequencies that would not be seen if the long period Q values applied to high frequencies as well (e.g. Der et al. 1980; Sipkin and Jordan 1979). It is shown in the present study that τ_m values which allow two to four Hz energy to pass through the mantle have strong effects on one to five second energy as well. Thus, the WWSSN signals constrain acceptable frequency dependence of this type. The long period level of the absorption band is described by $t^* = t_u/Q_m$ with t_u being the travel time, whether or not a τ_m roll-off is present. When τ_m is allowed to vary, the t^* level is held constant so that the model

amplitude variation can be attributed entirely to changes in τ_m. It is, of course, possible to permit greater flexibility by simultaneously varying both t^* and τ_m, but this is not warranted by our data, because we are presently unable to correct for the broadband receiver effects. Thus, this analysis does not encompass attenuation models such as proposed by Solomon (1972), which would allow short periods and long periods to vary independently. Such a refined model must await a better understanding of the long period amplitude and spectral effects apparent in the data.

The test of constant Q attenuation was performed as follows. Large amplitude, high frequency P and SH data were compared with synthetics generated for a wide range of source models and t^* values. We adopted the constraint that relative P and SH absorption is given by $t^*_\beta/t^*_\alpha = 4.0$, which implicitly assumes that all attenuation is caused by shear losses in the mantle (Anderson et al. 1965). The validity of this assumption is based on absolute t^* determinations such as those by Helmberger and Hadley (1981) and Burdick (1978), and relative attenuation measurements by Solomon and Toksöz (1970) and Der et al. (1980), as well as much work done with surface waves. Once the high frequency, high amplitude signals were adequately modeled by a particular source model and t^* combination, differential attenuation, Δt^*, was applied by convolving this synthetic signal with Futterman filters, and the amplitude behavior relative to the initial model was recorded. As a consistency check, the data that were initially modeled were carefully digitized and also convolved with differential attenuation filters, and the amplitude decrease relative to the

original signal was recorded.

Figure III.1.19 shows some of the results of this procedure, where the amplitude behavior relative to the initial signal (either reference synthetic model or digitized data) are plotted versus Δt^*_α. The curves for LP SH and SP SH were generated using $\Delta t^*_\beta = 4\Delta t^*_\alpha$. The theoretical source time functions for all of the models shown except for SP P was a symmetric triangle of one second total duration. The initial t^* for the LP P model was $t^*_\alpha = 0.8$ sec, while it was $t^*_\beta = 3.2$ sec for the short and long period SH models, though as discussed below, the absolute t^* values are not important in this procedure. Selection of this source model produced short period to long period SH amplitude ratios in the range of those observed in the data. The deep short period P waves were from smaller events of considerably higher frequency content, and a shorter source time function of 0.2 seconds duration and $t^*_\alpha = 0.6$ sec were used for the synthetics. Also shown in Figure III.1.19 are the curves representing the decrease in amplitude when digitized data were convolved with differential attenuation operators. Other data produced very similar curves. These curves are closely tracked by the models, which indicates that the inital source frequency content has been adequately accounted for. For a fairly large range of alternate source model-t^* combinations similar curves can be found that fit the data behavior as well as the ones shown. Thus, this procedure is relatively insensitive to the particular parameters selected; what is important is the initial frequency content. For the range in Δt^*_α shown, the synthetic waveforms are compatible with the range in observed waveforms and amplitudes. As

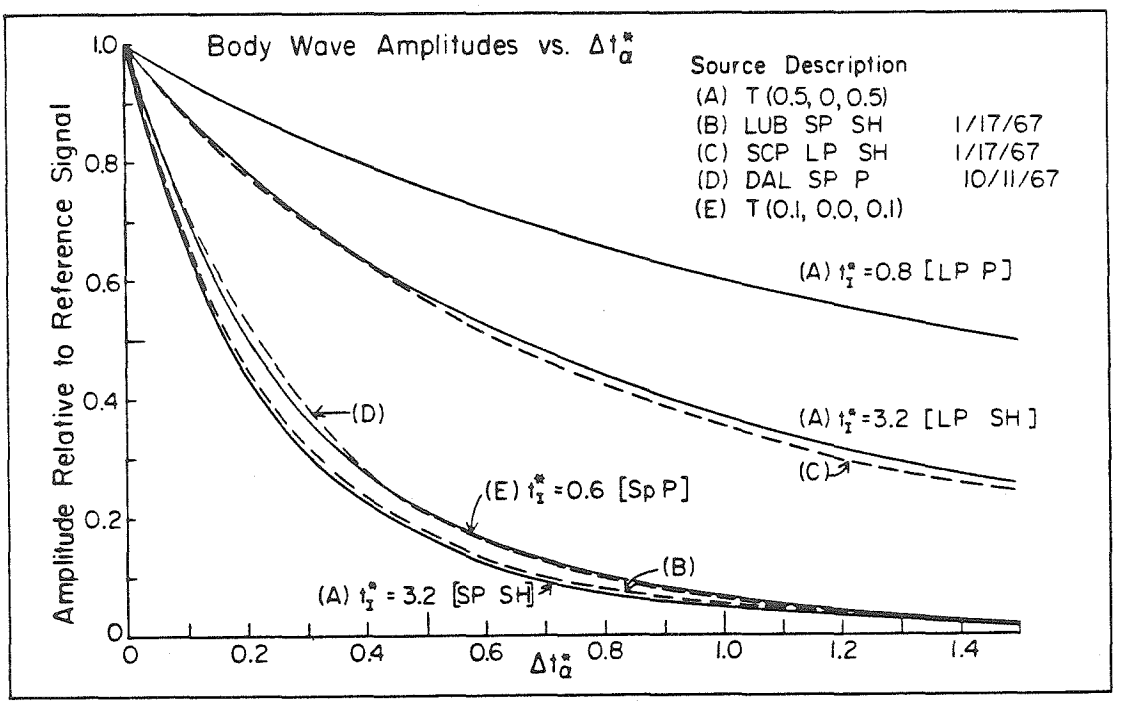

Figure III.1.19. Amplitude of body waves versus Δt^*_α. The amplitudes are given relative to the reference signal amplitude of either observed data or synthetic model with initial reference attenuation given by t^*_I. Curves B and C and the LPSH and SPSH curves are generated with $\Delta t^*_\beta = 4\Delta t^*_\alpha$. The similarity in behavior of the attenuated data and corresponding model indicates that the models have an appropriate spectral content. The synthetic time functions are trapezoids described by T(rise time, constant duration, fall time) in seconds.

has been shown by Butler and Ruff (1980), the change in waveform is not dramatic even for large changes in t^*. This waveform behavior is discussed in more detail below.

Figure III.1.19 clearly shows the insensitivity of long period waves to even large changes in t^*. The range in Δt^*_α required to span a factor of two in amplitude is 1.5 sec for long period P, which produces a factor of 3 variation in long period SH amplitudes. Thus, it is clear that regional variations of at least this range would have to be invoked to explain the observed amplitude behavior with constant Q attenuation alone. The relative amplitude behavior of the short periods is, of course, much more sensitive to Δt^*_α, at least as long as there is significant high frequency information in the signal. It is clear from the short period P and SH curves that it will be possible to explain the observed tendency of short period P and SH amplitudes to track closely by Δt^* variations, and that for the total range in Δt^* needed to fit the observed long period amplitude variations, the predicted short period variations would be on the order of two times greater than observed.

A somewhat different procedure had to be adopted for the frequency dependent modeling. The effect of increasing τ_m from zero is to permit progressively more high frequencies to pass through to the receiver, thus the amplitudes increase with τ_m. To accommodate this, we initially modeled low amplitude, low frequency content data, and then for a range in t^* and source time functions, generated synthetics with attenuation operators that had increasing τ_m. The amplitude behavior was then measured relative to the $\tau_m = 0.001$ sec

reference, at which the attenuation operator is very similar to a Futterman operator with the same t^*. τ_m was allowed to increase only as much as would still generate waveforms compatible with the data. This restricted the acceptable range in t^*, τ_m, and source models significantly, unlike for the constant Q model, where t^* and reasonable source duration trade off almost indistinguishably.

The results for short period P waves are shown in Figure III.1.20, where the amplitudes were measured relative to a signal generated with a Futterman operator of the t^* value indicated for each curve. The upper three curves were generated by delta function sources convolved with short period instrument and attenuation operators of varying t^* and τ_m. These demonstrate the predictable result that the relative enhancement in amplitude caused by increasing τ_m is greater for larger values of t^*, at least over this small range in t^*. The lower curves show that for a given t^*, the higher the source frequency content the higher the relative enhancement caused by increasing τ_m. The three triangular source models and t^* values of 0.6-0.8 sec produce waveforms spanning the range of observed variations for a given event when τ_m varies from 0.001 to 0.25 sec. This variation in frequency dependence produces a range in amplitudes of a factor of from 4 to 6, comparable with the range observed in the data. Larger values of τ_m produce unacceptably spiky waveforms for almost any simple triangular, trapezoidal, or Savage-type (Savage 1966) source model.

Figure III.1.21 shows a similar set of curves for short period SH waves, which have somewhat more complicated behavior. Again, the

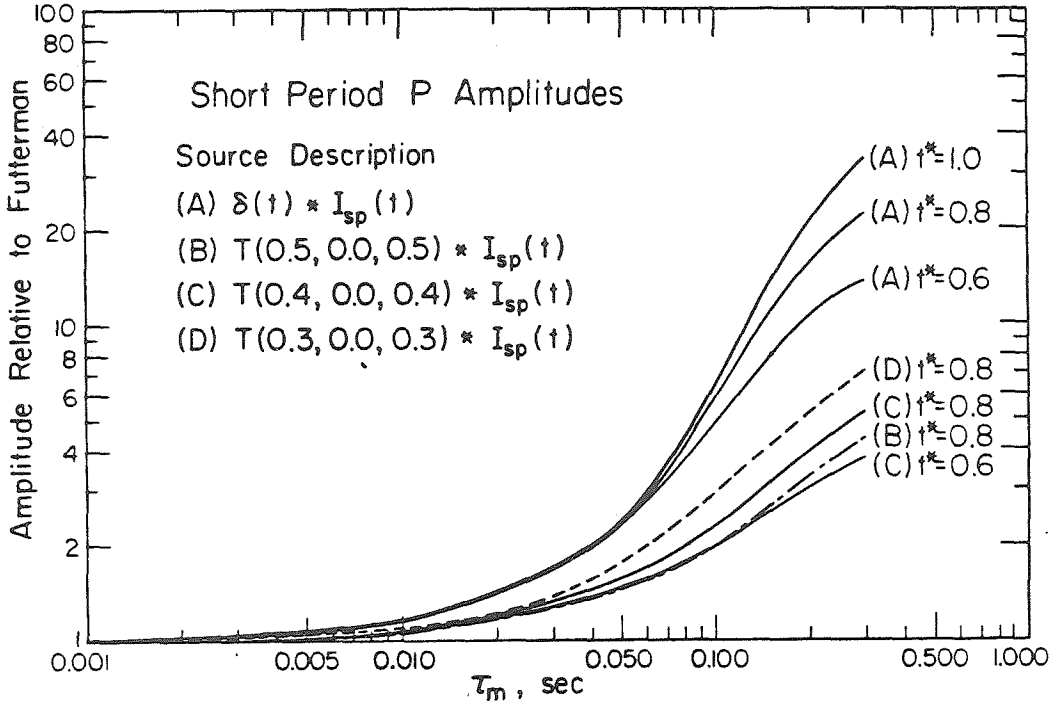

Figure III.1.20. Amplitude of short period P wave synthetics generated with frequency dependent attenuation operators. For each curve t^* is held constant and τ_m is varied. Curves (A) are generated with delta functions and the indicated attenuation operators and the other curves are generated with trapezoidal sources. All signals are convolved with a short period WWSSN instrument response $I_{sp}(t)$. The amplitudes are given relative to the τ_m = 0.001, Futterman operator amplitude.

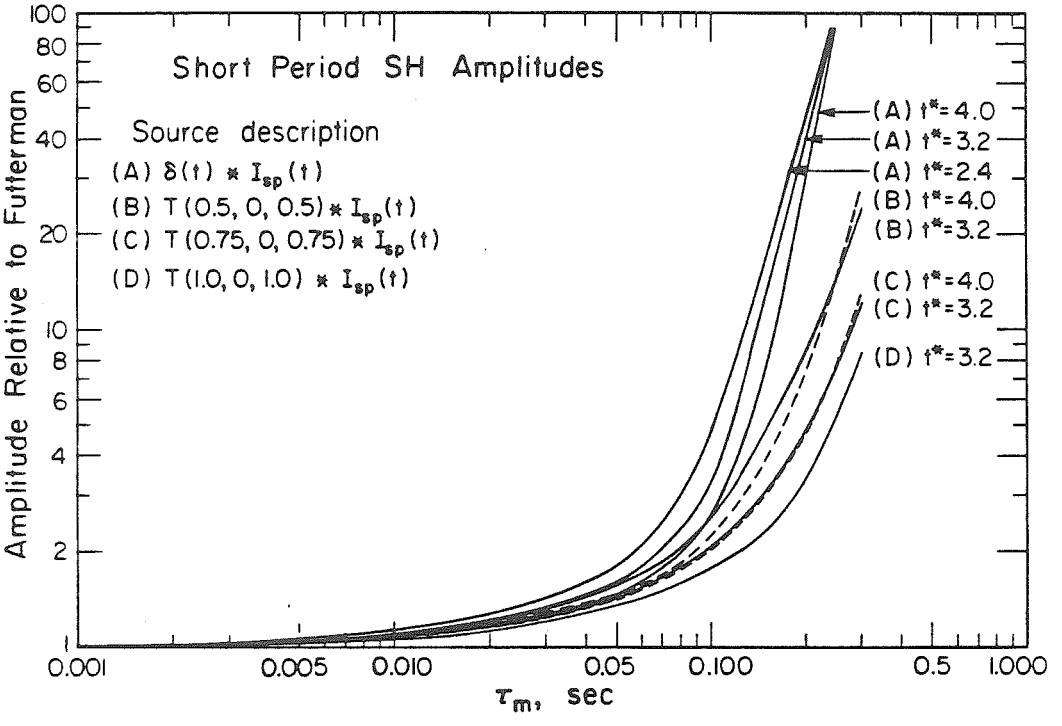

Figure III.1.21. Amplitude of short period SH wave synthetics generated with frequency dependent attenuation operators. For each curve t^* is held constant and τ_m is varied. Curves (A) are generated with delta functions and the indicated attenuation operators, and the other curves are generated with trapezoidal sources. All signals are convolved with a short period WWSSN instrument response $I_{sp}(t)$. The amplitudes are given relative to the τ_m = 0.001, Futterman operator amplitude.

upper three curves were generated using a delta function source, but over the range in τ_m up to 0.3 sec the effect of varying t_β^* is different than for the P waves. This is because of the greater range in t_β^* considered, as well as the larger dominant period of the SH waves due to longer source duration and higher t_β^*. It takes larger τ_m values to overcome the longer period nature of the source, but there is ultimately a cross-over point at which the relative enhancement of the higher t_β^* signal is greater, as seen in models (B) and (C). For the trapezoidal and Savage source models examined, fairly large t_β^* values of around 3.0 sec and τ_m values less than 0.25 sec were in best agreement with the data. For the January 17, 1967 and the December 20, 1966 events we checked the source models shown in Figure III.1.21 against several short period and long period P signals to help constrain the range of acceptable models. For $\tau_m \geq 0.25$ sec the models shown in Figure III.1.21 no longer produce acceptable short period P waves. For lower reference t^* values one requires source models that look like Futterman type attenuation filters to produce acceptable waveforms for any substantial range in τ_m, but there is again the unavoidable tradeoff between reference t^* and source time function. Because simple trapezoidal time functions and Savage source models are theoretically reasonable source representations for these small, deep events, we tend to prefer the results with $t_\alpha^* = 0.8$ sec and $t_\beta^* = 3.2$ sec.

The variation in long period amplitudes produced by varying τ_m from 0.001-0.25 sec are relatively minor, as shown in Figure III.1.22. For $t_\alpha^* = 0.8$ sec, and a source time function that adequately models

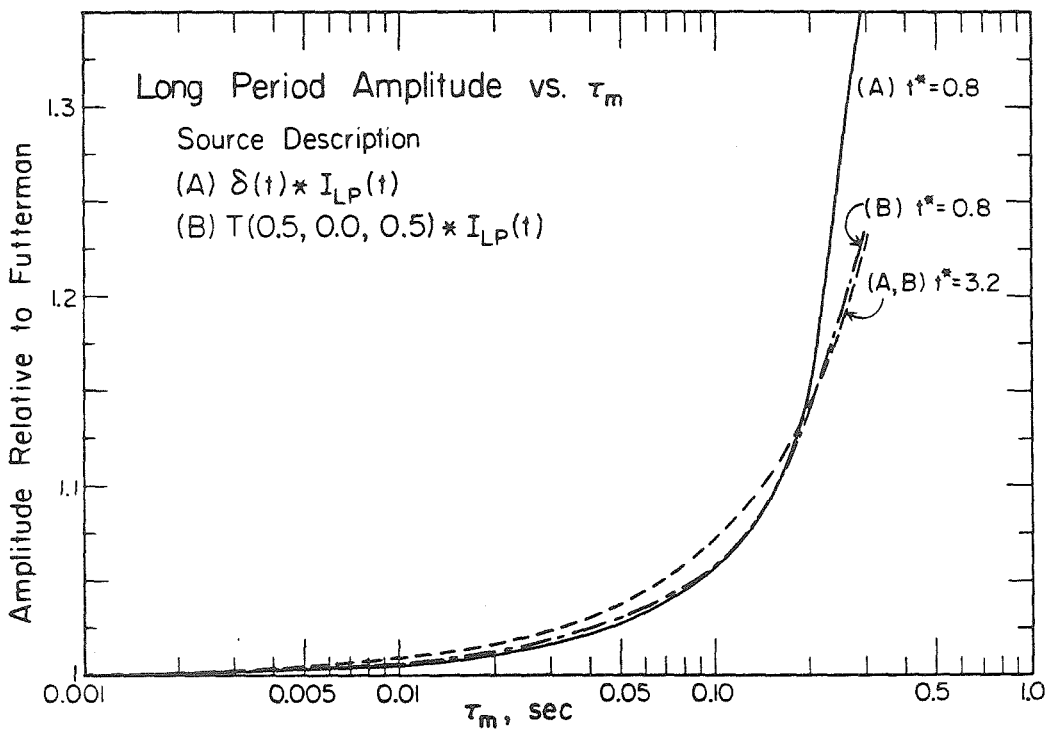

Figure III.1.22. Amplitude of long period P wave (t^* = 0.8 sec) and SH wave (t^* = 3.2 sec) synthetics generated with frequency dependent attenuation operators, as in Figures III.1.20 and III.1.21. $I_{lp}(t)$ is the long period WWSSN instrument response.

the long period P waves, only an amplitude variation of a factor of 1.2 is produced. The same is true of models that fit the SH data, regardless of source model or t_β^* selection. It is apparent that changes in the long period level of the relaxation spectrum produced by varying t^* are the only way to produce significant amplitude variations for these periods.

To more clearly compare the results of the synthetic models, we have employed the procedure of utilizing the data from one phase to predict the amplitude variations of another. This tests the degree to which the amplitudes behave consistently with lateral variations in attenuation. The curves in Figures III.1.19 to III.1.22 are readily adapted to this procedure. Figure III.1.23 shows the results of predicting the short period SH data from the short period P data. The Δt_α^* results were obtained by taking the P wave amplitude means and determining the Δt_α^* for each station, as read from Figure III.1.19, that yield the variations from the highest amplitude station. Then, for each station, that Δt_α^* predicted the short period SH behavior from Figure III.1.19, and the relative amplitudes were plotted against the data. Similarly, Figure III.1.20 was used to determine the τ_m values needed to produce the P pattern, assuming a particular source model (in this case source D), and the resulting τ_m values then predicted the SH amplitudes using Figure III.1.21 and a particular source model (in this case C with $t_\beta^* = 3.2$ sec). The predicted amplitudes were plotted with the data after linearly minimizing the scatter at each station. Some stations may lack either observed values or predictions depending upon the coverage of the data set.

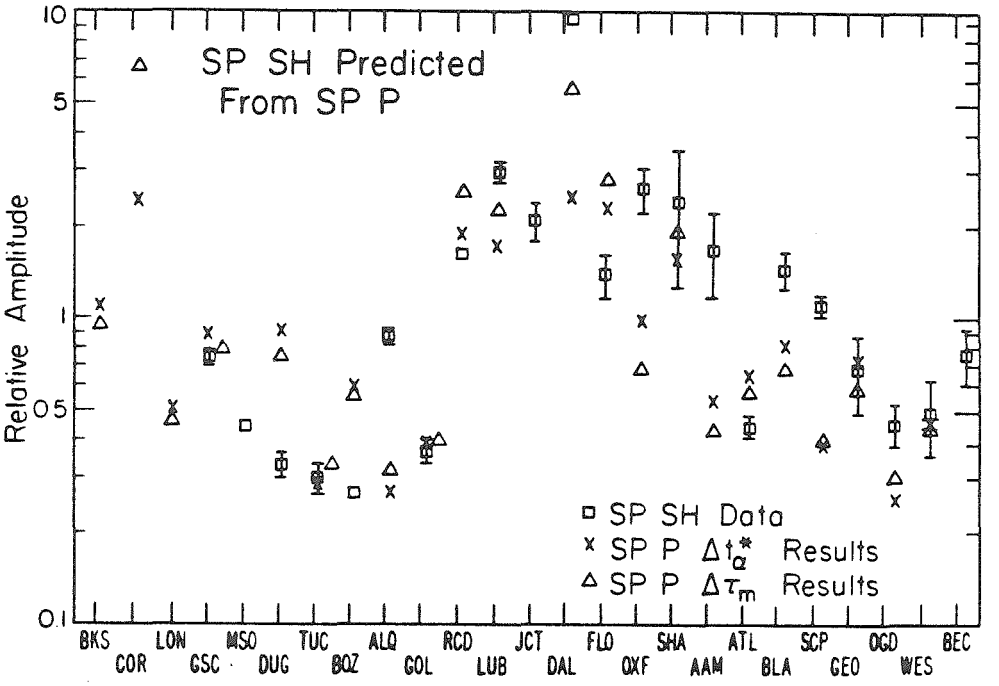

Figure III.1.23. Observed short period SH amplitudes versus predicted SH amplitudes utilizing the station values of Δt_α^* and $\Delta \tau_m$ which reproduce the short period P amplitudes.

It is clear that in a gross sense, describing the P wave amplitude variations by either Δt^*_α or a range in τ_m predicts the general behavior of the SH amplitudes. This basically reflects the fact that the amplitudes track, but more specifically, the degree to which they track is similar to what would result from lateral variations in attenuation. Of course, it may be possible to find receiver functions that produce a similar effect. The more important point to draw from Figure III.1.23 is that the short period WWSSN amplitudes do not clearly demand nor preclude frequency dependent attenuation. Since the amplitude and waveform behavior have been checked for consistency throughout, this means that one cannot base a strong argument for or against frequency dependence from the short period amplitude and waveform behavior alone. There do not appear to be any strong trends in the data which suggest alternate selection of t^*_β/t^*_α ratios or different reference models.

Though this is clearly a crude prediction, it is of some interest to look at the individual stations a bit closer. The predicted amplitudes at DUG are larger than observed in the SH data, but this station does have complex SH wave codas which may account for this discrepancy. BOZ has strong azimuthal variations (Butler and Ruff, 1980) and only a single SH observation, so its behavior is uncertain. Though ALQ is predicted to be on the level of TUC and GOL, which are well predicted, the SH amplitudes are significantly higher than expected. It is difficult to explain this with attenuation. Both OXF and AAM have high frequency SH waves and complex codas and their amplitudes are underpredicted. Most other stations, with the

Table III.1.3 Model results for Δt^*, τ_m.

Station	Deep spP		Shallow spP		1pSH
	Δt^*_α, sec	τ_m, sec (t^*_α=0.6)	Δt^*_α, sec	τ_m, sec (t^*_α=1.3)	Δt^*_β, sec
AAM	-0.11	0.034	-0.05	0.081	1.46
ALQ	0.11	0.009	0.06	0.061	1.01
ATL	-0.16	0.068	-0.12	0.100	2.03
BEC	-	-	-	-	2.92
BKS	-0.31	0.110	-0.21	0.115	0.94
BLA	-0.23	0.088	-0.22	0.119	0.24
BOZ	-0.14	0.064	0.41	0.001*	2.98
COR	-0.49	0.280	-0.46	0.180	-
DAL	-0.50	0.265	-0.50	0.240	-0.23
DUG	-0.26	0.096	-0.20	0.112	1.19
FLO	-0.46	0.200	-0.50	0.212	4.80
GEO	-0.18	0.072	-0.12	0.100	1.00
GOL	-0.01	0.032	0.15	0.047	1.25
GSC	-0.25	0.100	-0.15	0.107	1.24
JCT	-	-	-0.28	0.131	0.38
LON	-0.10	0.049	0.21	0.035	-
LUB	-0.41	0.180	-0.53	0.021	0.38
MSO	-	-	-0.08	0.090	-
OGD	0.13	0.001*	0.15	0.047	1.07
OXF	-0.28	0.089	-0.52	0.200	4.30
RCD	-0.44	0.190	-	-	1.34
SCP	0.00*	0.029	0.00*	0.072	0.00*
SHA	-0.39	0.165	-	-	0.47
TUC	0.09	0.012	0.05	0.064	3.54
WES	-0.05	0.040	0.05	0.069	3.90

*Reference station

exception of SCP, are quite well predicted.

The entire analysis described above was reproduced using the shallow and intermediate depth P data of Butler et al. (1979) with appropriate source models and Δt^*_α, and τ_m behavior as in Figures III.1.19 and III.1.20. The predictions are very similar, despite the longer period sources and different t^*_α level of the shallow data. Table III.1.3 lists the Δt^*_α and τ_m results for each P data set. The similarity in numbers indicate the stability of the process. The actual numbers are intended only to convey an appreciation of the range in Δt^*_α and τ_m indicated by the data, and are not to be taken as definitive station values.

Since the short period data are most subject to large receiver effects, we have also attempted to test the compatibility of the long period P and SH data, and the relative short period-long period behavior. By analogous procedures to those outlined above, we have predicted long period P using the long period SH amplitudes, with the results shown in Figure III.1.24. Only a Δt^* comparison is made, since the frequency dependent model cannot encompass the observed amplitude variations. The resulting values of Δt^*_β are listed in Table III.1.3, and as expected, a large range in Δt^*_β is necessary to explain the data. The interesting result is that the P waves are rather well predicted, with the largest single exception being at station FLO. This success attests to the degree to which the long periods track compatibly with constant Q attenuation and $t^*_\beta/t^*_\alpha = 4.0$.

In order to compare the short period data with the long periods, we have exercised some selectivity in only comparing the East Coast

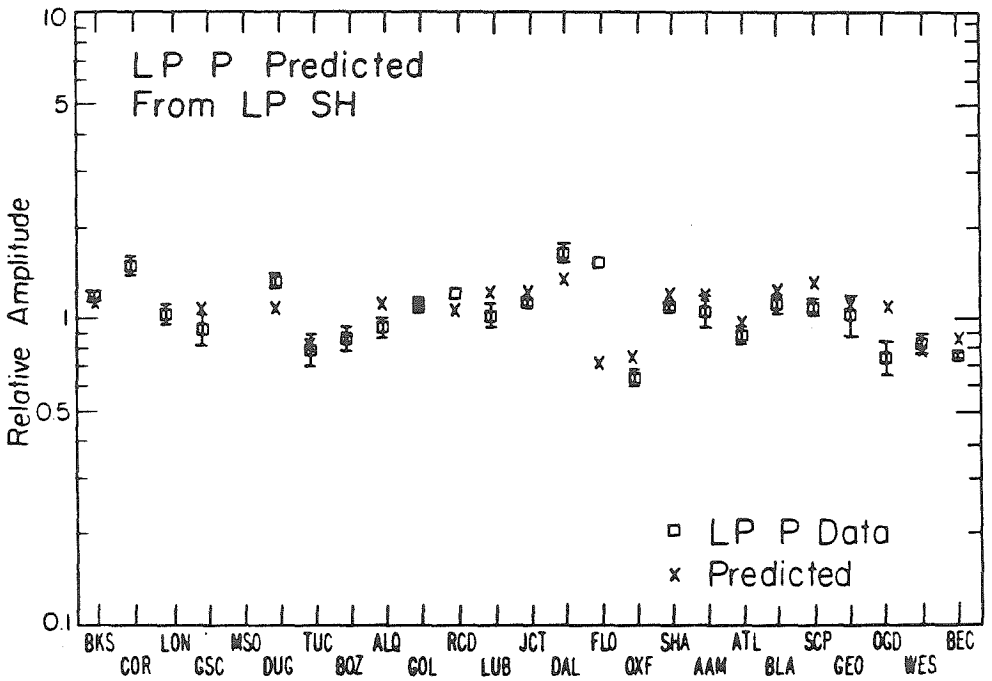

Figure III.1.24. Observed long period P amplitudes versus predicted P amplitudes utilizing the station values of Δt^*_β which reproduce the long period SH amplitudes.

and Rocky Mountain stations after determining Δt^*_α and Δt^*_β values appropriate for this subset. This was done to avoid the large anomalies of OXF and FLO, as well as the probable sediment amplifications in the central states. This also enables a more direct comparison of the two subregions. In Figure III.1.25 the predicted long period P amplitudes for these subregions are shown, with the success of the prediction even better than for the entire data set. Figure III.1.26 shows the predicted short period P amplitudes based on the long period SH Δt^*_β values, and Figure III.1.27 shows the predicted short period SH pattern. There is a fair amount of mismatch in the P data, with several eastern stations being overpredicted, whereas the SH data are slightly better matched. Considering the crudeness of this test, the most important feature is that although the details of the short period amplitude patterns are not well predicted, the overall range of amplitudes is not adequately outside the range of possible receiver effects to argue for frequency dependence. The Δt^*_β values involved in this comparison are as large as 3.8 sec, so with smaller variations expected if receiver corrections for long periods can be applied, it seems that the fit will improve. In this test it is difficult to argue against frequency dependent effects as well, for allowing for a second parameter in the attenuation variations enables one to fit the short periods much better, but this is not warranted by the present data set, at least until receiver corrections can be made.

The effects of possible frequency dependence are important to resolve, because if there is an appreciable impact on the short period WWSSN amplitudes, then source studies or nuclear test yield estimates

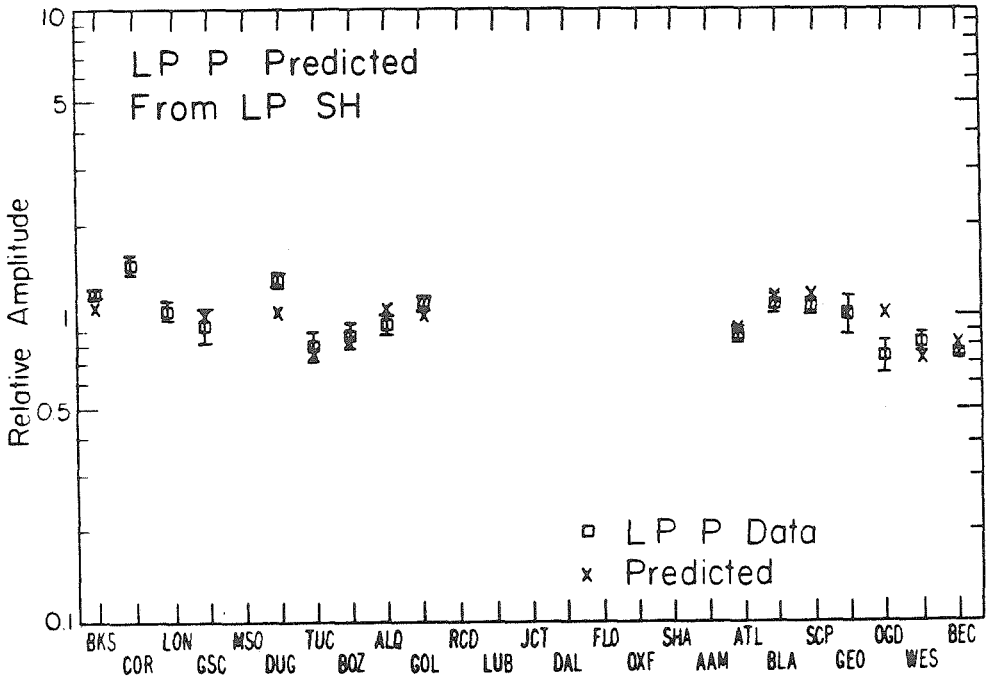

Figure III.1.25. Observed long period P amplitudes versus predicted P amplitudes utilizing the station values of Δt^*_β which reproduce the long period SH amplitudes in East Coast and western stations.

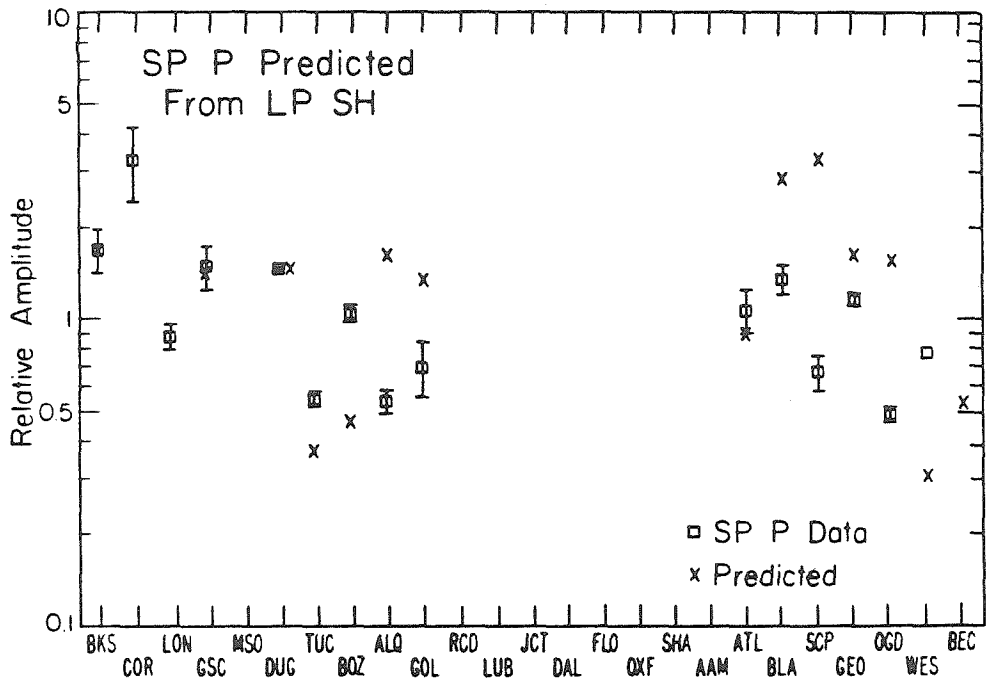

Figure III.1.26. Observed short period P amplitudes versus predicted P amplitudes utilizing the station values of Δt^*_β which reproduce the long period SH amplitudes in East Coast and western stations.

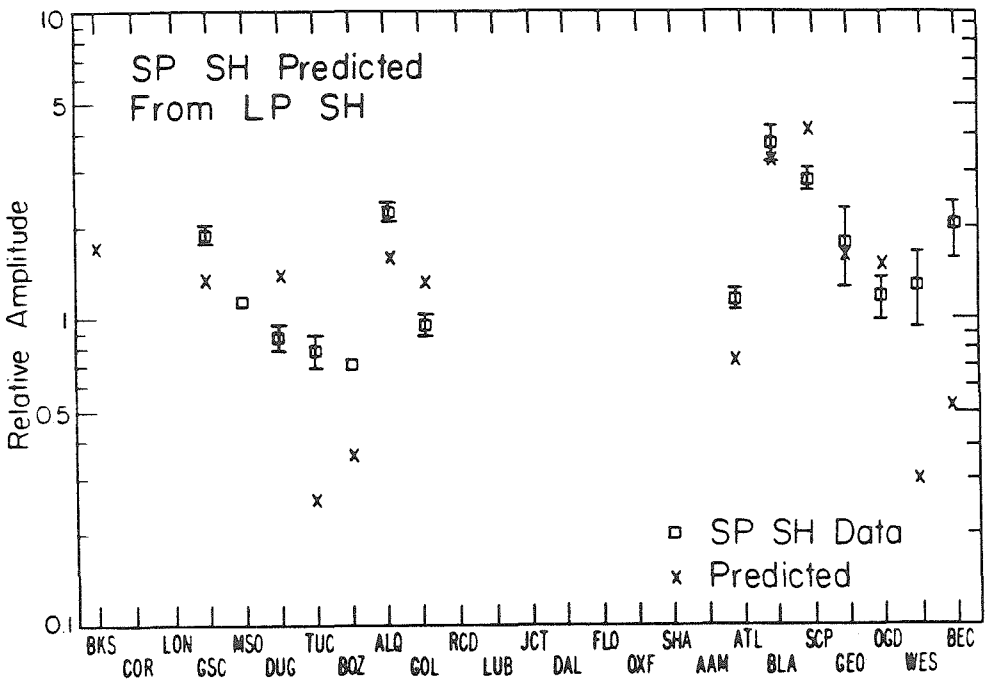

Figure III.1.27. Observed short period SH amplitudes versus predicted SH amplitudes utilizing the station values of Δt^*_β which reproduce the long period SH amplitudes in East Coast and western stations.

using these phases may be in significant error. Consider Figure III.1.28 which shows short period P wave data from one of the shallow events studied by Butler and Ruff (1980), and some of the short period SH waves from this study, as well as synthetics produced by varying t^* and τ_m. The source time function for all of the synthetics was a symmetric triangle of one second duration, with a reference $t^*_\alpha = 1.0$ sec and $t^*_\beta = 3.2$ sec. Values of τ_m and Δt^* are shown which produce relative amplitude variations in increments of 20% of the inital source model amplitude. This demonstrates two important features; one is the relatively minor change in waveform even for large values of Δt^*, and the other is the difference in resulting waveforms for the same source time function and t^* level between the constant Q and frequency dependent models. The frequency dependent synthetics could be brought into closer agreement with the data by using a longer period source time function or larger t^* values, which indicates the importance of attenuation in constraining the source model. When a longer period source is adopted, the waveform changes for the frequency dependent operator are as small as shown here for the constant Q model. The P and SH data shown in this figure do suggest a correlation between low frequency content and low amplitude, such as would be expected for either attenuation model, but this is not always observed in the data.

Since the details of the amplitude variations in the frequency dependent attenuation synthetic tests are sensitive to the t^* of the long period relaxation band, the value of which is controversial, we attempted to make an absolute t^* determination with the best quality

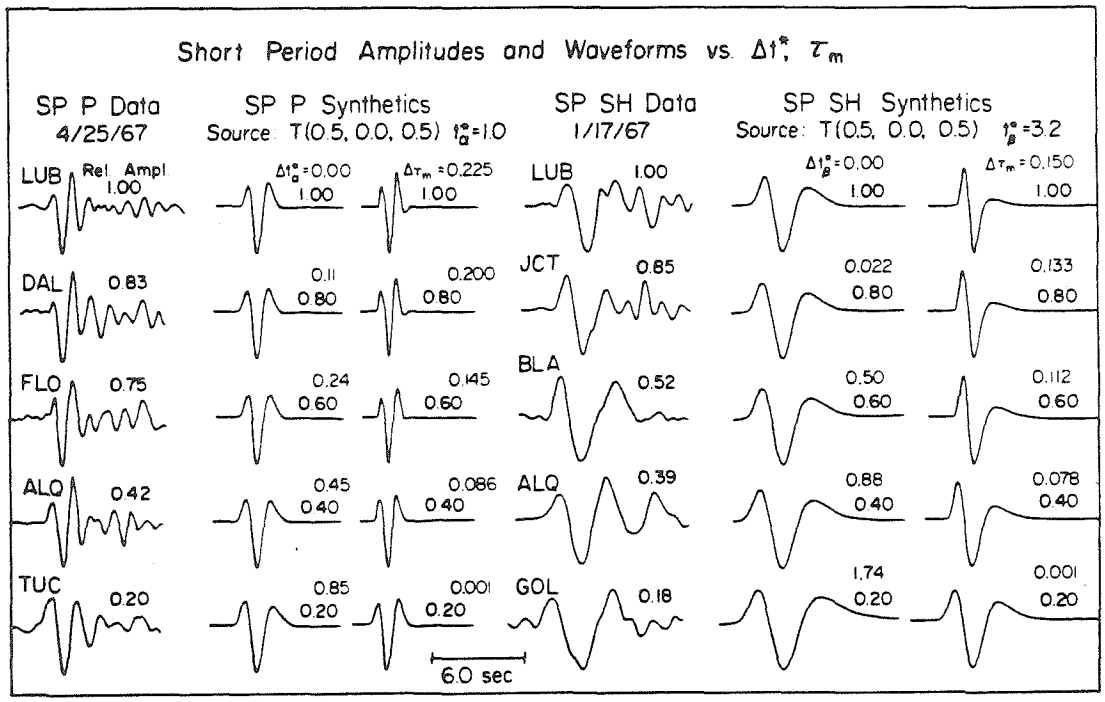

Figure III.1.28. Amplitude and waveform variations versus Δt^* and changes in τ_m for short period P and SH. The short period P data are from a shallow Argentine event, and the SH data are from a deep Argentinan event. Synthetics for a triangular source time function of one second duration are shown with the reference $t^*_\alpha = 1.0$ sec for the P synthetics and $t^*_\beta = 3.2$ sec for the SH synthetics. The variation in attenuation needed to produce a factor of five range in amplitudes for each case is shown. The frequency independent models provide a good fit to the data, whereas a longer time function or larger reference t^* would be needed for the frequency dependent models to match the data.

event in these data. The event of January 17, 1967, was selected for this, and in addition to the SH data, several high quality short period P and long period P waves were digitized. We examined the body wave complexity and stability at all azimuths for this event and found it to be as simple and well behaved as any we know of. This simplicity and the small size of the event allowed us to assume that the source spectrum is almost the same for the P and S waves, and thus that the only difference between P and S observed at a station is in absolute amplitude governed by relative radiation pattern and geometric spreading, differential attenuation between P and S, and differences in receiver effects which are assumed to be small. This point source approximation tends to bias t^* determinations toward larger values, but given the small size of the source involved this effect should not be excessive. Then, having interpolated, detrended and tapered the data, we applied differential attenuation operators to the short period and long period P waves, varying the attenuation until the amplitude ratio $R_{sp,lp}$ = max amp $|$(filtered $P_{sp,lp}$)$|$/max amp $|SH_{sp,lp}|$ was the same for short periods and long periods. In determining the optimal differential attenuation operator we actually minimized the parameter γ:

$$\gamma = [(C_{sp} + C_{lp})^2/4 + (1 - |R_{sp} - R_{lp}|\cdot 2/|R_{sp} + R_{lp}|)^2]$$

where C_{sp} is the normalized cross correlation coefficient of the filtered short period P and observed short period SH signals, and C_{lp} is the corresponding long period normalized cross correlation coefficient. This parameter, γ, which is just a weighted measure of the crosscorrelations and amplitude fits, weights the amplitude match

more heavily, but provides some control on the waveform fit. The normalized cross correlations were only performed over the first pulse half cycle in order to increase their sensitivity. Given the differential operator that minimizes γ, $F^* = t^*_\beta - t^*_\alpha$, one can determine the absolute value of t^*_α under the assumption that $t^*_\beta / t^*_\alpha = 4.0$.

The results of this experiment are listed in Table III.1.4, and shown in Figure III.1.29. For North American stations, the results indicate t^*_α values of 0.8-1.0 sec, with smaller values yielding very poor amplitude agreement. It must be emphasized that this procedure is most sensitive to the dominant periods of the signals, and hence the resulting t^* values are appropriate for the period range 5-20 sec. Note that the P waveforms map rather well into the SH waveforms, over at least the first few cycles. This indicates the validity of some of the assumptions made in the procedure. The resulting t^*_α values are in agreement with the results of Burdick (1978), who included this event in his determination of $t^*_\beta = 3.2$ sec. Two African stations were also included in this test, PRE and SDB, with the interesting result that $t^*_\alpha = 0.4$ sec. This may indicate significant differences in upper mantle attenuation beneath southern Africa relative to the United States, or possible directivity effects in the source. The comparison for the African stations was done with SV phases since the radiation pattern is more favorable for these than for SH, as shown in Figure III.1.2.

We also allowed the differential attenuation operator to be frequency dependent according to equation (2). Selecting a reference

Table III.1.4

Absolute t_α^* determinations

STA	t_α^*	R	C_{sp}	C_{lp}	γ
BLA	1.00	0.060	0.972	0.997	0.984
GEO	0.72	0.115	0.986	0.993	0.988
SCP	0.79	0.101	0.975	0.997	0.984
ALQ	0.96	0.047	0.999	0.986	0.992
DUG	1.03	0.074	0.935	0.962	0.949
PRE	0.38	0.648	0.989	0.907	0.948
SDB	0.39	0.568	0.905	0.949	0.929

τ_m determinations with $t_\alpha^* = 0.8$

STA	τ_m	R	C_{sp}	C_{lp}	γ
BLA	0.05	0.140_{sp} 0.073_{lp}	0.986	0.998	0.560
GEO	0.04	0.108	0.985	0.994	0.989
SCP	0.01	0.100	0.976	0.996	0.984
PRE	0.15	0.446	0.959	0.956	0.958
SDB	0.17	0.402	0.872	0.983	0.930

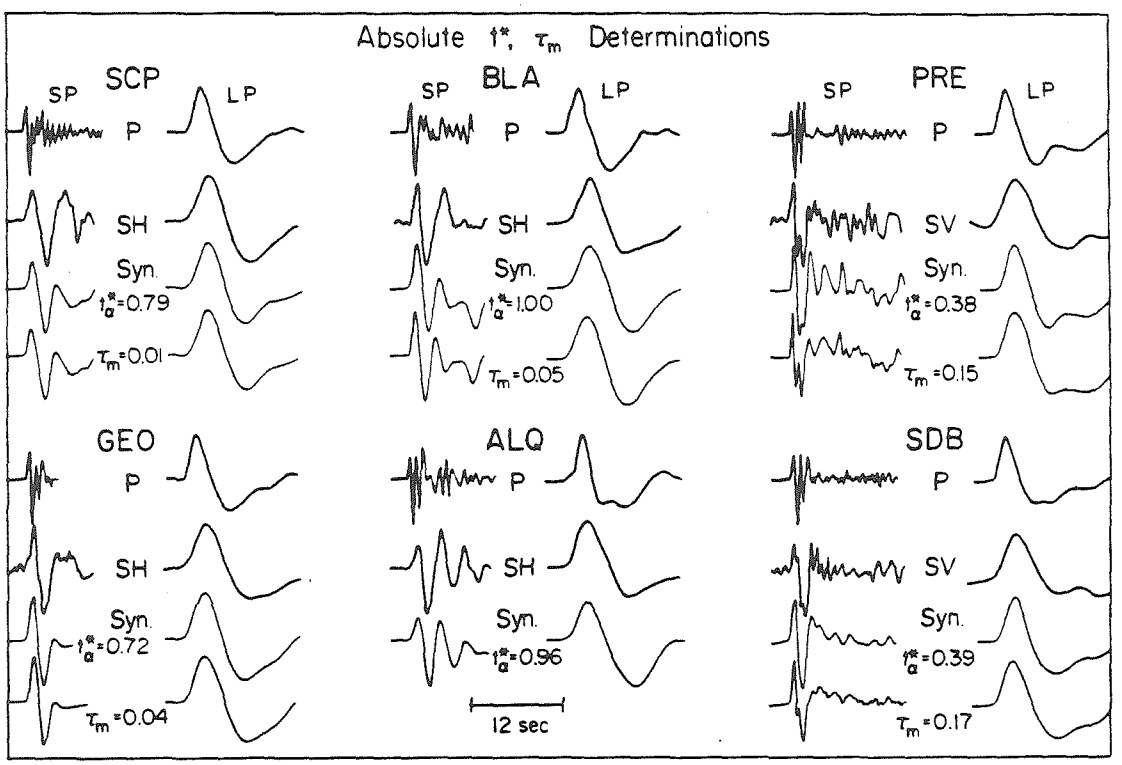

Figure III.1.29. Determination of t^*_α by obtaining a differential attenuation operator which maps the P waves into the SH waves. The t^*_α values which produce the best fitting SH synthetics are shown along with the synthetics. The τ_m value which produces the best fitting SH synthetics assuming $t^*_\alpha = 0.8$ sec are also shown with the corresponding synthetics.

t_α^* of 0.8 sec and varying τ_m produced the τ_m values in Table III.1.4 and the waveforms in Figure III.1.29. The BLA amplitudes were not well fit, though the short period normalized cross correlation is better in this case, and ALQ and a similar station DUG are only well fit with higher t_α^* values so that no τ_m values were determined for the latter two. The fits at the remaining stations are as good or better than for the Futterman operator test, and the African stations have predictably high τ_m values. This procedure is certainly subject to errors in digitization and the assumptions about the source and receivers. However, the consistency of the results indicates the validity of selecting long period t_α^* values of 0.8-1.0 sec as done in the time domain modeling.

Spectral ratio results

As an alternate approach to determining Δt^* variations, we have applied the spectral ratio technique to the long period SH data presented above. Under the assumption that the source spectrum and receiver crustal transfer functions are the same, the spectral ratio of a given body wave phase recorded at two stations by similar instruments will be a function only of the differences of attenuation along the raypaths:

$$\frac{A_i(f)}{A_j(f)} = g_{ij} \frac{\exp(-\pi f t_i^*)}{\exp(-\pi f t_j^*)}$$

where g_{ij} is a constant correction for geometric spreading. Thus, the natural log of the spectral ratio gives

$$\log(A_i(f)/A_j(f)) = C_{ij} - \pi f \Delta t_{ij}^*$$

Fitting a line to the log ratio enables determination of Δt_{ij}^*. For the distance range between stations in these data existing laterally

homogeneous Q_β models would not cause more than a Δt^*_β variation of 0.1 sec (Lundquist and Cormier 1980), so we did not attempt to correct the values to any standard model as was done by Solomon and Toksöz (1970). Data with ScS in the time window were excluded. We took a 30 second time window interpolated in 0.25 second intervals, removed the mean, detrended the signal, tapered it with a 10% cosine termination filter, and computed the spectra. The spectra were smoothed with a running mean over a window of 0.04 Hz, and the log ratio was performed and divided by π. A least squares fit line was found for the ratioed spectra. We performed the analysis with and without Gaussian band pass filtering and found that filtering the data does not significantly affect the results. However selection of the frequency window over which to fit the ratio slope does. The spectral slopes were determined over the period range from 6.3 to 25.0 sec. In Table III.1.5a we list the resulting values of Δt^*_β and standard deviations with SCP as the reference station. A band pass filter of 1-60 seconds has been applied to elimate digitization and rotation noise. The spectral ratios for the January 17, 1967 event are shown in Figure III.1.30, and the exceptional quality of the ratios indicates that source complexity and receiver structure are not important in the bulk of the data. This figure is representative of the quality of all of the ratios obtained. Several stations, BEC, SHA and TUC do have strong second arrivals which produce some interference peaks in the ratios, and the results for these stations are questionable. In Table III.1.5b we list the results for data band pass filtered over the band 5-25 seconds, with the spectral slopes being determined between 6.7

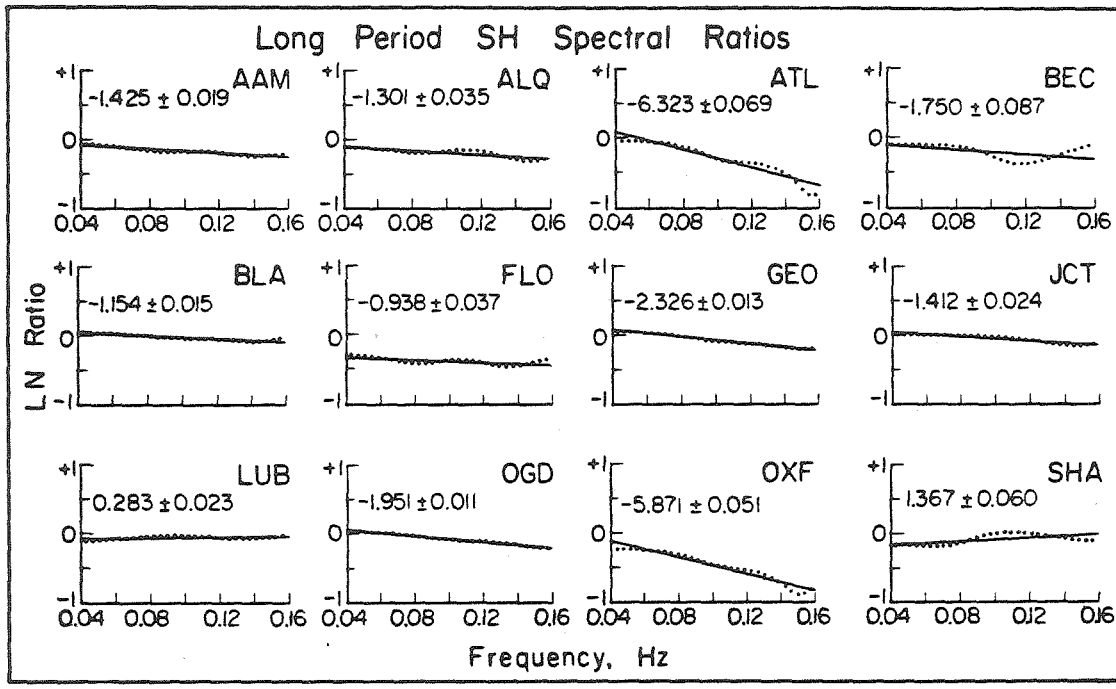

Figure III.1.30. Spectral ratios of long period SH waves, with station SCP as reference, for the January 17, 1967 event. The numbers shown are the least square determinations of the spectral ratio slope with one standard deviation. The data were bandpass filtered with a Gaussian filter of (1,60) seconds.

Table III.1.5a Δt^*_β from long period SH spectral ratios in the band 6.3-25.0 sec.[†]

Station	Dec. 20, 1966	Jan. 17, 1967	Sep. 9, 1967	Jul. 25, 1969	Jan. 3, 1973[*]
AAM	-	1.43 ± 0.02	1.23 ± 0.03	0.02 ± 0.02	1.69 ± 0.01
ALQ	0.38 ± 0.03	1.30 ± 0.04	-	-	0.40 ± 0.06
ATL	-	6.32 ± 0.07	-	3.44 ± 0.09	4.85 ± 0.03
BEC[ξ]	2.85 ± 0.08	1.75 ± 0.09	-	1.20 ± 0.06	2.52 ± 0.08
BLA	1.06 ± 0.02	1.15 ± 0.02	-	1.21 ± 0.02	1.14
DAL	-	-	-	-	-0.51 ± 0.04
FLO	0.66 ± 0.06	0.94 ± 0.04	0.39 ± 0.04	1.34 ± 0.06	-
GEO	-	2.33 ± 0.01	2.20 ± 0.04	4.40 ± 0.03	-
GOL	4.74 ± 0.09	4.25 ± 0.08	3.97 ± 0.09	4.52 ± 0.08	-
JCT	3.15 ± 0.04	1.41 ± 0.02	-	2.25 ± 0.02	1.49 ± 0.03
LUB	-	-0.28 ± 0.02	-	0.65 ± 0.03	-
OGD	1.03 ± 0.04	1.95 ± 0.01	-	3.16 ± 0.04	3.48 ± 0.04
OXF	-	5.87 ± 0.05	4.55 ± 0.03	3.19 ± 0.08	-
SHA[ξ]	-	-1.37 ± 0.06	-1.01 ± 0.09	-2.79 ± 0.04	-1.74 ± 0.05
TUC[ξ]	1.99 ± 0.05	1.74 ± 0.07	3.11 ± 0.02	3.92 ± 0.06	3.70 ± 0.05
WES	-	-	5.01 ± 0.05	5.02 ± 0.05	-

[†]Reference station: SCP

[*]BLA reference corrected to SCP

[ξ]Strong second arrival in signal

Table III.1.5b Δt^*_β from long period SH spectral ratios in the band 6.7-14.3 sec.†

Station	Dec. 20, 1966	Jan. 17, 1967	Sep. 9, 1967	Jul. 25, 1969	Jan. 3, 1973*
AAM	-	1.08 ± 0.01	0.49 ± 0.02	-0.80 ± 0.02	1.15 ± 0.01
ALQ	-0.20 ± 0.02	1.15 ± 0.04	-	-	-1.03 ± 0.05
ATL	-	6.65 ± 0.03	-	3.60 ± 0.08	4.24 ± 0.02
BEC$^\xi$	3.08 ± 0.08	2.19 ± 0.08	-	1.73 ± 0.04	3.49 ± 0.07
BLA	0.69 ± 0.01	1.15 ± 0.01	-	0.93 ± 0.01	0.89
DAL	-	-	-	-	-1.17 ± 0.02
FLO	-0.96 ± 0.04	0.75 ± 0.02	0.15 ± 0.03	0.08 ± 0.04	-
GEO	-	2.30 ± 0.01	2.30 ± 0.03	4.32 ± 0.01	-
GOL	5.71 ± 0.05	5.25 ± 0.03	5.97 ± 0.05	4.56 ± 0.01	-
JCT	3.89 ± 0.02	2.07 ± 0.02	-	2.41 ± 0.01	1.08 ± 0.02
LUB	-	0.47 ± 0.01	-	1.40 ± 0.01	-
OGD	0.28 ± 0.02	1.85 ± 0.01	-	3.15 ± 0.03	3.11 ± 0.01
OXF	-	6.52 ± 0.01	5.70 ± 0.01	2.35 ± 0.04	-
SHA$^\xi$	-	-1.16 ± 0.06	0.30 ± 0.08	-2.73 ± 0.04	-1.51 ± 0.04
TUC$^\xi$	0.67 ± 0.03	1.11 ± 0.03	2.63 ± 0.02	3.85 ± 0.04	3.61 ± 0.02
WES	-	-	5.07 ± 0.01	4.31 ± 0.04	-

†Reference station: SCP

*BLA reference corrected to SCP

$^\xi$Strong second arrival in signal

and 14.3 seconds. The choice of band pass filter again does not significantly affect the results. The variation in resulting values indicates the sensitivity of such measurements, and the degree of arbitrariness in selecting a suitable window.

These Δt_β^* determinations can be compared with the time domain results above and the results of Solomon and Toksöz (1970), bearing in mind that we have removed a factor of π from our slopes and errors. Despite the very smooth ratios that were found, there is significant scatter between events. Table III.1.6 lists the mean Δt_β^* values and standard deviations from this study, as well as the results of Solomon and Toksöz (1970) with π removed from their numbers. The large Δt_β^* values at ATL and OXF are consistent with the broadened nature of their waveforms mentioned above. GOL, even after instrument correction, has a very large Δt_β^* value, as does WES. The remainder of the data have Δt_β^* values within the range found in the time domain analysis, but a comparison with Table III.1.3 shows that individual stations, such as FLO, GEO and OGD, have significantly different results. Comparison with Solomon and Toksöz's (1970) values, which were dominated by SV determinations, shows similar large deviations. The high quality of this data set indicates that the new results are more reliable, but they are still subject to large error bars. There is no obvious east-west trend in the results listed in Table III.1.6.

In order to provide a comparison of the observed long period SH amplitude behavior with that predicted from the spectral ratio results, we utilized Figure III.1.19 to predict the relative amplitude patterns from the results in Table III.1.6. Figure III.1.31 shows the

Table III.1.6 Average Δt^*_β from spectral ratios†.

Station	N	Table 5a	Table 5b	Solomon & Toksöz (1970)
AAM	4	1.1 ± 0.7	0.5 ± 0.9	0.99
ALQ	3	0.7 ± 0.5	0.0 ± 1.1	0.06
ATL	3	4.9 ± 1.4	4.8 ± 1.6	-1.08
BEC$^{\xi}$	4	2.1 ± 0.7	2.6 ± 0.8	-
BLA	3	1.1 ± 0.1	0.9 ± 0.2	-
DAL	1	-0.5	-1.2	-
FLO	4	0.8 ± 0.4	0.0 ± 0.7	-3.72
GEO	3	3.0 ± 1.2	3.0 ± 1.2	2.26
GOL	4	4.4 ± 0.3	5.4 ± 0.6	-
JCT	4	2.1 ± 0.8	2.4 ± 1.2	1.43
LUB	2	0.2 ± 0.7	0.9 ± 0.7	-0.95
OGD	4	2.4 ± 1.1	2.1 ± 1.4	-
OXF	3	4.5 ± 1.3	4.9 ± 2.2	-1.43
SHA$^{\xi}$	4	-1.7 ± 0.8	-1.3 ± 1.2	-2.42
TUC$^{\xi}$	5	2.9 ± 1.0	2.4 ± 1.4	0.83
WES	2	5.0 ± 0.1	4.7 ± 0.5	3.02

† reference station SCP

ξ strong second arrival

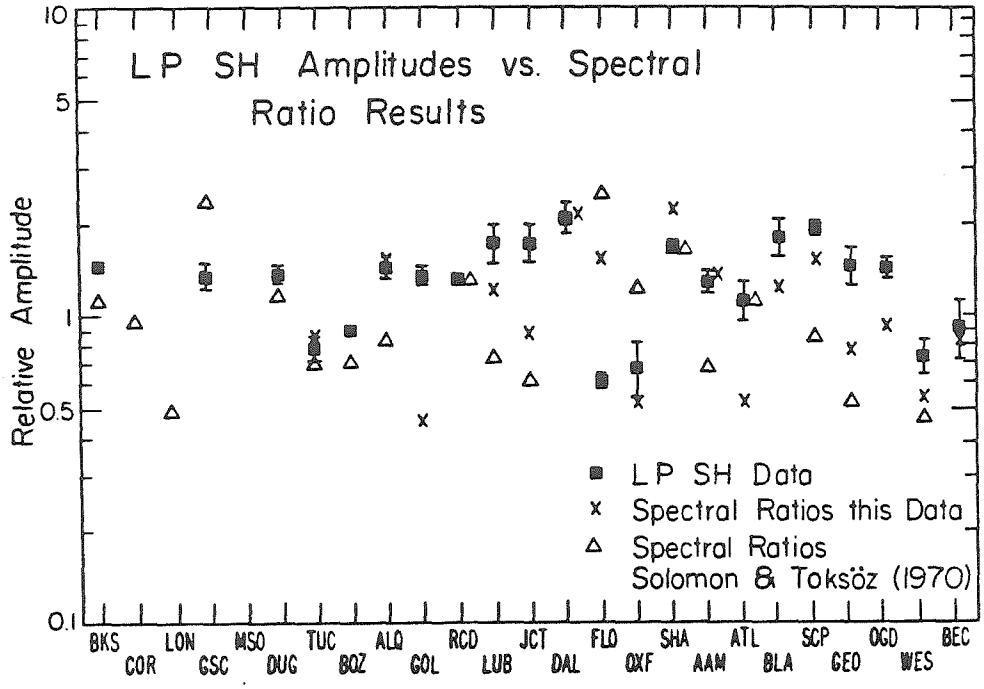

Figure III.1.31. Comparison of observed long period SH amplitude behavior with that expected given the Δt^*_β values determined by spectral ratios in this work and by Solomon and Toksöz (1970).

observed data versus the pattern predicted for the Δt^*_β values from Table III.1.5b, and from the results of Solomon and Toksöz (1970). There is large scatter in the comparison, which suggests that either the spectral ratio techniques are subject to large uncertainties due to the processing procedure, or the amplitudes are profoundly affected by receiver structures which do not disturb the amplitude spectra excessively. Probably the reality is somewhere between, with it being very difficult to dismiss the spectral evidence for attenuation variations, but almost equally difficult to accommodate as much amplitude variation as needed for receiver functions affecting 15 second period SH waves.

Discussion

The tests discussed above were not intended to provide accurate station dependent attenuation operators, rather they quantitatively examine the consistency of the relative amplitude behavior throughout the band from one to 20 seconds. The variations in long period behavior are perhaps the most suggestive that attenuation mechanisms are controlling the basic patterns, with the P and SH amplitudes behaving as predicted for constant Q and $t^*_\beta/t^*_\alpha = 4.0$. The discrepancy between the time domain amplitude results and the spectral analysis do argue for very large receiver effects in the long period data, though the P and SH relative behavior must still be similar to that produced by attenuation. Either technique indicates very large Δt^*_β values of up to 4.0 sec, consistent with the general results of Solomon and Toksöz (1970), but we feel that a better understanding of the frequency dependent receiver effects will lower this range

considerably. The next section addresses this problem in more detail.

Time domain modeling of the short period P and SH waves does not unambiguously resolve frequency dependence of attenuation, emphasizing as it does the longer periods in the waveform. Analysis of short period and long period digitial recordings may permit more reliable spectral analysis of the broadband frequency content, but we did not attempt such techniques for these data because of the limitations of hand digitization and rotation of the SH components. To first order, the P and SH amplitude behavior is consistent with regional variations in attenuation, with many of the deviations from this consistency occuring at stations with apparently large receiver effects. As it may be possible to generate receiver structures which produce relative P and SH amplitude behavior similar to that seen for the attenuation models, this does not conclusively indicate variations in attenuation, rather it demonstrates the general consistency of that hypothesis.

Comparison of the the long period and short period amplitudes indicates that individual station behavior is not entirely consistent with frequency independent attenuation variations, although the inconsistency is not such as to make a strong case for frequency dependence. The range of Δt^* values found by Der et al. (1980) for LRSM stations is within the range determined by our amplitude data, however we do not detect large systematic regional differences between the East Coast and western stations. The structure of the short period amplitude pattern is dominated by the high amplitudes of the central states, as also demonstrated by Butler and Ruff (1980). Much of this trend can be attributed to amplification due to sedimentary

receiver structures, and further analysis is required to resolve to what degree differential attenuation governs the pattern.

Conclusions

Short period and long period P and SH amplitude patterns across WWSSN stations in the United States tend to follow the same regional trends. Stations in the midwestern and Gulf Coast states record large amplitude, high frequency arrivals relative to the East Coast and western stations which record similar amplitudes. Efforts have been made to ensure that the amplitude data is free from bias due to source complexity, radiation pattern, and source structure. The relative amplitude and waveform behavior are tested for compatibility with constant Q and frequency dependent lateral attenuation variations. The short period data do not resolve frequency dependence of attenuation, and either a range of Δt^*_α of 0.5 sec or a range in τ_m of 0.001-0.25 sec proves consistent with the P and SH behavior in the 1 to 7 sec period range. The long period amplitude behavior is very consistent with Δt^*_β variations of up to 4.0 sec, though these variations are not in close agreement with the short period amplitudes. A technique was developed for determining absolute t^*_α levels, and indicates that t^*_α = 0.8-1.0 sec for the deep South American events recorded in North America, and lower t^*_α values or significant frequency dependence for paths to southern African stations. Spectral analysis of the long period SH data yields a large range in Δt^*_β of up to 4.0 sec, though the individual station values are not in close agreement with the amplitude behavior. This indicates that long period receiver functions may be more significant

than usually assumed.

References

Anderson, D. L., A. Ben-Menahem and C. B. Archambeau (1965). Attenuation of seismic energy in the upper mantle J. Geophys. Res., 70, 1441- 1448.

Booth, D. C., P. D. Marshall and J. B. Young (1974). Long and short period P-wave amplitudes from earthquakes in the range of 0^{o}-114^{o}, Geophys. J. Roy. Astron. Soc., 39, 523-537.

Burdick, L. J. (1978). t^{*} for S waves with a continental ray path, Bull. Seismol. Soc. Amer., 68, 1013-1030.

Burdick, L. J. and C. A. Langston (1977). Modeling crustal structure through the use of converted phases in teleseismic body-wave forms, Bull. Seismol. Soc. Amer., 67, 677-691.

Butler, R. and R. S. Hart (1979). Summary of current research on seismic waveform analysis of underground nuclear explosions, Sierra Geophysics Technical Report #SGI-R-79-004.

Butler, R. and L. Ruff (1980). Teleseismic short period amplitudes: Source and receiver variations, Bull. Seismol. Soc. Amer., 70, 831-850.

Butler, R., L. J. Ruff, R. S. Hart and G. R. Mellman (1979). Seismic waveform analysis of underground nuclear explosions, Sierra Geophysics Technical Report #SGI-R-79-011.

Cleary, J. (1967). Analysis of the amplitudes of short-period P waves recorded by long range seismic measurements stations in the distance range 30^{o} to 102^{o}, J. Geophys. Res., 72, 4705-4712.

Der, Z. A., R. P. Masse and J. P. Gurski (1975). Regional attenuation of short-period P and S waves in the United States,

Geophys. J. Roy. Astron. Soc., 40, 85-106.

Der, Z. A. and T. W. McElfresh (1977). The relationship between anelastic attenuation and regional amplitude anomalies of short period P waves in North America, Bull. Seismol. Soc. Amer., 67, 1303-1317.

Der, Z. A., T. W. McElfresh and C. P. Mrazek (1979). Interpretation of short-period P-wave magnitude anomalies at selected LRSM stations, Bull. Seismol. Soc. Amer., 69, 1149-1160.

Der, Z. A., E. Smart and A. Chaplin (1980). Short-period S-wave attenuation under the United States, Bull. Seismol. Soc. Amer., 70, 101-125.

Evernden, J. F. and D. M. Clark (1970). Study of teleseismic P. II. - Amplitude data, Phys. Earth Planet. Interiors, 4, 24-31.

Evernden, J. F. and J. Filson (1971). Regional dependence of surface-wave versus body-wave magnitudes, J. Geophys. Res., 76, 3303-3308.

Futterman, W. I. (1962). Dispersive body waves, J. Geophys. Res., 67, 5279-5291.

Helmberger, D. V. and D. M. Hadley (1981). Seismic source functions and attenuation from local and teleseismic observations of the NTS events Jorum and Handley, Bull. Seismol. Soc. Amer., 71, 51-67.

Isacks, B. and P. Molnar (1971). Distribution of stresses in the descending lithosphere from a global survey of focal-mechanism solutions of mantle earthquakes, Rev. Geophys. Space Phys., 9,

103-174.

Kanamori, H. and G. S. Stewart (1976). Mode of strain release along the Gibbs fracture zone, Mid-Atlantic Ridge, Phys. Earth Planet. Interiors, 11, 312-332.

Khattri, K. N. (1969). Focal mechanism of the Brazil deep focus earthquake of November 3, 1965, from the amplitude spectra of isolated P waves, Bull. Seismol. Soc. Amer., 59, 691-704.

Langston, C. A. (1977). Corvallis, Oregon, crustal and upper mantle receiver structure from teleseismic P and S waves, Bull. Seismol. Soc. Amer., 67, 713-724.

Langston, C. A. (1978). Structure under Mt. Rainier, Washington inferred from teleseismic body waves, J. Geophys. Res., 84, 4749-4762.

Langston, C. A. and D. E. Blum (1977). The April 29, 1965 Puget Sound earthquake and the crustal and upper mantle structure of western Washington, Bull. Seismol. Soc. Amer., 67, 693-711.

Lundquist, G. M. and V. Cormier (1980). Constraints on the absorption band model of Q, J. Geophys. Res., 85, 5244-5256.

Marshall, P. D., D. L. Springer and H. C. Rodean (1979). Magnitude corrections for attenuation in the upper mantle, Geophys. J. R. Astron. Soc., 57, 609-638.

Mikumo, T. and T. Kurita (1968). Q distribution for long-period P waves in the mantle, J. Phys. Earth, 16, 11-29.

Minster, J. B. (1978a). Transient and impulse responses of a one-dimensional linearly attenuating medium - I. Analytical results, Geophys. J. R. Astron. Soc., 52, 479-501.

Minster, J. B. (1978b). Transient and impulse responses of a one-dimensional linearly attenuating medium - II. A parametric study, Geophys. J. R. Astron. Soc., 52, 503-524.

Savage, J. C. (1966). Radiation from a realistic model of faulting, Bull. Seismol. Soc. Amer., 56, 577-592.

Sipkin, S. A. and T. H. Jordan (1979). Frequency dependence of Q_{ScS}, Bull. Seismol. Soc. Amer., 69, 1055-1080.

Solomon, S. C. (1972). Seismic-wave attenuation and partial melting in the upper mantle of North America, J. Geophys. Res., 77, 1483-1502.

Solomon, S. C. and M. N. Toksöz, (1970). Lateral variation of attenuation of P and S waves beneath the United States, Bull. Seismol. Soc. Amer., 60, 819-838.

Stauder, W. (1973). Mechanism and spatial distribution of Chilean earthquakes with relation to subduction of the oceanic plate, J. Geophys. Res., 78, 5033-5061.

Stauder, W. (1975). Subduction of the Nazca Plate under Peru as evidenced by focal mechanisms and by seismicity, J. Geophys. Res., 80, 1053-1064.

Teng, T. L. (1968). Attenuation of body waves and the Q structure of the mantle, J. Geophys. Res., 73, 2195-2208.

Ward, R. W. and M. N. Toksöz (1971). Causes of regional variations of magnitudes, Bull. Seismol. Soc. Amer., 61, 649-670.

Section III.2 Azimuthal Variation in S Wave Amplitude Patterns: Implications for Attenuation and Receiver Structure Variations

Abstract

Amplitude patterns for short and long period SH signals recorded at North American WWSSN and Canadian stations for two azimuths of approach are compared. Short period S wave amplitudes tend to be relatively low in the western tectonic region and enhanced in the shield and mid-continental regions. The East Coast has intermediate amplitude anomalies. Long period amplitude anomalies show surprisingly large variations with substantial azimuthal dependence. There is no simple correspondence between the short and long period anomalies. Along with the azimuthal dependence, this indicates that attenuation variations alone are not responsible for the long period variations. A frequency domain spectral ratio stacking procedure is applied to determine relative receiver functions for the long period SH waves from South American events recorded at WWSSN stations. These filters show a clear association between complex receiver functions and long period amplitude anomalies.

Introduction

Chapter III.1 presented an analysis of broadband P and S wave amplitude behavior at North American WWSSN stations for deep South American earthquakes. It was shown that for that azimuth of approach short and long period P and S wave amplitudes track quite closely, with the relative behavior being consistent with variations in attenuation under the assumption that all losses are in shear. This is true for the short and long period amplitudes separately, but there

is poor agreement between the differential t^* estimates made in the two pass bands. In particular, it was found that the range in t^* required to fit the entire range of long period amplitude variations exceeds that required to produce the short period patterns. It was suggested that this is due to much stronger influence of receiver structure on long period waveforms and amplitudes than is commonly assumed.

In this chapter the amplitude analysis is extended by comparing the relative amplitude patterns for short and long period S waves for an additional azimuth of approach, using events in the Sea of Okhotsk. The azimuthal behavior of the amplitude patterns provides a means by which to further isolate the effects of attenuation variations and geometric effects. The spectral ratio analysis presented in Chapter III.1 is also extended to develop long period relative receiver transfer functions for the southern azimuth of approach to North American WWSSN stations. The relative complexity of these filters is indicative of propagational effects.

Amplitude and Travel Time Data

The S wave travel time and amplitude observations presented here were recorded at North American WWSSN and Canadian Seismic Network (CSN) stations. Seventeen moderate size (m_b = 5.5 to 6.0) intermediate and deep focus earthquakes in Argentina and the Sea of Okhotsk were selected for analysis on the basis of their simple, impulsive waveforms and stable SH radiation patterns to North America. The station and event epicenter locations are shown in Figure III.2.1. The short and long period horizontal components in the distance range

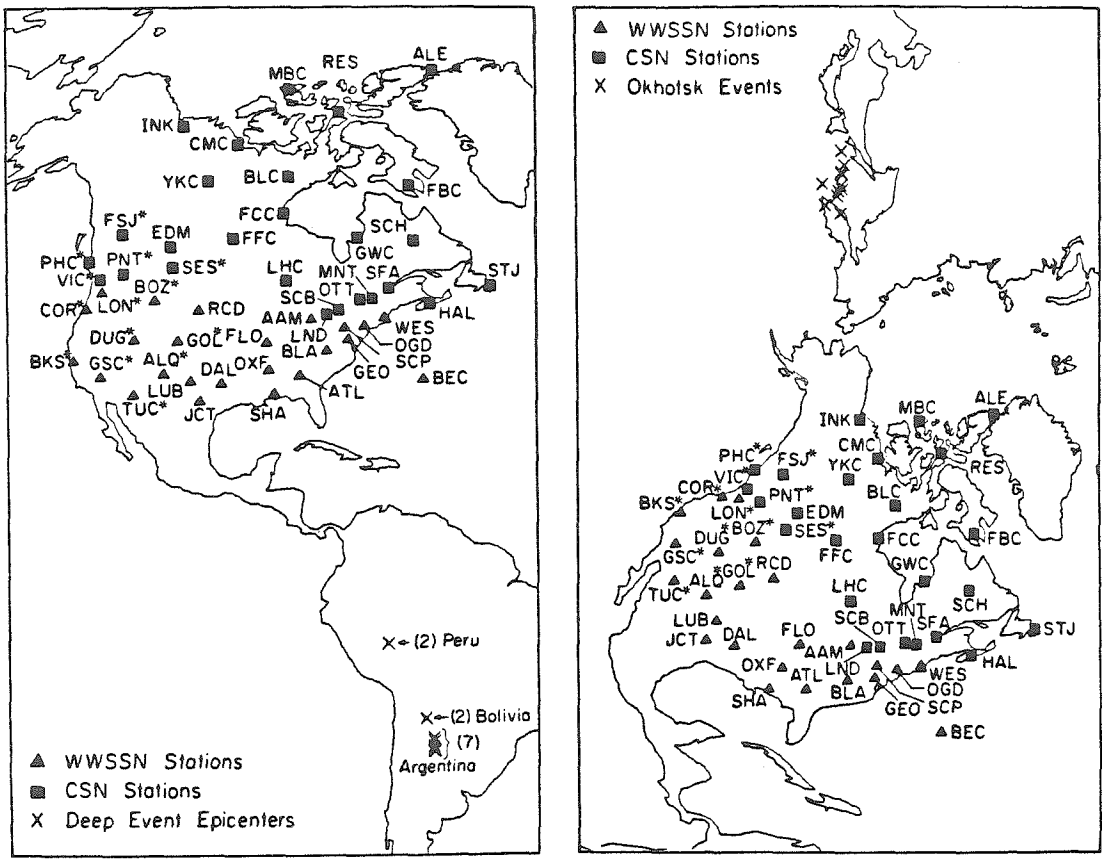

Figure III.2.1. Azimuthal equidistance projections centered on the Argentine (left) and Sea of Okhotsk (right) source regions. The locations of the intermediate and deep focus event epicenters and recording stations used in this study are shown. The stations with an asterisk are designated as stations within the western tectonic province. GSC, RCD and SCH are approximately 80^{o} from the Argentine source region. SHA ranges from 78^{o} to 88^{o} from the Sea of Okhotsk events used.

40^{o} to 80^{o} were digitized and rotated into transverse and radial polarizations, and amplitude and travel time measurements were made for the SH components. The first peak-to-first trough and first peak amplitudes were measured for the short and long period signals respectively. Figures III.1.3 to III.1.10 show SH waveforms for the Argentine events. Figures III.2.2 to III.2.10 show many of the SH waveforms for the Sea of Okhotsk events. The travel times and amplitudes of these simple phases can be reliably measured. The travel time information from these phases is discussed in Chapter II and Section III.3.

The Sea of Okhotsk earthquakes tend to be slightly more complicated than the deep South American events of similar size, with small precursory foreshocks and double events being common. The distance range spanned by North American WWSSN stations is somewhat larger for the Sea of Okhotsk events as well, and the coda of the signals in Figures III.2.2 to III.2.10 frequently contain ScS and the lower mantle triplication arrivals described in Chapter I. However, the general characteristics of the waveforms are similar to those of the South American events described in detail in the previous chapter. The Mississippi Valley and Texas stations show the highest frequency arrivals and the largest short period/long period amplitude ratios. Stations along the East Coast tend to be intermediate in behavior, and stations in the western tectonic province (identified in Figure III.2.1) typically record lower amplitude, more attenuated short period arrivals. Stations such as TUC and OXF, which were noted to have anomalous waveform and amplitude behavior in the Argentine data

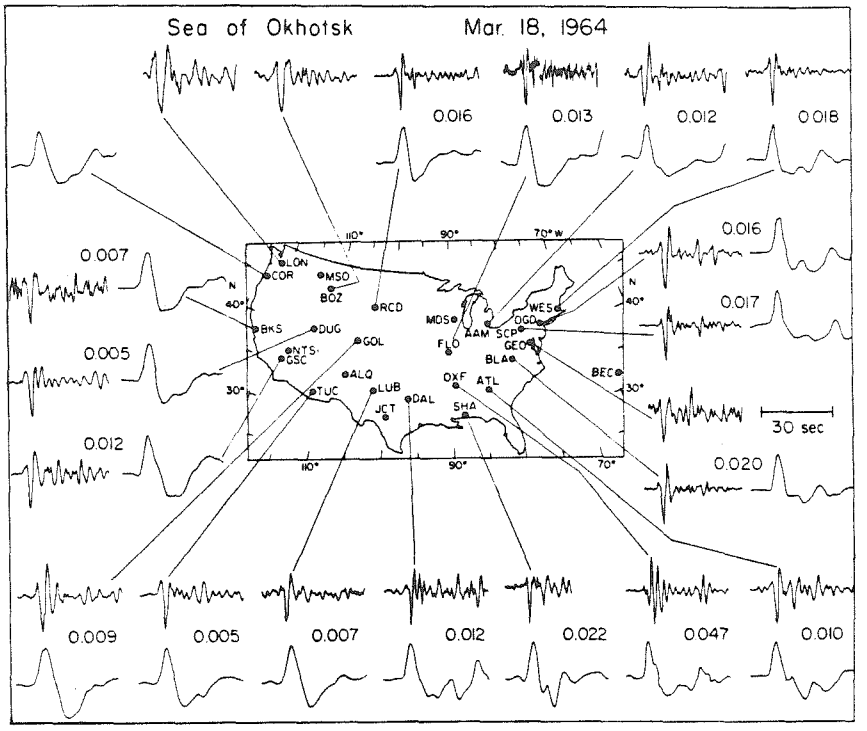

Figure III.2.2. Short and long period SH components of the March 18, 1964 event. The numbers are the gain corrected short period to long period amplitude ratios.

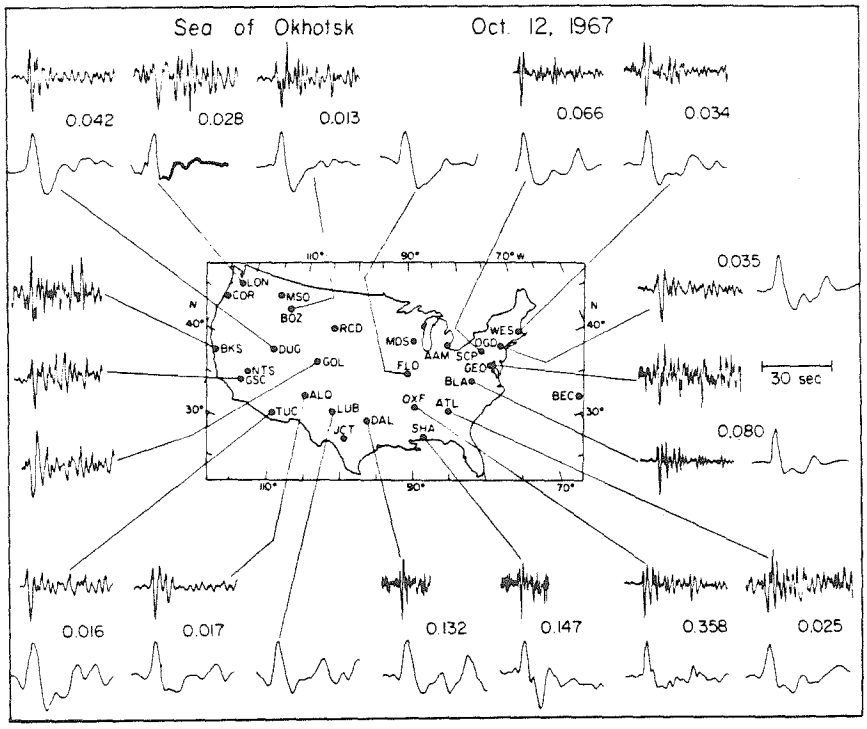

Figure III.2.3. Short and long period SH components of the October 12, 1967 event. The numbers are the gain corrected short period to long period amplitude ratios.

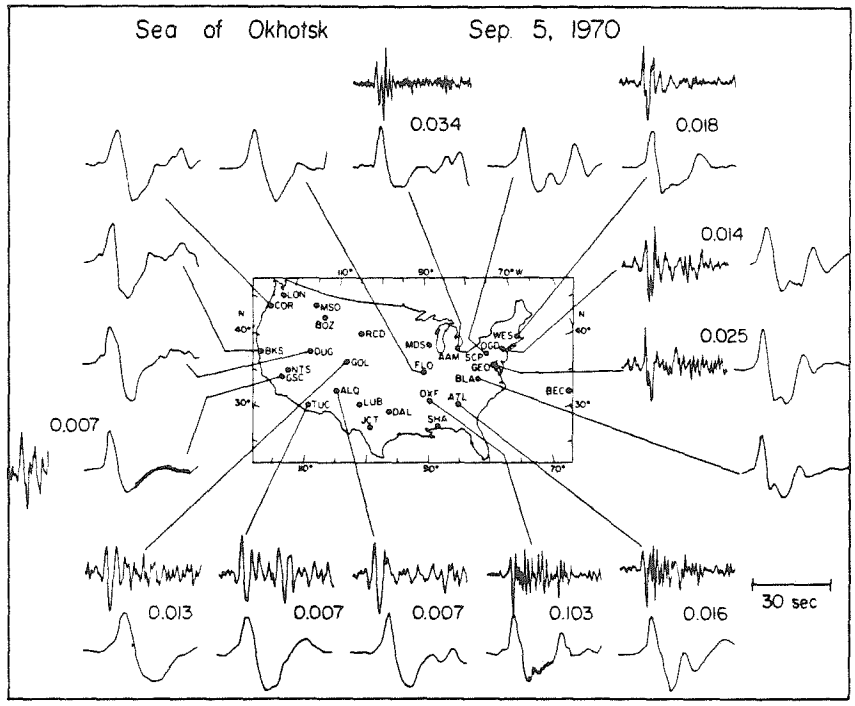

Figure III.2.4. Short and long period SH components of the September 5, 1970 event. The numbers are the gain corrected short period to long period amplitude ratios.

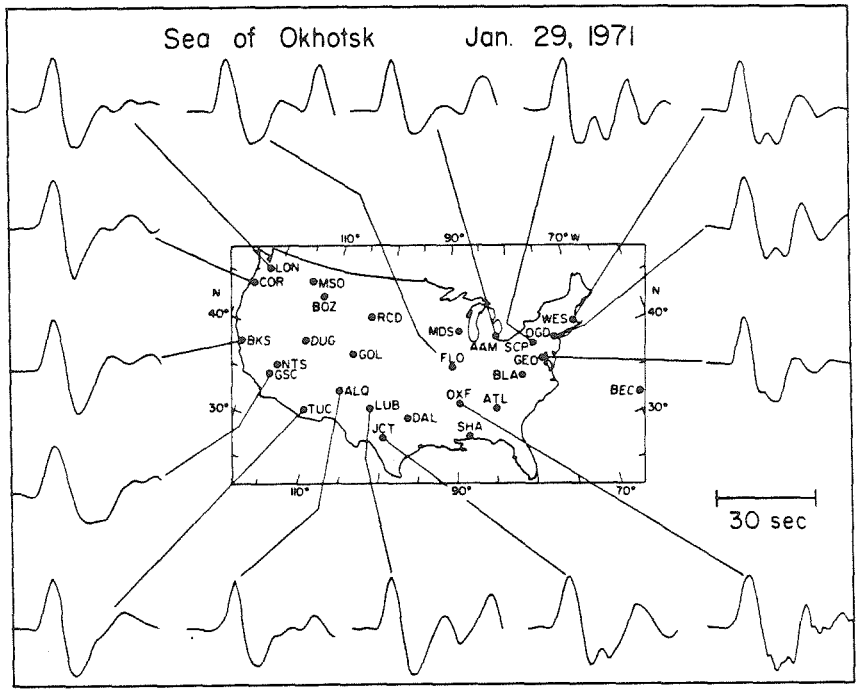

Figure III.2.5. Short and long period SH components of the January 29, 1971 event. The numbers are the gain corrected short period to long period amplitude ratios.

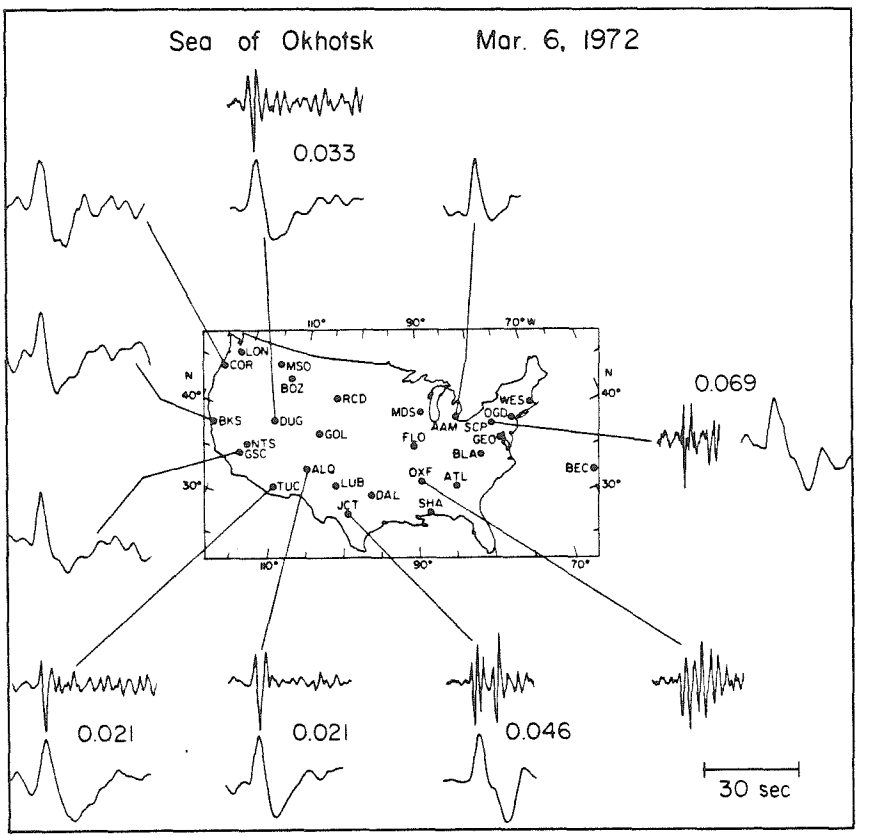

Figure III.2.6. Short and long period SH components of the March 6, 1972 event. The numbers are the gain corrected short period to long period amplitude ratios.

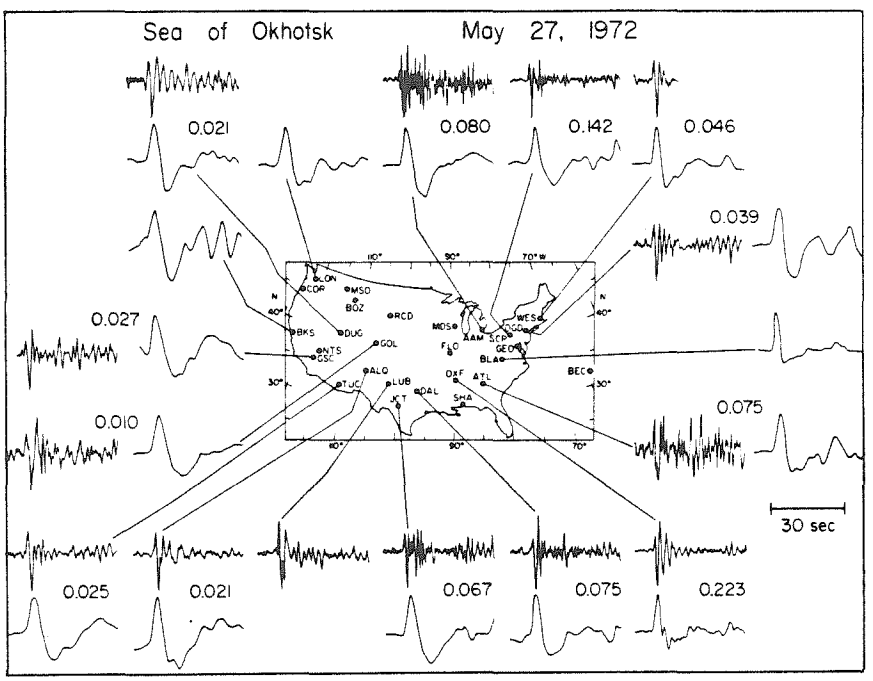

Figure III.2.7. Short and long period SH components of the May 27, 1972 event. The numbers are the gain corrected short period to long period amplitude ratios.

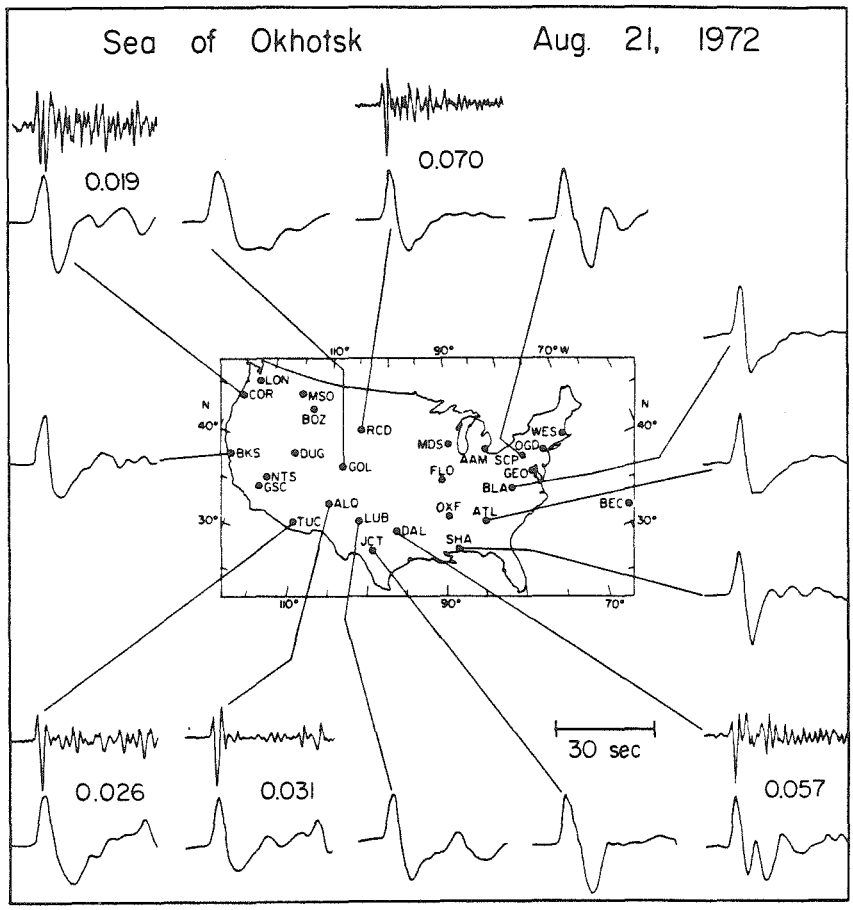

Figure III.2.8. Short and long period SH components of the August 21, 1972 event. The numbers are the gain corrected short period to long period amplitude ratios.

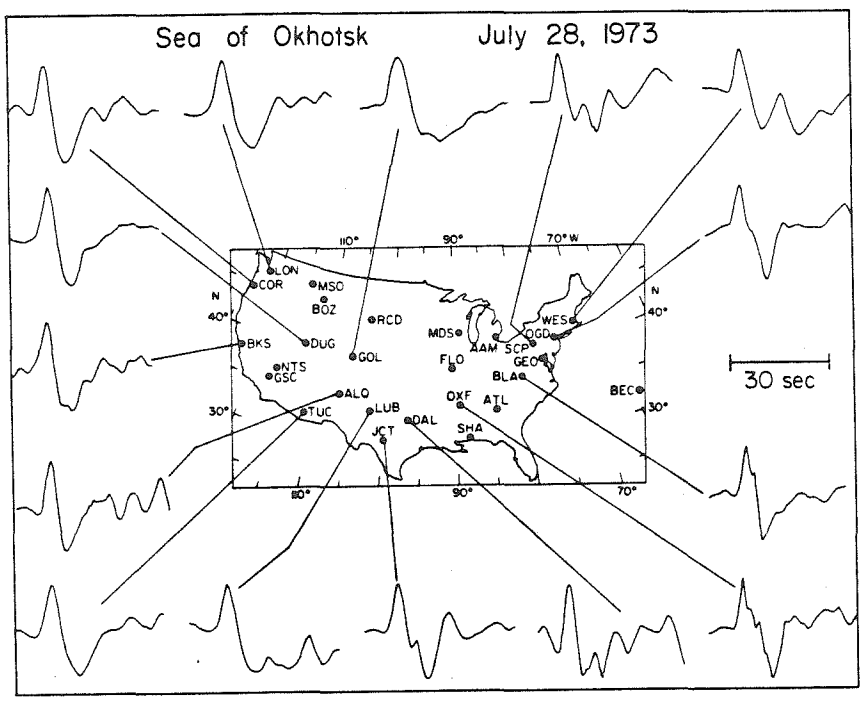

Figure III.2.9. Short and long period SH components of the July 28, 1973 event. The numbers are the gain corrected short period to long period amplitude ratios.

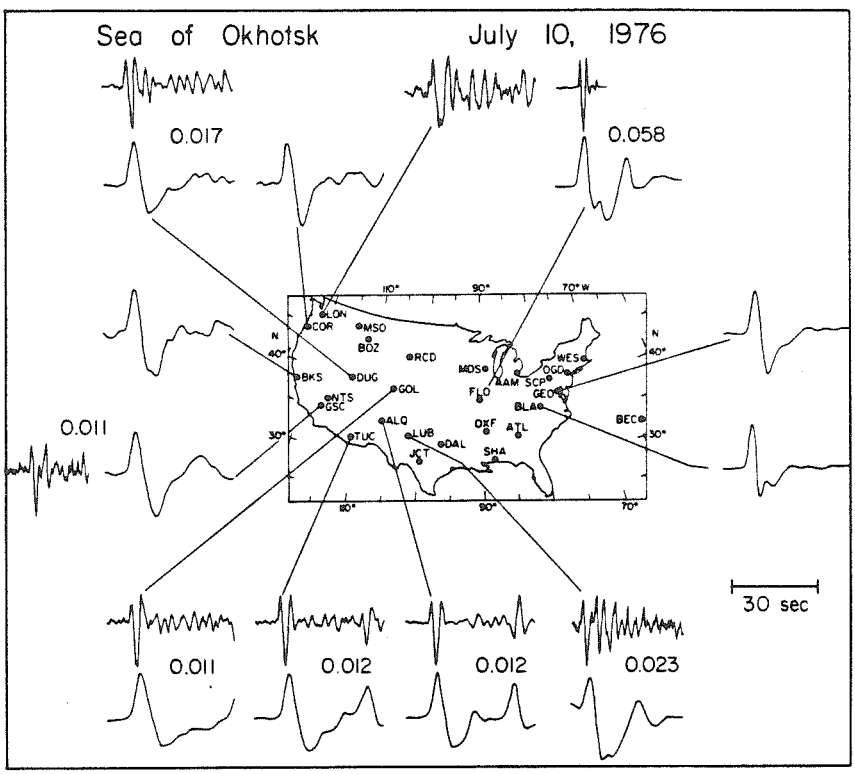

Figure III.2.10. Short and long period SH components of the July 10, 1976 event. The numbers are the gain corrected short period to long period amplitude ratios.

set, show clear multiple arrivals in the Sea of Okhotsk data.

Radiation pattern corrections were determined from focal mechanisms constrained by P wave first motions, S wave polarizations, and long period SV/SH amplitude ratios, and these corrections were applied to both the Sea of Okhotsk and South American amplitude data, along with instrument gain and geometric spreading corrections. The focal mechanisms are listed in Table I.1.2. Station anomalies were then determined by removing relative event size factors using the procedures described in Section III.1. The data for the two source regions were processed separately.

The average relative station anomalies for the long period SH arrivals for the two source regions are compared in Figure III.2.11. The Argentine data show larger relative variations than the Okhotsk data, of a factor of 4, which is surprisingly large for 20 s period signals. As shown in Figure III.1.19, the range in Δt^*_β for a constant Q attenuation operator required to produce a factor of four variation in long period S wave amplitudes is about 6 sec. The corresponding short period S waves would vary by a factor of 100 in amplitude, and would have dramatic waveform changes. If the amplitude variations were to be explained by upper mantle attenuation variations, there would be no reason to expect significant azimuthal variations for teleseismic body wave amplitudes, all of which are traversing the upper mantle at steep angles. There is no simple pattern in the long period amplitude variations associated with regional tectonics, and it is clear that several stations show strong azimuthal variations, particularly BOZ, DAL, RCD, SHA, OXF and FLO.

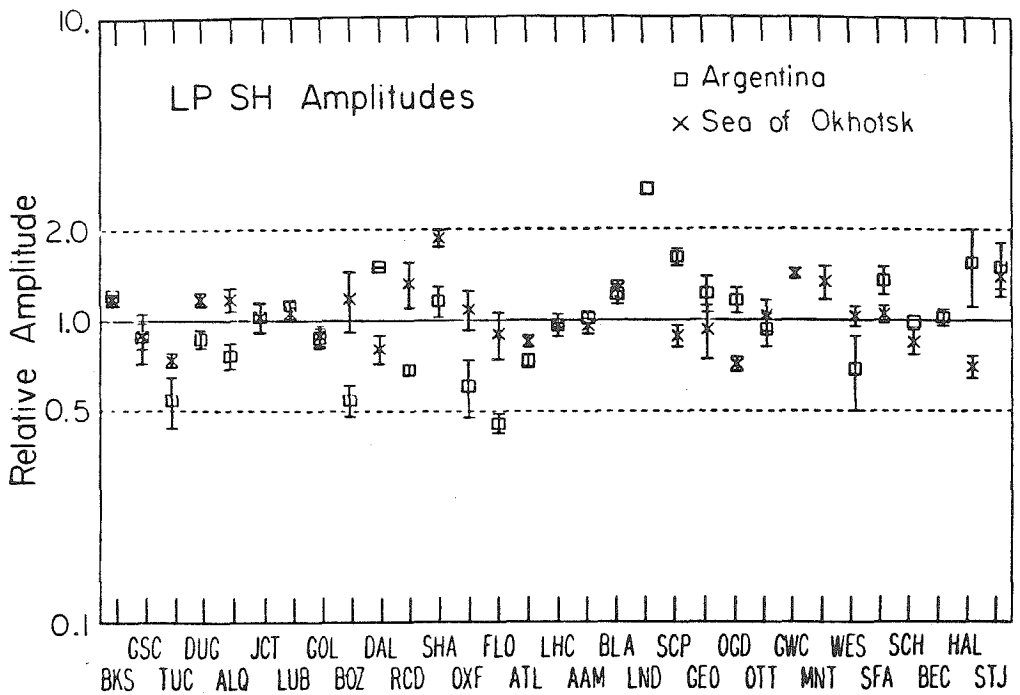

Figure III.2.11. Comparison of the station amplitude anomalies from the Sea of Okhotsk and Argentine long period SH data. The relative amplitudes have been adjusted to minimize the scatter at each station following the procedure described in Section III.1. Note the greater amplitude variation in the Argentine data.

To illustrate the relative behavior better, the ratios of the Argentina to Okhotsk stations amplitude anomalies are shown in Figure III.2.12. Note that the ratios at SCP, GEO, OGD, SCH, SFA and HAL are relatively large, indicating that the Argentina S wave data at the East Coast stations is enhanced by as much as a factor of 2 as concluded in Chapter II. OTT and WES do not show this enhancement, though WES has a complicated SH receiver function as shown below. Another interesting feature in Figure III.2.12 is the group of low ratios at SHA, OXF, FLO, RCD and BOZ. The latter two stations do not appear to sample the Caribbean travel time anomaly described in Chapter II, though RCD is along the same azimuth. BOZ lies about 100 to 200 km northwest of the Yellowstone hotspot and the diminished amplitudes from the southern azimuth may be associated with the presence of the hotspot. Butler (1983) notes a similar pattern for short period P waves at BOZ. DAL, which is close in distance and azimuth to SHA, shows a very high amplitude ratio, perhaps suggesting a scattering type interference effect associated with the diminished amplitudes at SHA, OXF and FLO. These stations all have substantial low velocity sediments beneath the recording sites, but the azimuthal variations are very consistent over the broad region spanned by the stations, indicating that the near surface effects are not responsible.

A comparison of the short period SH amplitude station averages for Okhotsk and Argentina is shown in Figure III.2.13. The overall amplitude variations are quite a bit larger than for the long periods and the amplitude ratios (Figure III.2.14) indicate greater azimuthal

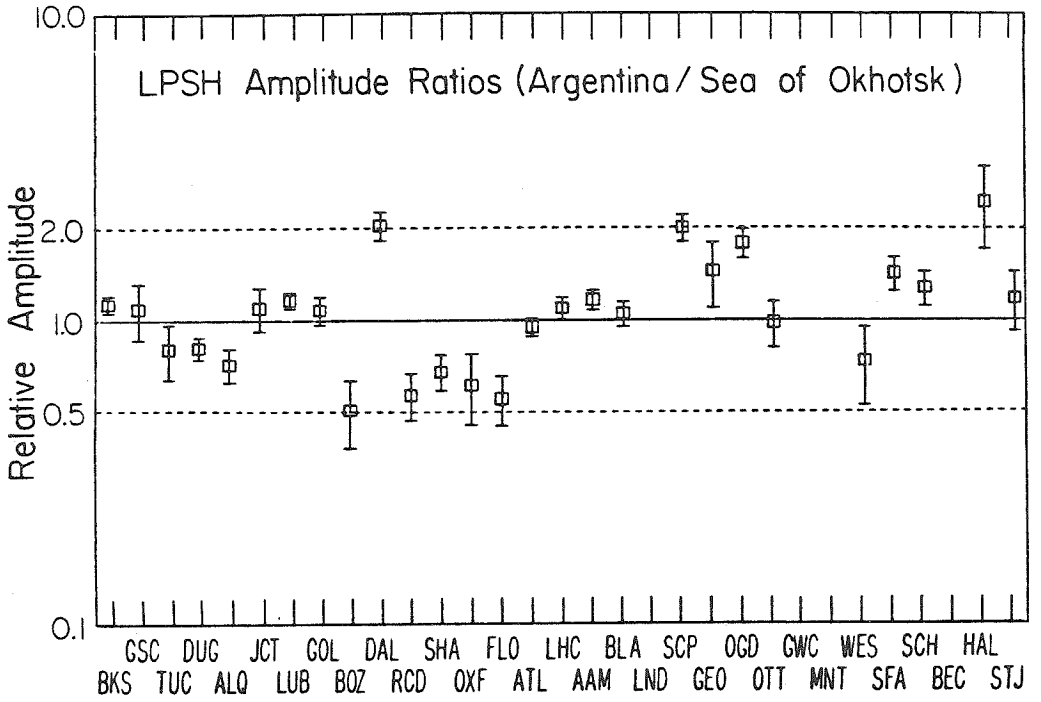

Figure III.2.12. Ratios of the long period SH station anomalies for Argentina over those for the Sea of Okhotsk. The East Coast stations for the Argentine data are relatively enhanced, whereas SHA, OXF and FLO are relatively low amplitude.

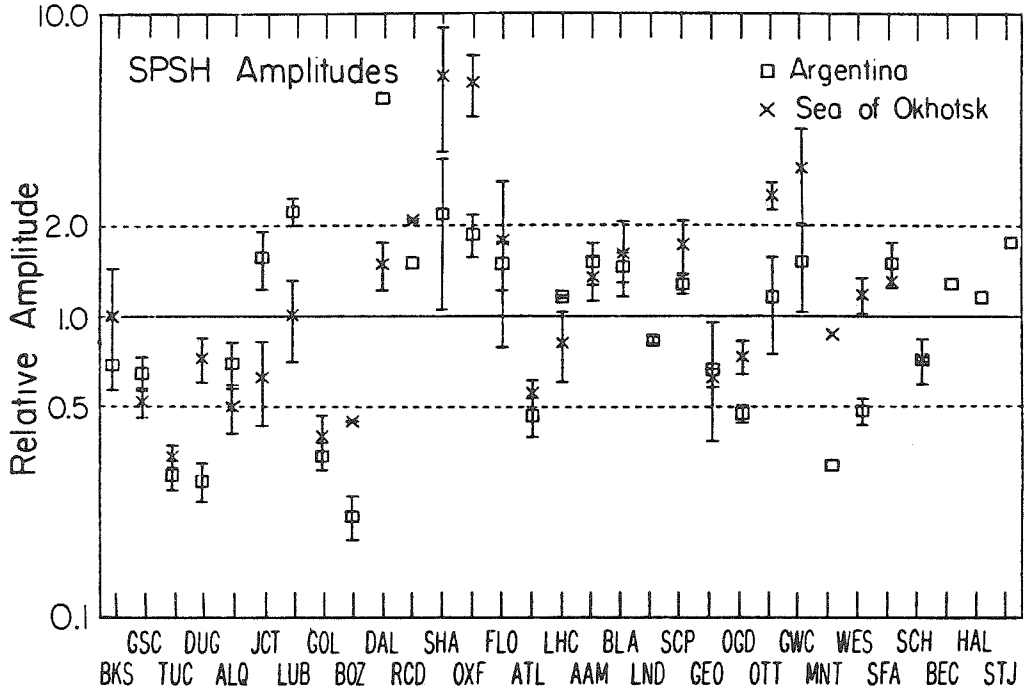

Figure III.2.13. Comparison of the station amplitude anomalies from the Sea of Okhotsk and Argentine short period data, which have been processed in the same way as the long period data in Figure III.2.11. The short period signals show greater relative variations than the long periods.

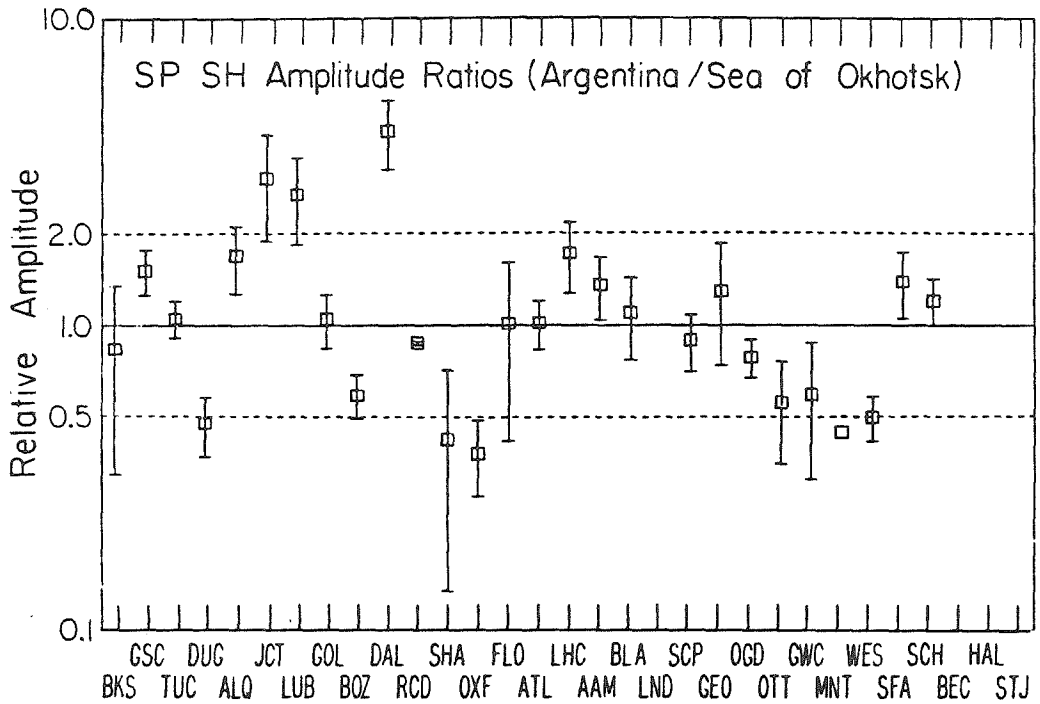

Figure III.2.14. Ratios of the short period SH station anomalies for Argentina over those for the Sea of Okhotsk. SHA and OXF are slightly diminished from Argentina, and the Texas stations are relatively enhanced. No clear East Coast anomaly is apparent.

variations, as might be expected for these shorter period (2 to 5 s) signals. The Argentina S waves in the East Coast do not appear to be enhanced, but the short period signals at SHA and OXF are a bit low. The most enhanced amplitudes from Argentina are found at the Texas stations which are in the same distance range and fairly close in azimuth to SHA and OXF, but do not show velocity anomalies. Again, this may reflect a defocusing or multipathing effect associated with the lower mantle anomlies discussed in Chapter II.

Figure III.2.13 clearly shows the jump in amplitude levels between stations in the tectonic province (TUC, DUG, ALQ, GOL, BOZ) and the midwestern and Texas stations. It is clear that the East Coast stations record intermediate amplitudes at least a factor of 2 higher than the tectonic province stations. It is also clear that stations with large sedimentary deposits beneath the site are enhanced (LUB, DAL, RCD, SHA, OXF and FLO). Though the exact amplitude effects of these sediments are unknown, the calculated effects for a suite of low velocity receiver structures indicates short period amplification factors of from 1.3 to 2.0. Allowing for this, the range in amplitudes can be reduced to a factor of about 8, which is twice as large as the variation in 1 sec P wave amplitudes for these stations (Butler, 1983). The average relative P wave amplitudes for North American WWSSN stations found by Butler are shown in Figure III.2.15. These values are the averages of amplitude patterns independently derived for three azimuths of approach to each station. The lowest P wave amplitudes are recorded at TUC, ALQ and GOL. TUC and GOL are also very low amplitude for short period S waves. Other features are

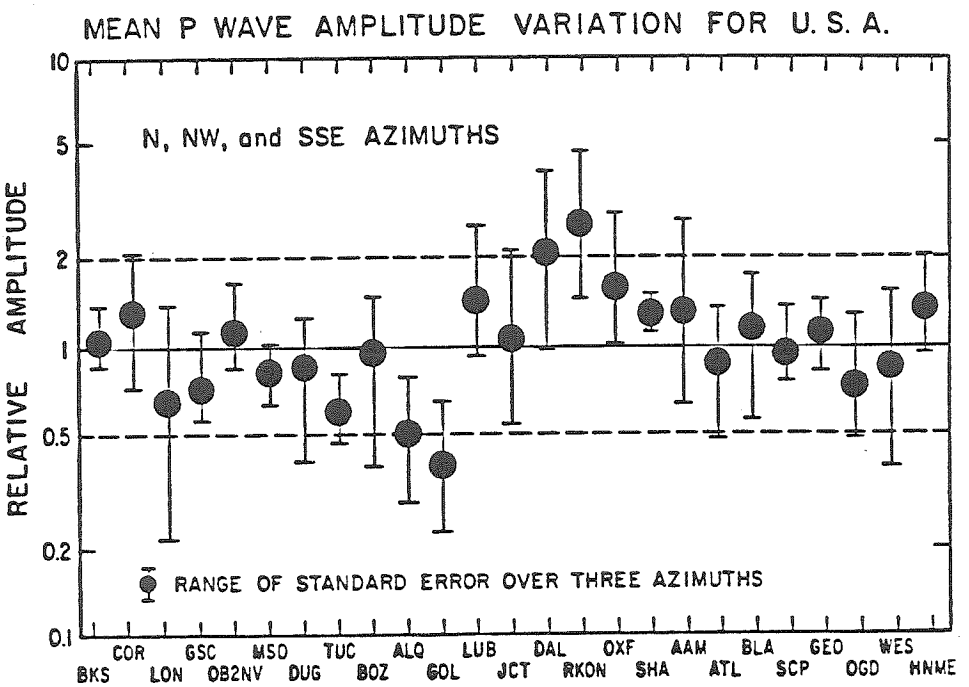

Figure III.2.15. The relative short period P wave amplitude variation for the N, NW and SSE azimuths are averaged to obtain mean P wave amplitude variations for stations in the United States and southern Canada. The error bars represent the total range of the standard errors of the means for the three azimuths. (From Butler, 1983).

very similar between the P and S waves, with ATL, SCP and OGD being relatively low within the East Coast set of stations. These variations cannot be attributed to sedimentary structure, for these stations are all on hard rock sites. The azimuthal stability of the relative amplitudes for these stations indicates that differential attenuation is a likely cause of the variation for these stations. A factor of 4 amplitude variation in the short period S waves would require Δt^*_β = 1.2 sec (Figure III.1.19). As shown in the next section the <u>average</u> short period amplitude variation between stations east of and west of the Rocky Mountains is a factor of 2.4.

The azimuthal variation of the short period P waves analyzed by Butler (1983) is shown in Figure III.2.16. The values shown are the ratio of the station amplitude anomalies for the northwestern azimuth to those for the South American azimuth. Note that these ratios are inverted relative to the S wave ratios in Figure III.2.14. Butler (1983) discussed the slight trend apparent in the P wave data, which shows a west to east increase in the amplitude ratios. He concluded that the South American P wave amplitudes are anomalously low at East Coast stations (SCP, GEO, OGD, WES, ATL, BLA). He attributed this to an attenuating or defocusing body beneath Colombia. There is a slight suggestion of a similar trend in the SH ratios in Figure III.2.14, if one eliminates DUG, BOZ, SHA and OXF. As discussed in Chapter II, the East Coast observations of South American events appear to be anomalously late, and the long period SH amplitudes are enhanced. If the lower mantle body responsible for this is also a low Q region, the pattern in the P wave amplitude ratios may be due to the same lower

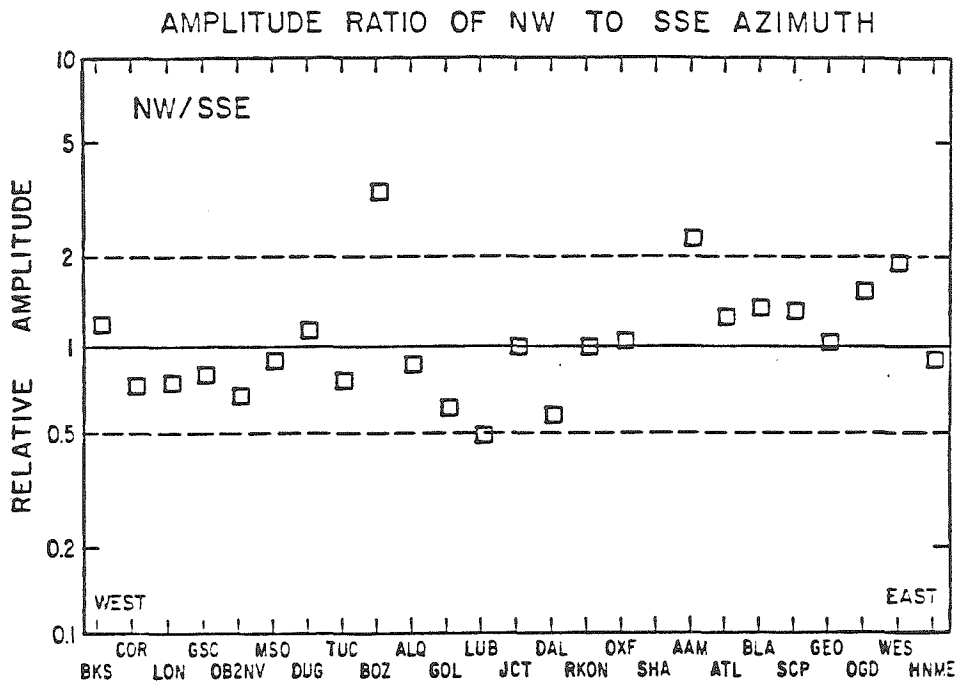

Figure III.2.16. The ratio of the relative short period P wave amplitudes for northwest and south southeastern azimuths are graphed with the northwest amplitude as numerator and the south southeast amplitude as denominator. From Butler (1983).

mantle heterogeneity.

In the previous chapter the long period SH signals from South America were used to determine Δt^*_β estimates using spectral ratio techniques. The results of this simple processing are difficult to interpret, for the Δt^*_β values found have a larger range than indicated by the short period signals, and they are poorly correlated with either short or long period amplitude variations. It is necessary to better understand the long period amplitude and spectral behavior before detailed models of variation in attenuation can be constructed. Because the South American data are exceptionally simple and reliable, a more detailed spectral analysis was applied with the intent of assessing the relative complexity of the receiver functions. The band limited nature of the data makes it difficult to determine attenuation differences, however, within the pass band of the long period instrument the combined effects of differential attenuation and receiver structure can be separated from source complexity.

The procedure adopted reduces the variance of individual spectral ratio estimates by using a log-spectral stack. As in Section III.1, SCP was chosen as the reference station, because of its relatively high frequency impulse-like waveforms. All other observations for each South American event were deconvolved by the corresponding SCP observation. The phase pairs are indicated in Table III.2.1. The time windows deconvolved were either 50 or 60 sec long, with ScS being omitted from the window. The ratios for a given station were then averaged in the log-frequency domain. The passband over which this averaging was done was .015 to 0.5 Hz. The stacked ratios were then

inverted into the time domain yielding relative receiver functions. Between 2 and 5 ratios were averaged for each station. The averaging procedure helps to suppress noise and radiation effects, and allows a somewhat broader frequency band to be analyzed.

The relative receiver functions determined in this procedure have lost any receiver or attenuation character common to the reference and secondary station. A test of the adequacy of these transfer functions is to convolve the reference trace signals with the relative receiver functions and compare the results with the observed traces. Figure III.2.17 shows the SCP reference traces for each event. The number after the station name indicates the event number in Table III.2.1. Figures III.2.18 to III.2.22 show the observed traces for each station (dotted lines) and the synthetic for each station produced by convolving the SCP observation for that event with the relative receiver function for that station (solid lines). Note that for the 35 to 40 sec time windows shown the comparisons are quite good. The signals do not vary substantially in waveform so this agreement is not surprising, but the validity of the averaging procedure is demonstrated by the comparisons between stations with dramatically different frequency content from SCP such as ATL, TUC and OXF.

The relative receiver functions determined in this analysis are shown in Figure III.2.23. These traces are the time domain representation of the stacked spectral ratios. The filters are acausal due to a phase shift introduced in the stacking procedure, and their band limited nature must be emphasized. However, the relative character of the filters can still be constructively assessed. Note

TABLE III.2.1

EVENT	AAM	ALQ	ATL	BLA	FLO	GEO	JCT	LUB	OGD	OXF	SCP	SHA	TUC	WES
1 Dec. 9, 1964		X	X							X	X			
2 Mar. 5, 1965		X	X	X					X		X		X	
3 Dec. 20, 1966	X	X		X	X		X		X		X	X	X	
4 Jan. 17, 1967	X	X	X	X	X	X	X	X	X	X	X	X	X	
5 Sep. 9, 1967	X				X	X				X	X	X	X	X
6 Jul. 25, 1969	X	X	X	X	X	X	X	X	X	X	X	X	X	X

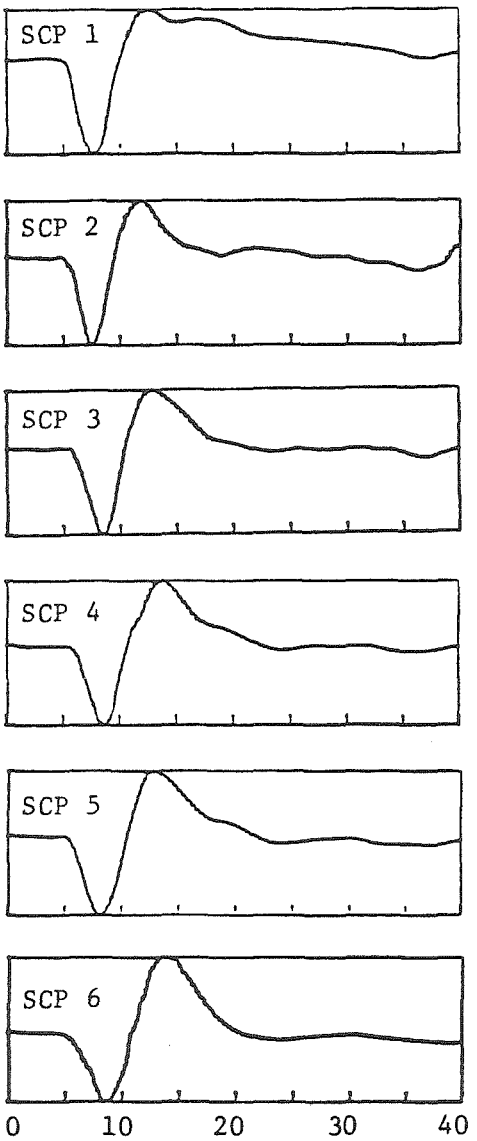

Figure III.2.17. The long period SH observations for the Argentine events at SCP. The numbers indicate the corresponding event in Table III.2.1. These traces are deconvolved from the other observations for each event and the ratios for a given station are stacked in the log frequency domain.

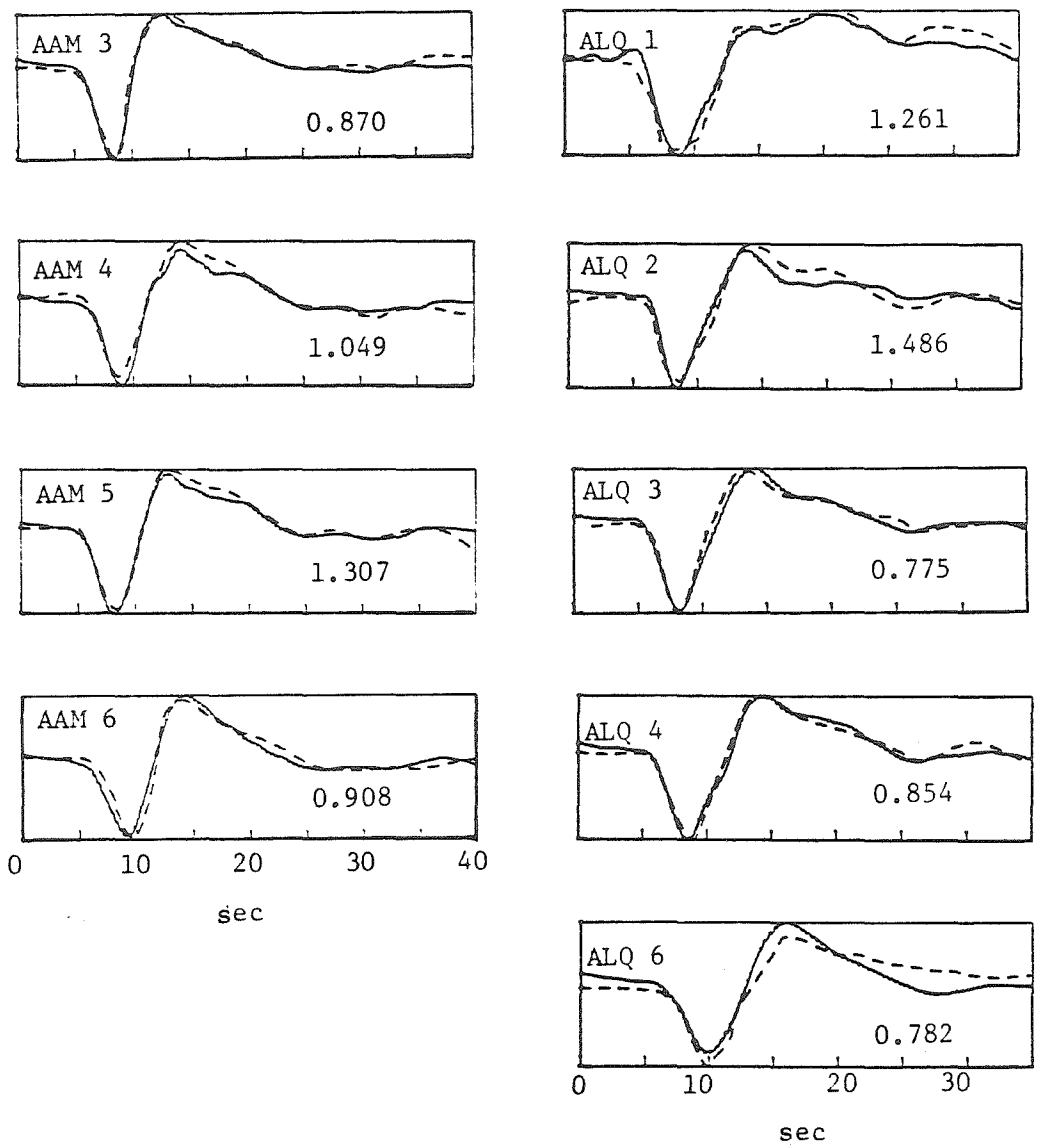

Figure III.2.18. The observed trace for the secondary stations AAM and ALQ (dotted lines) compared with the convolution of the SCP observation for the same event and the stacked relative receiver function for that station (solid line). The number after the station name indicates the corresponding event in Table III.2.1, and the number below each trace is the scale factor applied to the synthetic trace in plotting it over the observed signal.

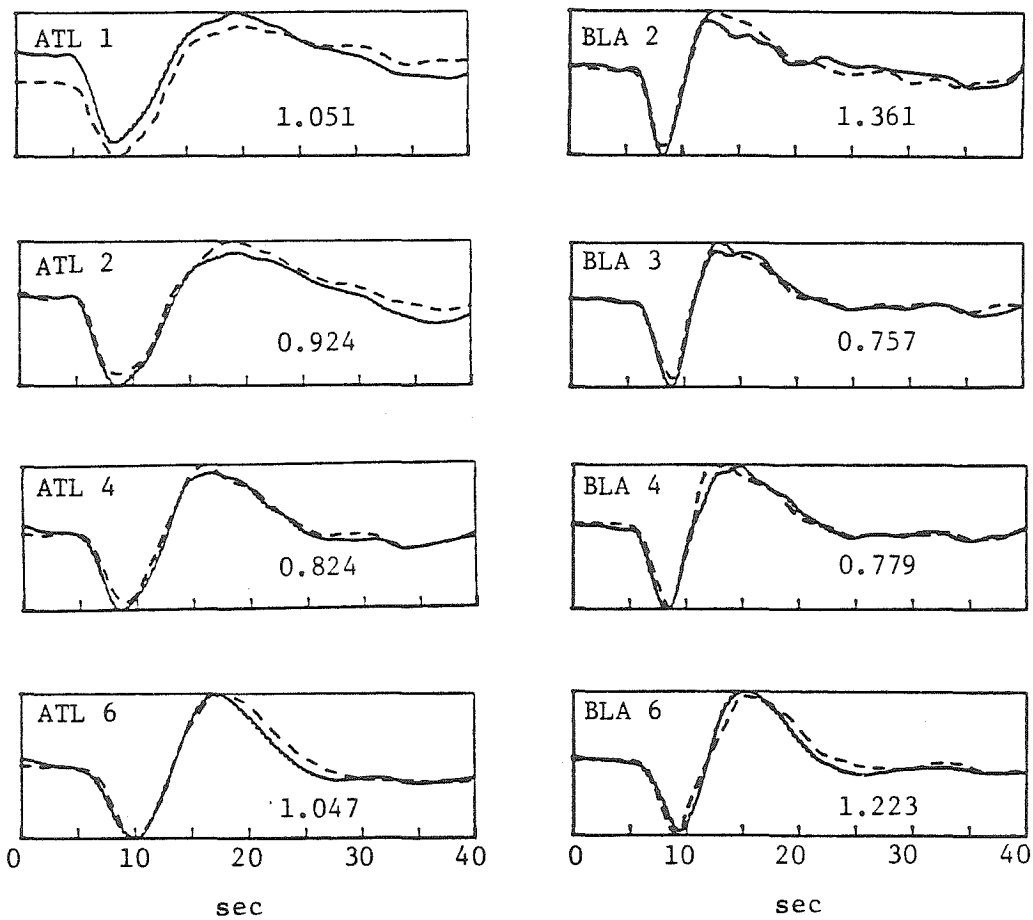

Figure III.2.19. The observed trace for the secondary stations ATL and BLA (dotted lines) compared with the convolution of the SCP observation for the same event and the stacked relative receiver function for that station (solid line). The number after the station name indicates the corresponding event in Table III.2.1, and the number below each trace is the scale factor applied to the synthetic trace in plotting it over the observed signal.

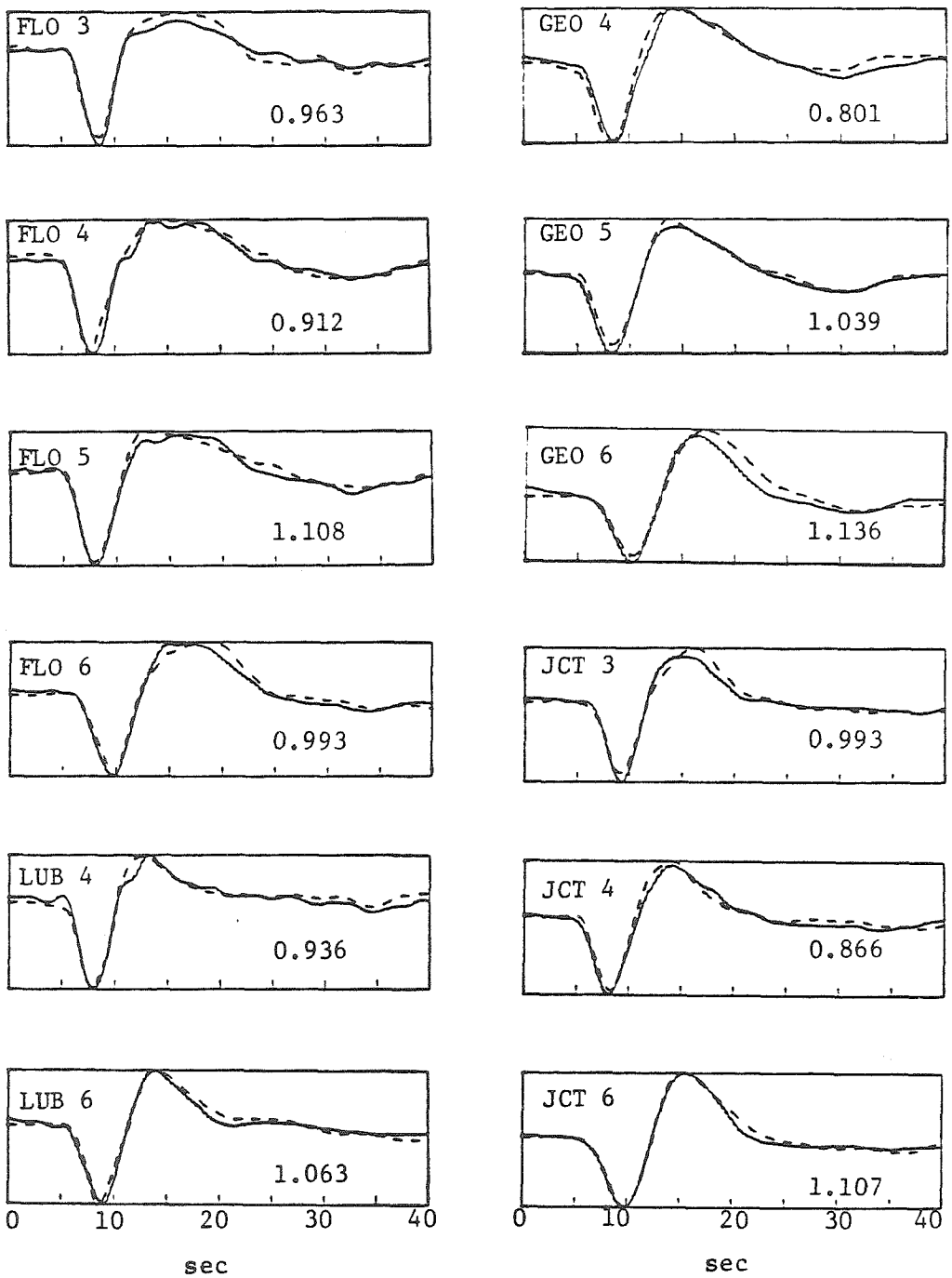

Figure III.2.20. The observed trace for the secondary stations FLO, GEO, LUB and JCT (dotted lines) compared with the convolution of the SCP observation for the same event and the stacked relative receiver function for that station (solid line). The number after the station name indicates the corresponding event in Table III.2.1, and the number below each trace is the scale factor applied to the synthetic trace in plotting it over the observed signal.

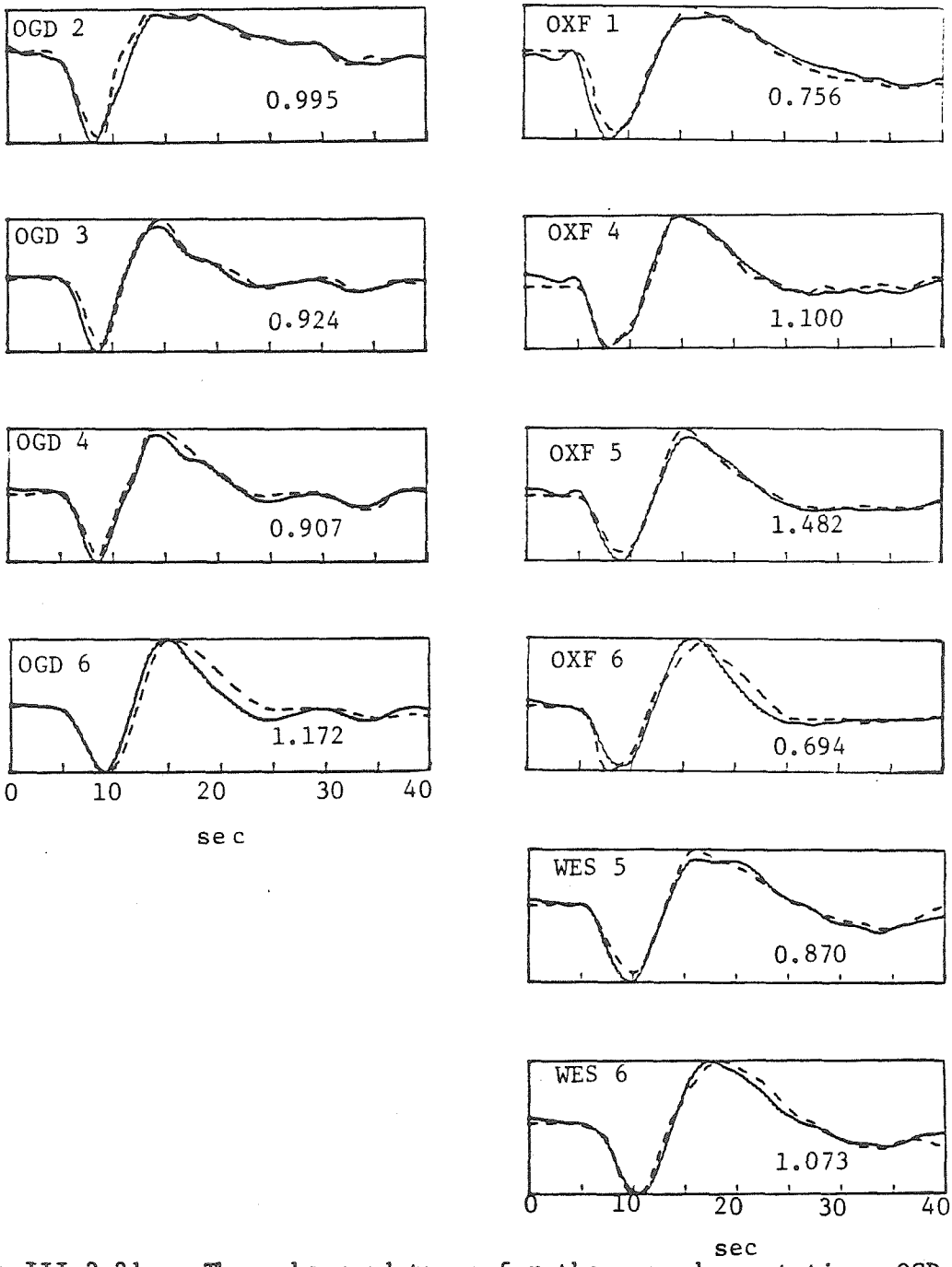

Figure III.2.21. The observed trace for the secondary stations OGD, OXF and WES (dotted lines) compared with the convolution of the SCP observation for the same event and the stacked relative receiver function for that station (solid line). The number after the station name indicates the corresponding event in Table III.2.1, and the number below each trace is the scale factor applied to the synthetic trace in plotting it over the observed signal.

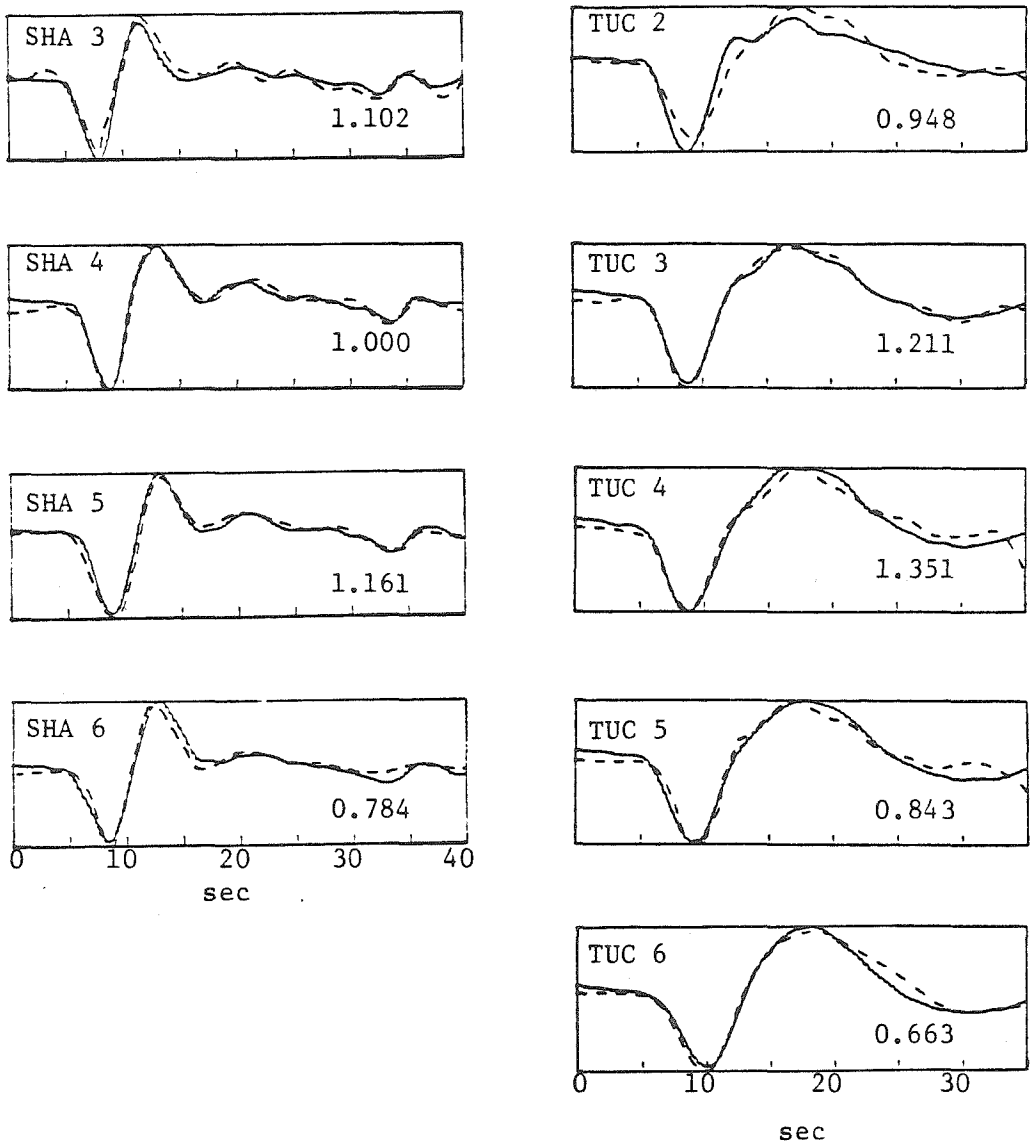

Figure III.2.22. The observed trace for the secondary stations SHA and TUC (dotted lines) compared with the convolution of the SCP observation for the same event and the stacked relative receiver function for that station (solid line). The number after the station name indicates the corresponding event in Table III.2.1, and the number below each trace is the scale factor applied to the synthetic trace in plotting it over the observed signal.

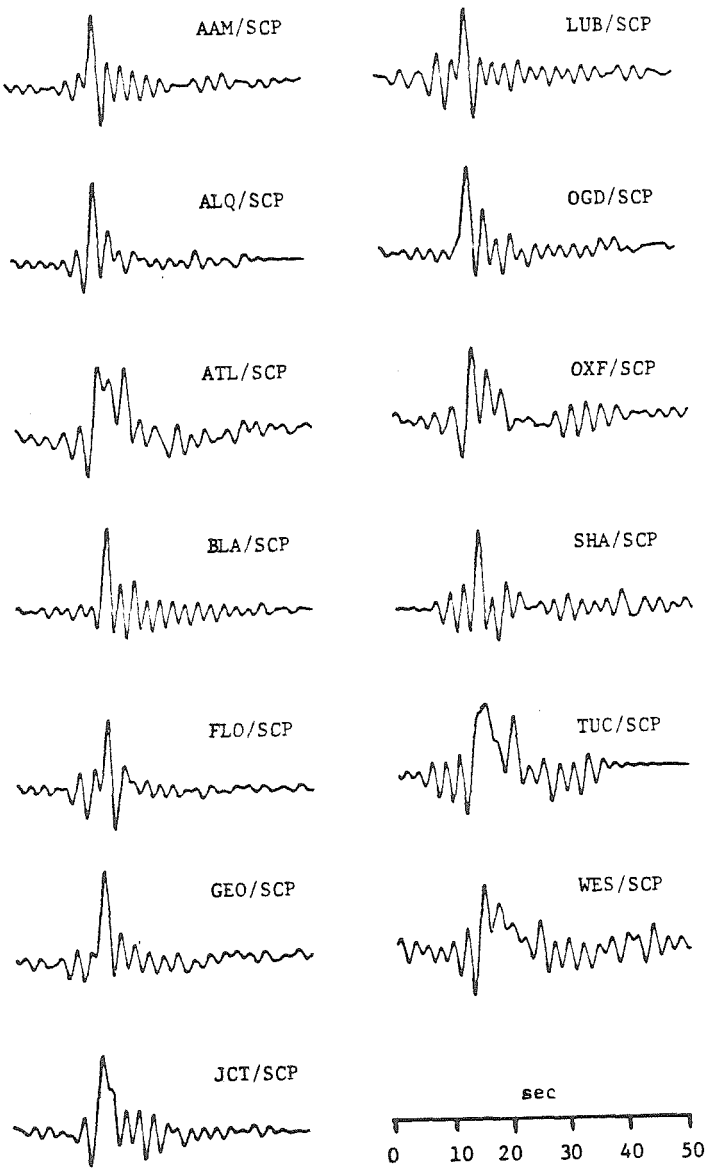

Figure III.2.23. Time domain representations of the stacked spectral ratios for each WWSSN station. These filters are acausal due to a phase shift introduced in the stacking algorithm, and the band limited character produces some of the ringing. However, the relative complexity of the receiver is still apparent.

that the stations which are similar to SCP in having very simple high frequency waveforms, such as AAM, BLA, GEO and LUB, have simple spike-like transfer functions. Stations with substantial complexity and apparent frequency differences visible in the raw waveforms such as ATL, OXF, TUC and WES, have complicated transfer functions. In each of these cases, rather than simply having a broadened transfer function, there are multiple peaks in the transfer function. These are partially artifacts of the band-limited nature of the traces, but they also represent multiple arrivals.

In order to interpret the relative receiver functions further the minimum entropy deconvolution method developed by Lundquist et al. (1980) was applied. This procedure attempts to determine the transfer function for the reference station by finding a linear operation which, when convolved with each trace in the set, minimizes the entropy of the set as a whole. The constraint employed is that all of the receiver functions are as simple or "delta-like" as possible. Any factor common to all of the stations is still lost, but this procedure permits an assessment of the reference trace contribution to each relative receiver function in Figure III.2.23.

The measure of simplicity employed is the weighted varimax norm (Wiggins, 1978)

$$V = \sum_j w_j v_j = \sum_j w_j \frac{\int r_j^4(t)dt}{(\int r_j^2(t)dt)^2}$$

where w_j is the weight of each receiver function r_j. From n known values of $d_i = r_i / r_o$, n+1 unknown receiver functions r_o, r_i, ...r_n

are determined. Hart et al. (1979) showed that maximizing V in the frequency domain is equivalent to solving the system of non-linear simultaneous equations:

$$\hat{r}_o^*(\omega) = \frac{\sum_j \frac{w_j}{u_j^2} \hat{r}_j^3(\omega) d_j^*(\omega)}{\sum_j \frac{v_j w_j}{u_j} d_j^*(\omega) d_j(\omega)}$$

were (^) implies an estimated value and (*) implies complex conjugate. Using an initial guess that r_o is a delayed delta function, $r_j = r_o d_j$; and $u_j = \int r^2(t)dt$ is the energy in each trace. This procedure emphasizes low amplitude spectral content and flattens the spectrum of r_o, as it shapes the spectrum of the transfer functions to be as spike-like as possible. After 5 or 6 iterations the procedure converges to a maximum of the varimax norm which depends on the choice of reference station and weighting.

Figure III.2.24 shows the resulting transfer functions for the receiver function processing using SCP as a reference trace. The results are shown for the fifth iteration. Note that SCP is very impulse-like, consistent with the observed transparency of the station. The complexities of ATL, OXF, TUC and WES are still apparent, with the multiple arrivals being quite distinctive. TUC appears to have substantial differential attenuation relative to SCP or BLA, but also has a strong second arrival which is apparent in the original data in Figures III.1.3 to III.1.10. The influence of the choice of reference station was assessed by changing the reference station to LUB and AAM. The receiver functions found in each case are shown in Figures III.2.25 and III.2.26. The general features are

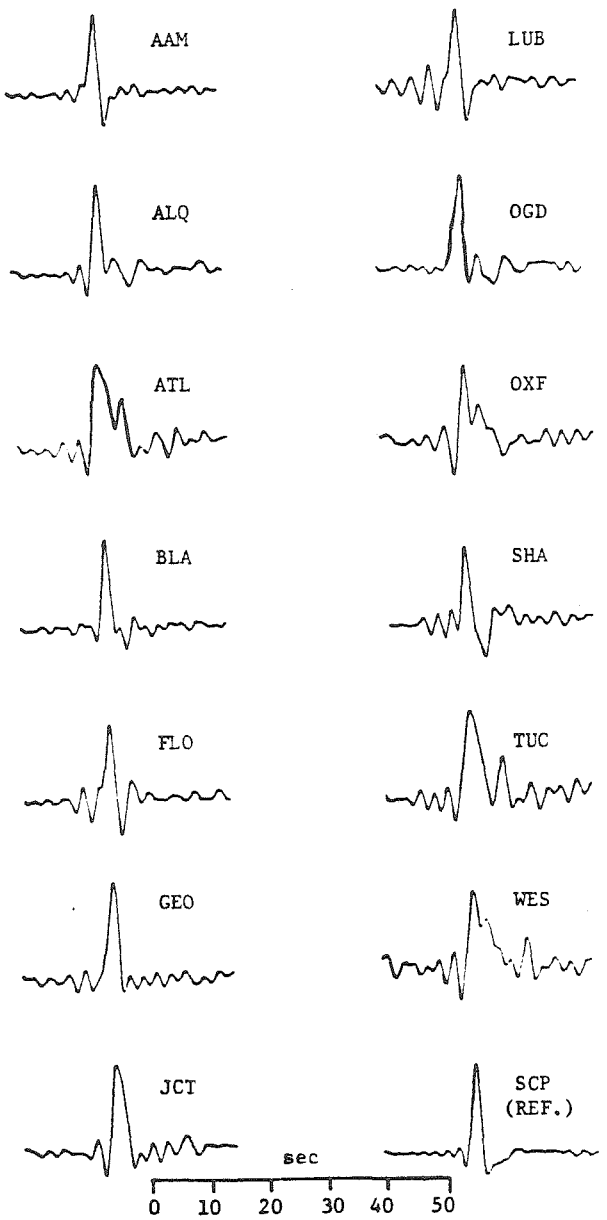

Figure III.2.24. The relative receiver functions for the WWSSN stations after the processing described in the text is applied to the stacked spectral ratios to extract the common contribution due to reference station SCP.

quite consistent independent of reference station. The most important result of this analysis is that the stations which have the largest long-period amplitude anomalies and differential attenuation estimates (Table III.1.6) such as ATL, OXF, TUC and WES, have clear evidence for multiple arrivals in the receiver functions. Such complexity produces scalloping of the spectra, which produces instability in the Δt^* estimates made using spectral ratio techniques for band limited data. The interference of the multiple arrivals produces observable amplitude and waveform variations. Thus, the large Δt^*_β estimates for OXF made from long period amplitude or spectral ratio techniques are incorrect. This is not surprising since OXF records large amplitude, high frequency, short period signals which would be inconsistent with a low Q receiver function.

An attempt was made to extend the bandwidth of the relative receiver functions by incorporating the short period observations, but the spectral stacking procedure was far less successful for the short period signals. This probably reflects the lower signal-to-noise ratio of the short period signals. It was not possible to analyze the Sea of Okhotsk data for the same stations because ScS and the lower mantle triplication phases arrive within 20 to 30 sec after the S arrival for most of the stations of interest.

Discussion

While it is not presently possible to fully characterize the long period receiver functions, several very important lessons can be learned from this long period amplitude analysis. The factor of 4 range in long period (T = 20 sec) amplitude variations observed over a

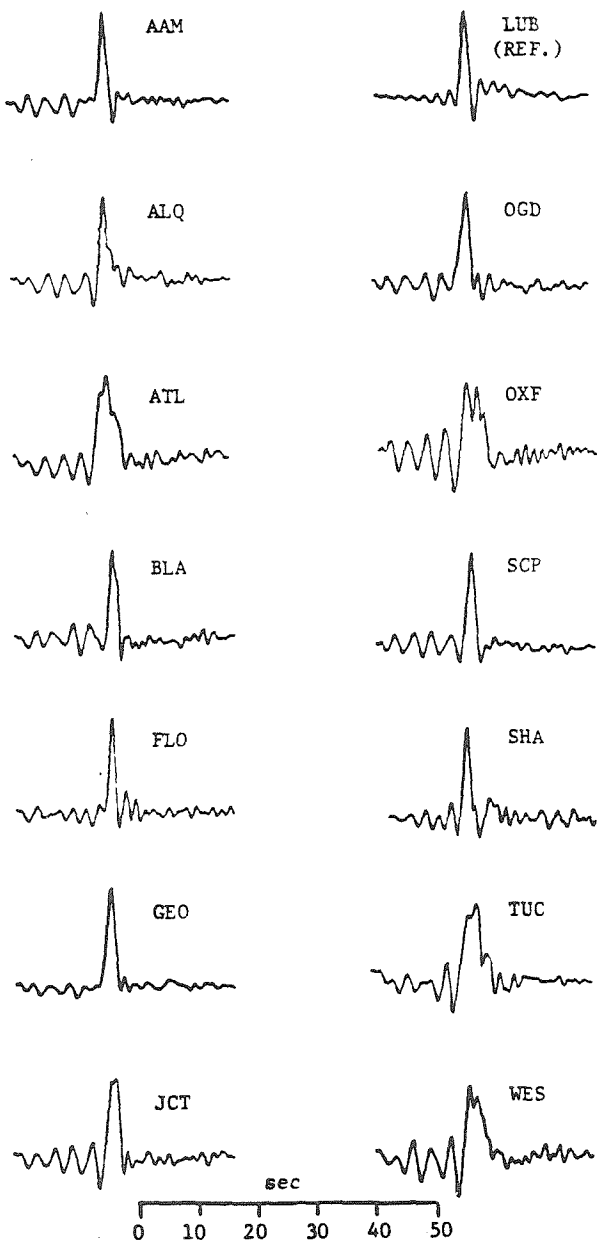

Figure III.2.25. The relative receiver functions determined when LUB is interchanged with SCP as the reference station.

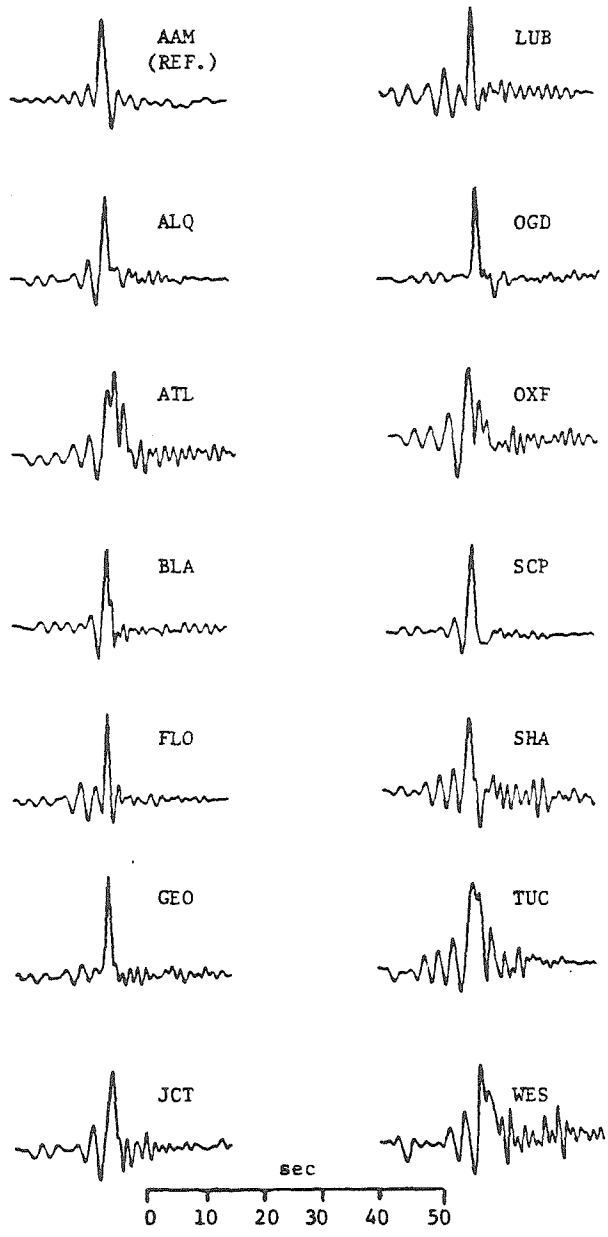

Figure III.2.26. The relative receiver functions determined when AAM is interchanged with SCP as the reference station.

limited range in azimuth from very simple sources indicates the intrinsic amplitude variability introduced by propagation and receiver effects. Large data sets are clearly required in order to justify the 10% accuracy often claimed in earthquake moment estimates and similar studies. The frequently made assumption of receiver transparency in the long period body wave band, crucial to most spectral ratio analyses, may be invalid for a large percentage of stations. This applies to studies which estimate Δt^* from spectral slopes as well as studies of spectral decay for diffracted phases. Careful receiver calibration or statistically large data sets must be employed to overcome these problems. Another point is that structural complexity can be significant for stations on bedrock such as ATL and TUC (both on Precambrian granite gneiss) as well as for stations on sediments like OXF and SHA.

Ultimately it will be desirable to map lateral variations in temperature and composition in the upper mantle, utilizing in part relative amplitude data such as presented here. At the moment this exercise is premature, for the uncertainty in the mechanisms affecting the amplitudes is great. Scattering effects are very difficult to assess, and the contribution from focussing and defocussing propagational effects has not been isolated. One can assume a composition for the upper mantle (say Olivine Forsterite); assume that thermally activated processes alone produce the relative amplitude patterns (E^* for Olivine Forsterite ranges from 57 kcal/mole to 125 kcal/mole depending on relaxation mechanism); and further assume scale lengths over which these mechanisms operate (100 to 600

km), and thereby estimate temperature variations (on the order of 50^{o} to 100^{o}) needed to account for the amplitude variations. For P waves this has been done by Butler (1983). In the future, hopefully, high quality broadband digital horizontal component data will become available with which to isolate the differential attenuation and geometric effects in similar S wave data with much greater precision.

Conclusions

Azimuthal amplitude patterns for short and long period SH waves are presented for North American stations. Sea of Okhotsk and Argentine deep focus earthquakes provide the data base. The relative amplitude variations for long period signals are more pronounced for the southern azimuth of approach, ranging over a factor of 4. The azimuthal variations indicate that the increased range in amplitudes for South American events is associated with travel time anomalies incurred in the lower mantle. Enhanced amplitudes are observed for late arrivals and diminished amplitudes are observed for early arrivals. Short period S waves show clear regional variations with low amplitudes in the western tectonic region, intermediate amplitudes along the eastern seaboard and high amplitudes in the central plains. Sediment amplification probably accounts for some of the latter feature. Long period amplitudes do not clearly show similar regional variations. Detailed spectral analysis of the long period waveforms from South America shows that stations with the largest long period amplitude anomalies have complicated receiver functions, with interference due to multiple arrivals. Spectral ratio techniques can be badly contaminated by these receiver complexities.

References

Butler, R. (1983). Energy, Q_α and Temperature: Variations on Seismic Amplitudes in the United States, Reviews of Geophysics and Space Physics, submitted.

Lundquist, G.M., G.R. Mellman and D. M. Hadley (1980). Relative receiver functions for three different array concepts, Sierra Geophysics Technical Report SGI-R-80-021.

Hart, R.S., D.M. Hadley, G.R. Mellman and R.Butler (1979). Seismic amplitude and waveform research, Sierra Geophysics Technical Report, SGI-R-79-012.

Wiggins, R. A. (1978). Minimum entropy deconvolution, Geoexploration, 16, 21-35.

Section III.3 Correlations Between Amplitude and Travel Time Anomalies

Abstract

Relationships between travel time and amplitude station anomalies are examined for short and long period SH waves and short period P waves recorded at North American WWSSN and CSN stations. Data for two azimuths of approach to North America are analyzed. To facilitate intercomparison of the data, the S wave travel times and amplitudes are measured from the same records, and the amplitude data processing is similar for both P and S waves. Short period P and S wave amplitudes have similar regional variations, being relatively low in the western tectonic region and enhanced in the shield and mid-continental regions. The east coast has intermediate amplitude anomalies and systematic, large azimuthal travel time variations. There is a general correlation between diminished short period amplitudes and late S wave arrival times and enhanced amplitudes and early arrivals. However, this correlation is not obvious within the eastern and western provinces separately, and the data are consistent with a step-like shift in amplitude level across the Rocky Mountain front. Long period S waves show no overall correlation between amplitude and travel time anomalies.

Introduction

It has long been indicated that there is a general association between P wave amplitude and travel time anomalies across North America (Herrin and Taggart, 1962; Romney et al., 1962). P and S wave amplitude and travel time station anomalies show similar regional variations with diminished amplitudes and late arrival times in the

Basin and Range and Rocky Mountain provinces, and enhanced amplitudes and early arrivals in the Great Plains and shield areas (e.g. Cleary, 1967; Evernden and Clark, 1970; Sengupta, 1975; North, 1977). However, this correlation is not a simple one, even for the few studies which measure the amplitudes and travel times from the same data (Cleary, 1967; Sengupta, 1975), and does not appear to exist on a global basis (Shore, 1982).

The North American observations are usually attributed to coupled lateral variations in the upper mantle low velocity and low Q zones between western and eastern North America, (e.g. Hales et al., 1968; Hales and Herrin, 1972), though it is only relatively recently that actual measurements of lateral variations in attenuation have been shown to correlate with amplitude anomalies (Der and McElfresh, 1977; Der et al., 1979, 1982; Section III.1). These studies have shown that there is a regional variation in attenuation associated with a baseline shift in amplitude levels between the two major provinces, but a large amount of amplitude variation within each region is not correlated with attenuation differences.

In this section we attempt to quantify the degree of correlation between body wave amplitude and travel time variations across North America for short and long period SH and short period P phases. Where possible, the amplitude and travel time measurements are made from the same records, and the method of amplitude analysis is the same for all observations, which allows us to more confidently compare the station anomalies than previous work. Data from two azimuths are processed and compared separately to avoid averaging out subtle trends.

Amplitude and Travel Time Data

The S wave amplitude observations presented in Section III.2, along with the travel time observations for the same signals reported in Chapter II, provide the S wave data set.

A similar set of short period P wave amplitudes has been presented by Butler and Ruff (1980) and extended by Butler et al. (1979). Earthquakes in South America and in source regions to the northwest of North America, as well as Russian nuclear explosions at five test sites were used to determine relative P wave amplitude patterns for three azimuths to North American WWSSN stations. The data were selected, measured, and processed in a manner similar to that used in the S wave analysis, though radiation pattern corrections were not applied to the earthquake data. The stability of the relative amplitude behavior between events and the coherence of the waveforms for each event indicate that the source radiation corrections are small for the narrow azimuth range spanned by the receivers, as was found for the S waves. The corresponding P wave travel times were not measured, but a recent study by Dziewonski and Anderson (1982) provides the most reliable azimuthally dependent P wave travel time station anomalies for North America presently available. The processing and quantity of data in that study were significantly different than for the other data sets, but it is of interest to compare the azimuthally dependent S and P wave station travel time anomalies.

Comparison of North American Station Anomalies

The Argentine and Sea of Okhotsk S wave travel time and short

period amplitude anomalies are shown in Figure III.3.1 and tabulated in Table III.3.1. The travel time residuals were determined using the short and long period data combined (see Chapter II for procedure), because the relative residuals are not frequency dependent. S wave station travel time anomalies for the Bolivian and Peruvian source regions are also shown in Figure III.3.1. The amplitudes for these events were not measured because the signals are complicated and dominated by SV radiation. In the top figure the travel time anomaly patterns for each source region have been baseline shifted to minimize the scatter at the first 11 stations from the left, which are western and Texas stations. These small shifts were applied in order to simplify comparison of the relative patterns across North America observed for each source region. The asterisked stations are located in western North America, as shown in Figure III.2.1. The stations are ordered in azimuth from the Argentine source region, and only those stations at which anomalies could be determined from both azimuths are shown.

Figure III.3.1 demonstrates that the SH travel times are relatively late (positive) and the amplitudes are relatively low at western stations for both azimuths. The central United States stations record arrivals 4 to 5 sec earlier than the western stations, and the amplitudes are 4 to 5 times larger as well. The east coast stations record intermediate amplitudes and show the clearest evidence for azimuthal variations in travel time anomalies. Relative to the central and western stations, the east coast stations record early arrivals from the Sea of Okhotsk and late arrivals from Argentina.

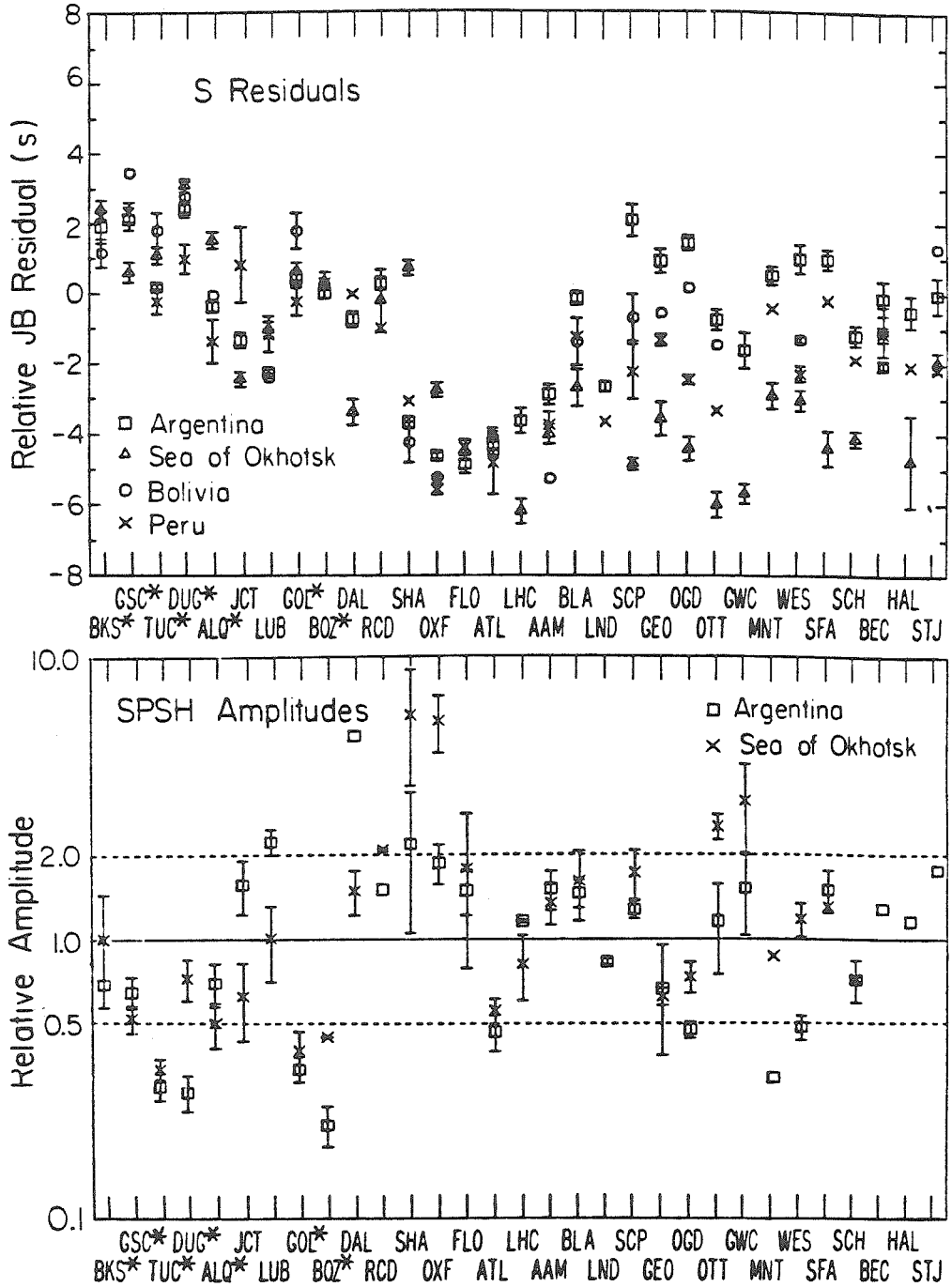

Figure III.3.1. Top: The mean and standard error of the mean of the S-wave JB residuals at North American stations for the Sea of Okhotsk and South American source regions. Only those stations at which anomalies could be determined for both azimuths are shown. Source region baseline corrections have been determined using the first 11 stations from the left. Bottom: Comparison of the station amplitude anomalies from the Sea of Okhotsk and Argentina short-period SH data. The relative amplitudes have been adjusted to minimize the scatter at each station following the procedure described in Section III.1.

Table III.3.1

	Sea of Okhotsk			Argentina			
STA	A_{SPS}	A_{LPS}	T_S	A_{SPS}	A_{LPS}	T_S	
AAM	0.63	0.50	-2.87	0.69	0.53	-1.86	E
ALE	0.77	0.63	-2.28	----	----	----	E
ALQ	0.26	0.60	2.81	0.32	0.40	0.62	W
ATL	0.28	0.45	-2.71	0.22	0.39	-3.29	E
BEC	----	----	----	0.59	0.54	0.87	E
BKS	0.38	0.61	3.62	0.32	0.63	2.91	W
BLA	0.73	0.64	-1.23	0.67	0.64	0.85	E
BLC	----	0.67	-3.04	----	----	----	E
BOZ	0.18	0.61	1.50	0.10	0.29	1.00	W
CMC	1.19	1.30	-1.31	----	----	----	E
COR	0.38	0.54	3.36	----	----	----	W
DAL	0.66	0.40	-1.98	2.43	0.79	0.26*	E
DUG	0.33	0.61	4.36	0.13	0.46	3.39	W
EDM	0.63	0.71	-0.88	----	----	----	E
FBC	0.51	0.55	-5.43	----	----	----	E
FCC	0.93	0.72	-1.62	----	----	----	E
FFC	1.04	0.65	-0.10	----	----	----	E
FLO	0.79	0.51	-3.26	0.69	0.24	-3.81*	E
FSJ	0.96	0.65	2.58	----	----	----	W
GEO	0.29	0.53	-2.33	0.31	0.64	1.89*	E
GOL	0.18	0.47	1.92	0.16	0.46	1.41	W
GSC	0.22	0.47	1.78	0.30	0.46	3.12	W
GWC	1.31	0.73	-4.19	0.70	----	-0.62*	E
HAL	----	0.39	-1.91	0.53	0.81	0.50*	E
INK	----	0.71	-1.61	----	----	----	E
JCT	0.34	0.51	-1.12	0.72	0.54	-0.34	E
LHC	0.37	0.49	-4.80	0.54	0.50	-2.61	E
LND	----	----	----	0.39	1.42	-1.64	E
LON	0.09	0.56	0.77	----	----	----	W
LUB	0.40	0.57	0.26	1.03	0.59	-1.26	E
MBC	0.76	0.73	-1.00	----	----	----	E
MNT	0.36	0.79	-1.62	0.15	0.23	1.49*	E
OGD	0.34	0.37	-3.12	0.22	0.61	2.40*	E
OTT	1.06	0.54	-4.61	0.53	0.49	0.24*	E
OXF	2.69	0.55	-1.42	0.86	0.32	-3.59*	E
PHC	----	0.56	2.16	----	----	----	W
PNT	----	0.56	-0.53	----	----	----	W
RCD	1.15	0.70	1.21	0.69	0.36	1.26	E
RES	0.41	0.76	-0.23	----	----	----	E
SCB	----	0.60	-4.66	----	----	----	E
SCH	0.36	0.44	-2.40	0.33	0.52	-0.20*	E
SCP	0.75	0.45	-3.44	0.59	0.85	3.06*	E
SES	0.90	0.75	2.80	----	----	----	W

SFA	0.79	0.55	-2.69	0.69	0.71	1.95*	E
SHA	2.39	0.97	2.00	1.01	0.61	-2.64*	E
STJ	----	0.76	-0.54	0.81	0.79	0.97*	E
TUC	0.17	0.39	2.42	0.14	0.28	1.17	W
VIC	0.46	0.49	1.38	----	----	----	W
WES	0.54	0.53	-1.72	0.22	0.36	1.97*	E
YKC	0.45	0.59	-1.64	----	----	----	E

*Argentine data with anomalous travel times.

Other South American source regions show relatively earlier arrivals on the east coast than observed for Argentina. This indicates that significant near-source or deep mantle velocity structure affects the relative travel time pattern from Argentina. This is discussed in greater detail below and in Chapter II where it is shown that the Argentine signals recorded on the east coast are anomalously late because they encounter a localized low-velocity region in the lower mantle. Some of the azimuthal variation observed at east coast stations may also be due to strong lateral gradients in upper mantle shear velocity structure, with the velocity increasing toward the Canadian shield. The short period SH amplitudes do not show similar azimuthal variations.

In Figure III.3.2 the S wave amplitude and travel time anomalies for both source regions are compared. All of the available determinations are included, with the solid symbols indicating Argentine observations. The general features are similar for both azimuths, though the long period amplitudes from Argentina have more scatter than observed for the Sea of Okhotsk data. The short period amplitude anomalies clearly have a much greater range in variation than the long periods, as has been observed for P waves (Booth et al., 1974; Sengupta, 1975). The short periods also show a tendency for late arrivals (positive residuals) to be low amplitude, which is not apparent in the long periods. Booth et al. (1974) found little correlation between short and long period P wave amplitude variations, and argued that this supports the interpretation that the short period amplitude variations are due to Q variations.

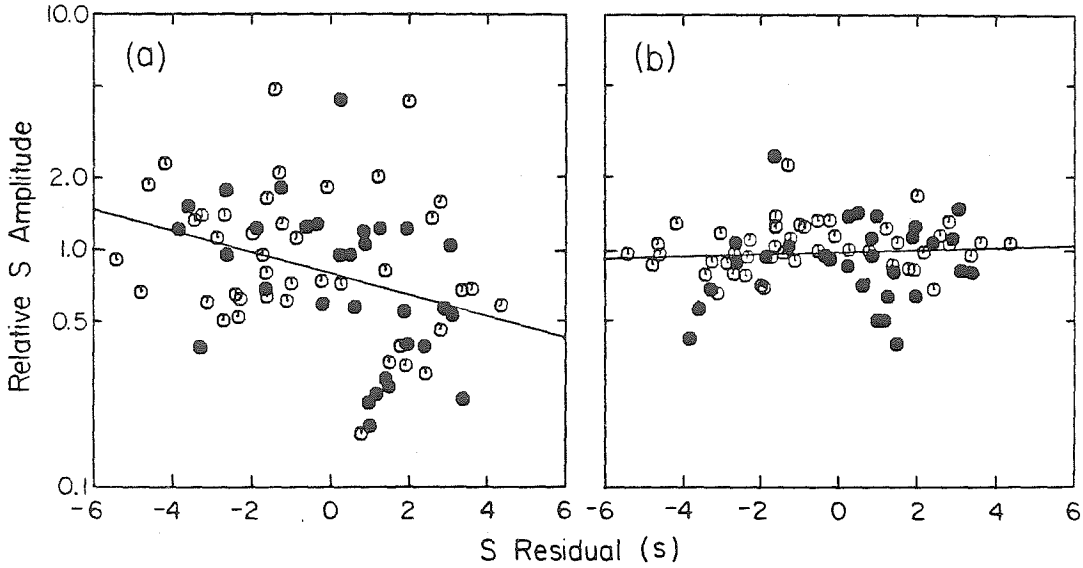

Figure III.3.2. (a) Comparison of short-period S-wave amplitude anomalies and station S-wave residuals in North America for the Sea of Okhotsk (empty symbols) and Argentina (filled symbols) source regions. (b) A similar comparison for long-period S-wave amplitude anomalies and S residuals. The curves are major axis regressions assuming equal weighting.

Using the major axis regression described by York (1966), relations between the logarithms of the short period S wave amplitudes (A_{SPS}) and long period S wave amplitudes (A_{LPS}) and the S wave travel time anomalies (T_S) have been determined. The relations found for equal weighting of each data point and using all of the data are indicated in Figure III.3.2 and given by:

$$\log A_{SPS} = -0.340(\ 0.035) - 0.047(\pm 0.015)T_S$$

$$\log A_{LPS} = -0.256(\pm 0.016) + 0.004(\pm 0.007)T_S$$

The intercept values are not significant due to the arbitrary baselines in both parameters. There is a weak, resolvable correlation between the log of the short period amplitudes and the travel time anomalies, with a linear correlation coefficient, r, of -0.341, but the long period amplitudes do not show similar behavior, as the correlation coefficient it 0.077. More sophisticated weighting schemes can be employed, but the errors involved in amplitude and travel time measurements are quite different in nature, and rigorous statistics may not be useful. The regressions presented here are intended only to indicate the relative degree of correlation between parameters.

In a detailed investigation of S and ScS S travel time anomalies for deep South American and Sea of Okhotsk events recorded in North America, it was demonstrated in Chapter II that the Argentine S wave data is contaminated by lower mantle anomalies. Large, localized velocity anomalies are observed at East Coast and Mississippi Valley stations. As seen in Figure III.3.1, these stations show strong azimuthal variations in S residuals as well as distance dependence of

S residuals between source regions in Peru, Bolivia and Argentina. The travel time anomalies are as much as 5 sec, and are not apparent in the ScS arrivals from the same events, which suggests a lower mantle origin. The greater range in long period amplitude anomalies for the Argentine data appears to be associated with these travel time anomalies as well. To ensure that these strong anomalies do not dominate the patterns in Figure III.3.2, we have omitted the Argentine observations identified as anomalous in Chapter II (see Table III.3.1) in Figure III.3.3. Different symbols have been used for stations to the east (circles) and to the west (triangles) of the Rocky Mountains. The stations placed in each category are indicated in Table III.3.1 and Figure III.2.1. Because the station distribution is rather sparse, we do not attempt to define more subregions, though there is ample evidence for distinct behavior for the Pacific Coast stations and central U.S. stations. Figure III.3.3 clearly indicates the tendency for western stations, which are slow, to record diminished short period S wave amplitudes, but the long periods show no regional pattern. The regression curves shown in Figure III.3.3 are given by:

$$\log A_{SPS} = -0.344(\pm 0.040) - 0.042(\pm 0.017)T_S$$

$$\log A_{LPS} = -0.250(\pm 0.016) - 0.001(\pm 0.006)T_S$$

The results are not significantly changed if all East Coast observations from the Sea of Okhotsk are omitted as well. The short period correlation coefficient is $r = -0.316$ and the long periods yield $r = -0.013$.

The short period S wave amplitudes in Figure III.3.3 appear to have more of a baseline shift between the eastern and western

provinces than a smoothly varying distribution of amplitudes. The filled squares in Figure III.3.3a indicate the average amplitude and travel time anomalies for each region. There is an amplitude factor of 2.4 and a 4.0 sec travel time shift between the means. Romanowicz and Cara (1980) have shown that if more than one physical parameter varies in the upper mantle (e.g. both velocity and thickness of the low velocity zone), it is possible to have baseline shifts in relative travel time variations. A similar line of argument applies to Δt^* variations and, thus, possibly to amplitude variations. To test this, we performed regressions for the short period S wave amplitudes and station travel time residuals for the eastern and western provinces separately. The following relations were found;

$$\log A_{SPS} = -0.130(\pm 0.053) + 0.038(\pm 0.022)T_S \quad \text{(East)}$$

$$\log A_{SPS} = -0.861(\pm 0.142) + 0.118(\pm 0.057)T_S \quad \text{(West)}$$

While the absolute levels of these lines are resolvably different, it is interesting to note that the slopes have reversed in sign from that for the overall trend, as have the corresponding correlation coefficients, $r = 0.272$ (East) and $r = 0.428$ (West). This may be an artifact of the reduced population sizes and large intrinsic amplitude scatter, however it may also be taken as a breakdown of the correlation between amplitudes and attenuation if one adopts the assumption that attenuation variations are coupled to velocity variations. There are clearly many scattering and focusing effects that would produce anomalous amplitude behavior with no travel time signature, or with a correlation opposite to that expected for attenuation variations.

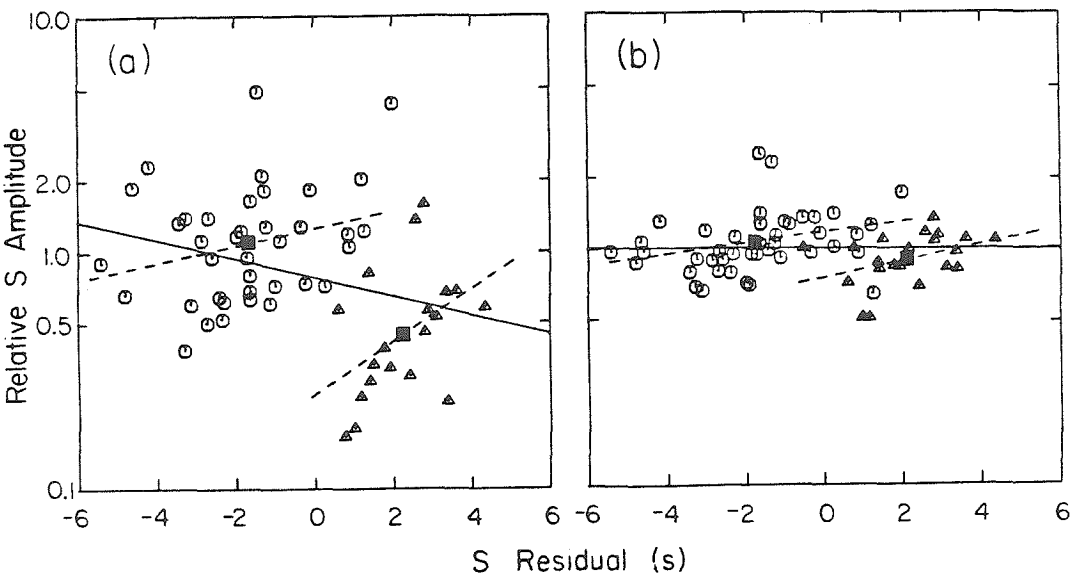

Figure III.3.3. (a) Comparison of short-period S-wave amplitude anomalies and S residuals after anomalous East Coast and Mississippi Valley observations from Argentina are removed. Tectonic province stations are indicated by triangles. The squares indicate the mean travel time and amplitude values for the eastern and western provinces. The solid curve is a major axis regression for the whole data set, and the dashed curves are for the two provinces separately. (b) Same as in (a) but for the long-period S wave amplitudes.

The results of Chapter II suggest that the most pronounced long period amplitude anomalies for the Argentine data are associated with the anomalous travel times produced by lower mantle anomalies, with enhanced amplitudes accompanying large travel time delays and diminished amplitudes accompanying large travel time advances. This indicates a geometric effect rather than attenuation-controlled behavior. If the eastern and western long period data in Figure III.3.3b are considered separately, the following regressions are found:

$$\log A_{LPS} = -0.190(\pm 0.026) + 0.021(\pm 0.011)T_S \quad \text{(East)}$$

$$\log A_{LPS} = -0.374(\pm 0.045) + 0.035(\pm 0.019)T_S \quad \text{(West)}$$

The correlations are given by r = 0.289 (East) and r = 0.381 (West). This indicates that even after the anomalous Argentine data are omitted there is a weak tendency for long period amplitudes to be enhanced for late arrivals, but this is only apparent when the two provinces are isolated. The average long period amplitude levels in Figure III.3.3b only differ by 18%.

Several authors have noted that while S wave travel time residuals have an overall variation 4 times greater than the P wave residuals for North America, the short period amplitudes have more comparable variations, with S waves varying about twice as much as P waves (Sengupta, 1975; Der et al., 1975, 1982; Section III.1). The latter observation is consistent with the trend expected for attenuation-controlled amplitudes for predominantly shear losses (Section III.1). The short period S and P wave amplitude anomalies are compared in Figure III.3.4. Figure III.3.4a presents the data for

South American earthquakes. The relation between the S and P (A_{SPP}) amplitudes is given by:

$$\log A_{SPS} = -0.397(\pm 0.059) + 1.926(\pm 0.338) \log A_{SPP}$$

This indicates a factor of two greater range in the S wave anomalies and a relatively good degree of correlation ($r = 0.802$) for the southern azimuth. For the northwestern azimuth (Figure III.3.4b) a similar relation is found:

$$\log A_{SPS} = -0.414(\pm 0.050) + 1.698(\pm 0.310) \log A_{SPP}$$

The correlation coefficient is $r = 0.767$. In both cases the amplitude anomalies have been determined for earthquakes spanning a fairly small range in azimuth from each station. Comparison of the S anomalies from the Sea of Okhotsk with the average P anomalies from all Russian test sites (which generally span a northern azimuth from each station) shows greater scatter (Figure III.3.4c). The corresponding relation is:

$$\log A_{SPS} = -0.292(\pm 0.142) + 2.591(\pm 1.581) \log A_{SPP}$$

This increase in scatter ($r = 0.337$) may reflect the azimuthal sensitivity of the receiver structures beneath the WWSSN stations, or it may indicate the greater variability of amplitude patterns for shallow high frequency events. The similarity of the relations for the northwestern and southern azimuths argues against the first alternative, whereas Butler and Ruff (1980) have shown that amplitude patterns for explosions at sites in as close a proximity as Northern and Southern Novaya Zemlya can have significant relative trends. This may be due to near source structure or contamination due to tectonic release.

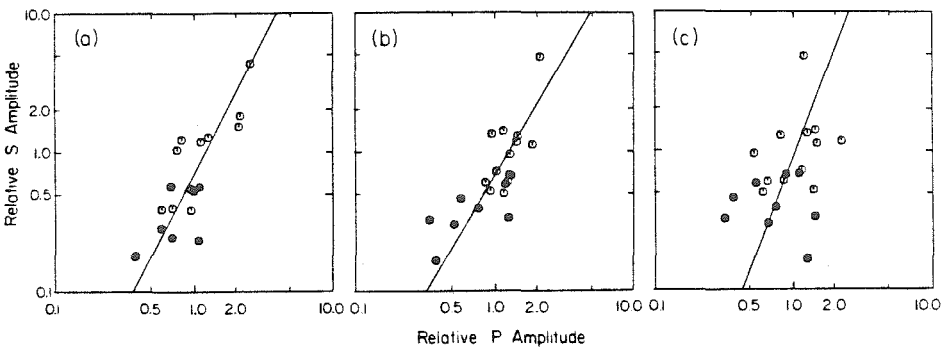

Figure III.3.4. Comparison between short-period WWSSN S and P amplitude anomalies for (a) South American earthquakes; (b) northwestern azimuth earthquakes; and (c) Sea of Okhotsk earthquakes (S) and Russian nuclear tests (P). Solid symbols indicate western U.S. stations.

In Section III.1 it was shown that long period P and SH amplitude patterns from South America track rather closely as well, with relative variations being consistent with attenuation variations assuming all losses are in shear. However, the long period amplitude variations are so large that explaining them by frequency-independent Q variations predicts short period amplitude patterns that are poorly correlated with and have a larger range than those observed. While frequency dependent models can be contrived to reconcile the data there is little correlation with geographic province or travel time anomalies. This indicates that receiver structure or propagational effects dominate the long period amplitudes, as was proposed by Booth et al. (1974), and it is possible that part of the correlation in short period amplitudes for P and SH is produced by receiver variations as well. Computation of amplification effects for plane layered receiver structures using the Haskell matrix techniques indicate that relative short period P and S wave amplitudes can track closely for a wide range of models. It is also interesting to note that Δt^* estimates made from long period body wave spectra do not accurately predict short or long period amplitude variations for North America (Section III.1), nor are they well correlated with short period travel time anomalies on a global scale (Mikami and Hirahara, 1981). This may suggest that the Δt^* estimates at long periods are contaminated by three dimensional receiver structure or other effects not related to upper mantle attenuation.

The correlations shown above between short period S amplitudes and travel times and short period P and S amplitudes predict a

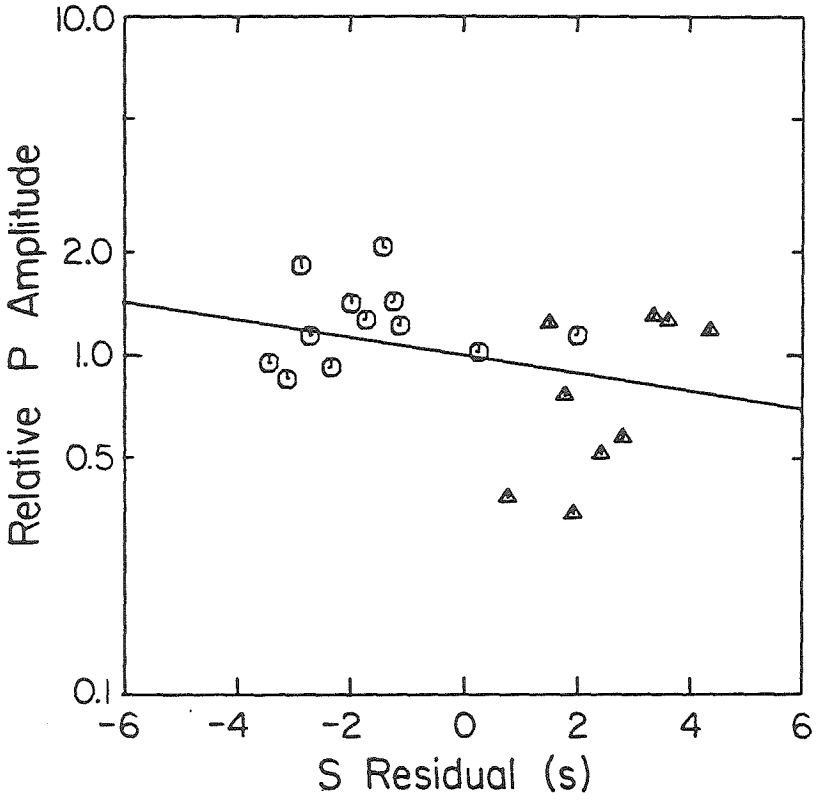

Figure III.3.5. Comparison between P wave amplitude anomalies and S wave travel time residuals for the northwestern azimuth. Triangles indicate western North America stations.

correlation between P amplitudes and S travel times. This is in fact observed as shown in Figure III.3.5. The P amplitude anomalies from the northwestern azimuth are compared with the S travel times from the Sea of Okhotsk, with the relation between them being

$$\log A_{SPP} = -0.001(\pm 0.043) - 0.026(\pm 0.017)T_S$$

A correlation of r = -0.318 was found for this comparison. Once again, it appears that a steplike shift in the amplitude level between the fast eastern (circles) and slow western (triangles) provinces is an equally valid interpretation.

Numerous studies have found that for North America S wave travel time anomalies are roughly four times the corresponding P wave anomalies (Doyle and Hales, 1967; Hales and Roberts, 1970; Sengupta, 1975). This requires upper mantle variations preferentially affecting the rigidity (Hales and Doyle, 1967; Hales and Herrin, 1972). On a global basis the relation between S and P anomalies appears to be different from that for North America, with a relative factor of 1.8 to 2.4, which does not require significant lateral variations in Poisson's ratio (Poupinet, 1977; Wickens and Buchbinder, 1980). It has also been proposed that the relation for North America has been misinterpreted if more than one physical parameter varies in the upper mantle (Romanowicz and Cara, 1980).

In Figure III.3.6 we compare the S wave travel time residuals from the Sea of Okhotsk and Argentina with the azimuthally dependent P wave station anomalies (T_p) of Dziewonski and Anderson (1982), which have the form

$$T_p = A + B\cos(\phi-\phi_1) + C\cos(2(\phi-\phi_2))$$

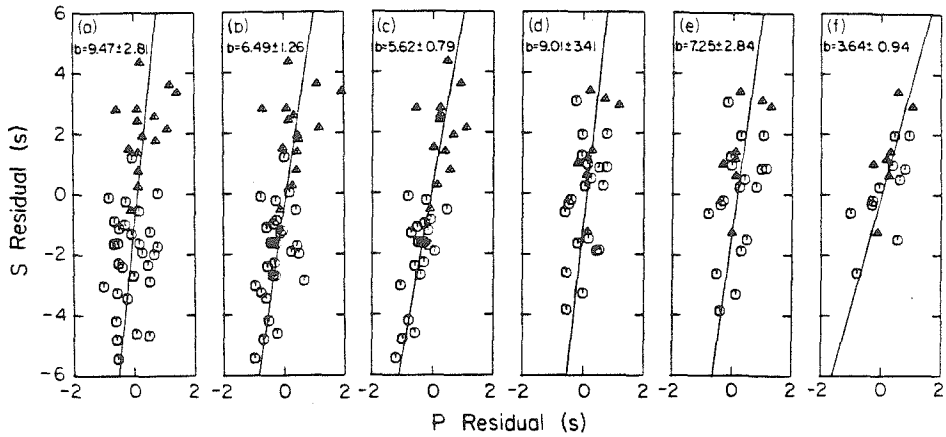

Figure III.3.6. S and P travel time residuals for the Sea of Okhotsk azimuth (a)-(c) and the Argentina azimuth (d)-(f). The P-wave station anomalies of Dziewonski and Anderson (1982) are used with the azimuthally independent term alone (a),(d); inclusion of the first cosϕ term (b),(e); and inclusion of both the cosϕ and cos2ϕ terms (c),(f). The value of the slope in the correlation $T_S = a + bT_P$ is given for each panel. Triangles indicate stations in the western tectonic province.

The azimuths, ϕ, used to compute the P residuals are the appropriate azimuths from each station to the Sea of Okhotsk and Argentine source regions. Figures III.3.6a-III.3.6c show the northwestern azimuth comparison, with the first panel using the azimuthally independent term (A) of the P residual only; the second including the $\cos\phi$ term; and the third including the $\cos 2\phi$ term as well. Since not all 5 coefficients could be determined for each station there is a slight attrition as higher order terms are added. However, this does not account for the significant reduction in scatter of the correlations as the azimuthal terms are included ($r = 0.45$, 0.62 and 0.77 in Figures III.3.6a, III.3.6b and III.3.6c respectively). The value of the slope given by the major axis regression is indicated in each panel. Stations in western North America are indicated by triangles. Note that these are slow for both P and S, and there is little overlap between the provinces. The slope in Figure III.3.6c is somewhat higher than the typical value of approximately 4, and the small scatter indicates that this may be significant. The lower value has always been determined using azimuthally averaged data, which may have resulted in an underestimation of the relative behavior, or it may be that the Sea of Okhotsk source region and/or lower mantle path effects account for the discrepancy.

The Argentine comparisons are shown in Figures III.3.6d-III.3.6f. Here the reduction in number of stations with higher order P anomaly azimuthal terms is more severe, but there is again some indication that a slope significantly higher than 4 may be appropriate ($r = 0.45$, 0.45 and 0.68 in Figures III.3.6d, III.3.6e and III.3.6f

respectively). The separation between the eastern and western provinces is not as clear as for the other azimuth, which results from the anomalous S and P travel time anomalies that affect the East Coast stations. The azimuthal variations are similar for both P and S for the latter stations, and are too strong to be produced at shallow depth in the upper mantle. It is likely that some of the lower mantle path anomaly detected in the S waves by Chapter II has been mapped into the P wave station anomalies for the southern azimuth. For both azimuths the correspondence between P and S travel time anomalies is quite good and there is little evidence for a baseline shift and decreased slope between the eastern and western provinces like those indicated by Romanowicz and Cara (1980). The importance of azimuthal terms in the station anomalies is strongly supported by these data.

Discussion

By determining the relationships between travel time residuals, amplitude anomalies and attenuation variations it will ultimately be possible to constrain some important upper mantle processes, following approaches similar to that first employed by Solomon (1972). This section has shown that there is a clear, though weak, correlation between short period P and S amplitude anomalies and S wave travel time residuals. In general, western North America records low amplitudes and late arrivals relative to the east. While this result is qualitatively consistent with many previous studies, it is the first to compare a large data set of short period S amplitudes and travel times obtained from the same signals with P amplitudes that are similarly processed.

It is strongly indicated that a steplike change in amplitude level occurs across the Rocky Mountain front, with amplitudes within the eastern and western provinces being poorly correlated with travel time variations. The step between the average short period S wave amplitude levels is a factor of 2.4, which approximately corresponds to a $\Delta t^*_\beta = 0.8$ sec for the 2-4 sec periods of the observations (Section III.1). Assuming all losses are in shear, this indicates $\Delta t^*_\alpha = 0.2$ sec, which produces a factor of two variation in amplitude at 1 sec period. This is consistent with the average Δm_b (0.26) value between the provinces (Booth et al., 1974; Der et al., 1975), and with average differences in Δt^*_α from high frequency spectral analysis (Der et al., 1982). The long period S wave amplitude variation predicted for $\Delta t^*_\beta = 0.8$ sec is about 20% (Section III.1), which is consistent with the 18% variation found in Figure III.3.5b. The associated S wave travel time step is about 4 sec. Superimposed on this attenuation-controlled amplitude variation are many individual station variations that are not associated with travel time anomalies and presumably reflect receiver structure or scattering effects within the mantle. These amplitude variations are comparable to those produced by attenuation variations. The long period SH wave amplitudes show no overall correlation with travel time anomalies, though within each province there is a tendency for later arrivals to be enhanced, thus it is probable that receiver structure or other propagation effects are responsible for much of the substantial variation in long period amplitudes. There is recent work using body waves that shows that lateral variations in upper mantle shear

velocity structure beneath North America are distributed throughout the upper mantle to a depth of 400 km (Grand and Helmberger, 1983). Future work with body waves will be needed to determine whether the variations in Q are similarly distributed or concentrated in a narrow channel.

The relative variation of S and P residuals may have a steeper slope than previously found in studies which neglect the azimuthal variations in station anomaly terms. If this proves generally valid, even more dramatic variations in rigidity in the upper mantle are required, or possibly alternate mechanisms such as anisotropy.

References

Booth, D. C., P. D. Marshall and J. B. Young (1974). Long and short period P wave amplitudes from earthquakes in the range 0^{o}-114^{o}, Geophys. J. Roy. Astr. Soc., 39. 523-537.

Butler, R. and L. Ruff (1980). Teleseismic short period amplitudes: source and receiver variations, Bull. Seism. Soc. Am., 70, 831-850.

Butler, R.,.L. J. Ruff, R. S. Hart and G. R. Mellman (1979). Seismic waveform analysis of underground nuclear explosions, Technical Report, SGI-R-79-011, Sierra Geophysics.

Cleary J. (1967). Analysis of the amplitudes of short period P waves recorded by Long Range Seismic Measurements stations in the distance range 30^{o} to 102^{o}, J. Geophys.Res., 72, 4705-4712.

Der, Z. A., R. P. Massé and J. P. Gurski (1975). Regional attenuation of short period P and S waves in the United States, Geophys. J. Roy. Astr. Soc., 40, 85-106,.

Der, Z. A. and T. W. McElfresh (1977). The relationship between anelastic attenuation and regional amplitude anomalies of short period P waves in North America, Bull. Seism. Soc. Amer., 67, 1303-1317.

Der, Z. A., T. W. McElfresh, C. P. Mrazek (1979). Interpretation of short period P wave magnitude anomalies of selected LRSM stations, Bull. Seism. Soc. Amer., 69, 1149-1160.

Der, Z. A., T. W. McElfresh, A. O'Donnell (1982). An investigation of the regional variations and frequency dependence of anelastic attenuation in the mantle under the United States in the 0.5-4.0

Hz band, Geophys. J. Roy. Astr. Soc., 69, 67-99.

Doyle, H. A. and A. L. Hales (1967). An analysis of the travel times of S waves to North American stations, in the distance range 28° to 82°, Bull. Seism. Soc. Amer., 57, 761-771.

Dziewonski, A. M. and D. L. Anderson (1982). Travel times and station corrections for P waves at teleseismic distances, J. Geophys. Res., submitted.

Evernden, J. F. and D. M. Clark (1970). Study of teleseismic P II-amplitude data, Phys. Earth. Planet. Int., 4, 24-31.

Grand, S. and D. V. Helmberger (1983)., Modeling upper mantle structure using SS, in preparation.

Hales, A. L. and H. A. Doyle (1967). P and S travel time anomalies and their interpretation, Geophys. J. Roy. Astr. Soc., 13, 403-415.

Hales, A. L. and E. Herrin (1972). Travel times of seismic waves, in Nature of the Solid Earth, pp. 172-215, ed. Robertson, E. C. McGraw-Hill, New York.

Hales, A. L. and J. L. Roberts (1970). The travel times of S and SKS, Bull. Seism. Soc. Amer., 60, 461-489.

Hales, A. L., J. R. Cleary, H. A. Doyle, R. Green and J. Roberts (1968). P wave station anomalies and the structure of the upper mantle, J. Geophys. Res., 73, 3885-3896.

Herrin, E. and J. Taggart (1962). Regional variations in Pn velocity and their effect on the location of epicenters, Bull. Seism. Soc. Amer., 52, 1037-1046.

Marshall, P. D., D. Springer and H. Rodean (1979). Magnitude

corrections for attenuation in the upper mantle, Geophys. J. Roy. Astr. Soc., 57, 609-638.

Mikami, N. and K. Hirahara (1981). Global distribution of long period P wave attenuation and its tectonic implications, J. Phys. Earth, 29, 97-117.

North, R. G. (1977). Station magnitude bias: Its determination, causes and effects, Report No. ESD-TR-77-85, Lincoln Laboratory, Lexington, Massachusetts.

Poupinet, G. (1977). Hétérogéneitiés du manteau terrestre déduites de la propagation des ondes de volume: implication géodynamique, Thèse présentée à l'Université Scientifique et Médicale de Grenoble.

Romanowicz, B. A. and M. Cara (1980). Reconsideration of the relations between S and P station anomalies in North America, Geophys. Res. Letters, 7, 417-420.

Romney, C., B. C. Brooks, R. H. Mansfield, D. S. Carter, J. N. Jordan and D. W. Gordon (1962). Travel times and amplitudes of principal body phases recorded from Gnome, Bull. Seism. Soc. Amer., 52, 1057-1074.

Sengupta, M. K. (1975). The Structure of the Earth's Mantle from Body Wave Observations, ScD thesis, Massachusetts Institute of Technology, 578pp..

Shore, M. J. (1982). Seismic travel-time anomalies from events in the western Soviet Union, Bull. Seism. Soc. Amer., 72, 113-128.

Solomon, S. C. (1970). Seismic wave attenuation and partial melting in the upper mantle of North America, J. Geophys. Res., 77,

1483-1502.

Wickens, A. J. and G. G. R. Buchbinder (1980). S wave residuals in Canada, Bull. Seism. Soc. Amer., 70, 809-822.

York, D. (1966). Least-squares fitting of a straight line, Canadian J. of Phys., 44, 1079-1086.